

THE MOTHER BODY PHASE TRANSITION IN THE NORMAL MATRIX MODEL

PAVEL M. BLEHER AND GUILHERME L. F. SILVA

ABSTRACT. The normal matrix model with algebraic potential has gained a lot of attention recently, partially in virtue of its connection to several other topics as quadrature domains, inverse potential problems and the Laplacian growth.

In this present paper we consider the normal matrix model with cubic plus linear potential. In order to regularize the model, we follow Elbau & Felder and introduce a cut-off. In the large size limit, the eigenvalues of the model accumulate uniformly within a certain domain Ω that we determine explicitly by finding the rational parametrization of its boundary.

We also study in details the mother body problem associated to Ω . It turns out that the mother body measure μ_* displays a novel phase transition that we call the *mother body phase transition*: although $\partial\Omega$ evolves analytically, the mother body measure undergoes a “one-cut to three-cut” phase transition.

To construct the mother body measure, we define a quadratic differential ϖ on the associated spectral curve, and embed μ_* into its critical graph. Using deformation techniques for quadratic differentials, we are able to get precise information on μ_* . In particular, this allows us to determine the phase diagram for the mother body phase transition explicitly.

Following previous works of Bleher & Kuijlaars and Kuijlaars & López, we consider multiple orthogonal polynomials associated with the normal matrix model. Applying the Deift-Zhou nonlinear steepest descent method to the associated Riemann-Hilbert problem, we obtain strong asymptotic formulas for these polynomials. Due to the presence of the linear term in the potential, there are no rotational symmetries in the model. This makes the construction of the associated g -functions significantly more involved, and the critical graph of ϖ becomes the key technical tool in this analysis as well.

CONTENTS

1. Introduction	3
2. Statement of main results	7
2.1. Phase diagram of the cubic model	7
2.2. The limiting boundary of eigenvalues as a polynomial curve	8
2.3. Spectral curve	10
2.4. Phase transition of the spectral curve	11
2.5. The parameters (r, a_0) as a change of variables	12
2.6. The mother body problem	13
2.7. Associated multiple orthogonality	16

2010 *Mathematics Subject Classification.* Primary: 60B20; Secondary: 30C99, 30Exx, 30F30, 31A15, 44A60.

Key words and phrases. Random matrix theory, normal matrix model, mother body problem, Schwarz function, Riemann-Hilbert problems, multiple orthogonal polynomials, trajectories of quadratic differentials.

2.8. Behavior at the boundary of the phase diagram	22
2.9. The S-property	23
2.10. Statement of Results - $t_1 < 0$	24
2.11. Phase transition along the mother body critical curve	28
2.12. Setup for the remainder of the paper	31
3. Limiting boundary of eigenvalues. Proofs of Propositions 2.1 and 2.7 and Theorems 2.2, 2.5 and 2.8	31
3.1. Proof of Proposition 2.1	31
3.2. Proofs of Theorems 2.2, 2.5 and 2.8 and Proposition 2.7	37
4. Geometry of the spectral curve. Proof of Theorem 2.6	40
4.1. The spectral curve for $t_1 = 0$	41
4.2. The spectral curve for $t_1 > 0$. Proof of Theorem 4.1	42
4.3. Sheet structure for \mathcal{R}	48
5. Meromorphic quadratic differential on \mathcal{R}	50
5.1. Technical computations for the three-cut case	52
5.2. Technical computations for the one-cut case	54
5.3. Quadratic differential on the spectral curve: general principles	59
5.4. Critical graph in the three-cut case	63
5.5. Critical graph in the one-cut case	70
6. Proofs of Theorems 2.3, 2.4, 2.9 and 2.10	73
7. Riemann-Hilbert analysis in the three-cut case	81
7.1. Multiple orthogonality in terms of Airy functions	81
7.2. The Riemann-Hilbert problem Y	83
7.3. First transformation: $Y \mapsto X$	83
7.4. Second transformation: $X \mapsto T$	86
7.5. Opening of lenses: $T \mapsto S$	91
7.6. The global parametrix	94
7.7. The local parametrices	95
7.8. Final transformation: $S \mapsto R$	95
8. Riemann-Hilbert analysis in the one-cut case	96
9. Construction of the global parametrix	104
9.1. The inverse of the rational parametrization	105
9.2. Construction of the global parametrix in the three-cut case	107
9.3. Construction of the global parametrix in the one-cut case	109
9.4. Explicit construction of the first row	111
10. Proofs of Theorems 2.14 and 2.15	112
Appendix A. Analysis of the width parameters	113
A.1. Width parameters in the three-cut case	115
A.2. Width parameters in the one-cut case	118
Acknowledgements	125
References	125

1. INTRODUCTION

We are interested in the eigenvalues of the normal matrix model given by the probability distribution

$$d\pi_n(M) = \frac{1}{Z_n} e^{-n \operatorname{Tr} \mathcal{V}(M)} dM, \quad (1.1)$$

where M is an $n \times n$ normal matrix and \mathcal{V} is a given function of M . Its induced joint probability distribution on the eigenvalues $\lambda = (\lambda_1, \dots, \lambda_n) \in \mathbb{C}^n$ is given explicitly by

$$d\pi_n(\lambda) = \frac{1}{Z_n} \prod_{j < k} |\lambda_j - \lambda_k|^2 e^{-n \sum_{j=1}^n \mathcal{V}(\lambda_j)} d\lambda, \quad (1.2)$$

where $d\lambda$ is the Lebesgue measure on \mathbb{C}^n and Z_n is the corresponding partition function [17, 22].

This model has been studied in the literature for different choices of the potential \mathcal{V} and under various perspectives [2, 3, 17, 30, 41–43, 49]. Of particular interest is the choice

$$\mathcal{V}(z) = \frac{1}{t_0} (|z|^2 - V(z) - \overline{V(z)}), \quad z \in \mathbb{C}, \quad V(z) = \sum_{k=1}^{d+1} \frac{t_k}{k} z^k, \quad t_{d+1} \neq 0. \quad (1.3)$$

As formally observed by Kostov, Krichever, Mineev-Weinstein, Wiegmann and Zabrodin [36], in this situation the eigenvalues should accumulate on a domain $\Omega = \Omega(t_0, t_1, \dots, t_d)$, whose boundary $\partial\Omega$ evolves in time $t_0 > 0$ according to the Laplacian growth model with given harmonic moments

$$\operatorname{Area}(\Omega) = \pi t_0, \quad -\frac{1}{\pi} \iint_{\mathbb{C} \setminus \Omega} \frac{dA(z)}{z^k} = t_k, \quad k = 1, 2, 3, \dots, \quad (1.4)$$

where we set $t_j = 0$, for $j \geq d+2$, and dA is the Lebesgue measure on \mathbb{C} .

However, the model (1.1) for \mathcal{V} given by (1.3) is in general purely formal. If $d \geq 2$, the density in (1.1) is not integrable, hence the normal matrix model is ill-defined. To overcome this essential issue, Elbau and Felder [22] proposed to consider a *cut off* model. Instead of integrating (1.1) over the whole set of normal matrices, they consider (1.1) as a distribution over normal matrices whose eigenvalues are constrained to lie within a fixed bounded domain $D \subset \mathbb{C}$. In this setup, the model becomes well-defined and the eigenvalue density (1.2) can be rewritten as

$$d\pi_n(\lambda) = \frac{1}{Z_n} \prod_{j < k} |\lambda_j - \lambda_k|^2 \prod_{j=1}^n \chi_D(\lambda_j) e^{-n \mathcal{V}(\lambda_j)} d\lambda, \quad (1.5)$$

where χ_D is the characteristic function of D . Let

$$d\mu_\lambda(z) = \frac{1}{n} \sum_{j=1}^n \delta(z - \lambda_j) dA(z)$$

be a probability atomic measure on D with atoms at the points λ_j of an eigenvalue configuration λ and

$$H(\mu) = \iint_{x \neq z} \log \frac{1}{|z - x|} d\mu(x) d\mu(z) + \int \mathcal{V}(z) d\mu(z) \quad (1.6)$$

the Coulomb gas Hamiltonian, where μ is an arbitrary probability measure on D , giving a distribution of the Coulomb gas particles. Then formula (1.5) can be written as

$$d\pi_n(\lambda) = \frac{1}{Z_n} e^{-n^2 H(\mu_\lambda)} d\lambda,$$

The factor n^2 in the exponent suggests that, as $n \rightarrow \infty$, the measure $d\pi_n(\lambda)$ concentrates in a shrinking neighborhood of the equilibrium measure μ_0 , which is the probability measure minimizing

$$\iint \log \frac{1}{|z-x|} d\mu(x) d\mu(z) + \int \mathcal{V}(z) d\mu(z) \quad (1.7)$$

over all probability measures supported on D . This concentration phenomenon has been proved rigorously for instance in [22, 30] under different assumptions.

Under the additional requirements that

- (1) the boundary ∂D of the cut off is sufficiently smooth,
- (2) the potential \mathcal{V} has exactly one minimum in the cut off D , and
- (3) the time parameter t_0 is *sufficiently small*,

Elbau and Felder proved that the (unique) probability measure on D minimizing (1.7) has the form

$$d\mu_0(z) = \frac{1}{\pi t_0} \chi_\Omega(z) dA(z), \quad (1.8)$$

where χ_Ω is the characteristic function of a simply connected domain $\Omega = \Omega(t_0, V)$ contained in D , whose boundary $\partial\Omega$ is a *polynomial curve* of degree d : there exists a rational function of the form

$$h(w) = rw + a_0 + \frac{a_1}{w} + \cdots + \frac{a_d}{w^d}, \quad w \in \mathbb{C}, \quad r > 0, \quad a_d \neq 0, \quad (1.9)$$

which is injective on the boundary of the unit disc \mathbb{D} and such that $\partial\Omega = h(\partial\mathbb{D})$. Moreover, h gives a conformal map of $\mathbb{C} \setminus \mathbb{D}$ onto $\mathbb{C} \setminus \Omega$. Furthermore, still for sufficiently small time t_0 , Elbau and Felder proved rigorously the connection of Ω with the Laplacian growth as in (1.4).

Concerning local statistics, Elbau [21] pointed out that the eigenvalue distribution (1.5) is a bona fide determinantal point process with kernel

$$K_n(z, w) = e^{-\frac{n}{2}(\mathcal{V}(z) + \mathcal{V}(w))} \sum_{j=0}^n \frac{q_{j,n}(z) \overline{q_{j,n}(w)}}{h_{n,j}},$$

where $q_{j,n}(z) = z^j + \dots$ are *planar orthogonal polynomials in the external field \mathcal{V}* (or simply POP's)

$$\iint_D q_{j,n}(z) \overline{q_{k,n}(z)} e^{-n\mathcal{V}(z)} dA(z) = h_{n,j} \delta_{j,k}, \quad j, k \in \mathbb{N}. \quad (1.10)$$

A natural question is to understand the behavior of the polynomials $(q_{n,n})$, and in particular of their zeros, as $n \rightarrow \infty$. Elbau showed that any weak limit μ_* of the zero counting measures

$$d\mu_n(z) = \frac{1}{n} \sum_{q_{n,n}(w)=0} \delta(z-w) dA(z)$$

should be supported in D and satisfy the mother body property for μ_0 , namely

$$\int \log |s-z| d\mu_0(s) = \int \log |s-z| d\mu_*(s), \quad z \in \mathbb{C} \setminus D. \quad (1.11)$$

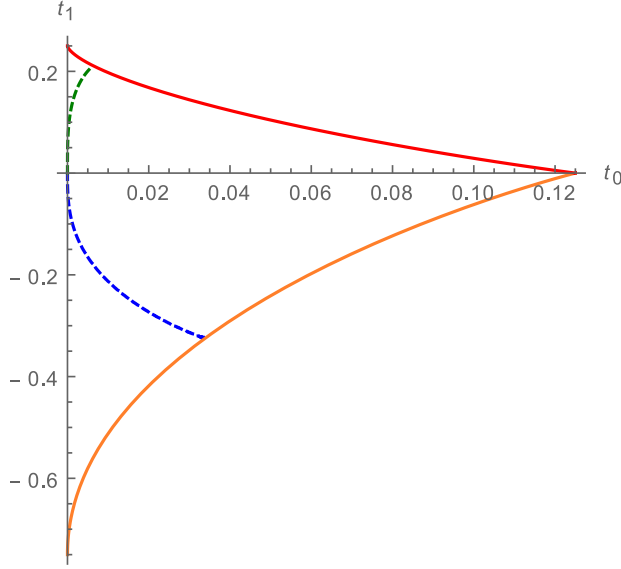


FIGURE 1. Phase diagram on the (t_0, t_1) -plane: the solid curves are the pairs $(t_{0,crit}, t_1)$, which correspond to the cusp phase transition. The dashed curves are the points of the form $(\tilde{t}_{0,crit}, t_1)$ and they correspond to the mother body phase transition. We should remark that the dashed curves on the upper and lower half planes are *not analytic continuation of each other*: the curve on the upper half plane is algebraic, whereas the one on the lower half plane is transcendental.

The goal of the present paper is to study in details the cubic plus linear model

$$\mathcal{V}(z) = \frac{1}{t_0}(|z|^2 - 2 \operatorname{Re} V(z)), \quad V(z) = \frac{z^3}{3} + t_1 z, \quad -\frac{3}{4} < t_1 < \frac{1}{4}, \quad (1.12)$$

for values of t_0 up to a critical time $t_{0,crit} = t_{0,crit}(t_1)$. The restriction on t_1 above comes from the corresponding potential \mathcal{V} : as a simple analysis shows, if either $t_1 \leq -3/4$ or $t_1 \geq 1/4$, then the potential \mathcal{V} has no local minimum. Consequently, for any choice of cut off D , the corresponding eigenvalues should accumulate on the boundary of D as $n \rightarrow \infty$, so that the limiting shape of eigenvalues Ω intersects ∂D and is very sensitive to the precise choice of D .

For t_1 as in (1.12), we are able to determine precisely the underlying phase diagram in the (t_0, t_1) -plane, as is shown in Figure 1. Given t_1 as above and for all positive values of t_0 up to the critical time $t_{0,crit} = t_{0,crit}(t_1)$, we find the parametrization h in (1.9) of the corresponding polynomial curve $\partial\Omega$, and consequently we obtain the associated limiting eigenvalue distribution (1.8) explicitly. When $t_0 \rightarrow t_{0,crit}$, the boundary of $\partial\Omega$ creates either one (if $t_1 > 0$) or two (if $t_1 < 0$) cusps: we call this phenomenon the *cusp phase transition*. We are able to compute the critical curve $(t_{0,crit}, t_1)$ explicitly.

For all values of (t_0, t_1) in our phase diagram, we also study the mother body equation (1.11) in detail. We construct a measure μ_* satisfying (1.11) and whose support consists of a finite union of analytic arcs. Furthermore, we find another

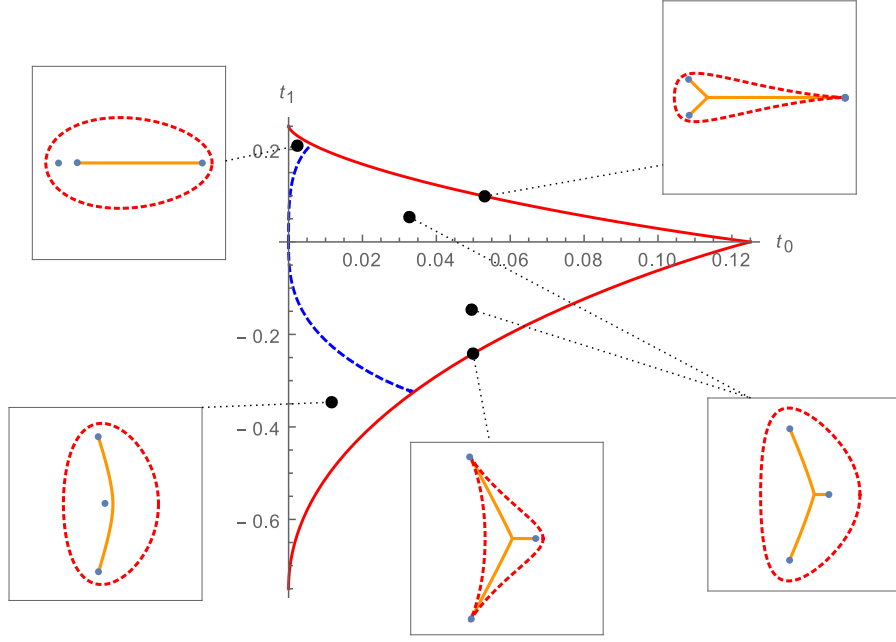


FIGURE 2. The phase diagram and the various topological configurations of $\partial\Omega$ (dashed lines in each frame) and $\text{supp } \mu_*$ (solid lines in each frame). The dots inside each frame are the branch points of the associated spectral curve.

critical time $\tilde{t}_{0,crit} = \tilde{t}_{0,crit}(t_1) < t_{0,crit}$ such that if $t_0 < \tilde{t}_{0,crit}$, then $\text{supp } \mu_*$ consists of one analytic arc, whereas for $t_0 > \tilde{t}_{0,crit}$ the set $\text{supp } \mu_*$ consists of three analytic arcs meeting at a common point. We call this transition the *mother body phase transition*.

The critical value $\tilde{t}_{0,crit}$ is depicted in Figure 1. We emphasize that the boundary of $\partial\Omega$ depends analytically on the parameters (t_0, t_1) in the phase diagram. So what our results show is that the measure μ_* solving the mother body problem (1.11) displays a phase transition that is not felt by $\partial\Omega$. We refer to Figure 2 for a visualization of this transition. To our knowledge, this is the first time such a phenomenon is described.

The construction of the measure μ_* is, in our opinion, our main technical contribution. We construct a quadratic differential on the three-sheeted Riemann surface (a.k.a. spectral curve) associated with the model, and lift the problem (1.11) to the trajectories of this quadratic differential. Following the recent work of Martínez-Finkelshstein and the second author [45], we use deformation techniques to describe the critical graph of this quadratic differential. When we project some of these trajectories back to the complex plane, we recover the measure μ_* . This critical graph displays some phase transitions; these transitions are determined by the critical value $\tilde{t}_{0,crit}$ and correspond to the phase transitions of $\text{supp } \mu_*$.

We follow previous works of Bleher and Kuijlaars [15] and Kuijlaars and López [37] and introduce a new sequence of polynomials $(P_{n,n})$ which has, at the heuristic

level, the same asymptotic behavior as the sequence $(q_{n,n})$ in (1.10). We characterize this sequence $(P_{n,n})$ in terms of multiple orthogonality of non-hermitian type, and using the Deift-Zhou steepest descent method we obtain strong asymptotic formulas for these polynomials. As one of the consequences, we prove that the sequence of zero counting measures for $(P_{n,n})$ converges weakly to the measure μ_* .

The case $t_1 = 0$ was studied before by Bleher and Kuijlaars [15], and it plays a substantial role here as well. Many auxiliary results require separate proofs depending whether $t_1 < 0$ or $t_1 > 0$, and a complete analysis would make the already lengthy paper much longer. So our main focus is on the case $t_1 > 0$, whose main results are stated in Section 2. The corresponding main results for $t_1 < 0$ are stated and discussed in Section 2.10, but their proofs are analogous and not provided.

2. STATEMENT OF MAIN RESULTS

2.1. Phase diagram of the cubic model. For the choice of potential (1.3) with V as in (1.12), the rational function h in (1.9) assumes the form

$$h(w) = rw + a_0 + \frac{a_1}{w} + \frac{a_2}{w^2}.$$

According to Elbau and Felder [22, page 442], the coefficients of h should be related to the normal matrix model (1.1) with cubic potential (1.12) through the system of equations

$$\begin{cases} \frac{a_2}{r^2} = 1, \\ \frac{a_1}{r} - \frac{2a_0a_2}{r^2} = 0, \\ a_0 - \frac{a_0a_1}{r} - \frac{a_2(2a_1r - a_0^2)}{r^2} = t_1, \\ r^2 - a_1^2 - 2a_2^2 = t_0. \end{cases} \quad (2.1)$$

This system of equations is obtained by computing the (expected) exterior harmonic moments of $\partial\Omega$ in terms of the rational function h . Solving in terms of r , it gives us

$$a_1 = 2ra_0, \quad a_2 = r^2, \quad a_0 = \frac{1 - 4r^2 + \delta\sqrt{(1 - 4r^2)^2 - t_1}}{2}. \quad (2.2)$$

where $\delta = \pm 1$. When $t_1 \rightarrow 0$, we expect $a_0 = 0$ [15]; thus $\delta = -1$, and h reduces to

$$h(w) = rw + a_0 + \frac{2a_0r}{w} + \frac{r^2}{w^2}, \quad (2.3)$$

where

$$a_0 = a_0(t_0, t_1) = \frac{1 - 4r^2 - \sqrt{(1 - 4r^2)^2 - 4t_1}}{2}, \quad (2.4)$$

and $r = r(t_0, t_1)$ is to be determined. Using the values (2.2) in the last equation in (2.1), after a lengthy calculation we conclude that r should be a root of the polynomial

$$\begin{aligned} p(x) = 128x^{10} - 124x^8 + (64t_0 - 16t_1 + 36)x^6 \\ + (16t_1^2 + 8t_1 - 28t_0 - 3)x^4 + t_0(2 - 8t_1)x^2 + t_0^2 \end{aligned} \quad (2.5)$$

When $t_1 \rightarrow 0$, we compare again with the results by Kuijlaars and the first author [15] to get that r should be the smallest positive root of p . An analysis of the

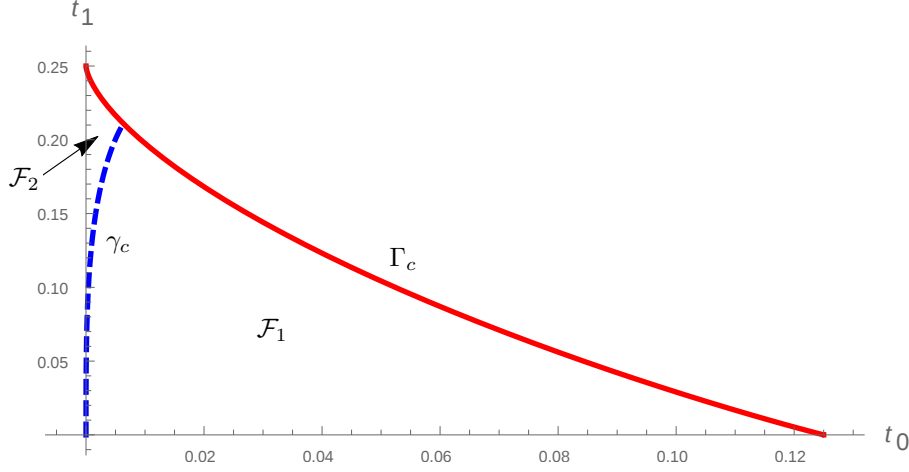


FIGURE 3. Phase diagram on the (t_0, t_1) -plane: The solid curve is Γ_c given in (2.6) and the dashed curve is γ_c given in (2.18). The region determined by Γ_c , γ_c and the t_0 -axis is the three-cut region \mathcal{F}_1 , whereas the region between Γ_c , γ_c and the t_1 -axis is the one-cut region \mathcal{F}_2 . Axes are scaled differently.

discriminant of p then leads us to consider the domain \mathcal{F} on the (t_0, t_1) -plane, bounded by the segments

$$\begin{aligned} (t_0, 0), \quad 0 \leq t_0 \leq 1/8, \\ (0, t_1), \quad 0 \leq t_1 \leq 1/4, \end{aligned}$$

and the critical curve Γ_c , parametrized by

$$\Gamma_c: \quad t_0 = -6s^4 + 4s^3, \quad t_1 = 4s^3 - 3s^2 + 1/4, \quad 0 \leq s \leq 1/2. \quad (2.6)$$

Proposition 2.1. *For $(t_0, t_1) \in \mathcal{F}$, the polynomial p in (2.5) has a smallest positive root $r = r(t_0, t_1)$, which is simple.*

Proposition 2.1 is proved in Section 3.1. Theorem 3.6 in Section 3.1 gives an important refinement of Proposition 2.1.

The curve Γ_c corresponds to the cusp phase transition for $t_1 > 0$. A plot of the region \mathcal{F} and the critical curve Γ_c are displayed in Figure 3.

Since the function $r = r(t_0, t_1)$ is a simple root of the polynomial p , it is analytic with respect to both variables t_0, t_1 , as long as $(t_0, t_1) \in \mathcal{F}$, and it is continuous up to the boundary of \mathcal{F} . The function r plays a fundamental role in the rest of the paper.

2.2. The limiting boundary of eigenvalues as a polynomial curve. As it was heuristically explained in Section 2.1, the rational function h in (2.3), with coefficients a_0 and r as in (2.4) and Proposition 2.1, should give the parametrization of the polynomial curve $\partial\Omega$ for the potential (1.12). This is rigorously established by our next result.

Theorem 2.2. *For $(t_0, t_1) \in \mathcal{F}$ and r, a_0 given respectively by Proposition 2.1 and equation (2.4), the rational function h is injective on $\mathbb{C} \setminus \mathbb{D}$. The image $h(\partial\mathbb{D})$ is*

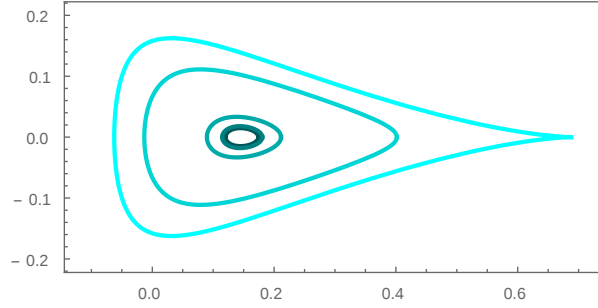


FIGURE 4. The boundary $\partial\Omega$ corresponding to $t_1 = \frac{1}{8}$ and $t_0 = \frac{1}{2500}, \frac{1}{1700}, \frac{1}{500}, \frac{1}{50}, \frac{5}{128}$ (from dark to bright color, respectively). For the pair $(t_0, t_1) = (\frac{5}{128}, \frac{1}{8})$, which belongs to the critical curve Γ_c , a cusp is created at the boundary. Numerical output.

an analytic curve whose interior is a simply connected domain Ω with area given by

$$\text{Area}(\Omega) = \pi t_0.$$

Moreover, the exterior harmonic moments of Ω with respect to any point $\zeta \in \Omega$ are given by

$$\frac{1}{2\pi i} \int_{\partial\Omega} \frac{\bar{z}}{(z - \zeta)^k} dz = \begin{cases} t_1 + \zeta^2, & k = 1, \\ 2\zeta, & k = 2, \\ 1, & k = 3, \\ 0, & k \geq 4. \end{cases} \quad (2.7)$$

Theorem 2.2 is proved in Section 3.2.

The equality $\partial\Omega = h(\partial\mathbb{D})$ with h rational and injective on $\partial\mathbb{D}$ says that $\partial\Omega$ is a *polynomial curve*, in the sense of Elbau and Felder [22]. We refer to Figure 4 for examples.

If $0 \in \Omega$ and $k \geq 3$, then the integrals in (1.4) are convergent for $\zeta = 0$ and Green's Theorem applied to $\mathbb{C} \setminus \Omega$ gives us the formula

$$-\frac{1}{\pi} \iint_{\mathbb{C} \setminus \Omega} \frac{dA(z)}{z^k} = \frac{1}{2\pi i} \int_{\partial\Omega} \frac{\bar{z}}{z^k} dz,$$

leading to the connection previously mentioned in (1.4).

For a measure ν on the complex plane, we denote by

$$U^\nu(z) = \int \log \frac{1}{|s - z|} d\nu(s), \quad z \in \mathbb{C}, \quad (2.8)$$

its logarithmic potential, which is harmonic in $\mathbb{C} \setminus \text{supp } \nu$ and superharmonic in \mathbb{C} [50].

Define the measure μ_0 by the formula

$$d\mu_0(z) = \frac{1}{\pi t_0} \chi_\Omega(z) dA(z). \quad (2.9)$$

Theorem 2.3. *Suppose $(t_0, t_1) \in \mathcal{F}$. Consider the potential \mathcal{V} in (1.3) for the cubic polynomial V in (1.12). There exist an open neighborhood D of $\bar{\Omega}$ and a constant*

l such that

$$2U^{\mu_0}(z) + \mathcal{V}(z) = l, \quad z \in \overline{\Omega}, \quad (2.10)$$

$$2U^{\mu_0}(z) + \mathcal{V}(z) > l, \quad z \in D \setminus \overline{\Omega}. \quad (2.11)$$

As an immediate consequence, we recover the connection with the normal matrix model.

Theorem 2.4. *Suppose $(t_0, t_1) \in \mathcal{F}$, and \mathcal{V} and V are as in Theorem 2.3. Suppose in addition that a given domain D contains $\overline{\Omega}$ and satisfies the conclusions of Theorem 2.3. Then the measure μ_0 in (2.9) is the limiting eigenvalue distribution of the normal matrix model with cubic potential (1.12) and cut off D .*

Theorems 2.3 and 2.4 are proved in Section 6. The evolution of the domain Ω in time $t_0 > 0$ is displayed in Figure 4.

2.3. Spectral curve. The pairs of points

$$(\xi, z) = (h(w^{-1}), h(w)), \quad w \in \overline{\mathbb{C}}$$

are expected to be solutions of an algebraic equation of the form

$$F(\xi, z) = 0,$$

where F is a symmetric polynomial in ξ and z , with $\deg_z F = \deg_\xi F = 3$. This equation is known in random matrix terminology as the *spectral curve* or *master loop equation*. Using equations (2.1)–(2.4), after a lengthy calculation we arrive at

$$F(\xi, z) := \xi^3 + z^3 - z^2\xi^2 - t_1(\xi^2 + z^2) - (1 + t_0)z\xi + (B + t_1)(\xi + z) + A = 0, \quad (2.12)$$

where

$$B = 4a_0^3r^2 + 4a_0^2r^4 + 4a_0r^4 - a_0r^2 \quad (2.13)$$

and

$$A = -\left(a_0^4(1 - 4r^2) - 2a_0^3(1 - 2r^2)^2 + a_0^2(-4r^6 + 6r^4 - 3r^2 + 1) + r^2(r^2 - 1)^3\right), \quad (2.14)$$

$r = r(t_0, t_1)$ is as in Proposition 2.1 and a_0 is given in (2.4).

For each z , there are three solutions ξ_1, ξ_2, ξ_3 to (2.12), labeled according to the expansions

$$\begin{aligned} \xi_1(z) &= z^2 + t_1 + \frac{t_0}{z} + \mathcal{O}(z^{-2}), \\ \xi_2(z) &= -z^{1/2} + \frac{t_1}{2z^{1/2}} - \frac{t_0}{2z} + \mathcal{O}(z^{-3/2}), \\ \xi_3(z) &= z^{1/2} - \frac{t_1}{2z^{1/2}} - \frac{t_0}{2z} + \mathcal{O}(z^{-3/2}), \end{aligned} \quad \text{as } z \rightarrow \infty, \quad (2.15)$$

where the square root is considered with a branch cut along the negative axis, and the branch is chosen such that $z^{1/2} > 0$ along the positive axis. In particular, the solution ξ_1 is meromorphic at $z = \infty$, whereas ξ_2, ξ_3 are branched at $z = \infty$.

A map $w \mapsto (\psi(w), \phi(w))$, ψ, ϕ rational, is a *rational parametrization* of (2.12) if

$$F(\psi(w), \phi(w)) = 0, \quad w \in \overline{\mathbb{C}}.$$

A rational parametrization as above is called *proper* if every but a finite number of pairs (ξ, z) satisfying (2.12) is generated by $(\xi, z) = (\psi(w), \phi(w))$ for exactly one choice $w \in \overline{\mathbb{C}}$.

Theorem 2.5. *Suppose that $(t_0, t_1) \in \mathcal{F}$. The map*

$$w \mapsto (\xi, z) = (h(w^{-1}), h(w)), \quad w \in \overline{\mathbb{C}}, \quad (2.16)$$

where h is given in (2.3), is a proper rational parametrization of the algebraic equation (2.12).

Moreover, the function ξ_1 is the Schwarz function of $\partial\Omega$. That is, there exists a simply connected domain $E \subset \overline{\mathbb{C}}$, containing $\partial\Omega$ and the point ∞ , and such that ξ_1 admits a meromorphic continuation to E , with pole only at ∞ , and satisfies

$$\xi_1(z) = \bar{z}, \quad z \in \partial\Omega. \quad (2.17)$$

Theorem 2.5 is proved in Section 3.2.

When $(t_0, t_1) \in \Gamma_c$, the function ξ_1 becomes branched in $\partial\Omega$ (see Section 2.8 below).

In particular, the existence of the Schwarz function implies that $\overline{\mathbb{C}} \setminus \overline{\Omega}$ is a quadrature domain, we refer the reader to [1, 40] for more details.

2.4. Phase transition of the spectral curve. The curve

$$\gamma_c : \quad t_0 = -2s^{12} + s^6 - 9s^{10}, \quad t_1 = \frac{3}{2}s^2 - \frac{9}{4}s^4 - 6s^8, \quad 0 \leq s \leq \frac{1}{2} \quad (2.18)$$

splits the parameter region \mathcal{F} into two parts $\mathcal{F}_1, \mathcal{F}_2$. The first part, \mathcal{F}_1 , consists of points (t_0, t_1) that lie to the right of γ_c , whereas the second part, \mathcal{F}_2 , consists of points that lie to the left of γ_c , see Figure 3. For reasons that will become apparent later, we call \mathcal{F}_1 the *three-cut* region and \mathcal{F}_2 the *one-cut* region.

Theorem 2.6. *For $(t_0, t_1) \in \mathcal{F} \setminus \gamma_c$, the spectral curve (2.12) has three branch points z_0, z_1, z_2 of order two, and no other branch points. These points are located as follows.*

(i) *For $(t_0, t_1) \in \mathcal{F}_1$,*

$$\operatorname{Im} z_1 < 0, \quad \bar{z}_2 = z_1, \quad z_0 > 0, \quad z_0, z_1, z_2 \in \Omega.$$

(ii) *For $(t_0, t_1) \in \mathcal{F}_2$,*

$$z_2 < z_1 < z_0, \quad z_0 > 0, \quad z_0, z_1 \in \Omega.$$

(iii) *For $(t_0, t_1) \in \gamma_c$, (2.12) has a branch point $z_0 > 0$ of order two and a branch point $z_1 = z_2 \in \mathbb{R}$ of order three, with $z_1 < z_0$. Furthermore, $z_0, z_1 \in \Omega$.*

Moreover, ∞ is always a branch point of order two of (2.12).

Finally, for $(t_0, t_1) \in \mathcal{F}$, (2.12) has three critical points $\hat{z}_0, \hat{z}_1, \hat{z}_2 \in \mathbb{C} \setminus \overline{\Omega}$, satisfying

$$\hat{z}_0 > z_0, \quad \hat{z}_1, \hat{z}_2 \in \mathbb{C} \setminus \mathbb{R}, \quad \operatorname{Im} \hat{z}_1 < 0, \quad \bar{\hat{z}}_2 = z_1.$$

The proof of Theorem 2.6 is provided in Section 4. In Theorem 2.6, by a critical point \hat{z}_j we mean that it satisfies

$$\frac{\partial F}{\partial \xi}(\xi_k, \hat{z}_j) = \frac{\partial F}{\partial z}(\xi_k, \hat{z}_j) = 0,$$

for some choice of $\xi_k = \xi_k(\hat{z}_j)$ for which the pair (ξ_k, \hat{z}_j) satisfies (2.12).

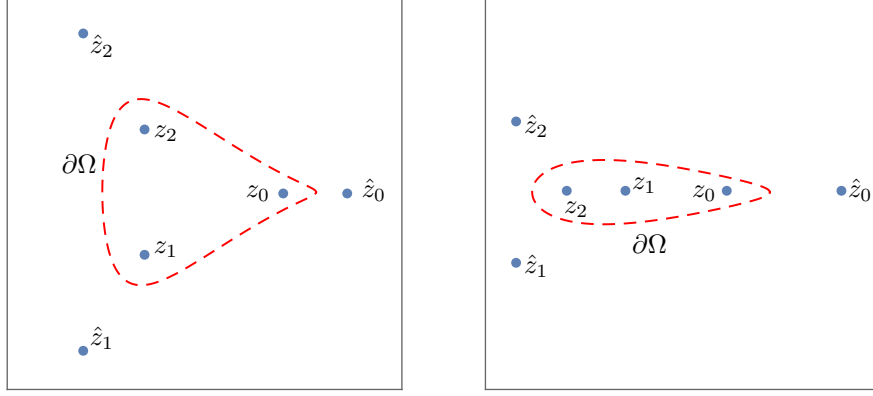


FIGURE 5. The boundary of Ω and the branch points and critical points in the three-cut (left-hand panel) and one-cut (right-hand panel) cases.

Theorem 2.6 can be summarized in the following manner. The critical curve γ_c determines two different regimes for the spectral curve: for pairs (t_0, t_1) to the left of γ_c the spectral curve has three real branch points, whereas for (t_0, t_1) to the right of γ_c the spectral curve has one real and two non real branch points. At γ_c , these non real branch points coalesce. We refer the reader to Figure 5 for a depiction of the branch points and critical points.

2.5. The parameters (r, a_0) as a change of variables. The functions $r = r(t_0, t_1)$ and $a_0 = a_0(t_0, t_1)$, given by Proposition 2.1 and equation (2.4), respectively, can be seen as a change of variables. It turns out that we can express the inverse change of coordinates $(r, a_0) \mapsto (t_0, t_1)$ explicitly.

Proposition 2.7. *Suppose $(t_0, t_1) \in \overline{\mathcal{F}}$. The functions r and a_0 satisfy the non-linear system*

$$2r^4 - r^2(1 - 4a_0^2) = -t_0 \quad (2.19)$$

$$a_0^2 - (1 - 4r^2)a_0 = -t_1 \quad (2.20)$$

The equations (2.19)–(2.20) are nothing but the last two equations in (2.1), taking into account the values of a_1 and a_2 in (2.2).

As a consequence of Proposition 2.7, we can compute our phase diagram in the (r, a_0) -plane, as it is established by the next Theorem and it is shown in Figure 6.

Theorem 2.8. *On the (r, a_0) -plane, the curve Γ_c assumes the form*

$$r = s, \quad a_0 = \frac{1 - 2s}{2}, \quad 0 < s < \frac{1}{2}, \quad (2.21)$$

and the curve γ_c assumes the form

$$r = s^3, \quad a_0 = \frac{3}{2}s^2, \quad 0 < s < \frac{1}{2}. \quad (2.22)$$

The proofs of Proposition 2.7 and Theorem 2.8 are given in Section 3.2.

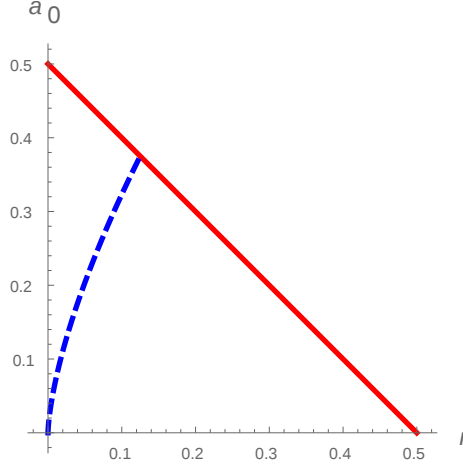


FIGURE 6. Image of the phase diagram in Figure 3 through the change of variables $(t_0, t_1) \mapsto (r, a_0)$. The solid curve is the image of Γ_c and the dashed curve is the image of γ_c . The region determined by the solid and dashed curves and the r -axis corresponds to \mathcal{F}_1 , whereas the region between the solid and dashed curves and the a_0 -axis corresponds to \mathcal{F}_2 .

2.6. The mother body problem. We now focus our attention on the mother body problem (1.11). In what follows, given a set $E \subset \mathbb{C}$ we denote

$$E^* = \{z \in \mathbb{C} \mid \bar{z} \in E\} \quad \text{and} \quad \mathbb{C}_\pm = \{z \in \mathbb{C} \mid \pm \operatorname{Im} z > 0\}. \quad (2.23)$$

Recall also that, according to Theorem 2.6, z_0, z_1 and z_2 are the branch points of the spectral curve (2.12).

Theorem 2.9. *There exists a contour Σ_* with*

$$\Sigma_* \subset \Omega, \quad (2.24)$$

and for which the solution ξ_1 in (2.15) admits an analytic continuation to $\mathbb{C} \setminus \Sigma_$ that satisfies*

$$(\xi_{1+}(s) - \xi_{1-}(s))ds \in i\mathbb{R}, \quad s \in \Sigma_*, \quad (2.25)$$

where ds is a tangent vector to Σ_ at the point s . The contour Σ_* is symmetric with respect to the real axis*

$$(\Sigma_*)^* = \Sigma_*$$

and has the following geometric properties.

(i) (Three-cut case) For $(t_0, t_1) \in \mathcal{F}_1$, the contour Σ_* can be decomposed into

$$\Sigma_* = \Sigma_{*,0} \cup \Sigma_{*,1} \cup \Sigma_{*,2},$$

where each $\Sigma_{,j}$ is a smooth oriented contour from a common point $z_* \in (-\infty, z_0)$ to the branch point z_j and*

$$\Sigma_{*,0} = [z_*, z_0], \quad (\Sigma_{*,2})^* = \Sigma_{*,1} \subset \overline{\mathbb{C}}_-.$$

(ii) (One-cut case) For $(t_0, t_1) \in \mathcal{F}_2$, the contour Σ_* is given by

$$\Sigma_* = [z_1, z_0].$$

Moreover, the measure

$$d\mu_*(z) = \frac{1}{2\pi i t_0} (\xi_{1-}(z) - \xi_{1+}(z)) dz, \quad z \in \Sigma_* \quad (2.26)$$

is a probability measure on Σ_* .

The phase diagram displayed in Figure 2 shows several configurations of $\text{supp } \mu_*$, and we refer to Figure 7 for more detailed numerical evaluations of $\text{supp } \mu_*$, displaying the evolution of $\text{supp } \mu_*$ in time t_0 while t_1 is kept fixed.

As we mentioned in the introduction, the construction of the measure μ_* in Theorem 2.9 is our main technical contribution, and it is quite involved. The first step, carried out in Section 4, is to construct the Riemann surface \mathcal{R} for (2.12); along the way we also collect several results that are used later on. The sheet structure of \mathcal{R} depends, in the terminology of Theorem 2.9, on whether we are in the three-cut or one-cut cases, and are explicitly given in Sections 4.3.1 and 4.3.2, respectively. In Section 5, we introduce a certain quadratic differential ϖ that encodes μ_* on some of its trajectories. The main goal of Section 5 is to describe the critical graph \mathcal{G} of ϖ . This is done by first computing \mathcal{G} for $t_1 = 0$ by “brute force”, and then deforming the parameter $t_1 > 0$, keeping track of all fundamental domains of \mathcal{G} . It turns out that the three-cut-to-one-cut phase transition for μ_* can be interpreted in terms of a phase transition for \mathcal{G} , and furthermore \mathcal{G} also plays a fundamental role in the asymptotic analysis of the multiple orthogonal polynomials that will be introduced in a moment. In Section 6 we use this critical graph \mathcal{G} to recover the measure μ_* .

It is a consequence of this analysis that the support Σ_* of μ_* , and in particular the point z_* , is determined as the projection of certain trajectories of ϖ . Roughly speaking, there are a number of points $y \in (-\infty, z_0)$ which are solutions to

$$\text{Re} \int_{z_2}^y (\xi_1(s) - \xi_2(s)) ds = 0,$$

where ξ_1, ξ_2 are (appropriate analytic continuations of) the functions in (2.15); the value $y = z_*$ is the largest of those solutions. We refer the reader to Sections 5 and 6 for details.

The measure μ_* is connected to the normal matrix model by the following theorem.

Theorem 2.10. *The measure μ_* in (2.26) relates to the limiting measure of eigenvalues μ_0 (1.8) through the conditions*

$$U^{\mu_0}(z) = U^{\mu_*}(z), \quad z \in \mathbb{C} \setminus \Omega, \quad (2.27)$$

$$U^{\mu_0}(z) < U^{\mu_*}(z), \quad z \in \Omega. \quad (2.28)$$

The proof of Theorem 2.10 is given in Section 6.

Given a domain $G \subset \mathbb{C}$, a measure ν is called a *mother body* (or also *potential-theoretic skeleton*) of G if [24]

- (M1) $\text{supp } \nu$ has null area measure;
- (M2) $\mathbb{C} \setminus \text{supp } \nu$ is connected;
- (M3) $\text{supp } \nu \subset G$;

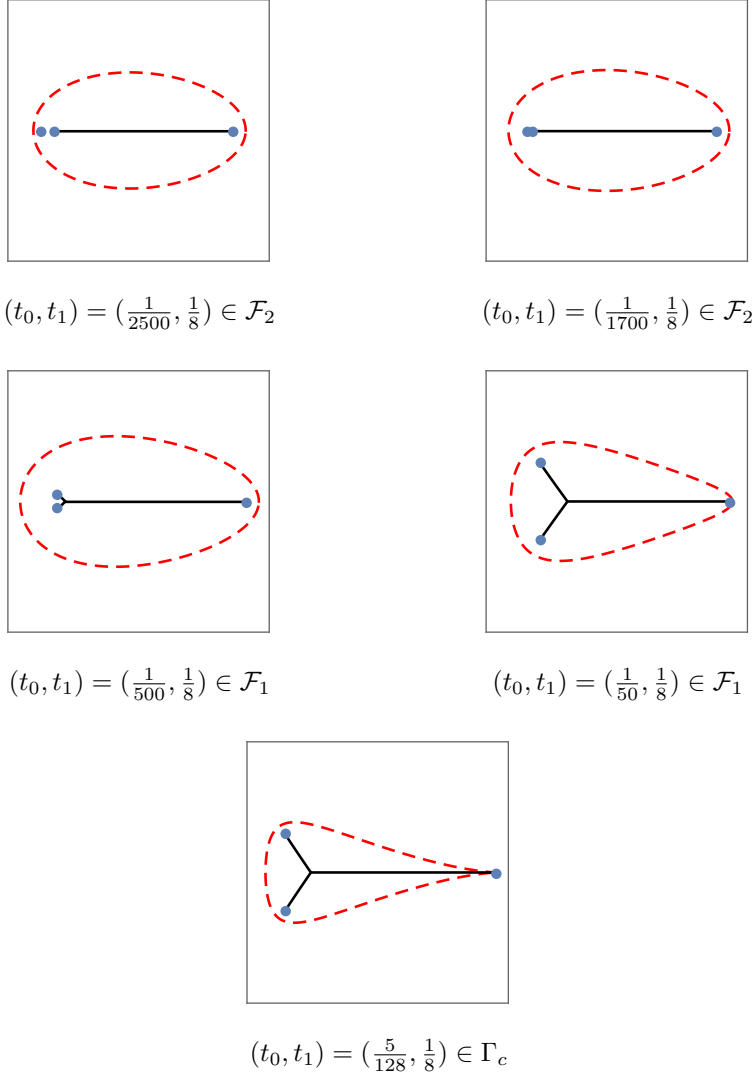


FIGURE 7. For the given values of (t_0, t_1) , the boundary $\partial\Omega$ (dashed contour), the support of the measure μ_* (solid lines) and the branch points z_0, z_1, z_2 (dots) are shown (the figures are scaled differently - compare with Figure 4). Note the transition when we move from \mathcal{F}_2 to \mathcal{F}_1 . We stress that the contours of $\text{supp } \mu_*$ outside the real line are not straight line segments. Numerical outputs.

(M4) for μ_G the normalized area measure of G , it holds true

$$\begin{aligned}
 U^{\mu_G}(z) &\leq U^\nu(z), \quad z \in \mathbb{C}, \\
 U^{\mu_G}(z) &= U^\nu(z), \quad z \in \mathbb{C} \setminus G.
 \end{aligned}$$

Conditions (M1)–(M4) are, generally speaking, quite demanding, and consequently domains with mother bodies are somewhat rare. Cases where the existence

of the mother body is known include discs, convex polyhedra [25] and ellipses [53], and mother bodies have also been numerically obtained for certain oval shapes [51]. Mother body measures appear in the context of quadrature domains [26], inverse problems in geophysics [58], zero distribution of orthogonal polynomials [28, 46], among others. We refer the reader to the lecture notes [24] by Gustafsson for more details.

Conditions (M1), (M2) and (M3) are satisfied for $\nu = \mu_*$ and $G = \Omega$. Equation (2.27) is the same as (1.11), and together with (2.28) they give (M4) and thus express that μ_* is a mother body for the domain Ω . For this reason, we call the “one-cut-to-three-cuts” phase transition for $\text{supp } \mu_*$ the *mother body phase transition*.

When the (boundary of the) domain G displays some topological transition, it is natural to expect that its mother body measure displays some phase transition as well. In fact, this has already been described in several previous works in the context of random normal matrices [6, 7, 15, 39], although in some cases without explicit mention. However, in our situation it is very interesting that the transition for μ_* occurs before any transition for Ω . In other words, the limiting domain for the eigenvalues of the normal matrix model (1.1) does not feel the mother body phase transition: as it is assured by Theorem 2.2, the boundary Ω depends analytically on the parameters (t_0, t_1) even across the critical curve γ_c .

To our knowledge, this is the first time a phase transition for the mother body, without any phase transition on the boundary of the underlying domain, is described in the literature. A somewhat related situation has already appeared in the work of Gustafsson and Lin [27, Example 5.2], where the authors identified, indirectly and without any detailed analysis, a phase transition for the branch points of the Schwarz function for a curve moving analytically in time: the branch points of the Schwarz function thus play the role of the end points of the mother body. Another similar phenomenon has been described in a previous work of the first author and Liechty [16, Section X], where they identified a phase transition for the zero distribution of the underlying orthogonal polynomials that is not reflected in the asymptotics of the partition function studied therein. In virtue of this latter work, it is also natural to expect that the partition function of (1.1) for the cubic potential (1.12) should not “feel” the mother body phase transition.

2.7. Associated multiple orthogonality. We follow [6, 15] and replace the planar orthogonality to an orthogonality over contours.

Construct a piecewise smooth curve

$$\Sigma = \Sigma_0 \cup \Sigma_1 \cup \Sigma_2, \quad (2.29)$$

where each set Σ_j is a smooth oriented arc, starting at a common point $a_* \in \mathbb{R}$ and ending at the critical point \hat{z}_j given by Theorem 2.6, $j = 0, 1, 2$. Recalling the notations introduced in (2.23), we assume

$$a_* < \hat{z}_0, \quad \Sigma_0 = [a_*, \hat{z}_0], \quad \Sigma_1 \subset \mathbb{C}_- \cup \{a_*\}, \quad \Sigma_2 \subset \mathbb{C}_+ \cup \{a_*\}. \quad (2.30)$$

we refer for instance to Figure 8 for a possible configuration of Σ . At this moment the contour Σ is rather arbitrary; in fact the conditions in (2.30) are made for simplicity and could even be loosen. But later the contour Σ will be chosen in an optimal way.

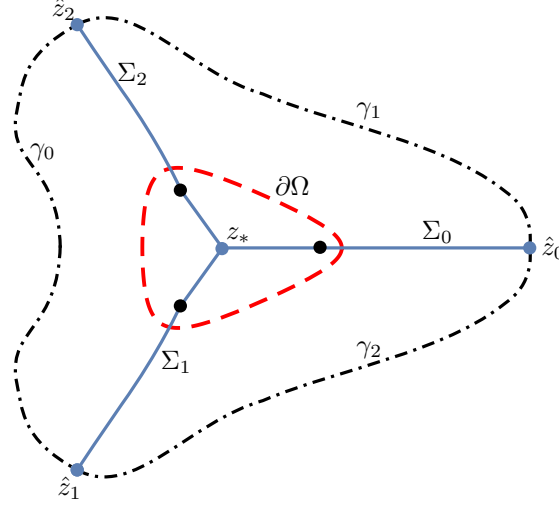


FIGURE 8. The dashed curve is $\partial\Omega$ and the dots inside it are the branch points z_0, z_1 and z_2 and the point z_* . The dot-dashed line is a possible configuration for $\partial D = \gamma_0 \cup \gamma_1 \cup \gamma_2$, and the points on ∂D are the critical points \hat{z}_0, \hat{z}_1 and \hat{z}_2 . The solid contour is a possible extension $\Sigma = \Sigma_0 \cup \Sigma_1 \cup \Sigma_2$ of the support Σ_* of the mother body measure Σ_* .

As a general notational convention, for the rest of the paper we use cyclic notation mod 3 without further mention when clear from the context. So for instance

$$\hat{z}_3 = \hat{z}_0, \quad \hat{z}_4 = \hat{z}_1, \quad \hat{z}_5 = \hat{z}_2,$$

and similarly for other quantities appearing later on.

Consider a compact, connected set $D \subset \mathbb{C}$, assuming in addition

$$\Sigma, \Omega \subset D, \quad \hat{z}_l \in \partial D, \quad l = 0, 1, 2,$$

where Σ is a curve as just explained above and Ω is the domain given by Theorem 2.2. The domain D should be interpreted as the cut off region in (1.10).

The points $\hat{z}_0, \hat{z}_1, \hat{z}_2$ split the boundary ∂D into three curves $\gamma_0, \gamma_1, \gamma_2$. For $l = 0, 1, 2$ (and again with cyclic notation mod 3), the curve γ_l is the oriented sub arc of ∂D going from \hat{z}_{l+2} to \hat{z}_{l+1} that does not contain \hat{z}_l , see Figure 8 for an example of a configuration of D, Σ and Ω .

For the third root of unity ω and the directions at infinity ∞_l given by

$$\omega = e^{\frac{2\pi i}{3}}, \quad \infty_l = -\omega^{-l} \infty, \quad l = 0, 1, 2, \quad (2.31)$$

let Γ_l be any unbounded oriented contour from ∞_{l+1} to ∞_{l+2} , $l = 0, 1, 2$. Also for $l = 0, 1, 2$ and any non negative integer k , define

$$\begin{aligned} w_{l,k,n}(z) &= \int_{\Gamma_l} s^k e^{-\frac{n}{t_0}(sz - V(s) - V(z))} ds, \quad z \in \mathbb{C}, \\ \tilde{w}_{l,k,n}(z) &= \int_{\infty_l}^{\bar{z}} s^k e^{-\frac{n}{t_0}(sz - V(s) - V(z))} ds, \quad z \in \mathbb{C}. \end{aligned} \quad (2.32)$$

where we recall that V is given in (1.12).

For $l = 0, 1, 2$, the union of contours $\gamma_l \cup \Sigma_{l+1} \cup \Sigma_{l+2}$ is the boundary of a domain $D_l \subset D$. An application of Green's Theorem to each of the pieces D_0, D_1, D_2 yields

Proposition 2.11. *For any polynomial Q and any integer $k \geq 0$, it is valid*

$$\begin{aligned} 2i \iint_D Q(z) \bar{z}^k e^{-\frac{n}{t_0}(|z|^2 - 2 \operatorname{Re} V(z))} dA(z) \\ = \sum_{l=0}^2 \int_{\Sigma_l} Q(z) w_{l,k,n}(z) dz + \sum_{l=0}^2 \int_{\gamma_l} Q(z) \tilde{w}_{l,k,n}(z) dz. \end{aligned} \quad (2.33)$$

The analogue to Proposition 2.11 for the monomial case $V(z) = \frac{z^d}{d}$, $d \geq 3$, is treated in [37, Proposition 1.1]. For the benefit of the reader we include the proof for V as in (1.12), which follows the same arguments presented in [37].

Proof. Let us apply the complex Green's theorem

$$2i \iint_S \frac{\partial f}{\partial \bar{z}} dA = \int_{\partial S} f dz$$

with $S = D_l$ and $f = Q(z) \tilde{w}_{l,k,n}(z)$. Then we obtain that

$$2i \iint_{D_l} Q(z) \bar{z}^k e^{-\frac{n}{t_0}(|z|^2 - V(\bar{z}) - V(z))} dA(z) = \int_{\partial D_l} Q(z) \tilde{w}_{l,k,n}(z) dz.$$

Summing over $l = 0, 1, 2$, we get that

$$2i \iint_D Q(z) \bar{z}^k e^{-\frac{n}{t_0}(|z|^2 - V(\bar{z}) - V(z))} dA(z) = \sum_{l=0}^2 \int_{\partial D_l} Q(z) \tilde{w}_{l,k,n}(z) dz. \quad (2.34)$$

The sum on the right can be partitioned as

$$\begin{aligned} \sum_{l=0}^2 \int_{\partial D_l} Q(z) \tilde{w}_{l,k,n}(z) dz &= \sum_{l=0}^2 \left[\int_{\gamma_l} Q(z) \tilde{w}_{l,k,n}(z) dz \right. \\ &\quad \left. + \int_{\Sigma_{l+2}} Q(z) \tilde{w}_{l,k,n}(z) dz - \int_{\Sigma_{l+1}} Q(z) \tilde{w}_{l,k,n}(z) dz \right]. \end{aligned}$$

Combining integrals over Σ_l , we obtain that

$$\begin{aligned} \sum_{l=0}^2 \int_{\partial D_l} Q(z) \tilde{w}_{l,k,n}(z) dz &= \sum_{l=0}^2 \int_{\gamma_l} Q(z) \tilde{w}_{l,k,n}(z) dz \\ &\quad + \sum_{l=0}^2 \int_{\Sigma_l} Q(z) [\tilde{w}_{l+1,k,n}(z) - \tilde{w}_{l+2,k,n}(z)] dz. \end{aligned}$$

We now observe that

$$\begin{aligned} \tilde{w}_{l+1,k,n}(z) - \tilde{w}_{l+2,k,n}(z) &= \int_{\infty_{l+1}}^{\bar{z}} s^k e^{-\frac{n}{t_0}(sz - V(s) - V(z))} ds \\ &\quad - \int_{\infty_{l+2}}^{\bar{z}} s^k e^{-\frac{n}{t_0}(sz - V(s) - V(z))} ds \\ &= \int_{\Gamma_l} s^k e^{-\frac{n}{t_0}(sz - V(s) - V(z))} ds \\ &= w_{l,k,n}(z), \end{aligned}$$

hence

$$\sum_{l=0}^2 \int_{\partial D_l} Q(z) \tilde{w}_{l,k,n}(z) dz = \sum_{l=0}^2 \int_{\gamma_l} Q(z) \tilde{w}_{l,k,n}(z) dz + \sum_{l=0}^2 \int_{\Sigma_l} Q(z) w_{l,k,n}(z) dz. \quad (2.35)$$

Equation (2.33) then follows from (2.34) and (2.35). \square

In particular, if $Q = q_{j,n}$ is the planar orthogonal polynomial (1.10), we conclude

$$\sum_{l=0}^2 \int_{\Sigma_l} q_{j,n}(z) w_{l,k,n}(z) dz + \sum_{l=0}^2 \int_{\gamma_l} q_{j,n}(z) \tilde{w}_{l,k,n}(z) dz = 0, \quad k = 0, \dots, j-1. \quad (2.36)$$

We are mostly interested in the behavior of $q_{j,n}$ in the limit $n \rightarrow \infty$ with j/n fixed. Under the conditions on D given in Theorem 2.4, that is, when the support $\bar{\Omega}$ of the equilibrium measure lies inside the cut off domain D , almost all the zeros of the polynomial $q_{j,n}$ lie inside D in this large n regime, as it was proven by Elbau [21, Lemma 5.2]. Consequently, $q_{j,n}$ should converge exponentially fast to zero in compact subsets of $\mathbb{C} \setminus \bar{\Omega}$, so in particular on the boundary ∂D .

It is then natural to expect that the integrals coming from $\partial D = \cup \gamma_l$ should be negligible compared to the integrals over Σ when $n \rightarrow \infty$. This fact motivates us to follow [15, 37] and neglect the integrals over ∂D in (2.36), and introduce the following family of polynomials.

Definition 2.12. We define $P_{j,n}$ to be the monic polynomial of degree j , if it exists, that satisfies

$$\sum_{l=0}^2 \int_{\Sigma_l} P_{j,n}(z) w_{l,k,n}(z) dz = 0, \quad k = 0, \dots, j-1, \quad (2.37)$$

where the weights $w_{l,k,n}$, $k, n \in \mathbb{N}$, $l = 0, 1, 2$, are given in (2.32).

Proposition 2.13. *The polynomial $P_{j,n}$, if it exists, fulfills the non-hermitian multiple orthogonality conditions*

$$\begin{aligned} \sum_{l=0}^2 \int_{\Sigma_l} P_{j,n}(z) z^k w_{l,0,n}(z) dz &= 0, \quad k = 0, \dots, \left\lceil \frac{j}{2} \right\rceil - 1, \\ \sum_{l=0}^2 \int_{\Sigma_l} P_{j,n}(z) z^k w_{l,1,n}(z) dz &= 0, \quad k = 0, \dots, \left\lfloor \frac{j}{2} \right\rfloor - 1. \end{aligned} \quad (2.38)$$

For a proof when $t_1 = 0$, we refer to [15, Lemma 5.1]. The case $t_1 \neq 0$ is treated similarly. For the sake of completeness we give the proof.

Proof. Equation (2.37) reads

$$\sum_{l=0}^2 \int_{\Sigma_l} P_{j,n}(z) \int_{\Gamma_l} s^k e^{-\frac{n}{t_0}(sz - V(s) - V(z))} ds dz = 0, \quad k = 0, \dots, j-1. \quad (2.39)$$

Let $Q(s)$ be any polynomial. Integration by parts gives the identity

$$\begin{aligned} \int_{\Gamma_l} Q'(s) e^{-\frac{n}{t_0}(sz-V(s)-V(z))} ds \\ = \frac{n}{t_0} \int_{\Gamma_l} Q(s) (z - V'(s)) e^{-\frac{n}{t_0}(sz-V(s)-V(z))} ds, \end{aligned}$$

hence

$$\begin{aligned} z \int_{\Gamma_l} Q(s) e^{-\frac{n}{t_0}(sz-V(s)-V(z))} ds \\ = \int_{\Gamma_l} \left(V'(s)Q(s) + \frac{t_0}{n} Q'(s) \right) e^{-\frac{n}{t_0}(sz-V(s)-V(z))} ds. \end{aligned} \quad (2.40)$$

Introduce the linear differential operator

$$\mathcal{A} : Q(s) \mapsto V'(s)Q(s) + \frac{t_0}{n} Q'(s). \quad (2.41)$$

Then the identity (2.40) can be written as

$$z \int_{\Gamma_l} Q(s) e^{-\frac{n}{t_0}(sz-V(s)-V(z))} ds = \int_{\Gamma_l} \mathcal{A}(Q)(s) e^{-\frac{n}{t_0}(sz-V(s)-V(z))} ds.$$

Applying it k times, we obtain that

$$z^k \int_{\Gamma_l} Q(s) e^{-\frac{n}{t_0}(sz-V(s)-V(z))} ds = \int_{\Gamma_l} \mathcal{A}^k(Q)(s) e^{-\frac{n}{t_0}(sz-V(s)-V(z))} ds,$$

thus

$$\begin{aligned} \sum_{l=0}^2 \int_{\Sigma_l} P_{j,n}(z) z^k \int_{\Gamma_l} Q(s) e^{-\frac{n}{t_0}(sz-V(s)-V(z))} ds dz \\ = \sum_{l=0}^2 \int_{\Sigma_l} P_{j,n}(z) \int_{\Gamma_l} \mathcal{A}^k(Q)(s) e^{-\frac{n}{t_0}(sz-V(s)-V(z))} ds dz. \end{aligned}$$

Observe that if $Q(s)$ is a polynomial, then $\mathcal{A}^k(Q)(s)$ is a polynomial as well, and since $\deg V' = 2$, we obtain from (2.41) that

$$\deg \mathcal{A}^k(Q) = \deg Q + 2k,$$

hence if $Q(s) \equiv 1$ and $2k < j$, then orthogonality condition (2.39) implies that

$$\begin{aligned} \sum_{l=0}^2 \int_{\Sigma_l} P_{j,n}(z) z^k \int_{\Gamma_l} e^{-\frac{n}{t_0}(sz-V(s)-V(z))} ds dz \\ = \sum_{l=0}^2 \int_{\Sigma_l} P_{j,n}(z) \int_{\Gamma_l} \mathcal{A}^k(1)(s) e^{-\frac{n}{t_0}(sz-V(s)-V(z))} ds dz = 0. \end{aligned}$$

This proves the first identity in (2.38). To prove the second one, we take $Q(s) \equiv s$ and any k such that $2k + 1 < j$. Then the orthogonality condition (2.39) implies

that

$$\begin{aligned} \sum_{l=0}^2 \int_{\Sigma_l} P_{j,n}(z) z^k \int_{\Gamma_l} s e^{-\frac{n}{t_0}(sz-V(s)-V(z))} ds dz \\ = \sum_{l=0}^2 \int_{\Sigma_l} P_{j,n}(z) \int_{\Gamma_l} \mathcal{A}^k(z)(s) e^{-\frac{n}{t_0}(sz-V(s)-V(z))} ds dz = 0. \end{aligned}$$

This proves (2.38). \square

We are mostly interested in the *diagonal* polynomials $P_{n,n}$. From Proposition 2.13 we obtain that the polynomial $P_{n,n}$ fulfills the non-hermitian multiple orthogonality conditions

$$\begin{aligned} \sum_{l=0}^2 \int_{\Sigma_l} P_{n,n}(z) z^k w_{l,0,n}(z) dz = 0, \quad k = 0, \dots, \left\lfloor \frac{n}{2} \right\rfloor - 1, \\ \sum_{l=0}^2 \int_{\Sigma_l} P_{n,n}(z) z^k w_{l,1,n}(z) dz = 0, \quad k = 0, \dots, \left\lfloor \frac{n}{2} \right\rfloor - 1. \end{aligned} \quad (2.42)$$

We remark that there is no complex conjugation on the integrands in (2.42). Consequently, it follows from the construction of the functions $w_{l,k,n}$ that the orthogonality conditions (2.42) do not depend on the precise choice of the contour Σ as in (2.29), but only on its endpoints \hat{z}_0, \hat{z}_1 and \hat{z}_2 .

As a consequence of (2.42), $P_{n,n}$ is additionally characterized through a Riemann-Hilbert problem (shortly RHP). We apply the nonlinear Deift/Zhou steepest descent analysis [18, 19] to this RHP and obtain the existence and asymptotic information for the polynomial $P_{n,n}$ for n sufficiently large. This analysis is carried out in Sections 7 and 8 for the three-cut and one-cut cases, respectively, and we refer the reader to these sections for more details. We also stress that several trajectories of the quadratic differential ϖ constructed in Section 5 play a fundamental role in this asymptotic analysis. One of the outcomes of it is regarding the zero counting measure

$$d\mu_n(z) = \frac{1}{n} \sum_{P_{n,n}(w)=0} \delta(z-w) dA(z). \quad (2.43)$$

Theorem 2.14. *Suppose $(t_0, t_1) \in \mathcal{F} \setminus \gamma_c$. The sequence of zero counting measures (μ_n) converges weakly to the measure μ_* given by (2.26).*

By Theorem 2.2, we know that the restriction of h to $\overline{\mathbb{C}} \setminus \mathbb{D}$ admits an inverse $\psi_1 : \overline{\mathbb{C}} \setminus \Omega \rightarrow \overline{\mathbb{C}} \setminus \mathbb{D}$. The function ψ_1 is alternatively characterized as the conformal map from $\mathbb{C} \setminus \overline{\Omega}$ to $\mathbb{C} \setminus \mathbb{D}$ that is uniquely determined by the conditions

$$\lim_{z \rightarrow \infty} \psi_1(\infty) = \infty, \quad \lim_{z \rightarrow \infty} \psi_1'(z) = \frac{1}{r},$$

where r is as in Proposition 2.1.

In addition, define the multivalued analytic function

$$G(z) = \int_{z_0}^z \xi_1(s) ds, \quad z \in \mathbb{C} \setminus \Sigma_*, \quad (2.44)$$

where z_0 is as in Theorem 2.6, ξ_1 is as in (2.15) and the path of integration is taken in $\mathbb{C} \setminus \Sigma_*$. As can be seen from the expansion (2.15), the residue of the function ξ_1 at ∞ is $-t_0$. In particular, this implies that G is well defined modulo $2\pi it_0$.

As for the uniform asymptotics for $P_{n,n}$, one of the consequences of our asymptotic analysis is given by the following result.

Theorem 2.15. *Suppose $(t_0, t_1) \in \mathcal{F} \setminus \gamma_0$. The map ψ_1 admits an analytic continuation to $\mathbb{C} \setminus \Sigma_*$, and for a certain constant c , the asymptotic formula*

$$P_{n,n}(z) = \sqrt{r\psi_1'(z)} e^{\frac{n}{t_0}(G(z)-V(z)+c)} (1 + \mathcal{O}(n^{-1})), \quad (2.45)$$

holds true uniformly on compacts of $\mathbb{C} \setminus \Sigma_$, where the branch of the square root is chosen with branch cut on Σ_* and so that $\sqrt{r\psi_1'(z)} \rightarrow 1$ as $z \rightarrow \infty$.*

Theorems 2.14 and 2.15 are proven in Section 10, after the conclusion of the steepest descent analysis.

Relation (2.27) is comparable with results by Elbau [21, Lemma 5.1 and Theorem 5.3]. As mentioned in the introduction, Elbau shows that any weak limit ν of the sequence of zero counting measures for the polynomials $(q_{n,n})$ in (1.10) should also satisfy (2.27) (with μ_* replaced by ν). Hence, what Theorem 2.14 says is that, at the level of weak asymptotics, our multiple orthogonal polynomials $(P_{n,n})$ have the same behavior as expected for the planar orthogonal polynomials $(q_{n,n})$. We also expect the formula (2.45) to hold true if we replace $P_{n,n}$ by the polynomial $q_{n,n}$.

The restriction $(t_0, t_1) \in \mathcal{F} \setminus \gamma_c$ in Theorems 2.14 and 2.15 is of technical nature. For these values of (t_0, t_1) , the density of μ_* vanishes as square root at the endpoints of its support, and as a consequence the required local parametrices in the steepest descent analysis are constructed out of solutions to the Airy differential equation. However, in the critical case $(t_0, t_1) \in \gamma_c$ the density of μ_* vanishes with order $1/3$ at the endpoint $z_1 = z_2$, and a different parametrix is required to complete the steepest descent analysis. This order of vanishing indicates that the local parametrix near $z_1 = z_2$ should be constructed in terms of solutions to the Pearcey differential equation (see for instance [14] and the references therein), but the rest of the analysis carried out here should work, after cosmetic changes, in this critical case as well. In particular, the conclusions of Theorems 2.14 and 2.15 should also hold true for $(t_0, t_1) \in \gamma_c$.

2.8. Behavior at the boundary of the phase diagram. When $(t_0, t_1) \in \Gamma_c$, the branch point z_0 and the double point \hat{z}_0 described in Theorem 2.6 come together at the boundary $\partial\Omega$. This corresponds to a branching of the Schwarz function ξ_1 on $\partial\Omega$, and explains the emerging of the cusp in $\partial\Omega$, as can be seen, for instance, in Figures 2, 4 and 7.

Consequently, when $(t_0, t_1) \in \Gamma_c$ the support of $\text{supp } \mu_*$ comes to the boundary of Ω as well, and the density of the measure μ_* vanishes with order $3/2$ at the endpoint $z_0 = \hat{z}_0$. This coalescence (for $t_1 = 0$) is already described in the literature (see for instance [15, 39, 41]), and the local behavior of the polynomial $P_{n,n}$ (after suitable regularization in terms of bilinear forms instead of a cut-off) near this point is expected to be given in terms of solutions to the Painlevé I equation, see for instance [11, 20] for related works. When $t_1 > 0$, nothing special happens near the other endpoints z_1, z_2 of $\text{supp } \mu_*$.

2.9. The S-property. Thanks to the precise manner we constructed the weights for the integrals in each contour Σ_l , the sum of integrals in (2.42) neither depends on the precise choice of contours Σ_1, Σ_2 and Σ_3 nor on their common point a_* . This freedom is reflected in Theorem 2.14, which says that the zeros of $P_{n,n}$ accumulate on $\text{supp } \mu_*$ regardless of the precise choice of the contour Σ . Furthermore, although the orthogonality conditions (2.42) do depend on the choice of endpoints \hat{z}_0, \hat{z}_1 and \hat{z}_2 for Σ , it becomes clear from our RH analysis that there is some flexibility in the choice of these points: in the large n limit the behavior of $P_{n,n}$ does not depend on these endpoints, as long as they are selected within some regions determined by certain critical trajectories of the underlying quadratic differential.

This freedom in the choice of the contour Σ is characteristic for non-hermitian orthogonality, and it is reflected in the behavior of the zeros of the respective orthogonal polynomials. Among all possible choices of contours, the zeros, in the large n limit, accumulate on a very particular one, determined by the so called *S-property*, as we discuss next.

Given a contour Σ for the orthogonality (2.42), construct three other oriented contours $L_j, j = 0, 1, 2$, starting at the point a_* in the inner sector between Σ_{j-1} and Σ_{j+1} , and extending to ∞ along the directions $\infty_j, j = 0, 1, 2$, as defined in (2.31). Assume in addition $L_j \cap L_k = L_j \cap \Sigma = \{a_*\}$ for $j \neq k$ and set $L = L_0 \cup L_1 \cup L_2$. We refer to Figure 29 in Section 7.3 for an example of the configuration of L and Σ .

To any pair of contours (Σ, L) as above, we associate a class of pairs of measures $\mathcal{M}(\Sigma, L) = \{(\nu_1, \nu_2)\}$, where each pair (ν_1, ν_2) satisfies the constraints

$$|\nu_1| = 2|\nu_2| = 1, \quad \text{supp } \nu_1 \subset \Sigma, \quad \text{supp } \nu_2 \subset L.$$

For a pair $(\nu_1, \nu_2) \in \mathcal{M}(\Sigma, L)$, we denote by

$$I(\nu_1, \nu_2) = \iint \log \frac{1}{|s - z|} d\nu_1(s) d\nu_2(s)$$

their mutual logarithmic energy and define the *vector energy*

$$E(\nu_1, \nu_2) = I(\nu_1, \nu_1) + I(\nu_2, \nu_2) - I(\nu_1, \nu_2) - \frac{1}{t_0} \int \text{Re}(V(x) - \Psi(x)) d\nu_1(x),$$

where $\Psi(z)$ is an appropriate branch of $\frac{2}{3}(z - t_1)^{3/2}$.

The *vector equilibrium problem* for the pair (Σ, L) and the energy $E(\cdot)$ asks for minimizing this vector energy on $\mathcal{M}(\Sigma, L)$. That is, asks for finding a pair $(\lambda_1, \lambda_2) \in \mathcal{M}(\Sigma, L)$, the so-called *vector equilibrium measure*, satisfying

$$E(\lambda_1, \lambda_2) = \inf_{(\mu_1, \mu_2) \in \mathcal{M}(\Sigma, L)} E(\mu_1, \mu_2).$$

We stress that the vector equilibrium measure (λ_1, λ_2) depends on the pair of contours (Σ, L) . Finally, the *S-property problem* asks for finding a pair of contours (Σ, L) for which the respective vector equilibrium measure (λ_1, λ_2) satisfies the *S-properties*

$$\begin{aligned} \frac{\partial}{\partial n_+} \left(2U^{\lambda_1}(z) - U^{\lambda_2}(z) - \frac{1}{t_0} \text{Re}(V(z) - \Psi(z)) \right) = \\ \frac{\partial}{\partial n_-} \left(2U^{\lambda_1}(z) - U^{\lambda_2}(z) - \frac{1}{t_0} \text{Re}(V(z) - \Psi(z)) \right), \quad z \in \text{supp } \lambda_1 \end{aligned}$$

and

$$\frac{\partial}{\partial n_+} (2U^{\lambda_2}(z) - U^{\lambda_1}(z)) = \frac{\partial}{\partial n_-} (2U^{\lambda_2}(z) - U^{\lambda_1}(z)), \quad z \in \text{supp } \lambda_2,$$

where n_{\pm} are the normal vectors to $\Sigma \cup L$ and U^{λ_j} is defined in (2.8). If the pair (Σ, L) has the S-property as above, we call it a pair of *S-contours*

The S-property has been originally introduced in the context of Padé approximants by H. Stahl [54–56] and further extended by A. Gonchar and E. Rakhmanov [23] to non-hermitian orthogonality with varying weights, see also [8, 10, 31, 38, 44, 48] for a more recent account of results when dealing with non-hermitian orthogonality, and [33–35] for related results in the context of differential equations.

However, the S-property for multiple orthogonality is much less clear. To our knowledge, the cases which have been studied so far are either restricted to multiple orthogonality with fixed (non varying) weights [5] or make strong symmetry assumptions for the weights [4, 12, 13, 15]. For all of those, the S-property followed directly from the symmetry at hand.

In the present setting, given a pair of contours (Σ, L) as above, the vector equilibrium energy exists, is unique and can be further characterized in terms of certain (Euler-Lagrange) variational conditions [9, 29]. However, finding the pair of S-contours is a much more delicate matter. To recover the S-property in our setting, we recall the condition (2.25), which allows us to define the *positive* measure μ_* as in (2.26). From our analysis of the underlying quadratic differential in Section 5, it is possible to construct two contours (Σ, L) such that the respective vector equilibrium measure is of the form (μ_*, λ_*) , where the measure μ_* is the one given by Theorem 2.9. The contour L satisfies the auxiliary condition

$$(\xi_{2+}(z) - \xi_{3+}(z))dz \in i\mathbb{R}, \quad z \in L, \quad (2.46)$$

and the measure λ_* can be constructed from this condition. It then follows that the S-property for this pair of contours (Σ, L) is actually equivalent to the conditions (2.25) and (2.46). Consequently, the measure μ_* can also be interpreted in terms of the S-property above, and conditions (2.25) and (2.46) can be regarded as *algebraic* S-properties. As we will see later, (2.25) and (2.46) also play a fundamental role in the construction of the g-functions used in the forthcoming RH analysis.

2.10. Statement of Results - $t_1 < 0$. As we mentioned in the introduction, after appropriate modifications the results of Sections 2.1–2.9 are also valid for $t_1 \in (-3/4, 0)$, as it is discussed next. Although the proofs of these results for $t_1 < 0$ go very much along the same lines as their respective results for $t_1 > 0$, some technical results collected on the way would have to be proved again taking into account $t_1 < 0$, what would make this already lengthy paper much longer. So for the sake of presentation we decided to not provide proof of these results.

The curve

$$\Gamma_c^- : \quad t_0 = -16s^6 + 6s^4, \quad t_1 = -12s^4 + 6s^2 - \frac{3}{4}, \quad 0 \leq s \leq \frac{1}{2},$$

together with the horizontal and vertical axes determine a bounded domain \mathcal{F}^- on the (t_0, t_1) -plane, see Figure 9. Note in particular that $t_1 < 0$, whenever $(t_0, t_1) \in \mathcal{F}^-$.

When $(t_0, t_1) \in \mathcal{F}^-$, Proposition 2.1 still holds true. That is, the polynomial p still has a smallest positive root, always simple, that we keep denoting by $r =$

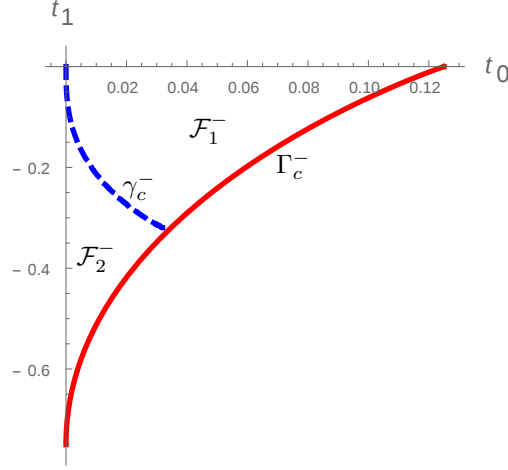


FIGURE 9. Phase diagram for t_1 negative. The dashed curve is γ_c^- , whereas the solid curve is Γ_c^- . The region to the right of γ_c^- is \mathcal{F}_1^- , whereas the region to the left of γ_c^- is \mathcal{F}_2^- .

$r(t_0, t_1)$. The coefficient a_0 in (2.4) is well-defined, but now it becomes negative. Nevertheless, the rational function h in (2.3) is also well-defined, and Theorems 2.2, 2.3 and 2.4 hold true without any modification in their statements. However, we emphasize that the behavior of the roots of p and of the coefficients r and a_0 , as functions of (t_0, t_1) , change when compared to $t_1 > 0$, so all the auxiliary results needed in their proofs have to be modified. We refer the reader to Figure 10 where, for a certain choice of $t_1 < 0$, the evolution in time $t_0 > 0$ of the boundary $\partial\Omega$ is displayed.

The quantities $B = B(t_0, t_1)$, $A = A(t_0, t_1)$, given respectively in equations (2.13) and (2.14), are still meaningful, and so is the spectral curve in (2.12), and Theorem 2.5 also holds true for $(t_0, t_1) \in \mathcal{F}^-$. As for the branch points and critical points of the spectral curve, we have the following result.

Theorem 2.16. *For $(t_0, t_1) \in \mathcal{F}^-$, the spectral curve (2.12) has three simple branch points $z_0, z_1, z_2 \in \mathbb{C}$ with*

$$z_0 \in \mathbb{R}, \quad z_1 \in \mathbb{C}_-, \quad z_2 = \bar{z}_1, \quad z_1, z_2 \in \Omega,$$

and three singular points $\hat{z}_0, \hat{z}_1, \hat{z}_2 \in \mathbb{C} \setminus \bar{\Omega}$ which satisfy

$$\hat{z}_0 \in \mathbb{R}, \quad \hat{z}_1 \in \mathbb{C}_-, \quad \hat{z}_2 = \bar{\hat{z}}_1.$$

Comparing Theorem 2.16 with the three-cut case $(t_0, t_1) \in \mathcal{F}_1$ in Theorem 2.6, the essential difference here is that the point z_0 is not always in the domain Ω . For t_1 negative and small, the three points z_0, z_1 and z_2 are branch points of the Schwarz function ξ_1 of $\partial\Omega$. However, when t_1 decreases (while $t_0 > 0$ is kept fixed), this point z_0 becomes a branch point of the other two solutions ξ_2, ξ_3 of the spectral curve (2.12), but it is not anymore a branch point of ξ_1 . If we keep decreasing t_1 the branch point z_0 might leave the domain Ω , even before t_1 reaches the critical value $-3/4$. This phenomenon is reflected in the mother body measure μ_* , as will be explained in a moment.

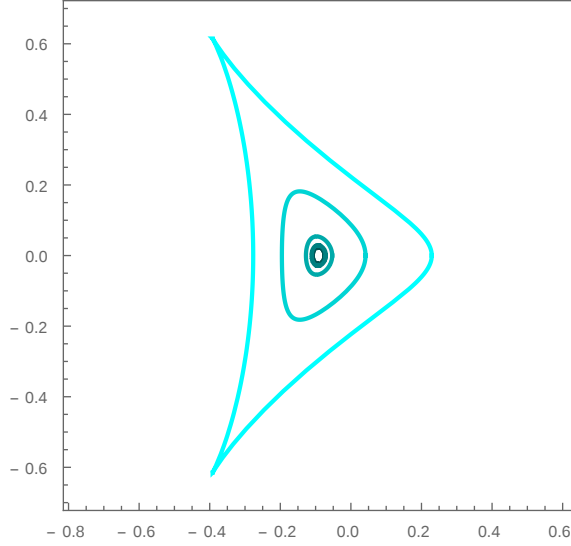


FIGURE 10. The boundary $\partial\Omega$ corresponding to $t_1 = -\frac{1}{10}$ and $t_0 = \frac{1}{2500}, \frac{1}{1700}, \frac{1}{500}, \frac{1}{50}$ and $\frac{35+4\sqrt{30}}{1800}$. (respectively from dark to bright color). For the pair $(t_0, t_1) = (\frac{35+4\sqrt{30}}{1800}, -\frac{1}{10})$, which belongs to the critical curve Γ_c^- , cusps are created at the boundary. Numerical output.

Theorem 2.17. *Suppose $(t_0, t_1) \in \mathcal{F}^-$ and z_0 and z_2 are the branch points given by Theorem 2.16. The implicit equation*

$$\operatorname{Re} \int_{z_0}^{z_2} (\xi_1(s) - \xi_2(s)) ds = 0 \quad (2.47)$$

defines an analytic curve γ_c^- on the (t_0, t_1) -plane, which connects the boundary Γ_c^- to the origin.

A plot of the curve γ_c^- can be seen in Figure 9. This curve determines two regions $\mathcal{F}_1^-, \mathcal{F}_2^- \subset \mathcal{F}^-$, labeled such that \mathcal{F}_1^- (\mathcal{F}_2^-) consists of the points in \mathcal{F}^- that are above (below) γ_c^- .

Proposition 2.7 holds true for $(t_0, t_1) \in \mathcal{F}_-$ without any modification, and Theorem 2.8 assumes the following form.

Theorem 2.18. *On the (r, a_0) -plane, the critical curve Γ_c^- is expressed as*

$$r = s, \quad a_0 = -\frac{1 - 4s^2}{2}, \quad 0 < s < \frac{1}{2},$$

and the curve γ_c^- is implicitly given by

$$(r + w_0^3) [(30a_0^2r^2 + 4a_0^3)w_0^3 + ra_0(r^2(12 - 8a_0) + 10a_0)w_0^2 + 6a_0r^2(5 - r^2)w_0 + 12r^3 + 3r^5] + 3w_0^6r^2(1 - 4a_0^2 - 2r^2) \log \frac{w_0^3}{r} = 0, \quad (2.48)$$

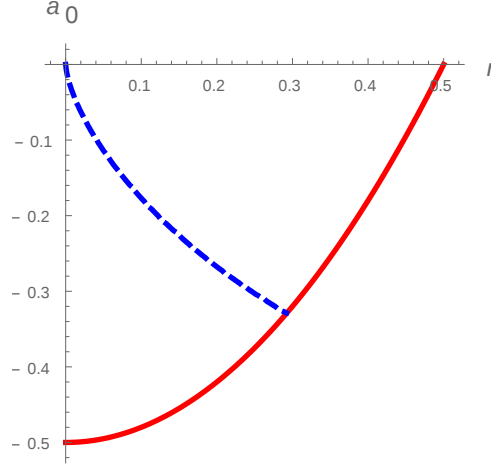


FIGURE 11. Image of the phase diagram in Figure 3 through the change of variables $(t_0, t_1) \mapsto (r, a_0)$. The solid curve is the image of Γ_c^- and the dashed curve is the image of γ_c^- . The region determined by the solid and dashed curves and the r -axis corresponds to \mathcal{F}_1^- , whereas the region between the solid and dashed curves and the a_0 -axis corresponds to \mathcal{F}_2^- .

where $w_0 = w_0(r, a_0)$ is the unique real solution to $h'(w) = 0$.

The critical curves Γ_c^- and γ_c^- on the (r, a_0) -plane are displayed in Figure 11.

The function w_0 is algebraic in r and a_0 , and the presence of the log term in (2.48) indicates that the curve γ_c^- is transcendental. In particular, γ_c^- is not the analytic continuation of γ_c (see also Section 2.11 below). For an indication on how to get (2.47)–(2.48), we refer to Remark A.2.

We are ready to state the result equivalent to Theorem 2.9.

Theorem 2.19. *For $(t_0, t_1) \in \mathcal{F}^-$, there exists a contour $\Sigma_* \subset \Omega$ for which the function ξ_1 in (2.15) admits an analytic continuation to $\mathbb{C} \setminus \Sigma_*$ that satisfies the property*

$$(\xi_{1+}(s) - \xi_{1-}(s))ds \in i\mathbb{R}, \quad z \in \Sigma_*.$$

The contour Σ_* is symmetric with respect to the real axis, and

(i) (Three-cut case) For $(t_0, t_1) \in \mathcal{F}_1^-$, the contour Σ_* decomposes as

$$\Sigma_* = \Sigma_{*,0} \cup \Sigma_{*,1} \cup \Sigma_{*,2},$$

where $\Sigma_{*,l}$ is a smooth oriented contour from a common point $z_* \in (-\infty, z_0)$ to the branch point z_l and

$$\Sigma_{*,0} = [z_*, z_0], \quad (\Sigma_{*,2})^* = \Sigma_{*,1} \subset \overline{\mathbb{C}}_-.$$

(ii) (One-cut case) For $(t_0, t_1) \in \mathcal{F}_1^-$, the contour Σ_* is a single analytic arc which connects the branch points z_1 and z_2 and intersects the real axis at a point $z_* > z_0$.

Furthermore, the measure

$$d\mu_*(z) = \frac{1}{2\pi it_0}(\xi_{1-}(z) - \xi_{1+}(z))dz, \quad z \in \Sigma_*$$

is a probability measure on Σ_* .

The arc Σ_* for various choices of the parameter (t_0, t_1) is displayed in Figure 12.

In the three-cut cases for $(t_0, t_1) \in \mathcal{F}_1$ and $(t_0, t_1) \in \mathcal{F}_1^-$ the geometry of the support Σ_* of μ_* is essentially the same. However, when (t_0, t_1) crosses γ_c^- and we move to the one-cut case for $t_1 < 0$, the part of Σ_* on the real line disappears, and we are only left with a single analytic arc, which is symmetric with respect to the real line. This is in contrast with the one-cut case for $t_1 > 0$, which corresponds to the shrinking of the arc outside the real line and reduction of Σ_* to a real interval.

The point z_* in Theorem 2.19 moves continuously with (t_0, t_1) and it is determined as one of the finitely many real solutions $y = z_*$ to the implicit equation

$$\int_{z_1}^y (\xi_1(s) - \xi_2(s))ds = 0. \quad (2.49)$$

The critical curve γ_c^- is then determined by the condition $z_* = z_0$ (compare (2.49) with (2.47)).

To conclude this section, we remark that Theorem 2.10 also extends to $(t_0, t_1) \in \mathcal{F}^-$ for the respective measure μ_0 and the measure μ_* given by Theorem 2.19.

2.11. Phase transition along the mother body critical curve. As we mentioned above, the critical curves γ_c and γ_c^- are not analytical continuation of each other. More precisely, if we consider them as functions $t_0(t_1)$, then they are both analytic at $t_1 = 0$ and their values and their first two derivatives are equal to 0 at $t_1 = 0$, but their third derivatives at $t_1 = 0$ are different. This can be characterized as a phase transition of the third order. To see this phase transition, let us evaluate the asymptotic behavior of the function $t_0(t_1)$ as $t_1 \rightarrow +0$ and $t_1 \rightarrow -0$.

We start with γ_c . When we approach the origin, we take into account the leading terms in (2.18) in order to get

$$t_0 = s^6(1 + \mathcal{O}(s^4)), \quad t_1 = \frac{3}{8}s^2(1 + \mathcal{O}(s^2)), \quad \text{as } s \rightarrow 0.$$

Hence we have the approximation

$$t_0 = \frac{8}{27}t_1^3(1 + \mathcal{O}(t_1)), \quad (2.50)$$

as we approach the origin along γ_c , where the implicit term is analytic in t_1 .

The similar analysis for γ_c^- is more involved. The relation $h'(w_0) = 0$ gives us that

$$a_0 = \frac{w_0^3 - 2r}{w_0}. \quad (2.51)$$

Replacing this expression into (2.48) we arrive at

$$\begin{aligned} (r + w_0^3) & (-24r^3 + 2r^5 + 36r^4w_0 + (10r^4 + 22r^2)w_0^3 \\ & - 48r^3w_0^4 - (4r^3 + r)w_0^6 + 15r^2w_0^7 + w_0^9) \\ & - 6r^2w_0^4(4r^2 + (2r^2 - 1)w_0^2 - 4rw_0^3 + w_0^6) \log \frac{w_0^3}{r} = 0. \end{aligned} \quad (2.52)$$

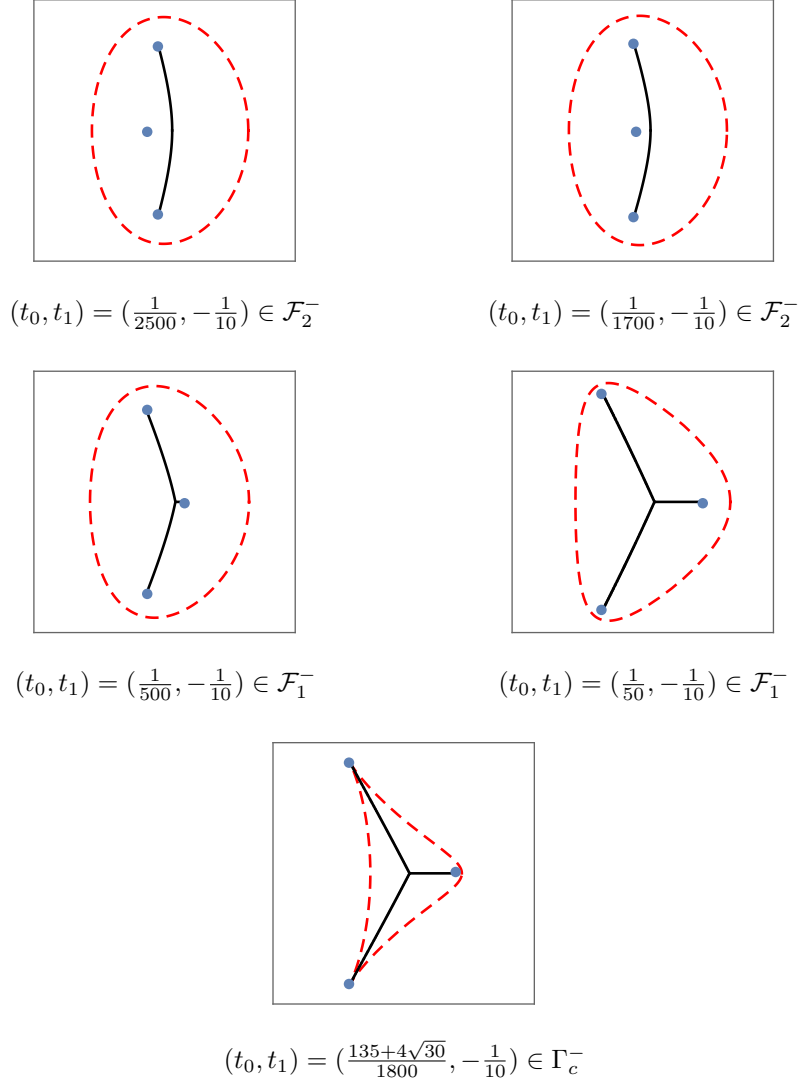


FIGURE 12. For the given values of (t_0, t_1) , the boundary $\partial\Omega$ (dashed contour), the support of the mother body measure μ_* (solid lines) and the branch points z_0, z_1, z_2 (dots) are shown (the figures are scaled differently - compare with Figure 4). Note the transition when we move from \mathcal{F}_2^- to \mathcal{F}_1^- . We stress that the contours of $\text{supp } \mu_*$ outside the real line are not straight line segments. Numerical outputs.

We now make the ansatz, to be verified in a moment, that w_0 can be expressed as

$$w_0 = (Cr)^{1/3} \quad (2.53)$$

along γ_c^- , where $C = C(r)$ is a positive function, to be determined later, which remains bounded away from 0 and ∞ when $r \rightarrow 0$. Using the change of variables (2.53) in (2.52), we get

$$\begin{aligned}
& r^4(1+C)(-24+22C-C^2+C^3+(2+10C-4C^2)r^2 \\
& \quad +C^{1/3}(36-48C+15C^2)r^{4/3}) \\
& \quad +r^4(6C^2-C^{1/3}(24C-24C^2+6C^3)r^{4/3}-12C^2r^2)\log C=0,
\end{aligned}$$

that is, $C = C(r)$ should satisfy

$$(1+C)(-24+22C-C^2+C^3)+6C^2\log C=-Q(r,C(r)) \quad (2.54)$$

where

$$\begin{aligned}
Q(r,c) &:= (2+10c-4c^2)r^2+c^{1/3}(36-48c+15c^2)r^{4/3} \\
&\quad -\left(c^{1/3}(24c-24c^2+6c^3)r^{4/3}+12c^2r^2\right)\log C
\end{aligned}$$

A simple application of the Implicit Function Theorem tells us that there exists a function $C = C(r)$ satisfying (2.54). Consequently, we get that along γ_c^- , we can express w_0 as a function of r as in (2.53). Furthermore, when $r \rightarrow 0$ it is easily seen that $Q(r,c) \rightarrow 0$, thus the constant $C_0 = C(0)$ solves

$$(1+C_0)(-24+22C_0-C_0^2+C_0^3)+6C_0^2\log C_0=0.$$

Numerically, we see that

$$C_0 = 1.075\dots \quad (2.55)$$

Hence, in virtue of (2.53) and (2.51) we get the first order approximation

$$w_0 = C_0^{1/3}r^{1/3}(1+\mathcal{O}(r)), \quad a_0 = \frac{(C_0-2)}{2C_0^{1/3}}r^{2/3}(1+\mathcal{O}(r)), \quad (2.56)$$

valid as $r \rightarrow 0$ along γ_c^- , and where the implicit terms are analytic in r . By (2.19)–(2.20), we know that

$$\begin{aligned}
t_0 &= -2r^4 + r^2 - \frac{(C_0-2)^2}{C_0^{2/3}}r^{10/3}(1+\mathcal{O}(r)) = r^2(1+\mathcal{O}(r)), \\
t_1 &= a_0(1-a_0-4r^2) = \frac{(C_0-2)}{2C_0^{1/3}}r^{2/3}(1+\mathcal{O}(r)),
\end{aligned}$$

so by the second equation in (2.56) we get the first order approximation

$$t_0 = \frac{8C_0}{(C_0-2)^3}t_1^3(1+\mathcal{O}(t_1)), \quad (2.57)$$

as $(t_0, t_1) \rightarrow (0, 0)$ along γ_c^- , and the implicit term is analytic in t_1 . Using (2.55) we also get

$$\frac{8}{27} < \left| \frac{8C_0}{(C_0-2)^3} \right|.$$

Thus, comparing (2.50) with (2.57), we see that the tangent vector and the curvature of γ_c and γ_c^- coincide at the origin, but the derivative of their curvatures do not coincide. In the terminology of statistical mechanics, the origin $(t_0, t_1) = (0, 0)$ determines a third order phase transition along the critical curve $\gamma_c \cup \gamma_c^-$.

2.12. Setup for the remainder of the paper. The rest of the paper is organized as follows.

In Section 3 we derive several technical results on the functions r and a_0 , which are extensively used in the rest of the paper. Propositions 2.1 and 2.7 and Theorems 2.2, 2.5 and 2.8 are proved in Section 3.

In Section 4 we study the spectral curve (2.12) and construct its associated Riemann surface \mathcal{R} as a three-sheeted cover of the complex plane. This sheet structure depends on whether we are in the three-cut (Section 4.3.1) or one-cut (Section 4.3.2) cases. Along the way, we also prove Theorem 2.6 in Section 4.

In Section 5 we introduce the quadratic differential ϖ on the Riemann surface \mathcal{R} (which was already mentioned after Theorem 2.9), and describe its critical graph. Using its critical graph, in Section 6 we prove Theorems 2.3, 2.4, 2.9 and 2.10.

In Sections 7 and 8 we carry out the asymptotic analysis of the Riemann-Hilbert problem characterizing the multiple orthogonal polynomial $P_{n,n}$ in Proposition 2.13, in the three-cut and one-cut cases, respectively. This analysis also heavily relies on the critical graph of the quadratic differential ϖ . The final ingredient in the analysis of this Riemann-Hilbert problem is the so-called global parametrix, whose construction is provided in Section 7.6.

In Section 10 we use the outcome of the asymptotic analysis in order to prove Theorems 2.14 and 2.15.

Finally, in the Appendix A we study the width parameters used in Section 5 to perform the deformation of the critical graph of ϖ .

3. LIMITING BOUNDARY OF EIGENVALUES. PROOFS OF PROPOSITIONS 2.1 AND 2.7 AND THEOREMS 2.2, 2.5 AND 2.8

In order to prove the main results of this section we need some technical lemmas, which are also used in the next sections.

3.1. Proof of Proposition 2.1. It is convenient to change variables for the polynomial p in (2.5) and instead consider

$$\begin{aligned} \tilde{p}(x) = p(\sqrt{x}) = & 128x^5 - 124x^4 + (-16t_1 + 64t_0 + 36)x^3 \\ & + (16t_1^2 + 8t_1 - 28t_0 - 3)x^2 + t_0(2 - 8t_1)x + t_0^2. \end{aligned} \quad (3.1)$$

With the help of Mathematica, the discriminant of \tilde{p} with respect to x is computed

$$\text{Discr}(\tilde{p}; x) = 16384 t_0^2 p_1(t_0)p_2(t_0)p_3(t_0), \quad (3.2)$$

where

$$\begin{aligned} p_1(s) &= 8192s^3 + 192(64t_1 - 7)s^2 - 48(1 - 4t_1)^2s + (108t_1 - 11)(4t_1 - 1)^3 \\ p_2(s) &= 1728s^2 - 432(1 + 4t_1)s + (3 + 4t_1)^2(3 + 16t_1), \\ p_3(s) &= (8s - 8t_1 - 1)^2. \end{aligned} \quad (3.3)$$

Lemma 3.1. *For $t_1 > 0$, the polynomials p_2, p_3 in (3.3) do not have zeros on $(0, 1/8)$.*

Proof. The discriminant of p_2 in s is

$$-1769472 t_1^3,$$

which is clearly negative for $t_1 > 0$, and hence p_2 does not have real zeros. The Lemma for p_3 follows trivially from the inequality

$$8s - 8t_1 - 1 < -8t_1 < 0,$$

which is valid if $0 < s < 1/8$. \square

Lemma 3.2. *The three roots $s_1, s_2, t_{0,crit}$ of the polynomial p_1 in (3.3) satisfy*

$$s_1 < 0 < s_2 < t_{0,crit}, \quad 0 < t_1 < \frac{11}{108}; \quad (3.4)$$

$$s_1 < s_2 = 0 < t_{0,crit}, \quad t_1 = \frac{11}{108}; \quad (3.5)$$

$$s_1 \leq s_2 < 0 < t_{0,crit}, \quad \frac{11}{108} < t_1 < \frac{1}{4}; \quad \text{and } s_1 = s_2 \text{ only for } t_1 = \frac{1}{8} \quad (3.6)$$

Moreover, the function

$$t_1 \mapsto t_{0,crit} = t_{0,crit}(t_1), \quad 0 < t_1 < 1/4,$$

is decreasing and

$$t_{0,crit}(0) = 1/8, \quad t_{0,crit}(1/4) = 0. \quad (3.7)$$

Finally, the curve Γ_c in (2.6) is parameterized by $(t_{0,crit}, t_1)$, that is,

$$\Gamma_c : (t_0, t_1) = (t_{0,crit}(t_1), t_1), \quad 0 < t_1 < \frac{1}{4}. \quad (3.8)$$

Proof. For a positive constant c , the discriminant of p_1 (with respect to s) is given by

$$\text{Discr}(p_1; s) = c t_1^3 (1 - 8t_1)^2 (1 - 4t_1)^3.$$

In particular, $\text{Discr}(p_1; s) \geq 0$ for $0 < t_1 < 1/4$, so p_1 has always three real roots for $0 < t_1 < 1/4$, and these are all distinct if $t_1 \neq 1/8$. For $t_1 = 1/8$, p_1 simply factors as

$$p_1(s) = \frac{1}{12} (1 + 32s)^2 (128s - 5), \quad (3.9)$$

so the largest positive root $t_{0,crit}$ of p_1 is always simple if $0 < t_1 < 1/4$, and also $s_1 = s_2 = -\frac{1}{32} < 0$ for $t_1 = 1/8$. Evaluating explicitly,

$$p_1(0) = (1 - 4t_1)^3 (11 - 108t_1),$$

which means that $p_1(0) < 0$ for $t_1 < \frac{11}{108}$, and $p_1(0) \geq 0$ otherwise. Therefore, combining continuity and what we already have, we get the inequalities claimed in (3.4)–(3.6).

We now verify that $t_{0,crit} < 1/8$. For $t_1 \in (11/108, 1/4)$, the value $t_{0,crit}$ is the unique positive root of p_1 . Since also

$$p_1(1/8) = 64t_1^2 (108t_1^2 - 92t_1 + 27) > 0, \quad 0 < t_1 < \frac{1}{4},$$

and the leading coefficient of p_1 is positive, we use continuity to conclude that the inequality $t_{0,crit} < 1/8$ always holds true.

The derivative of $t_{0,crit}$ is computed via the chain rule,

$$\frac{\partial}{\partial t_1} t_{0,crit} = -\frac{\frac{\partial p_1}{\partial t_1}}{\frac{\partial p_1}{\partial s}}. \quad (3.10)$$

Since $t_{0,crit}$ is the largest root of p_1 ,

$$\frac{\partial p_1}{\partial s}(t_{0,crit}) > 0, \quad 0 < t_1 < \frac{1}{4}. \quad (3.11)$$

The derivative of p_1 with respect to t_1 is explicitly computed to be

$$\frac{\partial p_1}{\partial t_1}(s) = 48(256s^2 + s(8 - 32t_1) - (1 - 4t_1)^2(5 - 36t_1)).$$

For $t_1 = 1/8$, (3.9) gives

$$t_{0,crit} = \frac{5}{128}, \quad \left. \frac{\partial p_1}{\partial t_1}(t_{0,crit}) \right|_{t_1=1/8} = \frac{81}{24}. \quad (3.12)$$

We claim that $\frac{\partial p_1}{\partial t_1}(t_{0,crit})$ is never zero. To the contrary, the discriminant $\text{Discr}(p_1; t_1)$ with respect to t_1 would be zero, and it is thus enough to show that $\text{Discr}(p_1; t_1)$ is different from zero. For a positive constant c ,

$$\text{Discr}(p_1; t_1) = c s^2(8s - 1)^3(1 + 32s)^2;$$

and since $t_{0,crit} < 1/8$ we conclude

$$\left. \text{Discr}(p_1; t_1) \right|_{s=t_{0,crit}} \neq 0,$$

so $\frac{\partial p_1}{\partial t_1}(t_{0,crit})$ is never zero for $0 < t_1 < 1/4$. From (3.12) and continuity,

$$\frac{\partial p_1}{\partial t_1}(t_{0,crit}) > 0, \quad 0 < t_1 < \frac{1}{4}.$$

Combining this last equation with (3.10) and (3.11), we finally get that $t_{0,crit}$ is a decreasing function of t_1 .

The limits (3.7) now follow directly from a combination of (3.4)–(3.6) and the explicitly expressions

$$p_1(s) \Big|_{t_1=0} = (1 - 8s)^2(11 + 128s), \quad p_1(s) \Big|_{t_1=1/4} = 64s^2(27 + 128s).$$

To conclude, we prove (3.8). Plugging the parametrization (2.6) into the definition of p_1 , one can easily verify

$$p_1(t_0) = 0, \quad (t_0, t_1) \in \Gamma_c,$$

so t_0 is always a root of p_1 if $(t_0, t_1) \in \Gamma_c$. For $s = 1/4$ in (2.6), we compute explicitly $(t_0, t_1) = (5/128, 1/8) = (t_{0,crit}, t_1)$, hence Γ_c intersects $(t_0, t_{0,crit})$ at $(5/128, 1/8)$. Since $t_{0,crit}$ is always a simple root and the pair $(t_0, t_1) \in \Gamma_c$ must always give rise to a root of p_1 , by continuity we conclude (3.8) \square

As a consequence of Lemma 3.2, the parameter region \mathcal{F} is alternatively described as

$$\mathcal{F} = \{(t_0, t_1) \mid 0 < t_1 < 1/4, \quad 0 < t_0 < t_{0,crit}(t_1)\}.$$

Lemma 3.3. *For $(t_0, t_1) \in \mathcal{F} \cup \Gamma_c$, $t_1 \neq 0, 1/4$, the polynomial \tilde{p} in (3.2) never has a triple root.*

Proof. If \tilde{p} has a triple root, then $\tilde{p}, \tilde{p}', \tilde{p}''$ share a common root, say x_0 . This means that $t_0 \mapsto \tilde{p}(x_0), \tilde{p}'(x_0), \tilde{p}''(x_0)$ all share a common root. We compute two of their

resultants with the help of Mathematica. Their full expressions are rather long, but we exhibit their first coefficients,

$$\text{Resultant}(p(x), p''(x); t_0) = -44040192 x^7 + 56033280 x^6 + \dots,$$

$$\text{Resultant}(p'(x), p''(x); t_0) = 245760 x^5 - 202752 x^4 + \dots,$$

and since $t_0 \mapsto \tilde{p}(x_0), \tilde{p}'(x_0), \tilde{p}''(x_0)$ all share a common root,

$$\text{Resultant}(p'(x_0), p''(x_0); t_0) = 0 = \text{Resultant}(p(x_0), p''(x_0); t_0)$$

We now see $\text{Resultant}(p(x), p''(x); t_0), \text{Resultant}(p'(x), p''(x); t_0)$ as functions of x . The equation above says that these polynomials share a common root x_0 , so their resultant with respect to x must be zero. Again with the help of Mathematica, we compute their resultant with respect to x to get

$$-c t_1^6 (1 + t_1)^3 (1 - 4t_1)^4 (3 + 4t_1)^3 (27 + 4t_1)^2 (775 + 864t_1 + 13824t_1^2)^2$$

for some large positive constant c . It is then not hard to see that this last expression is never zero for $0 < t_1 < 1/4$, and the Lemma follows. \square

Lemma 3.4. *For $(t_0, t_1) \in \mathcal{F}$, the polynomial \tilde{p} defined in (3.2) has a smallest positive root \tilde{r} , which is simple. When $(t_0, t_1) \rightarrow \Gamma_c$, \tilde{r} becomes a root of higher multiplicity, given explicitly as $\tilde{r} = s^2$, where s is the parameter on (2.6).*

Proof. When $t_0 \rightarrow 0$, the polynomial \tilde{p} factors into

$$\tilde{p}(x) = x^2 q(x), \quad q(x) := 128x^3 - 124x^2 + (36 - 16t_1)x + 16t_1^2 + 8t_1 - 3. \quad (3.13)$$

The discriminant and value at $x = 0$ of q are respectively given by

$$\text{Discr}(q; x) = -1024(1 + 8t_1)^2(3 + 16t_1)(108t_1 - 11), \quad (3.14)$$

$$q(0)|_{t_0=0} = 16t_1^2 + 8t_1 - 3 < 0, \quad 0 < t_1 < \frac{1}{4} \quad (3.15)$$

For the sake of clarity, we split the rest of the proof into three parts, the last of those being a limiting case of the others.

1st Case: $0 < t_1 < \frac{11}{108}$.

In this case, the discriminant (3.14) is positive, so q has three real roots. For $t_1 = 1/16$, these are given by

$$\left\{ \frac{3}{8}, \frac{1}{64}(19 - 3\sqrt{17}), \frac{1}{64}(19 + 3\sqrt{17}) \right\},$$

so in particular they are all positive. Since $q(0)$ is never zero, see (3.15), we conclude that these three roots are all positive for any choice $t_1 \in (0, 11/108)$. This is the same as saying that in the present situation and $t_0 = 0$, the polynomial \tilde{p} has a double root $x_1 = \tilde{r} = 0$ and three simple positive roots $x_2 < x_3 < x_4$.

Recall that s_2 is a root of p_1 as in Lemma (3.2). For $0 < t_0 < s_2$, a combination of Equation (3.2), Lemma 3.1 and Equation (3.4) assures \tilde{p} has only simple roots. By continuity from t_0 and the further observations $\tilde{p}(0) = t_0^2 > 0$ and $\tilde{p}(x) < 0$ when $x \rightarrow -\infty$, we learn that for $0 < t_0 < s_2$, the double root of \tilde{p} at $x = 0$ splits into two simple roots $x_1 < 0 < \tilde{r}$ and the remaining roots still satisfy $\tilde{r} < x_2 < x_3 < x_4$.

We now approach $t_0 \nearrow s_2$. In this situation, two roots of \tilde{p} collide, because p_1 - hence $\text{Discr}(\tilde{p}; x)$, see (3.2) - is zero for $t_0 = s_2$. For $t_1 = 1/16$, $t_0 = s_2$, the roots of \tilde{p} are computed numerically

$$s_2 = 0.0512061, \quad \{x_1, \tilde{r}, x_2, x_3, x_4\} \approx \{-0.0169, 0.0607, 0.1235, 0.4007, 0.4007\},$$

so in this case $x_3 = x_4$ and \tilde{r} is a simple root. By continuity and Lemma 3.3, we conclude $x_3 = x_4$ whenever $t_0 = s_2$, and hence \tilde{r} is always a simple root for $t_0 \leq s_2$. Again by Equation (3.2), Lemma 3.1 and Equation (3.4), we know that \tilde{p} does not have multiple roots for $s_2 < t_0 < t_{0,crit}$, and we finally conclude that \tilde{r} is always a simple root in the present case.

2nd Case: $\frac{11}{108} < t_1 < \frac{1}{4}$.

This case is somewhat simpler than the previous one. In the present case, the discriminant (3.14) is negative, so q has one real root and two non real roots. From (3.15) we see that this real root is positive. Similarly as before, it means \tilde{p} has a double root $\tilde{r} = x_1 = 0$, and simple roots $x_2 > 0$, $x_3, x_4 \in \mathbb{C} \setminus \mathbb{R}$.

As before, we compute $p(0) = t_0^2$, $\tilde{p}(x) < 0$ for $x \rightarrow -\infty$ and conclude that for $t_0 > 0$ and small, the double root splits into two simple roots $x_1 < 0 < \tilde{r}$ and the remaining roots still satisfy $x_2 > 0$, $x_3, x_4 \in \mathbb{C} \setminus \mathbb{R}$.

From Equation (3.2), Lemma 3.1 and Equation (3.4) we know \tilde{p} has no multiple roots for $0 < t_0 < t_{0,crit}$, so we conclude the smallest positive root \tilde{r} is always simple.

3rd Case: $t_1 = \frac{11}{108}$.

In this case the polynomial q simply factors as

$$q(x) = \frac{4}{729}(9x - 4)^2(288x - 23),$$

and it clearly has three positive roots. The rest follows the same lines as 2nd Case.

In either of the cases above, we consider the limit $(t_0, t_1) \rightarrow (t_{0,crit}, t_1) \in \Gamma_c$ and plug the parametrization (2.6) into the expression for \tilde{p} in (3.1), arriving at

$$\tilde{p}(x) = 4(s^2 - x)^2 (32x^3 + (64s^2 - 31)x^2 + (48s^3 - 50s^2 + 8) + 9s^4 - 12s^3 + 4s^2),$$

so s^2 is a root of \tilde{p} for $(t_0, t_1) \in \Gamma_c$. The discriminant (in x) of the polynomial inside brackets above is

$$144(1 - 2s)^3(2 - 3s)^2(8s^2 - 4s - 1)(64s^2 + 35s + 7) < 0, \quad 0 < s < 1/4,$$

so that polynomial has only one real root. Its value at $x = 0$ is $9s^4 - 12s^3 + 4s^2 > 0$, hence this root is negative.

Comparing to what we proved before, it means that for $(t_0, t_1) \in \Gamma_c$, the root \tilde{r} collides with the root x_2 , becoming the double root $\tilde{r} = s^2$, as we want. \square

Lemma 3.5. *The function*

$$t_1 \mapsto \tilde{r} = \tilde{r}(t_0, t_1), \quad (t_0, t_1) \in \mathcal{F},$$

is increasing and satisfies the inequalities

$$\tilde{r} < \frac{1}{4}, \tag{3.16}$$

$$4t_1 < (1 - 4\tilde{r})^2. \tag{3.17}$$

Proof. The chain rule tells us

$$\frac{\partial}{\partial t_1} \tilde{r} = -\frac{\frac{\partial \tilde{p}}{\partial t_1}}{\frac{\partial \tilde{p}}{\partial x}}. \tag{3.18}$$

As it followed from the calculations in the proof of Lemma 3.4, \tilde{r} is the second smallest real root of \tilde{p} , hence

$$\frac{\partial \tilde{p}}{\partial x}(\tilde{r}) < 0. \quad (3.19)$$

Moreover,

$$\frac{\partial \tilde{p}}{\partial t_1} = -8x(2x^2 - (4t_1 + 1)x + t_0).$$

For $t_1 = 1/8$, $t_0 = 1/32 < t_{0,crit} = 5/128$, we compute

$$\tilde{r} \approx 0.040736, \quad \frac{\partial \tilde{p}}{\partial t_1}(\tilde{r}) \approx 0.00864782 > 0,$$

thus the monotonicity follows from (3.18), (3.19) and the previous inequality once we prove that $\frac{\partial \tilde{p}}{\partial t_1}(\tilde{r})$ is never zero.

If $\frac{\partial \tilde{p}}{\partial t_1}(\tilde{r})$ were zero, then the polynomials \tilde{p} , $\frac{\partial \tilde{p}}{\partial t_1}$ would share a zero, hence their resultant with respect to x would be zero. But

$$\text{Resultant}\left(\tilde{p}, \frac{\partial \tilde{p}}{\partial t_1}(\tilde{r}); x\right) = c t_1^2 t_0^4 (1 + 8t_1 - 8t_0)^2,$$

and this last expression is never zero for $0 < t_1 < 1/4$, $0 < t_0 < t_{0,crit} < 1/8$.

We now prove (3.16). In the proof of Lemma 3.4, we already observed that $\tilde{r} \rightarrow 0$ when $t_0 \rightarrow 0$, see (3.13). In particular (3.16) is valid for t_0 very small. In addition

$$\tilde{p}(1/4) = \frac{1}{64}(1 + 8t_1 - 8t_0)^2 \neq 0,$$

because $0 < t_1 < 1/4$, $0 < t_0 < t_{0,crit} < 1/8$, implying that $\tilde{r} \neq 1/4$. By continuity from the case $t_0 = 0$, we get (3.16).

For (3.17), define

$$f(x) := (1 - 4x)^2 - 4t_1, \quad x \in \mathbb{C}.$$

We want to prove that $f(\tilde{r}) > 0$. Using (3.16) and the monotonicity of \tilde{r}

$$\frac{\partial}{\partial t_1}(f(\tilde{r})) = -8(1 - 4\tilde{r}) \frac{\partial \tilde{r}}{\partial t_1} - 4 < 0,$$

hence $t_1 \mapsto f(\tilde{r})$ is decreasing, so it is enough to prove $f(\tilde{r}) \geq 0$ for $(t_0, t_1) \in \Gamma_c$. But for this choice, we know that $\tilde{r} = s^2$, where s is the parameter in (2.6), and in this case

$$f(\tilde{r}) = 4s^2(1 - 2s^2)^2 > 0, \quad (t_0, t_1) \in \Gamma_c, \quad t_1 \neq 0, 1/4,$$

as desired. \square

As a consequence of Lemmas 3.4 and 3.5, we get the following refinement of Proposition 2.1.

Theorem 3.6. *For $(t_0, t_1) \in \mathcal{F}$, the polynomial p in (2.5) has a smallest positive root r . The function $t_1 \mapsto r$ is increasing and satisfies*

$$0 < r < \frac{1}{2}, \quad 4t_1 < (1 - 4r^2)^2, \quad (t_0, t_1) \in \mathcal{F}. \quad (3.20)$$

In the limit $(t_0, t_1) \rightarrow (t_{0,crit}, t_1) \in \Gamma_c$, r becomes a root of higher multiplicity of p , explicitly given as $r = s$, where s is the parameter in (2.6).

Still for $(t_0, t_1) \in \mathcal{F}$, the quantity $a_0 = a_0(t_0, t_1)$ in (2.4) is well defined and positive, and the function $t_1 \mapsto a_0$ is increasing.

Finally, for $(t_0, t_1) \in \mathcal{F}$, it is valid

$$0 < 2a_0 + 2r < 1, \quad (3.21)$$

and the equality

$$2a_0 + 2r = 1 \quad (3.22)$$

is attained when $(t_0, t_1) \in \Gamma_c$.

Proof. The first two claims about r follow directly as a consequence of Lemmas 3.4 and 3.5, having in mind the identification (3.1).

The positivity of a_0 follows directly from (2.4) and (3.20).

Simple computations show that a_0 is the smallest root of

$$q(x) := x^2 + x(4r^2 - 1) + t_1.$$

This implies

$$\frac{\partial a_0}{\partial t_1} = -\frac{\frac{\partial q}{\partial t_1}}{\frac{\partial q}{\partial x}} = -\frac{8a_0r \frac{\partial r}{\partial t_1} + 1}{\frac{\partial q}{\partial x}(a_0)}.$$

Note that the discriminant of q is given by $(1 - 4r^2)^2 - 4t_1$, which is strictly positive due to (3.20). So a_0 is always a simple root, and since it is the smallest one,

$$\frac{\partial q}{\partial x}(a_0) < 0.$$

Moreover, since $t_1 \mapsto r$ is increasing by Theorem 3.6, we also know that $\frac{\partial r}{\partial t_1} > 0$. Recalling that we already proved $a_0 > 0$, we conclude from the last two equations

$$\frac{\partial a_0}{\partial t_1} > 0,$$

so $t_1 \mapsto a_0$ is indeed increasing.

The positivity of $2a_0 + 2r$ is trivial since both a_0, r are positive for $(t_0, t_1) \in \mathcal{F}$. From the monotonicity of r and a_0 , it is enough to prove (3.22) in order to conclude (3.21). But (3.22) follows immediately from the definition of a_0 in (2.4), Equation (2.6) and the value $r = s$ given by Theorem 3.6. \square

3.2. Proofs of Theorems 2.2, 2.5 and 2.8 and Proposition 2.7. We proceed to the analysis of the rational function h given in (2.3).

Denote by

$$R_0 = R_0(h) = \sup\{|w| \mid h'(w) = 0\},$$

the *critical radius* of h . The relevance of R_0 comes from the fact that the rational function h is injective on $\mathbb{C} \setminus \overline{D}_{R_0}$, where D_R denotes the open disc centered at 0 and radius R .

Lemma 3.7. *For the rational function h in (2.3) and $(t_0, t_1) \in \mathcal{F}$, the inequality $R_0 < 1$ holds true.*

Proof. Note that

$$h'(w) = r - \frac{2a_0r}{w^2} - \frac{2r^2}{w^3},$$

so the zeros of h' are solutions to the equation

$$w^3 - 2a_0w - 2r = 0.$$

Using (3.21), we get

$$|(w^3 - 2a_0w - 2r) - w^3| \leq 2a_0 + 2r < 1 = |w^3|, \quad w \in \partial\mathbb{D}.$$

By Rouché's Theorem we conclude that all the roots of h' are on \mathbb{D} . \square

Corollary 3.8. *For $(t_0, t_1) \in \mathcal{F}$, h is a biholomorphism from $\overline{\mathbb{C}} \setminus \overline{\mathbb{D}}$ to $h(\overline{\mathbb{C}} \setminus \overline{\mathbb{D}})$.*

Proof. From Lemma 3.7, we know that $R_0 < 1$. In particular $\overline{\mathbb{C}} \setminus \overline{\mathbb{D}} \subset \overline{\mathbb{C}} \setminus \overline{D}_{R_0}$, and the result follows. \square

As a consequence of Corollary 3.8, the set $h(\partial\mathbb{D})$ is an analytic closed curve that splits $\overline{\mathbb{C}}$ into two simply connected domains; only one of which is bounded and henceforth denoted by Ω .

Proof of Theorem 2.5. A straightforward computation shows that

$$F(h(w^{-1}), h(w)) = 0, \quad w \in \mathbb{C},$$

where F is as in (2.12). For a rational function $\chi = \frac{\chi_1}{\chi_2}$, its *degree* is defined as

$$\deg \chi = \max\{\deg \chi_1, \deg \chi_2\}.$$

Since

$$\max\{\deg_{\xi} F, \deg_z F\} = 3 = \max\{\deg h(w), \deg h(w^{-1})\},$$

it follows from [52, Theorem 4.21] that $(h(w^{-1}), h(w))$ is a proper parametrization.

From Corollary 3.8 we know that h maps $V := \overline{\mathbb{C}} \setminus \overline{D}_{R_0}$ biholomorphically to an open simply connected set $G \subset \overline{\mathbb{C}}$ with $(\overline{\mathbb{C}} \setminus \Omega) \subset G$. This means that h admits a meromorphic inverse $g : G \rightarrow V$, so that

$$h(g(z)) = z, \quad z \in G. \quad (3.23)$$

From its definition, it follows that g maps $\partial\Omega$ to $\partial\mathbb{D}$, and we conclude

$$\overline{g(z)} = \frac{1}{g(z)}, \quad z \in \partial\Omega. \quad (3.24)$$

Furthermore,

$$F(h(1/g(z)), h(g(z))) = 0,$$

so that the meromorphic function

$$S(z) = h\left(\frac{1}{g(z)}\right), \quad z \in G, \quad (3.25)$$

is a solution to the algebraic equation (2.12). Since ξ_1 is the only solution in (2.15) that is not branched at ∞ , we conclude that S has to be a meromorphic continuation of ξ_1 to the neighborhood G of $\overline{\mathbb{C}} \setminus \Omega$. Thus using the fact that h has real coefficients and (3.23)–(3.24)

$$\bar{z} = \overline{h(g(z))} = h(\overline{g(z)}) = h\left(\frac{1}{g(z)}\right) = S(z), \quad z \in \partial\Omega,$$

which shows that the meromorphic continuation S of ξ_1 is the Schwarz function of $\partial\Omega$. \square

Corollary 3.9. *The Riemann surface \mathcal{R} defined by (2.12) has genus 0.*

Proof. From Theorem 2.5, we learn the rational parametrization h defines a biholomorphism between \mathcal{R} and $\overline{\mathbb{C}}$. Since the genus of $\overline{\mathbb{C}}$ is 0, the same holds true for \mathcal{R} [52, pg. 90, Remark (2)]. \square

Proof of Theorem 2.2. After Corollary 3.8, it only remains to compute the area and harmonic moments (2.7). The computations are very much the same as in [15, pg. 1290]. We include them here for completeness.

Using Green's formula on Ω ,

$$2i \operatorname{Area}(\Omega) = 2i \iint_{\Omega} dA(z) = \int_{\partial\Omega} \bar{z} dz. \quad (3.26)$$

By (2.17),

$$2i \operatorname{Area}(\Omega) = \int_{\partial\Omega} \xi_1(z) dz.$$

We now deform the above integral to $z = \infty$ and use the expansion (2.15) and the Residues Theorem to get that this last integral is equal to $2\pi i t_0$.

Having in mind the identity

$$\frac{1}{2\pi i} \int_{\partial\Omega} \frac{\bar{z}}{(z - z_0)^k} dz = \frac{1}{2\pi i} \int_{\partial\Omega} \frac{\xi_1(z)}{(z - z_0)^k} dz,$$

the equalities in (2.7) follow in a similar fashion. \square

Proof of Proposition 2.7. Equation (2.20) follows directly from identity (2.4). In fact, it was already used in the proof of Theorem 3.6.

Recall Equation (3.26),

$$2\pi i t_0 = 2i \operatorname{Area}(\Omega) = \int_{\partial\Omega} \bar{z} dz.$$

We now change coordinates $z = h(w)$ in the integral above, and the formula becomes

$$\begin{aligned} 2\pi i t_0 &= \int_{\partial\mathbb{D}} \overline{h(w)} h'(w) dw \\ &= \int_{\partial\mathbb{D}} h(\bar{w}) h'(w) dw \\ &= \int_{\partial\mathbb{D}} h(w^{-1}) h'(w) dw \end{aligned}$$

Expanding the integrand $h(w^{-1}) h'(w)$ and using Residues Theorem, we get

$$2\pi i t_0 = 2\pi i \operatorname{Res}(h(w^{-1}) h'(w), w = 0) = 2\pi i (-4a_0^2 r^2 - 2r^4 + r^2),$$

which is equivalent to (2.19) \square

Recall the curve γ_c splitting our phase diagram \mathcal{F} into two parts $\mathcal{F}_1, \mathcal{F}_2$, see (2.18). Lemma 3.7 assures us the critical points of h are on the unit disc, but it is important for later to have a better control on the position of these points, as it is stated in the next two lemmas.

Lemma 3.10. *The zeros w_0, w_1, w_2 of the function h' satisfy*

- For $(t_0, t_1) \in \mathcal{F}_1$,

$$w_0 \in (0, 1), \quad \bar{w}_2 = w_1, \quad w_1 \in \mathbb{D} \setminus \mathbb{R}.$$

- For $(t_0, t_1) \in \mathcal{F}_2$,

$$w_0 \in (0, 1), \quad -1 < w_1 < w_2 < 0.$$

- For $(t_0, t_1) \in \gamma_c$, h' has a simple root $w_0 \in (0, 1)$ and a double root $w_1 = w_2 \in (-1, 0)$.

Furthermore,

$$h\left(\frac{1}{w_j}\right) \neq 0, \quad j = 0, 1, 2. \quad (3.27)$$

Proof. The zeros of h' are the same as the zeros of the polynomial \tilde{h} given by

$$\tilde{h}(w) = \frac{w^3}{r} h'(w) = w^3 - 2a_0 w - 2r \quad (3.28)$$

For $t_1 = 0$, \tilde{h} reduces to $w^3 - 2r$, which has three simple zeros, only one of them real. The discriminant of \tilde{h} is given by

$$\text{Discr}(\tilde{h}; w) = 4(8a_0^3 - 27r^2) \quad (3.29)$$

so h' has a zero with multiplicity iff $a_0 = \frac{3}{2}r^{2/3}$. Plugging this into (2.19)–(2.20), we get that t_0, t_1 are given by (2.18) for $s = r^{1/3}$. In particular, this is only possible for $0 < r < 1/8$.

Furthermore, $\text{Discr}(\tilde{h}; w)$ does not change sign in each of the sets $\mathcal{F}_1, \mathcal{F}_2$. When we keep t_0 fixed and send $t_1 \rightarrow 0$, we know from (2.4) that $a_0 \rightarrow 0$, whereas r remains positive, so $\text{Discr}(\tilde{h}; w) < 0$ on \mathcal{F}_1 . On another hand, if we keep t_1 fixed and send $t_0 \rightarrow 0$, it follows from (2.19)–(2.20) that a_0 remains positive, whereas $r \rightarrow 0$, and hence $\text{Discr}(\tilde{h}; w) > 0$ on \mathcal{F}_2 .

In virtue of (3.29), the discussion above means that \tilde{h} - and thus h' - has exactly one real zero for $(t_0, t_1) \in \mathcal{F}_1$, and three real zeros for $(t_0, t_1) \in \mathcal{F}_2$.

From Lemma 3.7, we already know that all the zeros of h' belong to \mathbb{D} . Since $a_0 \geq 0, r > 0$ (see Theorem 3.6), from Descartes' Rule of sign we learn that h' has exactly one positive real zero for $(t_0, t_1) \in \mathcal{F}$.

It only remains to prove (3.27). Suppose to the contrary that $h(w_j^{-1}) = 0$ for some j . This means that the polynomial

$$\hat{h}(w) = w^2 h(w^{-1}) = r^2 w^3 + 2a_0 r w^2 + a_0 w + r$$

has the common root w_j with the polynomial \tilde{h} in (3.28). But,

$$\text{Resultant}(\tilde{h}, \hat{h}) = -r^3[1 - 4a_0^2 + r^2(6 - 16a_0^2) + r^4(12 - 16a_0^2) + 8r^6 + 32a_0^3 r^2],$$

and because $0 < r < 1/2$ and $0 \leq a_0 < 1/2$ (see Theorem 3.6), it is not hard to see that the term between brackets above is always positive, thus the resultant above is nonzero and consequently \tilde{h} and \hat{h} do not have common roots. The proof is complete. \square

Proof of Theorem 2.8. Equation (2.21) follows directly from (3.22).

Equation (3.29) and the arguments thereafter immediately show that in the coordinate system (r, a_0) , the critical curve γ_c is described as in (2.22). \square

4. GEOMETRY OF THE SPECTRAL CURVE. PROOF OF THEOREM 2.6

An important role for the analysis of the spectral curve (2.12) is played by the discriminant

$$\mathcal{D}(z) = \text{Discr}(F(\xi, z); \xi), \quad (4.1)$$

\mathcal{D} is a polynomial of degree 9 in z . It can be computed with the help of Mathematica, but its explicit expression is rather complicated to be dealt with directly. Its first coefficients are

$$\mathcal{D}(z) = 4z^9 - 4t_1 z^8 + (4B + 16t_1) z^7 + \cdots, \quad z \in \mathbb{C},$$

where B is as in (2.13).

Theorem 2.6 can be restated in terms of the discriminant \mathcal{D} .

Theorem 4.1. *For $(t_0, t_1) \in \mathcal{F}$ the discriminant \mathcal{D} in (4.1) has three double zeros $\hat{z}_0, \hat{z}_1, \hat{z}_2 \in \mathbb{C} \setminus \overline{\Omega}$ satisfying*

$$\hat{z}_0 > 0, \quad \text{Im } \hat{z}_1 < 0, \quad \bar{\hat{z}}_2 = \hat{z}_1. \quad (4.2)$$

In addition, \mathcal{D} always has a real simple zero $z_0 > 0$, $z_0 \in \Omega$. Its remaining zeros z_1, z_2 also belong to Ω and are located as follows.

(i) For $(t_0, t_1) \in \mathcal{F}_1$,

$$\text{Im } z_1 < 0, \quad \bar{z}_2 = z_1.$$

(ii) For $(t_0, t_1) \in \mathcal{F}_2$,

$$z_2 < z_1 < z_0.$$

(iii) For $(t_0, t_1) \in \gamma_c$,

$$z_1 = z_2 < z_0$$

that is, \mathcal{D} has a double zero at $z_1 = z_2$.

Assuming Theorem 4.1, we now prove Theorem 2.6. The proof of Theorem 4.1 is given in Section 4.2

Proof of Theorem 2.6. The zeros z_0, z_1, z_2 of \mathcal{D} given by Theorem 4.1 correspond to the branch points given by Theorem 2.6. The branch point at ∞ follows from the asymptotics (2.15) for the solutions ξ_1, ξ_2, ξ_3 . In virtue of Lemma 4.2 below, the double zeros $\hat{z}_0, \hat{z}_1, \hat{z}_2$ of \mathcal{D} are singular points of (2.12). \square

The spectral curve (2.12) can be seen as a (branched) three-sheeted cover \mathcal{R} of the Riemann sphere $\overline{\mathbb{C}}$. The main goal of the rest of the present section is to describe the three sheets $\mathcal{R}_1, \mathcal{R}_2, \mathcal{R}_3$ of \mathcal{R} . As an analytic counterpart, we ultimately prove Theorem 4.1. During this Section, t_0 is always considered to be a fixed parameter, and every deformation is taken with respect to the parameter t_1 .

4.1. The spectral curve for $t_1 = 0$. We briefly discuss the case $t_1 = 0$ studied by Bleher and Kuijlaars [15], describing their results in a suitable form for our needs. Besides being instructive both to fix notation and keep in mind the main lines of the rest of the section, this particular case is also used later.

For $t_1 = 0$ the quantities r, a_0, A, B appearing in Proposition 2.1, (2.4), (2.13) and (2.14), respectively, are explicitly given by

$$r = \frac{\sqrt{1 - \sqrt{1 - 8t_0}}}{2}, \quad (4.3)$$

$$a_0 = 0,$$

$$A = \frac{1 + 20t_0 - 8t_0^2 - (1 - 8t_0)^{3/2}}{32}, \quad (4.4)$$

$$B = 0.$$

The spectral curve (2.12) is invariant under rotation $(\xi, z) \mapsto (\omega^2 \xi, \omega z)$, $\omega = e^{2\pi i/3}$, and this symmetry is carried over to all related quantities. For instance, in this situation it is easy to see that $h(\omega w) = \omega h(w)$.

The discriminant \mathcal{D} in (4.1) is a cubic polynomial in z^3 , thus reflecting the aforementioned three-fold rotational symmetry. It has a simple real zero z_0 and a double real zero $\hat{z}_0 > z_0$ given by

$$z_0 = \frac{3}{4} (1 - \sqrt{1 - 8t_0})^{2/3}, \quad \hat{z}_0 = \frac{3 + \sqrt{1 - 8t_0}}{4}, \quad (4.5)$$

and the remaining zeros are

$$z_j = \omega^{-j} z_0, \quad \hat{z}_j = \omega^{-j} \hat{z}_0, \quad j = 1, 2. \quad (4.6)$$

In terms of the rational parametrization h , the branch points z_0, z_1, z_2 are obtained as

$$z_j = h(w_j), \quad j = 0, 1, 2, \quad (4.7)$$

where $w_0 \in (0, 1)$, $w_j = \omega^{2j} w_0$, $j = 1, 2$, are the zeros of h' as in Lemma 3.10.

Regarding Theorem 2.9, we are always in the three-cut situation and

$$\Sigma_* = \Sigma_{*,0} \cup \Sigma_{*,1} \cup \Sigma_{*,2}, \quad \Sigma_{*,j} = [0, z_j], \quad j = 0, 1, 2. \quad (4.8)$$

For

$$\mathcal{R}_1 = \overline{\mathbb{C}} \setminus \Sigma_*, \quad \mathcal{R}_2 = \overline{\mathbb{C}} \setminus ([-\infty, 0] \cup \Sigma_{*,1} \cup \Sigma_{*,2}), \quad \mathcal{R}_3 = \overline{\mathbb{C}} \setminus [-\infty, z_0], \quad (4.9)$$

the Riemann Surface \mathcal{R} is the resulting surface after gluing \mathcal{R}_1 to \mathcal{R}_2 along $\Sigma_{*,1} \cup \Sigma_{*,2}$, \mathcal{R}_1 to \mathcal{R}_3 along $\Sigma_{*,0}$ and \mathcal{R}_2 to \mathcal{R}_3 along $[-\infty, 0]$, always in the usual crosswise manner.

Each function ξ_j in (2.15) has an analytic continuation to the whole sheet \mathcal{R}_j , and for the values of z_0, z_1, z_2 as above, they satisfy

$$\xi_1(z_0) = \frac{r^{2/3} (2r^2 + 1)}{2^{1/3}} = \xi_3(z_0), \quad \xi_1(z_j) = \omega^{-j} \xi_1(z_0) = \xi_2(z_j), \quad j = 1, 2, \quad (4.10)$$

$$\xi_1(\hat{z}_0) = \hat{z}_0 = \xi_3(\hat{z}_0), \quad \xi_1(\hat{z}_j) = \omega^{-j} \hat{z}_j = \xi_2(\hat{z}_j), \quad j = 1, 2. \quad (4.11)$$

Careful readers may notice this sheet structure differs from the one given in [15], where the authors construct the sheets respecting the underlying three-fold symmetry. But for us it is more convenient to do it this way, because for $t_1 \neq 0$ the symmetry is unavoidably broken.

The preimage of a point $z \in \overline{\mathbb{C}}$ through the canonical projection $\pi : \mathcal{R} \rightarrow \overline{\mathbb{C}}$ on the sheet \mathcal{R}_j is denoted by $z^{(j)}$, $j = 1, 2, 3$. Equivalently, a point $z^{(j)} \in \mathcal{R}_j$ can be seen as the pair $(\xi_j(z), z)$ - we use both representations without further explanation.

At the branch points of \mathcal{R} , two of the preimages coincide. More precisely, \mathcal{R} is branched at the points

$$z_0^{(1)} = z_0^{(3)}, \quad z_1^{(1)} = z_1^{(2)}, \quad z_2^{(1)} = z_2^{(2)}, \quad \infty^{(2)} = \infty^{(3)},$$

and for $z \in \mathbb{C} \setminus \{z_0, z_1, z_2\}$ the points $z^{(1)}, z^{(2)}, z^{(3)}$ are all distinct.

4.2. The spectral curve for $t_1 > 0$. Proof of Theorem 4.1. We now focus on the case when t_1 is positive.

Consider the system of equations

$$F(\xi, z) = 0, \quad (4.12)$$

$$\frac{\partial F}{\partial \xi}(\xi, z) = 3\xi^2 - 2z^2\xi - 2t_1\xi - (1 + t_0)z + B + t_1 = 0, \quad (4.13)$$

$$\frac{\partial F}{\partial z}(\xi, z) = 3z^2 - 2z\xi^2 - 2t_1z - (1 + t_0)\xi + B + t_1 = 0. \quad (4.14)$$

Lemma 4.2. *If $z \in \mathbb{C}$ is a zero of \mathcal{D} but the point $z^{(j)} \in \mathcal{R}$ is not a branch point of \mathcal{R} , then $(\xi_j(z), z)$ satisfies the system (4.12)–(4.14).*

Proof. For a generic point $(\xi, z) = (h(w^{-1}), h(w))$ satisfying (4.12) it is true

$$-\frac{h'(w^{-1})}{w^2} \frac{\partial F}{\partial \xi}(h(w^{-1}), h(w)) + h'(w) \frac{\partial F}{\partial z}(h(w^{-1}), h(w)) = 0.$$

If $z^{(j)}$ is a zero of the discriminant \mathcal{D} , then $(\xi_j(z), z)$ satisfies (4.13), hence from the previous equation

$$h'(w) \frac{\partial F}{\partial z}(h(w^{-1}), h(w)) = 0.$$

Since $z^{(j)}$ is not a branch point, $h'(w) \neq 0$, and the Lemma follows. \square

Subtracting Equation (4.14) from Equation (4.13), we get

$$(\xi - z)(3\xi + 3z + 2z\xi + 1 + t_0 - 2t_1) = 0,$$

and as a corollary of Lemma 4.2

Corollary 4.3. *If $z \in \mathbb{C}$ is a zero of \mathcal{D} but the point $z^{(j)} \in \mathcal{R}$ is not a branch point of \mathcal{R} , then the pair $(\xi_j(z), z)$ satisfies at least one of the equations below,*

$$\xi - z = 0, \quad (4.15)$$

$$3\xi + 3z + 2z\xi + 1 + t_0 - 2t_1 = 0. \quad (4.16)$$

Corollary 4.2 gives us an analytic tool for studying the dynamics of the singular points $\hat{z}_0, \hat{z}_1, \hat{z}_2$ when deforming t_1 , namely through the system (4.15)–(4.16). When $t_1 = 0$, $(\xi_1(\hat{z}_0), \hat{z}_0), (\xi_2(\hat{z}_0), \hat{z}_0)$ satisfy (4.15), whereas $(\xi_1(\hat{z}_j), \hat{z}_j), (\xi_3(\hat{z}_j), \hat{z}_j)$, $j = 1, 2$, satisfy (4.16), as can be verified by simply plugging the values (4.5), (4.6), (4.11) into (4.15)–(4.16).

Writing $(\xi, z) = (h(w^{-1}), h(w))$, equations (4.15)–(4.16) respectively become

$$\left(w - \frac{1}{w}\right)g(w) = 0, \quad (4.17)$$

$$f(w) = 0, \quad (4.18)$$

where

$$g(w) = 1 - 2a_0 - r \left(w + \frac{1}{w}\right), \quad (4.19)$$

$$f(w) = \tilde{f} \left(w + \frac{1}{w}\right), \quad (4.20)$$

$$\begin{aligned} \tilde{f}(w) = & 2r^3w^3 + 3r^2(1 + 2a_0)w^2 + r(3 + 8a_0 + 4a_0^2 + 4a_0r^2 - 6r^2)w \\ & + 6a_0 + 2a_0^2 - 4r^2 - 12a_0r^2 + 8a_0^2r^2 + 2r^4 + 1 + t_0 - 2t_1. \end{aligned} \quad (4.21)$$

Lemma 4.4. *For $(t_0, t_1) \in \mathcal{F}$, the function g in (4.19) has exactly one zero \hat{w}_0 on $(1, +\infty)$ and exactly one zero \hat{w}_0^{-1} on $(0, 1)$.*

Proof. We notice that $w \mapsto w + 1/w$ is a bijection from $(1, +\infty)$ to $(2, +\infty)$. Since $(1 - 2a_0)/r > 2$ (see (3.21)), the equation

$$w + \frac{1}{w} = \frac{1 - 2a_0}{r}$$

has precisely one solution \hat{w}_0 on $(1, +\infty)$. \square

For $t_1 = 0$, g simplifies to

$$g(w) = 1 - r \left(w + \frac{1}{w} \right),$$

so the point \hat{w}_0 and its images $h(\hat{w}_0), h(\hat{w}_0^{-1})$ in this case are given by

$$\hat{w}_0 = \frac{\sqrt{1 - 4r^2} + 1}{2r}, \quad h(\hat{w}_0^{-1}) = h(\hat{w}_0) = 1 - r^2 = \hat{z}_0, \quad (4.22)$$

where \hat{z}_0 is given in (4.5) and we used the explicit expression for r in (4.3).

Lemma 4.5. *For $(t_0, t_1) \in \mathcal{F}$, the polynomial \tilde{f} in (4.21) has exactly one root on $(-\infty, 0)$ and no other real roots.*

Proof. The function $(\tilde{f})'$ is a polynomial of degree 2, whose discriminant is given by

$$\text{Discr}((\tilde{f})') = 12r^2 (12r^2 - 3 - 4a_0 (1 + 2r^2 - a_0)).$$

Using the upper bound $r < 1/2$ given by Theorem 3.6 and the inequality (3.21), we get

$$12r^2 - 3 < 0, \quad 1 + 2r^2 - a_0 > 1 - a_0 \geq 2r + a_0 > 0,$$

so $\text{Discr}((\tilde{f})') < 0$ and hence $(\tilde{f})'$ has no real zeros. This implies that \tilde{f} has exactly one real root.

Moreover,

$$\begin{aligned} \tilde{f}(0) &= a_0^2 (8r^2 + 2) + a_0 (6 - 12r^2) + 1 + 2r^4 - 4r^2 + t_0 - 2t_1 \\ &\geq 1 + 2r^4 - 4r^2 + t_0 - 2t_1, \end{aligned} \quad (4.23)$$

where we used $a_0 \geq 0$ and $0 < r < 1/2$ (see Theorem 3.6). The derivative of the right-hand side is given by

$$\frac{\partial}{\partial t_1} (1 + 2r^4 - 4r^2 + t_0 - 2t_1) = -8r(1 - r^2) \frac{\partial r}{\partial t_1} - 2 < 0,$$

where again we used Theorem 3.6. This implies the minimum of the right-hand side in (4.23) is attained when $(t_0, t_1) \in \Gamma_c$, hence using (2.6) with parameter $s = r$ given by Theorem 3.6,

$$1 + 2r^4 - 4r^2 + t_0 - 2t_1 > -4r^4 - 4r^3 + 2r^2 + \frac{1}{2} > 0, \quad 0 < r < \frac{1}{2}.$$

Returning this conclusion back to (4.23), we get $\tilde{f}(0) > 0$, so the only real root of \tilde{f} needs to be negative. \square

As a consequence,

Corollary 4.6. *For $(t_0, t_1) \in \mathcal{F}$, the function f in (4.20) has two simple zeros $\hat{w}_1, \hat{w}_2 = \overline{\hat{w}_1}$, $\text{Im } \hat{w}_1 < 0$, on $\mathbb{D} \setminus \mathbb{R}$, two simple zeros $\hat{w}_1^{-1}, \hat{w}_2^{-1}$ on $\mathbb{C} \setminus (\mathbb{D} \cup \mathbb{R})$ and two zeros on $(-\infty, 0) \cup \partial\mathbb{D}$, the latter not necessarily distinct.*

Proof. The Corollary is a direct consequence of Lemma 4.5 and the 2-to-1 correspondence between the zeros of f and the zeros of \tilde{f} induced by the map $w \mapsto w + w^{-1}$. \square

Corollary 4.7. *The functions f, g given by (4.19)–(4.21) do not have a common root.*

Proof. This result follows directly from Lemma 4.4 and Corollary 4.6. \square

For $t_0 = 0$, f reduces to

$$f(w) = 2r^4 + 2r^3w^3 + \frac{2r^3}{w^3} + 3r^2w^2 + \frac{3r^2}{w^2} + 2r^2 \\ + (6r^3 + (3 - 6r^2)r)w + \frac{6r^3 + (3 - 6r^2)r}{w} + t_0 + 1$$

and the root \hat{w}_1 and the values $h(\hat{w}_1), h(\hat{w}_1^{-1})$ are given by

$$\hat{w}_1 = \omega^2 \hat{w}_0, \quad h(\hat{w}_1) = \omega^2 h(\hat{w}_0) = \omega^2 \hat{z}_0 = \hat{z}_1, \quad h(\hat{w}_1^{-1}) = \omega h(\hat{w}_0^{-1}) = \omega \hat{z}_0 = \omega^2 \hat{z}_1 \quad (4.24)$$

where we recall $\omega = e^{\frac{2\pi i}{3}}$, \hat{z}_0, \hat{z}_1 and \hat{w}_0 are given in (4.5), (4.6) and (4.22).

To get started to the deformation argument used for the proof of Theorem 4.1, we state the following weak form of Theorem 4.1 as a Lemma.

Lemma 4.8. *For $t_1 > 0$ small, the discriminant \mathcal{D} has three simple zeros, which are branch points of \mathcal{R} , and three double zeros, which are not branch points of \mathcal{R} .*

Proof. As explained in Section 4.1, the result is true for $t_1 = 0$. As a general fact that follows by continuity arguments, for small perturbations of t_1 , the multiplicity of a zero of \mathcal{D} cannot increase. That is, simple zeros of \mathcal{D} for $t_1 = 0$ stay simple for small t_1 , and double zeros of \mathcal{D} for $t_1 = 0$ either keep being double zeros or else split into two distinct simple zeros.

In particular, we get that for small perturbation of t_1 , \mathcal{D} still has *at least* three simple zeros.

By Riemann-Hurwitz formula and the genus 0 condition given by Corollary 3.9, we know that \mathcal{R} has four branch points. One of those is the point $z = \infty$, see (2.15), and each simple zero of \mathcal{D} is also a branch point. Hence, \mathcal{D} must have *at most* three simple zeros, and by the remarks above it follows that \mathcal{D} has exactly three simple zeros and exactly three double zeros for small perturbations of t_1 . \square

Remark 4.1. The discriminant \mathcal{D} can be expressed as

$$\mathcal{D}(z) = (\xi_1 - \xi_2)^2 (\xi_1 - \xi_3)^2 (\xi_2 - \xi_3)^2,$$

where ξ_j 's are the solutions to (2.12). In particular, at least two of the ξ_j 's coincide at each zero of \mathcal{D} . By continuity from the case $t_1 = 0$, it follows that for t_1 small, the solution ξ_1 coincides with one of the other two solutions at each zero of \mathcal{D} .

After this preparation, we can proceed to

Proof of Theorem 4.1. For w_j, \hat{w}_j , $j = 0, 1, 2$, the points given by Lemmas 3.10, 4.4 and Corollary 4.6, define

$$z_j = h(w_j), \quad \hat{z}_j = h(\hat{w}_j), \quad j = 0, 1, 2. \quad (4.25)$$

Our goal is to prove that these points satisfy the conclusions of Theorem 4.1. As a first step we prove their geometric properties (i)–(iii), and afterwards we prove

that these points are zeros of \mathcal{D} with the claimed multiplicities. At the end, we prove that $z_0, z_1, z_2 \in \Omega$ in the three-cut case and $z_0, z_1 \in \Omega$ in the one-cut case.

First note that $\hat{z}_0, \hat{z}_1, \hat{z}_2 \in \mathbb{C} \setminus \overline{\Omega}$, because $|\hat{w}_j| > 1$ and h maps $\mathbb{C} \setminus \mathbb{D}$ to $\mathbb{C} \setminus \Omega$, see Corollary 3.8 and also Lemma 4.4 and Corollary 4.6.

We verify (4.2). For $t_1 = 0$, (4.2) follows from (4.22) and (4.24). Since $\hat{w}_0 \in (1, +\infty)$ (Lemma 4.4) and h maps $(1, +\infty)$ to $(0, +\infty) \setminus \Omega$ (Corollary 3.8), it follows that $\hat{z}_0 \in (0, +\infty) \setminus \Omega$, and in particular $z_0 > 0$. Because \hat{w}_1 is never real and $|\hat{w}_1| > 1$, see Corollary 4.6, the point \hat{z}_1 cannot be real neither, again due to Corollary 3.8. Thus by continuity with respect to t_1 we get $\text{Im } \hat{z}_1 < 0$. The equality $\hat{z}_2 = \overline{\hat{z}_1}$ is trivial from (4.25) and the definition of \hat{w}_1, \hat{w}_2 given by Corollary 4.6.

We now prove that (i)-(iii) are satisfied by the points z_0, z_1, z_2 .

For $t_1 = 0$, (i) follows from (4.7). When we tune up t_1 , the point z_1 cannot become real for $(t_0, t_1) \in \mathcal{F}_1$. Indeed, the value w_j is a double zero of

$$z_j = h(w).$$

If z_1 becomes real for $(t_0, t_1) \in \mathcal{F}_1$ - hence also $z_2 = \overline{z_1}$ - then the equation $z_1 = h(w)$ has two distinct solutions w_1, w_2 with multiplicity two, see Lemma 3.10, which cannot occur because of the explicit form of h . By continuity, we get (i).

When $(t_0, t_1) \in \gamma_c$, we know that $w_1 = w_2 \in (-1, 0)$, see Lemma 3.10. This automatically implies $z_1 = z_2$. Choosing $s = 1/4$ in (2.22), we compute explicitly

$$w_0 = 1/2, \quad w_1 = w_2 = \frac{1}{4}, \quad z_0 = \frac{111}{1024} > \frac{21}{256} = z_1 = z_2,$$

so for the respective choice of parameters $(t_0, t_1) \in \gamma_c$ (iii) holds true. Since h' never has triple roots, see Lemma 3.10, by continuity we conclude (iii) holds true for every choice of parameters $(t_0, t_1) \in \gamma_c$.

When (t_0, t_1) enters \mathcal{F}_2 , we learn from (iii) and continuity that $z_1, z_2 < z_0$, so to get (ii) it only remains to prove that in this situation $z_2 < z_1$, or equivalently $h(w_2) < h(w_1)$.

The function $w \mapsto h(w)$ goes to $-\infty$ when $w \rightarrow -\infty$. On the negative axis its derivative has two simple zeros $w_1 < w_2$ and no others. This implies h is increasing in $(-\infty, w_1)$ and decreasing in (w_1, w_2) , and hence $h(w_1) > h(w_2)$, so finally (ii) is proven.

For $(t_0, t_1) \in \mathcal{F} \setminus \gamma_c$, we now prove z_0, z_1, z_2 are simple zeros of \mathcal{D} and $\hat{z}_0, \hat{z}_1, \hat{z}_2$ are double zeros of \mathcal{D} .

The points z_0, z_1, z_2 are the only branch points of \mathcal{R} , so surely they are zeros of \mathcal{D} . The remaining zeros of \mathcal{D} must be of multiplicity at least two, because they are not branch points. Since we already know the points $\hat{z}_1, \hat{z}_2, \hat{z}_3$ are pairwise distinct, a total counting of zeros (according to multiplicity) shows it is enough to prove $\hat{z}_1, \hat{z}_2, \hat{z}_3$ are always zeros of \mathcal{D} , and their multiplicity properties will follow.

For $t_1 = 0$, \mathcal{D} is given by

$$\begin{aligned} \mathcal{D}(z) = & 4z^9 + (t_0^2 + 4A + 12t_0 - 8)z^6 \\ & + (4t_0^3 + 18At_0 + 12t_0^2 - 36A + 12t_0 + 4)z^3 - 27A^2, \end{aligned}$$

where A is given in (4.4). Using (4.22), (4.24), after a lengthy calculation it follows that \hat{z}_j is a double zero of \mathcal{D} , $j = 0, 1, 2$.

From Lemma 4.8, we know \mathcal{D} has three double zeros for t_1 small, and these are not branch points. Let $h(\tilde{w}) = \tilde{z}$ be one of these zeros. We can assume

$h(\tilde{w}^{-1}) = \xi_1(\tilde{z})$, see Remark 4.1, so in particular

$$|\tilde{w}| > 1. \quad (4.26)$$

From Corollary 4.3 we know the pair $(\xi, \tilde{z}) = h((\tilde{w}^{-1}), h(\tilde{w}))$ satisfies one of Equations (4.15)–(4.16), and hence \tilde{w} must satisfy at least one of equations (4.17)–(4.18). Combining Equation (4.26) with Lemma 4.4 and Corollary 4.6, we thus get that \tilde{w}_j must be one of the points $\hat{w}_0, \hat{w}_1, \hat{w}_2$, so \tilde{z} must be one of the points $\hat{z}_1, \hat{z}_2, \hat{z}_3$.

Although carried out for t_1 small, the argument above works as long as none of the points z_j, \hat{z}_j pairwise coincide. But we already proved (4.2), (i)–(iii) are valid, so the only coalescence that can happen is $z_1 = z_2$, and only for $(t_0, t_1) \in \gamma_c$. By continuity it means that in this case \mathcal{D} has a unique simple zero z_0 and the other points $\hat{z}_0, \hat{z}_1, \hat{z}_2, z_1 = z_2$ are double zeros of \mathcal{D} - the double zero $z_1 = z_2$ is still a branch point of \mathcal{R} . When we move beyond γ_c , the double zero $z_1 = z_2$ splits into the two simple zeros z_1, z_2 and the point z_1 is still a simple zero. The genus 0 constraint then guarantees that the remaining zeros should still be of multiplicity at least two, and by analytic continuation these must be given by $\hat{z}_0, \hat{z}_1, \hat{z}_2$.

We now verify that $z_0, z_1, z_2 \in \Omega$ for $(t_0, t_1) \in \mathcal{F}_1$. For $t_1 = 0$ we know from (4.10) that

$$\xi_1(z_0) = \xi_3(z_0), \quad \xi_1(z_j) = \xi_2(z_j), \quad j = 1, 2,$$

where ξ_1, ξ_2, ξ_3 are (analytic continuations of) the solutions to (2.12) as in (2.15). Since we already proved that the points z_0, z_1 and z_2 do not pairwise coincide for $(t_0, t_1) \in \mathcal{F}_1$, we conclude that these equalities are valid for every choice $(t_0, t_1) \in \mathcal{F}_1$. Hence ξ_1 is branched at each of the points z_0, z_1 and z_2 . But from Theorem 2.5 we know that ξ_1 is the Schwarz function of $\partial\Omega$, hence ξ_1 is meromorphic on $\overline{\mathbb{C}} \setminus \Omega$ and consequently its branch points z_0, z_1 and z_2 have to belong to Ω .

It only remains to prove that $z_0, z_1 \in \Omega$ in the one-cut case $(t_0, t_1) \in \mathcal{F}_2$. When we cross γ_c , the branch point z_0 does not coalesce with any other zero of \mathcal{D} ; thus by continuity we get that $\xi_1(z_0) = \xi_3(z_0)$ for every $(t_0, t_1) \in \mathcal{F}_2$. The discriminant \mathcal{D} is a polynomial of degree 9 with positive leading coefficient, and for $(t_0, t_1) \in \mathcal{F}_2$ we already know that its only real zeros are z_2, z_1, z_0 and \hat{z}_0 , the first three of multiplicity one, and the last one of multiplicity two. Hence

$$\begin{aligned} \mathcal{D}(z) &< 0, & z \in (-\infty, z_2), \\ \mathcal{D}(z) &> 0, & z \in (z_2, z_1), \\ \mathcal{D}(z) &< 0, & z \in (z_1, z_0), \\ \mathcal{D}(z) &> 0, & z \in (z_0, \hat{z}_0) \cup (\hat{z}_0, +\infty). \end{aligned} \quad (4.27)$$

We already know that $\xi_1(z_2) = \xi_3(z_2)$. The third inequality in (4.27) then implies that the boundary values of the analytic continuations of ξ_1 and ξ_2 are complex conjugate of each other in the interval (z_1, z_0) . Combining with the second inequality in (4.27) we get that $\xi_1(z_1) = \xi_3(z_1)$, that is, the function ξ_1 is branched at z_1 as well. Since we already know from Theorem 2.5 that ξ_1 is the Schwarz function of $\partial\Omega$, the branch points of ξ_1 have to be in Ω , that is, $z_0, z_1 \in \Omega$, concluding the proof. \square

Remark 4.2. We stress that the proof of Theorem 4.1 also shows that the points z_j and \hat{z}_j , $j = 0, 1, 2$, given by Theorem 2.6 can be obtained through the equalities

$$h(w_j) = z_j, \quad h(\hat{w}_j) = \hat{z}_j, \quad j = 0, 1, 2,$$

where w_0 , w_1 and w_2 are the zeros of h' as in Lemma 3.10, and \hat{w}_0 , \hat{w}_1 and \hat{w}_2 are given by Lemma 4.4 and Corollary 4.6. We will use this fact extensively in the next sections.

4.3. Sheet structure for \mathcal{R} . To construct the sheet structure of \mathcal{R} , we make use of the following proposition.

Proposition 4.9. *For $(t_0, t_1) \in \mathcal{F}$, the (meromorphic continuation of) the functions ξ_1, ξ_2 and ξ_3 in (2.15) satisfy*

$$\xi_1(\hat{z}_0) = \xi_3(\hat{z}_0), \quad \xi_1(\hat{z}_j) = \xi_2(\hat{z}_j), \quad j = 1, 2.$$

Furthermore,

(i) for $(t_0, t_1) \in \mathcal{F}_1$,

$$\xi_1(z_0) = \xi_3(z_0), \quad \xi_1(z_j) = \xi_2(z_j), \quad j = 1, 2;$$

(ii) for $(t_0, t_1) \in \mathcal{F}_2$,

$$\xi_1(z_j) = \xi_3(z_j), \quad j = 0, 1, \quad \xi_2(z_2) = \xi_3(z_3);$$

(iii) for $(t_0, t_1) \in \gamma_c$,

$$\xi_1(z_0) = \xi_3(z_0), \quad \xi_1(z_1) = \xi_2(z_1) = \xi_3(z_1).$$

Proof. The first equality in (ii) was explicitly verified in the final part of the proof of Theorem 4.1. The other properties claimed by the proposition follow from similar continuity arguments. We skip the details. \square

Using Proposition 4.9 we are ready to construct the sheet structure of the Riemann surface \mathcal{R} associated with the algebraic equation (2.12). We see \mathcal{R} as a branched three-sheeted cover of \mathbb{C} and denote its sheets by \mathcal{R}_1 , \mathcal{R}_2 and \mathcal{R}_3 , so that

$$\mathcal{R} = \mathcal{R}_1 \cup \mathcal{R}_2 \cup \mathcal{R}_3.$$

The explicit construction of $\mathcal{R}_1, \mathcal{R}_2, \mathcal{R}_3$ is carried out below and depends on whether we are in the three-cut or one-cut case. In both situations, for $j = 1, 2, 3$, the function ξ_j in (2.15) admits a meromorphic continuation to the whole sheet \mathcal{R}_j . As usual, these functions ξ_1, ξ_2, ξ_3 are regarded as branches of the same meromorphic function

$$\xi : \mathcal{R} \rightarrow \overline{\mathbb{C}}, \quad \xi \equiv \xi_j \text{ on } \mathcal{R}_j,$$

which is the global solution to (2.12).

Moreover, given the sheet structure $\mathcal{R} = \mathcal{R}_1 \cup \mathcal{R}_2 \cup \mathcal{R}_3$, we denote the restriction of the canonical projection $\pi : \mathcal{R} \rightarrow \overline{\mathbb{C}}$ to \mathcal{R}_j by π_j , $j = 1, 2, 3$. With this notation, the function π_j is invertible outside the branch cuts connecting the sheets, and its inverse π_j^{-1} extends continuously to the branch cuts if one considers appropriate limiting boundary values. As at the end of Section 4.1, we denote by $p^{(j)}$ the inverse image of a point $p \in \overline{\mathbb{C}}$ through π_j . That is, $p^{(j)}$ denotes the point in \mathcal{R}_j which is uniquely defined through the relation

$$\{p^{(j)}\} = \pi_j^{-1}(\{p\}), \quad j = 1, 2, 3.$$

The point $p^{(j)}$ is also well defined at branch points. However, if p belongs to the projection of the open arcs constituting the branch cuts of \mathcal{R}_j , then the set

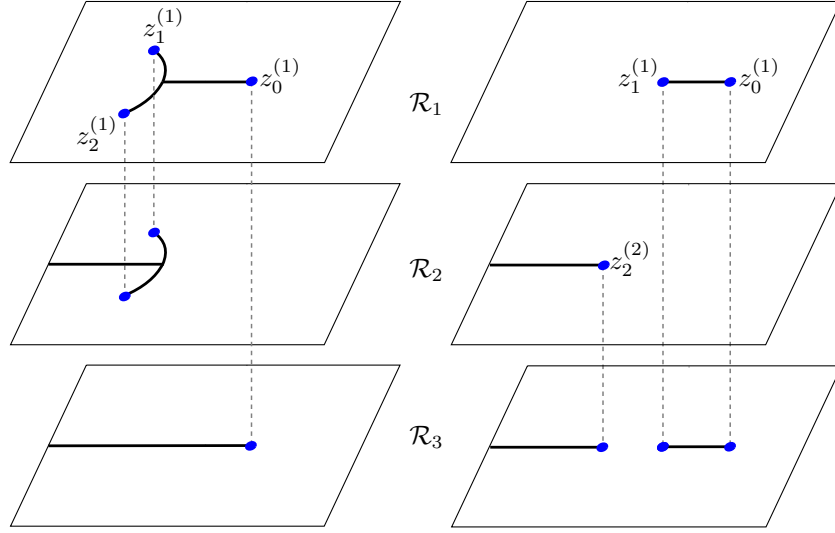


FIGURE 13. Sheet structure of \mathcal{R} for $(t_0, t_1) \in \mathcal{F}_1$ (left) and $(t_0, t_1) \in \mathcal{F}_2$ (right).

$\pi_j^{-1}(\{p\})$ contains two points on \mathcal{R}_j , one on each side of the branch cut. We denote these two points by $p_+^{(j)}, p_-^{(j)} \in \mathcal{R}_j$, labeled according to

$$\{p_+^{(j)}\} = \pi_{j+}^{-1}(\{p\}), \quad \{p_-^{(j)}\} = \pi_{j-}^{-1}(\{p\}).$$

In particular, if p belongs to the branch cut connecting two sheets \mathcal{R}_j and \mathcal{R}_k , then $p_\pm^{(j)} = p_\mp^{(k)}$.

4.3.1. Sheet structure in the three-cut case. Consider a Jordan arc γ_0 connecting z_1 to z_2 and intersecting \mathbb{R} exactly once, say at the point z_* . Assume in addition $\gamma_0^* = \gamma_0$ and $z_* < z_0$. Set

$$\Sigma_* = \gamma_0 \cup [z_*, z_0]$$

and define

$$\mathcal{R}_1 = \mathbb{C} \setminus \Sigma_*, \quad \mathcal{R}_2 = \mathbb{C} \setminus (\gamma_0 \cup [-\infty, z_0]), \quad \mathcal{R}_3 = \mathbb{C} \setminus [-\infty, z_0].$$

We construct the three-sheeted Riemann surface

$$\mathcal{R} = \mathcal{R}_1 \cup \mathcal{R}_2 \cup \mathcal{R}_3$$

connecting \mathcal{R}_1 to \mathcal{R}_2 along γ_0 , \mathcal{R}_1 to \mathcal{R}_3 along $[z_*, z_0]$ and \mathcal{R}_2 to \mathcal{R}_3 along $[-\infty, z_*]$, always in the usual crosswise manner. For $t_1 = 0$ and the choice $\gamma_0 = [0, z_1] \cup [0, z_2]$, this is in agreement with the sheet structure for $t_1 = 0$ carried over in Section 4.1. This sheet structure is illustrated in Figure 13.

The Riemann surface \mathcal{R} is branched at the points

$$z_0^{(1)} = z_0^{(3)}, \quad z_1^{(1)} = z_1^{(2)}, \quad z_2^{(1)} = z_2^{(2)}, \quad \infty^{(2)} = \infty^{(3)}.$$

We emphasize here the freedom in the choice of γ_0 . This freedom is exploited later. We also remark that this sheet structure preserves the equalities

$$\begin{aligned} \xi_1(\hat{z}_0) &= \xi_3(\hat{z}_0), & \xi_1(\hat{z}_j) &= \xi_2(\hat{z}_j), & j &= 1, 2, \\ \xi_1(z_0) &= \xi_3(z_0), & \xi_1(z_j) &= \xi_2(z_j), & j &= 1, 2, \end{aligned} \tag{4.28}$$

claimed by Proposition 4.9. In addition, the following properties hold true

$$\xi_2(x) < \xi_3(x) < \xi_1(x), \quad x > \hat{z}_0, \quad (4.29)$$

$$\xi_2(x) < \xi_1(x) < \xi_3(x), \quad z_0 < x < \hat{z}_0, \quad (4.30)$$

$$\xi_{1\pm}(x) = \overline{\xi_{3\pm}(x)} = \xi_{3\mp}(x), \quad \text{Im } \xi_2(x) = 0, \quad z_* < x < z_0, \quad (4.31)$$

$$\xi_{2\pm}(x) = \overline{\xi_{3\pm}(x)} = \xi_{3\mp}(x), \quad \text{Im } \xi_1(x) = 0, \quad x < z_*, \quad (4.32)$$

as it follows from the asymptotic behavior (2.15) and an analysis of the sign of the discriminant \mathcal{D} as in (4.27). We skip the details.

Furthermore, from the construction of the Riemann surface, it also holds true

$$\xi_{1\pm}(z) = \xi_{3\mp}(z), \quad z \in [z_*, z_0],$$

$$\xi_{1\pm}(z) = \xi_{2\mp}(z), \quad z \in \gamma_0$$

4.3.2. *Sheet structure in the one-cut case.* For $(t_0, t_1) \in \mathcal{F}_2$, we define

$$\mathcal{R}_1 = \overline{\mathbb{C}} \setminus [z_1, z_0], \quad \mathcal{R}_2 = \overline{\mathbb{C}} \setminus [-\infty, z_2], \quad \mathcal{R}_3 = \overline{\mathbb{C}} \setminus ([-\infty, z_2] \cup [z_1, z_0]).$$

In the present case, \mathcal{R}_1 is connected to \mathcal{R}_3 along $[z_1, z_0]$ and \mathcal{R}_2 is connected to \mathcal{R}_3 along $[-\infty, z_2]$, in the usual crosswise way. This sheet structure is shown in Figure 13.

The branch points of \mathcal{R} are given by

$$z_0^{(1)} = z_0^{(3)}, \quad z_1^{(1)} = z_1^{(3)}, \quad z_2^{(2)} = z_2^{(3)}, \quad \infty^{(2)} = \infty^{(3)},$$

see Figure 13. In the same spirit as in (4.28)–(4.32), we also have the following equalities,

$$\begin{aligned} \xi_1(\hat{z}_0) &= \xi_3(\hat{z}_0), \quad \xi_1(\hat{z}_j) = \xi_2(\hat{z}_j), \quad j = 1, 2, \\ \xi_2(z_2) &= \xi_3(z_2), \quad \xi_1(z_j) = \xi_3(z_j), \quad j = 0, 1, \end{aligned} \quad (4.33)$$

and the relations

$$\begin{aligned} \xi_2(x) &< \xi_3(x) < \xi_1(x), & x > \hat{z}_0, \\ \xi_2(x) &< \xi_1(x) < \xi_3(x), & z_0 < x < \hat{z}_0, \\ \xi_{1\pm}(x) &= \overline{\xi_{3\pm}(x)} = \xi_{3\mp}(x), \quad \text{Im } \xi_2(x) = 0, & z_1 < x < z_0, \\ \xi_{2\pm}(x) &= \overline{\xi_{3\pm}(x)} = \xi_{3\mp}(x), \quad \text{Im } \xi_1(x) = 0, & x < z_2. \end{aligned} \quad (4.34)$$

5. MEROMORPHIC QUADRATIC DIFFERENTIAL ON \mathcal{R}

Given any point $p \in \mathcal{R}$ which is not a branch point, we define the following function element in a neighborhood of p

$$Q(z) = \begin{cases} \xi_2(z) - \xi_3(z), & \text{if } p \in \mathcal{R}_1, \\ \xi_1(z) - \xi_3(z), & \text{if } p \in \mathcal{R}_2, \\ \xi_1(z) - \xi_2(z), & \text{if } p \in \mathcal{R}_3. \end{cases} \quad (5.1)$$

The function element Q cannot be extend to a (single-valued) meromorphic function on the whole Riemann surface \mathcal{R} , but it admits an analytic extension along any path on \mathcal{R} . Hence given any path γ on \mathcal{R} , it is meaningful to talk about contour integrals of Q along γ . More importantly, the square Q^2 extends to a (single-valued!) meromorphic function on the whole Riemann surface \mathcal{R} , as it is shown in a general framework in [45, Theorem 1.8]. Due to our explicit sheet structure, this can also be verified directly, but we skip the details.

We are interested in the associated quadratic differential

$$\varpi = -(Q(z))^2 dz^2. \quad (5.2)$$

Zeros and poles of ϖ are the zeros and poles of Q^2 , along with their multiplicities, and also the branch points of \mathcal{R} . Simple poles and zeros are called finite critical points, whereas poles of order at least 2 are called infinite critical points. An arc $\gamma \subset \mathcal{R}$ is said to be an *arc of trajectory* of ϖ if

$$\operatorname{Re} \int^z \sqrt{-\varpi} = \operatorname{Re} \int^z Q(s) ds = \text{const}, \quad z \in \gamma. \quad (5.3)$$

A trajectory is a maximal arc of trajectory, and it is called critical if it extends to a finite critical point of ϖ on at least one of its ends. Two trajectories can only intersect at the critical points. The union of all critical trajectories of ϖ is denoted by $\mathcal{G} = \mathcal{G}(\varpi)$ and is called the *critical graph* of ϖ .

The main goal of this Section is to describe the critical graph \mathcal{G} . As we will see later on, the critical graph plays a substantial role in the Riemann-Hilbert/Steepest Descent analysis carried over in Sections 7 and 8. Some of its trajectories also encode Equation (2.25): Theorem 2.9 will follow almost immediately once we describe the critical graph \mathcal{G} .

To describe the trajectories of ϖ , we follow the methodology of the recent work [45] by Martínez-Finkelshtein and the second author. The main conclusion of this analysis is that the topology of the critical graph of ϖ only depends on whether (t_0, t_1) belongs to \mathcal{F}_1 or \mathcal{F}_2 .

In our setting, the analysis works as follows. We first describe the trajectories for $t_1 = 0$, for which the underlying rotational symmetry plays a fundamental role. It turns out that in this case $\mathcal{R} \setminus \mathcal{G}$ consists only of strip and half plane domains, and no short trajectories. When we increase t_1 , the critical graph is deformed, and we control its dynamics by means of analyzing the widths of the strip domains, showing that they do not vanish on \mathcal{F}_1 , and thus the critical graph is preserved for values of (t_0, t_1) in this domain. When we cross γ_c , moving from \mathcal{F}_1 to \mathcal{F}_2 , we are able to identify the phase transitions for the trajectories, and describe the critical graph for values of $(t_0, t_1) \in \mathcal{F}_2$ that are sufficiently close to γ_c . Once again the critical graph consists only of strip and half plane domains, but now there are also short trajectories. We again analyze the widths of the strip domains, and also the short trajectories, and prove that the critical graph remains unchanged on \mathcal{F}_2 .

The standard references on quadratic differentials are the books by Strebel [57] and by Jenkins [32]. We follow closely the aforementioned work [45], where the reader can also find a discussion on the general theory of quadratic differentials in a form suitable for our needs.

The present Section is organized in the following manner. In Sections 5.1 and 5.2 we derive some technical lemmas that are needed for the computation of the critical graph, first for the three-cut case $(t_0, t_1) \in \mathcal{F}_1$ and then for the one-cut case $(t_0, t_1) \in \mathcal{F}_2$. In Section 5.3 we compute the zeros and poles of ϖ , and discuss some general principles that are used for the computation of the critical graph. Finally, in Sections 5.4 and 5.5 we derive the critical graph in the three-cut and one-cut cases, respectively.

When describing the trajectories and dynamics of the critical graph of ϖ , instead of a precise formulation of the behavior of each trajectory we opt for a more “reader friendly” approach, with visual description and illustration of the results

by a number of pictures. And of course, we always provide rigorous proofs of the results.

5.1. Technical computations for the three-cut case. When $t_1 = 0$, the sheet structure constructed in Section 4.3.1 is consistent with the sheet structure in Section 4.1. However, for the analysis of the trajectories of ϖ when $t_1 = 0$, it is more convenient (although, strictly speaking, not necessary) to construct the sheets in a different way that better reflects the underlying discrete rotational symmetry.

According to Theorem 2.6, z_j, \hat{z}_j , $j = 1, 2, 3$, denote the branch points and the singular points of (2.12), respectively. In the case $t_1 = 0$, these points are explicitly given in (4.5)–(4.6).

We set

$$L_j = [0, \infty e^{\frac{(2j+3)\pi i}{3}}], \quad j = 0, 1, 2, \quad L = \bigcup_{j=0}^2 L_j, \quad (5.4)$$

and recalling the set Σ_* given explicitly for $t_1 = 0$ in (4.8), we define

$$\tilde{\mathcal{R}}_1 = \overline{\mathbb{C}} \setminus \Sigma_*, \quad \tilde{\mathcal{R}}_2 = \overline{\mathbb{C}} \setminus (\Sigma_* \cup L), \quad \tilde{\mathcal{R}}_3 = \overline{\mathbb{C}} \setminus L. \quad (5.5)$$

We then connect the sheets $\tilde{\mathcal{R}}_1$ and $\tilde{\mathcal{R}}_2$ along Σ_* and the sheets $\tilde{\mathcal{R}}_2$ and $\tilde{\mathcal{R}}_3$ along L , always in the crosswise manner, and denote by $\tilde{\mathcal{R}}$ the resulting three-sheeted Riemann surface,

$$\tilde{\mathcal{R}} = \tilde{\mathcal{R}}_1 \cup \tilde{\mathcal{R}}_2 \cup \tilde{\mathcal{R}}_3.$$

This construction can be compared to (4.9) through the identities

$$\tilde{\mathcal{R}}_1 = \mathcal{R}_1, \quad \tilde{\mathcal{R}}_2 = \begin{cases} \mathcal{R}_3, & -\frac{\pi}{3} < \arg z < \frac{\pi}{3}, \\ \mathcal{R}_2, & \text{otherwise,} \end{cases} \quad \tilde{\mathcal{R}}_3 = \begin{cases} \mathcal{R}_2, & -\frac{\pi}{3} < \arg z < \frac{\pi}{3}, \\ \mathcal{R}_3, & \text{otherwise.} \end{cases} \quad (5.6)$$

That is, we interchange the sectors $-\pi/3 < \arg z < \pi/3$ between the sheets \mathcal{R}_2 and \mathcal{R}_3 . We refer the reader to Figure 14 for a comparison of these sheets structures.

Clearly this new sheet structure also affects the analytic continuation of the function germs in (2.15). Each function germ in (2.15) admits an analytic continuation to the whole sheet $\tilde{\mathcal{R}}_j$, and these analytic continuations satisfy the equalities

$$\xi_1(z_j) = \xi_2(z_j), \quad \xi_1(\hat{z}_j) = \xi_2(\hat{z}_j), \quad j = 0, 1, 2,$$

and the identities

$$\xi_3(x) < \xi_2(x) < \xi_1(x), \quad x > \hat{z}_0, \quad (5.7)$$

$$\xi_3(x) < \xi_1(x) < \xi_2(x), \quad z_0 < x < \hat{z}_0, \quad (5.8)$$

$$\xi_{1\pm}(x) = \overline{\xi_{2\pm}(x)} = \xi_{2\mp}(x), \quad \operatorname{Im} \xi_3(x) = 0, \quad 0 < x < z_0, \quad (5.9)$$

$$\xi_{2\pm}(x) = \overline{\xi_{3\pm}(x)} = \xi_{3\mp}(x), \quad \operatorname{Im} \xi_1(x) = 0, \quad x < 0, \quad (5.10)$$

which are compatible with (4.28)–(4.32), keeping in mind (5.6). During Section 5, for $t_1 = 0$ we always use the analytic continuations of the functions ξ_1, ξ_2, ξ_3 in accordance to the sheet structure for $\tilde{\mathcal{R}}$, unless otherwise stated. For $t_1 > 0$ we keep using the sheet structure constructed in Sections 4.3.1 and 4.3.2.

For $t_1 = 0$, define

$$h_j(x, y) = \int_x^y (\operatorname{Re} \xi_{j+}(s) - \operatorname{Re} \xi_{3+}(s)) ds, \quad x, y \in \mathbb{R}, \quad j = 1, 2, \quad (5.11)$$

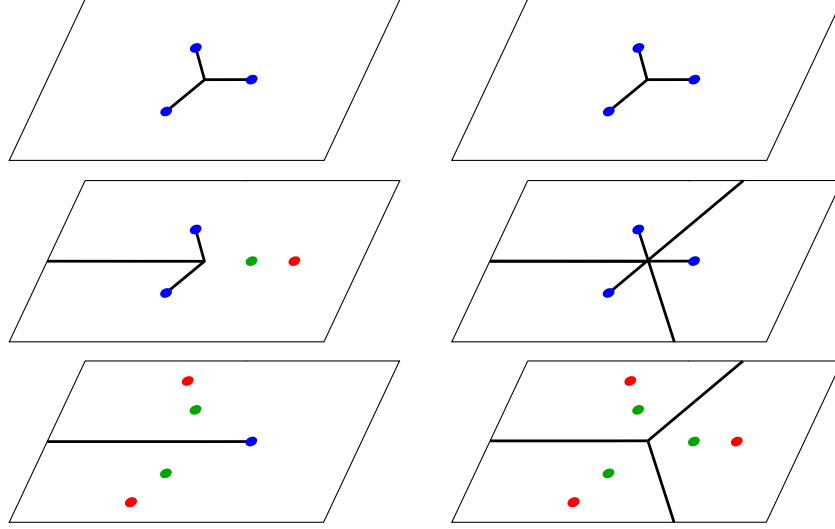


FIGURE 14. For $t_1 = 0$, the cut structure and the zeros of ϖ before (left) and after (right) the regluing $\mathcal{R}_j \mapsto \tilde{\mathcal{R}}_j$.

where the integrals above are computed along the real axis. We emphasize that the functions ξ_1, ξ_2, ξ_3 in the expression above correspond to the sheet structure $\tilde{R}_1, \tilde{R}_2, \tilde{R}_3$.

Lemma 5.1. *Suppose that $t_1 = 0$. For $j = 1, 2$, the following properties hold true for h_j .*

- (i) *If $x, y \in [0, z_0]$, $x \neq y$, then $h_j(x, y) \neq 0$.*
- (ii) *If $h(x_j, y_j) = 0$, for $x_j < y_j \leq 0$, $j = 1, 2$, then $(x_1, y_1) \cap (x_2, y_2) \neq \emptyset$.*

Proof. We first prove (i). If $h_j(x, y) = 0$ for $x, y \in [0, z_0]$, then we conclude that there exists u_0 between x and y for which

$$\operatorname{Re} \xi_{j+}(u_0) = \operatorname{Re} \xi_{3+}(u_0).$$

It follows from the first equation in (4.5) that $z_0 < 1$. In particular, this implies

$$0 < u_0 < z_0 < 1. \quad (5.12)$$

From (5.9) we know that $\overline{\xi_{1+}(u_0)} = \xi_{2+}(u_0)$, so

$$\operatorname{Re} \xi_{2+}(u_0) = \operatorname{Re} \xi_{1+}(u_0) = \xi_3(u_0).$$

For $t_1 = 0$, the coefficient of ξ^2 in (2.12) is $-z^2$. Using Vieta's relations we hence conclude

$$u_0^2 = \xi_{1+}(u_0) + \xi_{2+}(u_0) + \xi_3(u_0) = 3\xi_3(u_0).$$

Plugging in the pair $(\xi_3(u_0), u_0) = (u_0^2/3, u_0)$ back to (2.12), we see that u_0 must be a root of

$$\phi(u) = \frac{2}{27}u^6 - \left(\frac{2}{3} - t_0\right)u^3 - A = 0,$$

where the coefficient A , given explicitly in (4.4), is positive because $t_0 \in (0, 1/8)$. Due to the rotational symmetry $\phi(\omega u) = \phi(u)$, the polynomial ϕ has at most two

real roots. Straightforward computations show

$$\phi(0) = -A < 0, \quad \phi(1) = t_0 - A - \frac{16}{27} < 0.$$

Since the degree of ϕ is even and its leading coefficient is positive, the inequalities above imply that ϕ does not have roots on the interval $[0, 1]$, thus $u_0 \in \mathbb{R} \setminus [0, 1]$. But this is in contradiction with (5.12).

To get (ii), we first note that arguments similar as the analysis above show that ϕ has a zero in each of the intervals (x_1, y_1) and (x_2, y_2) . On the other hand, the inequality and comments above also show that ϕ has exactly one zero on $(-\infty, 0)$, so this zero must belong to both intervals (x_1, y_1) and (x_2, y_2) . \square

For $(t_0, t_1) \in \mathcal{F}_1$ and recalling the definition of the function germ Q in (5.1) and the sheet structure described in Section 4.3.2, the quantities

$$\tau_1 = \operatorname{Re} \int_{z_2^{(3)}}^{z_0^{(3)}} Q(s) ds = \operatorname{Re} \int_{z_2}^{z_0} (\xi_1(s) - \xi_2(s)) ds, \quad (5.13)$$

$$\tau_2 = \operatorname{Re} \int_{z_0^{(2)}}^{z_2^{(2)}} Q(s) ds = \operatorname{Re} \int_{z_0}^{z_2} (\xi_1(s) - \xi_3(s)) ds, \quad (5.14)$$

$$\tau_3 = \operatorname{Re} \int_{z_2^{(3)}}^{\hat{z}_2^{(3)}} Q(s) ds = \operatorname{Re} \int_{z_2}^{\hat{z}_2} (\xi_1(s) - \xi_2(s)) ds, \quad (5.15)$$

$$\tau_4 = \operatorname{Re} \int_{z_2^{(3)}}^{z_1^{(2)}} Q(s) ds = \operatorname{Re} \int_{z_2}^{x_*} (\xi_1(s) - \xi_2(s)) ds + \operatorname{Re} \int_{x_*}^{z_1} (\xi_1(s) - \xi_3(s)) ds, \quad (5.16)$$

$$\tau_5 = \int_{z_0^{(2)}}^{\hat{z}_0^{(2)}} Q(s) ds = \int_{z_0}^{\hat{z}_0} (\xi_1(s) - \xi_3(s)) ds, \quad (5.17)$$

are of interest for what comes later. In the formulas above, the paths of integration are taken in $\mathbb{C} \setminus (-\infty, z_*] \cup \Sigma_*$ and x_* is any point in the interval $(-\infty, z_*)$: the value τ_4 does not depend on the precise choice of x_* , as it is indicated by the first integral defining it.

What is important here is that τ_j , $j = 1, \dots, 5$, do not vanish for $(t_0, t_1) \in \mathcal{F}_1$. The analysis of these quantities is carried out in the Appendix A.1.

5.2. Technical computations for the one-cut case. It is a simple observation that if you fix $(\tilde{t}_0, \tilde{t}_1) \in \gamma_c$, then any pair of the form $(\tilde{t}_0, t_1) \in \mathcal{F}$, with t_1 larger than \tilde{t}_1 , actually belongs to \mathcal{F}_2 , as can be seen in Figure 3. In other words, \mathcal{F}_2 consists of points in \mathcal{F} of the form (\tilde{t}_0, t_1) , where $(\tilde{t}_0, \tilde{t}_1) \in \gamma_c$ for some \tilde{t}_1 and $t_1 > \tilde{t}_1$. We use this fact without further mention.

Recall that w_0, w_1, w_2 denote the zeros of h' (see Lemma 3.10) and, moreover, $w_1 = w_2$ for $(t_0, t_1) \in \gamma_c$. For $(t_0, t_1) \in \mathcal{F}_2$, denote additionally by \tilde{w}_j the simple root of $h(w) - z_j = h(w) - h(w_j)$, $j = 0, 1, 2$, and extend \tilde{w}_j for values $(t_0, t_1) \in \gamma_c$ by continuity.

When $(t_0, t_1) \in \gamma_c$, we recall that r, a_0 are given in terms of $s \in (0, 1/2)$ by (2.22), so that

$$h'(w) = r - \frac{2a_0 r}{w^2} - \frac{2r^2}{w^3} = -\frac{s^3(2s - w)(s + w)^2}{w^3}.$$

In particular $w_0 = 2s$, so

$$h(w) - h(w_0) = \frac{s^3(2s - w)^2(s + 4w)}{4w^2}.$$

Summarizing, the last two equations tell us that when $(t_0, t_1) \in \gamma_c$, the quantities w_0, w_1, w_2 and \tilde{w}_0 mentioned above are given in terms of the parameter $s \in (0, 1/2)$ by

$$w_1 = -s = w_2, \quad \tilde{w}_0 = -\frac{s}{4}, \quad w_0 = 2s. \quad (5.18)$$

For the choice $a_0 = \frac{1}{4}$, $r = \frac{1}{32}$, corresponding to the pair $(t_0, t_1) = (\frac{639}{524288}, \frac{191}{1024}) \in \mathcal{F}_2$, we compute numerically

$$\begin{aligned} z_2 &\approx 0.18352, & w_2 &\approx -0.12932, & \tilde{w}_2 &\approx -1.86844, \\ z_1 &\approx 0.20797, & w_1 &\approx -0.63351, & \tilde{w}_1 &\approx -0.07786, \\ z_0 &\approx 0.29599, & w_0 &\approx 0.76284, & \tilde{w}_0 &\approx -0.05370. \end{aligned}$$

so for this choice

$$\tilde{w}_2 < w_1 < w_2 < \tilde{w}_1 < \tilde{w}_0 < w_0. \quad (5.19)$$

If $(t_0, t_1) \in \mathcal{F}_2$, then none of the points w_j, \tilde{w}_j 's can pairwise coincide. Indeed, we already know from Lemma 3.10 that the points w_0, w_1 and w_2 do not pairwise coincide. If $\tilde{w}_j = \tilde{w}_k$ (or also $\tilde{w}_j = w_k$) for some pair j, k , then consequently

$$z_j = h(w_j) = h(\tilde{w}_j) = h(\tilde{w}_k) = h(w_k) = z_k,$$

which cannot occur on \mathcal{F}_2 (see Theorem 4.1). Hence by continuity we conclude that (5.19) holds for every pair $(t_0, t_1) \in \mathcal{F}_2$.

Lemma 5.2. *Fix $(\tilde{t}_0, \tilde{t}_1) \in \gamma_c$. Then*

$$\lim_{t_1 \rightarrow \tilde{t}_1+} \frac{\partial w_1}{\partial t_1} = -\infty, \quad \lim_{t_1 \rightarrow \tilde{t}_1+} \frac{\partial w_2}{\partial t_1} = +\infty$$

Proof. We deal with the equality for w_1 . The case w_2 is analogous. Let $(\tilde{t}_0, t_1) \in \mathcal{F}_2$, so $t_1 > \tilde{t}_1$. In this situation, w_1 is a simple zero of h' , so

$$\frac{\partial w_1}{\partial t_1} = -\frac{\frac{\partial h'}{\partial t_1}(w_1)}{h''(w_1)}. \quad (5.20)$$

We see $(t_0, t_1) \mapsto (r, a_0)$ as a change of coordinates, so that from the chain rule

$$\left(\frac{\partial h'}{\partial t_0}, \frac{\partial h'}{\partial t_1} \right) = \left(\frac{\partial h'}{\partial r}, \frac{\partial h'}{\partial a_0} \right) \frac{D(r, a_0)}{D(t_0, t_1)}, \quad (5.21)$$

where $D(r, a_0)/D(t_0, t_1)$ is the Jacobian of the change of coordinates. From the Inverse Function Theorem,

$$\begin{aligned} \frac{D(r, a_0)}{D(t_0, t_1)} &= \left(\frac{D(t_0, t_1)}{D(r, a_0)} \right)^{-1} \\ &= \det \left(\frac{D(t_0, t_1)}{D(r, a_0)} \right)^{-1} \begin{pmatrix} \partial t_1 / \partial a_0 & -\partial t_0 / \partial a_0 \\ -\partial t_1 / \partial r & \partial t_0 / \partial r \end{pmatrix}. \end{aligned}$$

We use this expression to compute the second component in (5.21), arriving at

$$\frac{\partial h'}{\partial t_1} = \det \left(\frac{D(t_0, t_1)}{D(r, a_0)} \right)^{-1} \left(\frac{\partial t_0}{\partial r} \frac{\partial h'}{\partial a_0} - \frac{\partial t_0}{\partial a_0} \frac{\partial h'}{\partial r} \right). \quad (5.22)$$

Using (2.19)–(2.20), we compute explicitly

$$\begin{aligned}\frac{\partial t_0}{\partial r} &= 2(1 - 4a_0^2)r - 8r^3, & \frac{\partial t_0}{\partial a_0} &= -8a_0r^2, \\ \frac{\partial t_1}{\partial r} &= -8a_0r, & \frac{\partial t_1}{\partial a_0} &= 1 - 2a_0 - 4r^2,\end{aligned}$$

and after a lengthy calculation

$$\det \left(\frac{D(t_0, t_1)}{D(r, a_0)} \right) = 2r \left(8a_0^3 - 4a_0^2(4r^2 + 1) + a_0(8r^2 - 2) + (1 - 4r^2)^2 \right).$$

Similarly,

$$\frac{\partial t_0}{\partial r} \frac{\partial h'}{\partial a_0} - \frac{\partial t_0}{\partial a_0} \frac{\partial h'}{\partial r} = -\frac{4r^2(8ar - 2aw^3 - 4r^2w + w)}{w^3}$$

We are interested in the values of $\partial h' / \partial t_1$ for parameters on γ_c , so using (2.22) and (5.18) in the last two equations, we get

$$\frac{D(t_0, t_1)}{D(r, a_0)} = 2s^3(1 - s^2)^3(2s^2 + 1)^2(1 - 4s^2) > 0, \quad s \in (0, 1/2)$$

and

$$\frac{\partial t_0}{\partial r} \frac{\partial h'}{\partial a_0} - \frac{\partial t_0}{\partial a_0} \frac{\partial h'}{\partial r} = -4s^4(1 - 15s^4 - 4s^6) < 0, \quad s \in (0, 1/2).$$

In virtue of (5.22), we conclude

$$\frac{\partial h'}{\partial t_1}(w_1) < 0, \quad (\tilde{t}_0, \tilde{t}_1) \in \gamma_c.$$

Additionally, since w_1 is the smallest root of the continuous function h' on $(-\infty, 0)$ and $h'(w) \rightarrow r > 0$ when $w \rightarrow -\infty$, we conclude

$$h''(w_1) < 0, \quad (t_0, t_1) \in \mathcal{F}_2.$$

When t_1 approaches \tilde{t}_1 , w_1 becomes a double root of h' , and hence $h''(w_1)$ approaches zero. The result then follows by combining the last two inequalities with (5.20). \square

Having in mind (2.20), set

$$\begin{aligned}G(w) &= h\left(\frac{1}{w}\right) - \frac{t_1 + h(w)^2}{3} \\ &= \frac{2r^2w^2}{3} + \frac{4a_0rw}{3} + \frac{2a_0}{3} + \frac{r(3 - 4a_0^2 - 2r^2)}{3w} \\ &\quad - \frac{2a_0r^2(1 + 2a_0)}{3w^2} - \frac{4a_0r^3}{3w^3} - \frac{r^4}{3w^4}, \quad w \in \mathbb{C}.\end{aligned}$$

When $(t_0, t_1) \in \gamma_c$ we use (2.22) and (5.18) to compute

$$G(w_1) = 0 = G(w_2), \quad G(\tilde{w}_0) = -\frac{3}{8}s^2(7s^6 + 12s^4 + 8) < 0. \quad (5.23)$$

Lemma 5.3. *If $(\tilde{t}_0, \tilde{t}_1) \in \gamma_c$, then $G'(w) < 0$ on $(-\infty, 0)$.*

Proof. On γ_c , the quantities a_0 and r are explicitly given in terms of $s \in (0, 1/2)$ by (2.22). Substituting these values in the definition of G , we can rewrite

$$G'(w) = \frac{s^3}{3w^5}p(w),$$

$$p(w) = 4s^3w^6 + 6s^2w^5 + (2s^6 + 9s^4 - 3)w^3 + 6s^5(1 + 3s^2)w^2 + 18s^8w + 4s^9.$$

The discriminant of p can be decomposed as

$$\text{Discr}(p; w) = c (s^2 - 1)^3 s^{24} (s^{30} + \dots),$$

where the polynomial between parentheses has rational coefficients and is symbolically computed with Mathematica. Its zeros are computed numerically and verified to not belong to $(0, 1/2)$.

As a consequence, we conclude that p - and hence G' - does not have zeros with multiplicity on $(-\infty, 0)$. For $s = 1/2$,

$$p(w) = \frac{(w-1)(64w^5 + 256w^4 + 256w^3 - 52w^2 - 10w - 1)}{1024}$$

and the set of zeros (with nonnegative imaginary part) of the polynomial between parentheses above is numerically computed to be

$$\{-4.14697 + 1.16757i, -0.144709 + 0.158865i, 0.58336\}.$$

so in particular $p(w)$ has no negative zeros for $s = 1/2$, and the same holds true for G' . Since G' is never zero at $w = 0$ and, as we just observed, G' does not have zeros with multiplicity, by continuity of the zeros of G' with respect of s we get that G' is never zero on $(-\infty, 0)$. The result then follows from the extra observation that $G'(w) \rightarrow -\infty$ when $w \rightarrow -\infty$. \square

Lemma 5.4. Fix $(\tilde{t}_0, \tilde{t}_1) \in \gamma_c$. There exists $\varepsilon > 0$ such that for any pair $(\tilde{t}_0, t_1) \in \mathcal{F}_2$ with $0 < t_1 - \tilde{t}_1 < \varepsilon$, the following inequalities hold true

$$G(w_2) < 0 < G(w_1).$$

Proof. We will prove

$$\lim_{t_1 \rightarrow \tilde{t}_1+} \frac{\partial}{\partial t_1}(G(w_1)) = +\infty, \quad \lim_{t_1 \rightarrow \tilde{t}_1+} \frac{\partial}{\partial t_1}(G(w_2)) = -\infty. \quad (5.24)$$

By continuity, it then follows that $t_1 \mapsto G(w_1)$ ($t_1 \mapsto G(w_2)$) is increasing (decreasing) for t_1 sufficiently close to \tilde{t}_1 . Since $G(w_1) = 0 = G(w_2)$ for $t_1 = \tilde{t}_1$ (see (5.23)), the result will follow.

From the definition of G and $j = 1, 2$,

$$\frac{\partial}{\partial t_1}(G(w_j)) = -\frac{1}{w_j^2}h'\left(\frac{1}{w_j}\right)\frac{\partial w_j}{\partial t_1} + \frac{\partial h}{\partial t_1}\left(\frac{1}{w_j}\right) - \frac{2}{3}h(w_j)\frac{\partial h}{\partial t_1}(w_j) - \frac{1}{3}, \quad (5.25)$$

where we also used $h'(w_j) = 0$. Additionally, we use (5.18) to get

$$h'\left(\frac{1}{w_j}\right) \rightarrow h'\left(-\frac{1}{s}\right) = 2s^9 - 3s^7 + s^3 > 0, \quad \text{as } t_1 \rightarrow \tilde{t}_1.$$

From Lemma 5.2 and the inequality above, we know that the first term on the right hand side of (5.25) goes to $(-1)^{j+1}\infty$ when $t_1 \searrow \tilde{t}_1$. Since $w_j \rightarrow -s \neq 0$ in the limit $t_1 \searrow \tilde{t}_1$, the remaining terms remain bounded, concluding the proof of (5.24). \square

Proposition 5.5. *Suppose $(\tilde{t}_0, \tilde{t}_1) \in \gamma_c$. There exists $\varepsilon > 0$ such that for every choice $(\tilde{t}_0, t_1) \in \mathcal{F}_2$ with $0 < t_1 - \tilde{t}_1 < \varepsilon$, the function G has no zeros on the intervals $(-\infty, w_1]$ and $[w_2, \tilde{w}_0]$.*

Proof. Since $\tilde{w}_0 < 0$, it follows from continuity and Lemma 5.3 that

$$G'(w) < 0, \quad w \in (-\infty, \tilde{w}_0], \quad 0 < t_1 - \tilde{t}_1 < \varepsilon,$$

so if $0 < t_1 - \tilde{t}_1 < \varepsilon$, then G is strictly decreasing on the interval $(-\infty, \tilde{w}_0]$, and as a consequence G has at most one zero in this interval. From Lemma 5.4, this zero has to be on the subinterval (w_1, w_2) , thus G is never zero on $(-\infty, w_1] \cup [w_2, \tilde{w}_0]$. \square

Corollary 5.6. *Suppose $(\tilde{t}_0, \tilde{t}_1) \in \gamma_c$. There exists $\varepsilon > 0$ such that for every choice $(\tilde{t}_0, t_1) \in \mathcal{F}_2$ with $0 < t_1 - \tilde{t}_1 < \varepsilon$, the functions*

$$z \mapsto \xi_1(z) - \frac{t_1 + z^2}{3}, \quad z \mapsto \xi_2(z) - \frac{t_1 + z^2}{3},$$

do not vanish, respectively, on the intervals $(-\infty, z_2], [z_1, z_0]$.

Proof. Under the mapping $z = h(w)$, the functions

$$z \mapsto \xi_1(z) - \frac{t_1 + z^2}{3}, \quad z \in (-\infty, z_2], \quad z \mapsto \xi_2(z) - \frac{t_1 + z^2}{3}, \quad z \in [z_1, z_0]$$

transform to

$$w \mapsto G(w), \quad w \in (-\infty, \tilde{w}_2], \quad w \mapsto G(w), \quad w \in [\tilde{w}_1, \tilde{w}_0]$$

respectively, where we recall that \tilde{w}_j , $j = 1, 2$, is the simple root of $h(w) = z_j$. From (5.19) we know $(-\infty, \tilde{w}_2] \subset (-\infty, w_1]$, $[\tilde{w}_1, \tilde{w}_0] \subset [w_2, \tilde{w}_0]$, and the result follows from Proposition 5.5. \square

Similarly as it is done in (5.11) for $t_1 = 0$, we now define

$$h_j(x, y) = \int_x^y (\operatorname{Re} \xi_{j+}(s) - \operatorname{Re} \xi_{3+}(s)) ds, \quad x, y \in \mathbb{R}, \quad j = 1, 2, \quad (t_0, t_1) \in \mathcal{F}_2.$$

The next result is the analogous of Lemma 5.1 for the one-cut case, and its proof is also similar.

Lemma 5.7. *Suppose $(\tilde{t}_0, \tilde{t}_1) \in \gamma_c$. There exists $\varepsilon > 0$ such that for any pair $(\tilde{t}_0, t_1) \in \mathcal{F}$ with $0 < t_1 - \tilde{t}_1 < \varepsilon$, the following properties hold true.*

- (i) *If $x, y \in (-\infty, z_2]$, $x \neq y$, then $h_1(x, y) \neq 0$.*
- (ii) *If $x, y \in [z_1, z_0]$, $x \neq y$, then $h_2(x, y) \neq 0$.*

Proof. For simplicity, denote $J_1 = (-\infty, z_2]$, $J_2 = [z_1, z_0]$. If $h_j(x, y) = 0$ for some points $x, y \in J_j$, $x \neq y$, then there exists a point $u_0 \in J_j$ for which

$$\operatorname{Re} \xi_{j+}(u_0) = \operatorname{Re} \xi_{3+}(u_0).$$

Using the equalities in (4.34) we conclude

$$\operatorname{Re} \xi_{1+}(u_0) = \operatorname{Re} \xi_{2+}(u_0) = \operatorname{Re} \xi_{3+}(u_0).$$

According to the sheet structure constructed in Section 4.3.2, the function ξ_j is real on J_j and continuous across J_j , so the equality above implies

$$\operatorname{Re} \xi_{1+}(u_0) + \operatorname{Re} \xi_{2+}(u_0) + \operatorname{Re} \xi_{3+}(u_0) = 3\xi_j(u_0).$$

On the other hand, the sum $\xi_1 + \xi_2 + \xi_3$ is equal to minus the coefficient of ξ^2 in (2.12), that is,

$$\xi_j(u_0) = \frac{1}{3}(\operatorname{Re} \xi_{1+}(u_0) + \operatorname{Re} \xi_{2+}(u_0) + \operatorname{Re} \xi_{3+}(u_0)) = \frac{t_1 + u_0^2}{3}.$$

This last equality implies that the function

$$z \mapsto \xi_j(z) - \frac{t_1 + z^2}{3}$$

is zero at the point $u_0 \in J_j$, contradicting Corollary 5.6. \square

In the same spirit as at the end of Section 5.2, for $(t_0, t_1) \in \mathcal{F}_2$ we introduce the quantities

$$\tau_1 = \operatorname{Re} \int_{z_2^{(3)}}^{z_1^{(3)}} Q(s) ds = \operatorname{Re} \int_{z_2}^{z_1} (\xi_1(s) - \xi_2(s)) ds, \quad (5.26)$$

$$\tau_2 = \operatorname{Re} \int_{z_2^{(2)}}^{z_1^{(2)}} Q(s) ds = \operatorname{Re} \int_{z_2}^{z_1} (\xi_1(s) - \xi_3(s)) ds, \quad (5.27)$$

$$\tau_3 = \operatorname{Re} \int_{z_2^{(3)}}^{\hat{z}_2^{(3)}} Q(s) ds = \operatorname{Re} \int_{z_2}^{\hat{z}_2} (\xi_1(s) - \xi_2(s)) ds, \quad (5.28)$$

$$\tau_4 = \operatorname{Re} \int_{z_2^{(1)}}^{z_1^{(1)}} Q(s) ds = \operatorname{Re} \int_{z_2}^{z_1} (\xi_2(s) - \xi_3(s)) ds, \quad (5.29)$$

$$\tau_5 = \operatorname{Re} \int_{z_0^{(2)}}^{\hat{z}_0^{(2)}} Q(s) ds = \operatorname{Re} \int_{z_0}^{\hat{z}_0} (\xi_1(s) - \xi_3(s)) ds, \quad (5.30)$$

$$\tau_6 = -\operatorname{Re} \int_{z_1^{(1)}}^{z_0^{(1)}} Q(s) ds = \operatorname{Re} \int_{z_1}^{z_0} (\xi_3(s) - \xi_2(s)) ds, \quad (5.31)$$

The analysis of these quantities is carried over in the Appendix A.2. The important fact for what comes later is that these quantities never vanish for $(t_0, t_1) \in \mathcal{F}_2$.

5.3. Quadratic differential on the spectral curve: general principles. For a point $p \in \overline{\mathbb{C}}$, recall that $p^{(j)}$ denotes its preimage under the canonical projection $\pi : \mathcal{R} \mapsto \overline{\mathbb{C}}$ that lies on the sheet \mathcal{R}_j . Additionally, the points $z_j, \hat{z}_j, j = 0, 1, 2$, are given by Theorem 4.1.

We use Theorem 4.1, equations (4.28), (4.33) and the asymptotics (2.15) to find all critical points of ϖ . For $(t_0, t_1) \in \mathcal{F}_1$ they are as follows

- Double zeros at the branch points $z_0^{(1)} = z_0^{(3)}, z_1^{(1)} = z_1^{(2)}, z_2^{(1)} = z_2^{(2)}$;
- Double zeros at $\hat{z}_0^{(2)}, \hat{z}_1^{(3)}, \hat{z}_2^{(3)}$;
- Simple zeros at $z_0^{(2)}, z_1^{(3)}, z_2^{(3)}$;
- A pole of order 5 at $\infty^{(1)}$ and a pole of order 14 at $\infty^{(2)} = \infty^{(3)}$,

whereas for $(t_0, t_1) \in \mathcal{F}_2$ the critical points are given by

- Double zeros at the branch points $z_0^{(1)} = z_0^{(3)}, z_1^{(1)} = z_1^{(3)}, z_2^{(2)} = z_2^{(3)}$;
- Double zeros at $\hat{z}_0^{(2)}, \hat{z}_1^{(3)}, \hat{z}_2^{(3)}$;
- Simple zeros at $z_0^{(2)}, z_1^{(2)}, z_2^{(1)}$;
- A pole of order 5 at $\infty^{(1)}$ and a pole of order 14 at $\infty^{(2)} = \infty^{(3)}$.

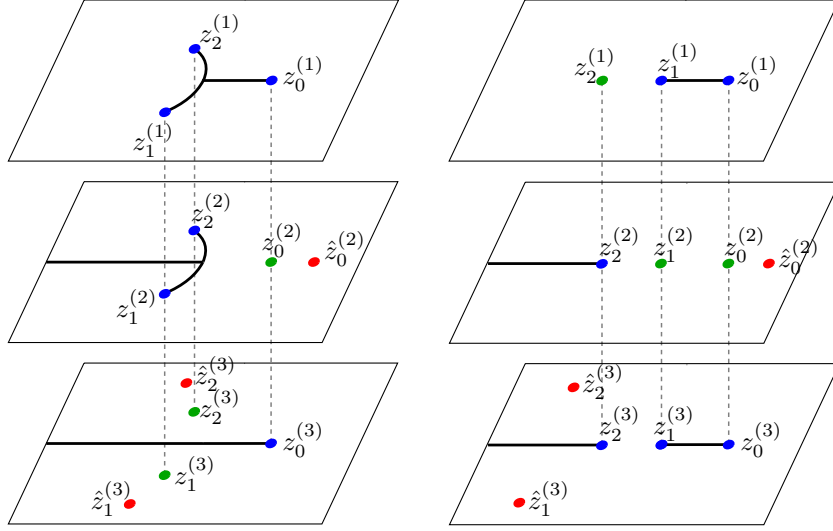


FIGURE 15. The critical points of ϖ : on the left for $(t_0, t_1) \in \mathcal{F}_1$ and on the right for $(t_0, t_1) \in \mathcal{F}_2$. Blue dots represent the zeros that are also branch points, red dots represent the remaining double zeros, and green dots represent simple zeros. In addition, there are also poles at the points at infinity.

These critical points are shown in Figure 15. From the general theory, it is known that there are $n + 2$ trajectories emanating from a given zero of order n , and any two consecutive trajectories form an angle $2\pi/(n + 2)$ at the zero.

It is time to fix some notation concerning the critical trajectories. From a given zero $p^{(j)} \in \mathcal{R}_j$ emanate a number of critical trajectories on \mathcal{R}_j , which we denote by $\gamma_0(p^{(j)}), \gamma_1(p^{(j)}), \dots$; we make the convention that these trajectories are labeled in such a way that their canonical projections $\pi(\gamma_0(p^{(j)})), \pi(\gamma_1(p^{(j)})), \dots$, are enumerated in the anti-clockwise direction, starting on the positive horizontal direction. This is well defined as long as there are no trajectories emanating along branch cuts, situation that will not occur. We also note that if $p^{(k)} = p^{(j)}$ is a branch point joining two sheets \mathcal{R}_j and \mathcal{R}_k , the trajectories $\gamma_l(p^{(j)}), \gamma_l(p^{(k)})$ are different, because they emanate from different sheets. We refer the reader to Figure 16 for an example.

Similar notation is adopted at the poles $\infty^{(1)}, \infty^{(2)} = \infty^{(3)}$. In this case, there are certain directions, henceforth called *critical directions* and denoted $\theta_0^{(k)}, \theta_1^{(k)}, \dots$, along which any trajectory extending to $\infty^{(k)}$ has to do so along one of the critical directions $\theta_0^{(k)}, \theta_1^{(k)}, \dots$. These directions are easily computed to be given by the angles

$$\theta_j^{(1)} = \frac{\pi}{3} + \frac{2\pi}{3}j, \quad j = 0, 1, 2, \quad \theta_j^{(2)} = \theta_j^{(3)} = \frac{\pi}{6} + \frac{\pi}{3}j, \quad j = 0, \dots, 5.$$

Note that \mathcal{R} is branched at $\infty^{(2)} = \infty^{(3)}$, so in the same spirit as for finite branch points, although the numerical values for $\theta_j^{(2)}$ and $\theta_j^{(3)}$ are the same, we refer to

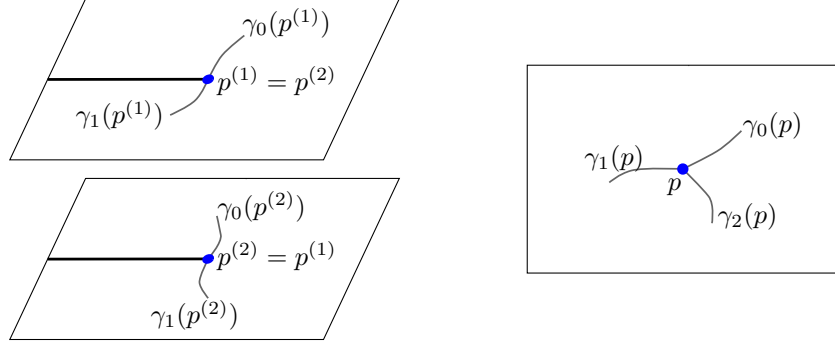


FIGURE 16. Example of critical trajectories' labeling around critical points. On the left-hand side, around the double zero $p^{(1)} = p^{(2)}$ connecting two sheets of the Riemann surface. On the right, around the simple zero p which is not a branch point.

$\theta_j^{(2)}$ as the critical direction on the sheet \mathcal{R}_2 , whereas $\theta_j^{(3)}$ as the critical direction on the sheet \mathcal{R}_3 .

Given $p \in \mathcal{R}$, we define the number $\eta(p)$ as follows.

- If p is a regular point of ϖ , then $\eta(p) = 0$.
- If p is a zero of ϖ , then $\eta(p)$ is its order as a zero.
- If p is a pole of ϖ , then $\eta(p)$ is minus its order as a pole.

Clearly $\eta(p) > 0$ iff p is a zero, and $\eta(p) < 0$ iff p is a pole.

A domain $D \subset \mathcal{R}$ is called a ϖ -*polygon* if its boundary ∂D is the union of a finite number of critical trajectories. For a ϖ -polygon D , we define the quantities

$$\lambda(D) = \sum_{p \in D} \eta(p)$$

and

$$\kappa(D) = \sum_{p \in \partial D} \beta(p),$$

where the summation for κ is over all critical points on the boundary of D ,

$$\beta(p) = 1 - \theta(p) \frac{\eta(p) + 2}{2\pi}$$

and $\theta(p) = \theta(D; p)$ is the inner angle of D at p .

If D is simply connected, the formula

$$\kappa(D) = 2 + \lambda(D) \tag{5.32}$$

holds true. It is a consequence of the argument principle and is known as *Teichmüller Lemma* or *Teichmüller formula* [57, Theorem 14.1].

Recall that \mathcal{G} denotes the critical graph of ϖ (see (5.3) and the discussion thereafter). The critical graph \mathcal{G} can be decomposed as a finite union

$$\mathcal{G} = \bigcup \mathcal{U}, \tag{5.33}$$

where the sets \mathcal{U} 's are pairwise disjoint ϖ -polygons without critical points. For a quadratic differential without recurrent trajectories, we can classify the sets on the decomposition above into four distinct groups, namely: *strip* domains, *half plane*

(or *end*) domains, *circle* domains and *ring* domains. This classification is known as the *Basic Structure Theorem* [32, Theorem 3.5]. For our quadratic differential ϖ in (5.2), only the first two types of domain appear, and we explain their definition and basic properties next, in a form suitable for our needs.

A ϖ -polygon \mathcal{U} in the decomposition (5.33) is called a half plane domain if the primitive

$$\Upsilon(z) = \int^z Q(s)ds, \quad z \in \mathcal{U} \quad (5.34)$$

is a conformal map from \mathcal{U} to a half plane on \mathbb{C} of the form

$$\{z \in \mathbb{C} \mid \delta \operatorname{Re} z > c\},$$

for some real constant c and some $\delta \in \{1, -1\}$. The boundary of a half plane domain contains exactly one infinite critical point p and at least one finite critical point of ϖ . Locally at p , $\partial\mathcal{U}$ consists of two arcs of trajectories that end at p along two consecutive critical directions.

Conversely, any two consecutive critical directions at a given infinite critical point uniquely determine a half plane domain in the decomposition (5.33).

In the same spirit, \mathcal{U} is called a strip domain if the primitive Υ in (5.34) is a conformal map from \mathcal{U} to a strip on \mathbb{C} of the form

$$\{z \in \mathbb{C} \mid c_1 < \operatorname{Re} z < c_2\}$$

for some real constants c_1, c_2 . The boundary of \mathcal{U} contains two infinite critical points p_1, p_2 (possibly $p_1 = p_2$). The set $\partial\mathcal{U} \setminus \{p_1, p_2\}$ has two connected components, and each of them contains at least one finite critical point. Moreover, the inner angle of $\partial\mathcal{U}$ at each finite critical point is zero (that is, $\beta(p_1) = \beta(p_2) = 1$).

The positive number

$$\sigma(\mathcal{U}) = c_2 - c_1$$

is well defined regardless of the exact choice of the integration constant in (5.34), and it is called the *width* of the strip domain. For the quadratic differential ϖ in (5.2), it can be explicitly computed by

$$\sigma(\mathcal{U}) = |\Upsilon(q_1) - \Upsilon(q_2)| = \left| \operatorname{Re} \int_{q_2}^{q_1} Q(s)ds \right|, \quad (5.35)$$

where q_1, q_2 are any two points on different connected components of $\partial\mathcal{U} \setminus \{p_1, p_2\}$, and the integral is computed along any path connecting q_1 and q_2 that lies entirely in $\overline{\mathcal{U}}$.

Recall that $\pi_j : \mathcal{R}_j \rightarrow \overline{\mathbb{C}}$ denotes the restriction of the canonical projection $\pi : \mathcal{R} \rightarrow \overline{\mathbb{C}}$ to the sheet \mathcal{R}_j . We follow [45] and list some general principles regarding trajectories of quadratic differentials. These principles will be extensively used later on.

- P.1** The quadratic differential ϖ does not have recurrent trajectories, as it follows from Jenkins' Three Poles Theorem [47, Thm. 8.5, page 226]. Consequently, any trajectory γ of ϖ has a well defined limiting point along its two directions (possibly the same, in case γ is closed).
- P.2** If $\gamma \subset \mathcal{R}_j$ is an arc of trajectory of ϖ , then the arc $\gamma^* = \pi_j^{-1}(\pi(\gamma)^*)$, obtained as the lift of the complex conjugate of $\pi(\gamma)$ to \mathcal{R}_j , is also an arc of trajectory.
- P.3** If a ϖ -polygon does not have poles on its interior, then it has to have poles on its boundary. This is a consequence of (5.32).

- P.4** The function Q^2 in (5.2) is analytic on the parameters (t_0, t_1) . Consequently the trajectories of ϖ change continuously (in any reasonable topology) with the parameters (t_0, t_1) . In our setting, it is enough to have the following observation. Choose a critical point p of ϖ , varying continuously with the parameter (t_0, t_1) . Fix $(\tilde{t}_0, \tilde{t}_1)$ and assume that for small perturbations of $(\tilde{t}_0, \tilde{t}_1)$ the order of the critical point p is preserved and that a given open set $U \subset \mathcal{R}$ does not contain critical points of ϖ . If for $(\tilde{t}_0, \tilde{t}_1)$ the critical trajectory emanating from p along a given direction intersects the open set U , then the same holds true for small perturbations of $(\tilde{t}_0, \tilde{t}_1)$.
- P.5** If for a given value $(\tilde{t}_0, \tilde{t}_1)$, a point p belongs to the half plane domain for the pole $\infty^{(k)}$ determined by the critical angles $\theta_j^{(k)}, \theta_{j+1}^{(k)}$, then the same holds true for parameters on a small neighborhood of $(\tilde{t}_0, \tilde{t}_1)$. The point p can depend continuously on (t_0, t_1) .
- P.6** If for a given value $(\tilde{t}_0, \tilde{t}_1)$, an arc of trajectory emerging from a certain point p intersects the real line at a *regular* point, then the same holds true for small perturbations of $(\tilde{t}_0, \tilde{t}_1)$. As before, the point p can depend continuously on the parameters.

When $t_1 = 0$ we will make use of one more principle, which will be enunciated in Section 5.4.

5.4. Critical graph in the three-cut case. This section is devoted to the description of the critical graph in the three-cut case $(t_0, t_1) \in \mathcal{F}_1$. We will use extensively the principle **P.1** without further mention. More precisely, in our situation this principle assures us that every trajectory has a limiting endpoint in its both directions, and our goal will be to, starting at a given critical trajectory emanating from a critical point, find its other endpoint.

5.4.1. Critical graph for $t_1 = 0$. We first describe the critical graph for $t_1 = 0$. To this end, we use the sheet structure in (5.5).

For $t_1 = 0$, the algebraic equation (2.12) is invariant under the action

$$(\xi, z) \mapsto (\omega^2 \xi, \omega z),$$

where we recall that $\omega = e^{2\pi i/3}$. With regard to the sheet structure (5.5), this discrete rotational symmetry is reflected on the trajectories of ϖ , and it leads to the following principle.

- P.7** Suppose $t_1 = 0$. If $\gamma \subset \tilde{\mathcal{R}}_j$ is an arc of trajectory, then the arc $\tilde{\gamma} = \pi_j^{-1}(\omega\pi(\gamma))$, obtained as the lift of $\omega\pi(\gamma)$ to $\tilde{\mathcal{R}}_j$, is also an arc of trajectory.

Some of the trajectories of ϖ are straightforward to describe. On the interval $(-\infty, 0)$, the solutions ξ_2 and ξ_3 are complex conjugate of each other (see (5.10)), and the same is true for ξ_1 and ξ_2 on $(0, z_0)$ (see (5.9)). It thus follows from the definition of a trajectory in (5.3) that

$$\gamma_1(z_0^{(3)}) = \pi_1^{-1}((-\infty, 0]) \cup \pi_3^{-1}([0, z_0]), \quad (5.36)$$

that is, the trajectory $\gamma_1(z_0^{(3)})$ starts to the left of $z_0^{(3)}$, moves to the sheet $\tilde{\mathcal{R}}_1$ and goes to $\infty^{(1)}$ along the negative axis. Using the principle **P.7**, we also get the trajectories $\gamma_0(z_1^{(3)})$ and $\gamma_2(z_2^{(3)})$. These are depicted in Figure 17.

We now focus on the trajectory $\gamma_0(z_0^{(1)})$.

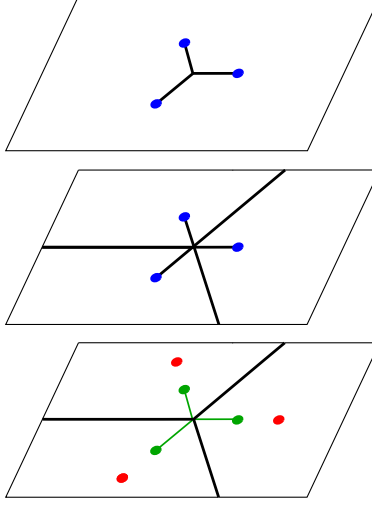


FIGURE 17. In thin lines the trivial trajectories of ϖ in the large are depicted; these are the trajectories described by equations (5.36)–(5.36). In thick lines the branch cuts for the Riemann surface.

Lemma 5.8. *The trajectory $\gamma_0(z_0^{(1)})$ goes to $\infty^{(1)}$ with angle $\theta_0^{(1)}$ and it is entirely contained in $\tilde{\mathcal{R}}_1$*

Proof. We first claim that the trajectory $\gamma_0(z_0^{(1)})$ cannot intersect the interval $\pi_1^{-1}((z_0, +\infty))$. Indeed, to the contrary we use the principle **P.2** to get the equality $\gamma_0(z_0^{(1)}) = \gamma_1(z_0^{(1)})$. In particular, this implies that $\gamma_0(z_0^{(1)})$ is the boundary of a ϖ -polygon without poles on its closure, contradicting **P.3**.

The trajectory $\gamma_0(z_0^{(1)})$ cannot intersect the interval $\pi_{1+}^{-1}([0, z_0])$ neither. To see this, suppose it does, say at a point which projects to $x_0 \in [0, z_0]$. It then follows from (5.3) and the definition of ϖ (5.2) that

$$\operatorname{Re} \int_{x_0}^{z_0} (\xi_2(z) - \xi_3(z)) dz = \int_{x_0}^{z_0} (\operatorname{Re} \xi_{2+}(x) - \operatorname{Re} \xi_{3+}(x)) dx = 0, \quad (5.37)$$

where the first integral is computed along $\pi(\gamma_0(z_0^{(1)}))$, and the second integral, obtained after deformation of the contour for the first one, is performed on \mathbb{R} . This is the same as saying that $h_2(x_0, z_0) = 0$, contradicting Lemma 5.1 (i).

In summary, we proved that the trajectory $\gamma_0(z_0^{(1)})$ does not intersect the arc $\pi_1^{-1}([0, +\infty))$. Since it cannot intersect the segment $\pi_1^{-1}([0, \infty e^{\pi i/3}))$, because this is an arc of the trajectory $\gamma_0(z_1^{(3)})$, the only possibility left is that it goes to $\infty^{(1)}$ with angle $\theta_0^{(1)}$, as we want. \square

Using the principles **P.2** and **P.7**, we also get the behavior of the trajectories $\gamma_1(z_0^{(1)})$, $\gamma_j(z_k^{(1)})$, $k = 1, 2$, $j = 0, 1$. The outcome we have so far is displayed in Figure 18.

Recall that L_0 , L_1 and L_2 denote the segments connecting the sheets $\tilde{\mathcal{R}}_2$ and $\tilde{\mathcal{R}}_3$ (see (5.4)).

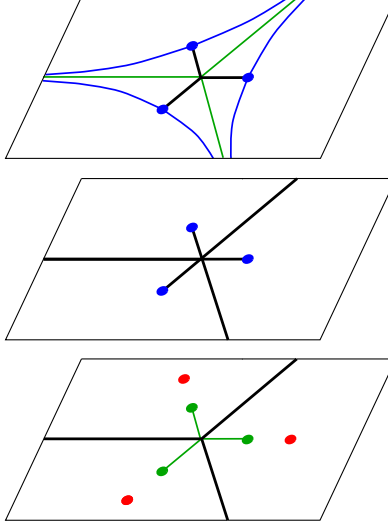


FIGURE 18. Trajectories of ϖ in the large after equations (5.36)–(5.36) and Lemma 5.8.

Lemma 5.9. *The trajectory $\gamma_0(z_0^{(3)})$, intersects the cut L_2 exactly once, moves to the sheet $\tilde{\mathcal{R}}_2$ and then extends to $\infty^{(2)}$ along the critical angle $\theta_1^{(2)}$.*

Proof. We first prove that $\gamma_0(z_0^{(3)})$ moves to $\tilde{\mathcal{R}}_2$.

The trajectory $\gamma_0(z_0^{(3)})$ cannot intersect $\pi_3^{-1}([z_0, +\infty))$, otherwise the principle **P.2** tells us that $\gamma_0(z_0^{(3)}) = \gamma_2(z_0^{(3)})$, and this trajectory then determines a ϖ -polygon without poles on its closure, contradicting the principle **P.3**. So if we assume it does not move to $\tilde{\mathcal{R}}_2$, it has to extend to $\infty^{(3)}$ with angle $\theta_0^{(3)}$, and as a consequence of the principle **P.2** we further get that $\gamma_2(z_0^{(3)})$ ends up at $\infty^{(3)}$ with angle $\theta_3^{(5)}$. We then apply Teichmüller's formula (5.32) to the ϖ -polygon determined by these two trajectories that contains $\hat{z}_0^{(3)}$. On the boundary there are two critical points, namely $z_0^{(3)}$ and $\infty^{(3)}$, and the sum on the left hand side of (5.32) is equal to 2. On the interior, there is only the double zero $\hat{z}_0^{(3)}$, so the sum on the right hand side of (5.32) is 4, a contradiction.

It is a conclusion of the last paragraph that the trajectory $\gamma_0(z_0^{(3)})$ goes to $\tilde{\mathcal{R}}_2$. Combining **P.2** and **P.7**, we further get that the trajectories $\gamma_2(z_0^{(3)})$, $\gamma_j(z_1^{(3)})$ and $\gamma_{j-1}(z_2^{(3)})$ also move to $\tilde{\mathcal{R}}_2$, $j = 1, 2$.

We now prove that $\gamma_0(z_0^{(3)})$ intersects L_2 exactly once. Again in virtue of the principles **P.2** and **P.7**, it is enough to verify that $\gamma_1(z_2^{(3)})$ intersects L_0 exactly once.

We already showed that $\gamma_1(z_2^{(3)})$ intersects L_0 at least once, say at a point projecting to $x \in (-\infty, 0)$. Suppose now that $\gamma_1(z_2^{(3)})$ intersects L_0 at another point, say projecting to $y \in (-\infty, 0)$. For simplicity, assume $x < y$, the case $x > y$ is analogous. Proceeding as in (5.37), we conclude that

$$h(x, y) = h(y, 0) = 0.$$

From Lemma 5.1 (ii), we learn that $(x, y) \cap (y, 0) \neq \emptyset$, which is certainly not true. We also remark that a combination of the principles **P.2** and **P.7** yield that $\gamma_0(z_2^{(3)})$ intersects the cut L_2 exactly once.

As a final step, we prove that $\gamma_0(z_0^{(3)})$ extends to $\infty^{(2)}$ with critical angle $\theta_1^{(2)}$. Again due to **P.2** and **P.7**, it is enough to prove that $\gamma_0(z_2^{(3)})$ extends to $\infty^{(2)}$ with angle $\theta_1^{(2)}$. The latter fact follows if we prove that $\gamma_0(z_2^{(3)})$ stays in the sector of $\tilde{\mathcal{R}}_2$ determined by the positive real axis and L_2 . Since we already noticed that $\gamma_0(z_2^{(3)})$ intersects L_0 exactly once and then enters this sector, it is enough to verify that $\gamma_0(z_2^{(3)})$ does not intersect the positive real axis on $\tilde{\mathcal{R}}_2$.

Suppose the latter happens, say at a certain point projecting to $x \in [0, \infty)$. There are two possibilities, namely either $0 \leq x \leq z_0$ or $x > z_0$.

For the first situation, we note that in this case the integral

$$\int_{0^{(3)}}^{x^{(2)}} Q(s) ds,$$

computed along the contour $\gamma_2(z_2^{(3)}) \cup \gamma_0(z_2^{(3)})$, is purely imaginary. Deforming this integral to the interval $\pi_{2+}^{-1}([0, x])$ we conclude

$$\int_0^x (\operatorname{Re} \xi_{1+}(s) - \operatorname{Re} \xi_{3+}(s)) ds = 0,$$

and the equation above contradicts Lemma 5.1 (i).

Now let us assume that $x > z_0$. Using **P.2**, this assumption implies that $\gamma_0(z_2^{(3)}) = \gamma_2(z_1^{(3)})$. The trajectories $\gamma_2(z_2^{(3)})$, $\gamma_0(z_2^{(3)})$, $\gamma_2(z_1^{(3)})$ then determine a ϖ -polygon whose only critical point in its interior is the double zero $z_0^{(1)} = z_0^{(2)}$ (this is the shaded domain in Figure 19). The right hand side of (5.32) is then 4, whereas the left hand side is 2, which is a contradiction. \square

Again after an application of the principles **P.2** and **P.7**, we get the partial configuration in Figure 20

Lemma 5.10. *The trajectories $\gamma_0(z_0^{(2)})$ and $\gamma_1(z_0^{(2)})$ extend to $\infty^{(2)}$ along critical angles $\theta_0^{(2)}$ and $\theta_5^{(2)}$, respectively.*

Proof. The trajectory $\gamma_0(z_0^{(2)})$ cannot intersect $\pi_{2+}^{-1}([0, z_0])$ neither. Otherwise, if it does so at a point $x_+^{(2)}$, then

$$0 = \int_0^{x_+^{(2)}} Q(s) ds = \int_0^x (\operatorname{Re} \xi_{2+}(s) - \operatorname{Re} \xi_{3+}(s)) ds,$$

where for the first integral we integrate over $\gamma_0(z_0^{(2)})$, and then we deform this contour of integration to the real line to get the second equality. Since $x \in (0, z_0]$, this is in contradiction with Lemma 5.1 (i).

Having in mind **P.2**, a consequence of the discussion above is that the trajectories $\gamma_0(z_0^{(2)})$ and $\gamma_1(z_0^{(2)})$ have to stay in the region on $\tilde{\mathcal{R}}_2 \cup \tilde{\mathcal{R}}_3$ determined by the contour $\gamma_0(z_2^{(3)}) \cup \gamma_2(z_2^{(3)}) \cup \gamma_0(z_1^{(3)}) \cup \gamma_2(z_1^{(3)})$. Additionally, the trajectory $\gamma_0(z_0^{(2)})$ cannot intersect $\pi_2^{-1}([z_0, \infty))$, otherwise using **P.2** we conclude that $\gamma_0(z_0^{(2)}) = \gamma_1(z_0^{(2)})$, and this trajectory then determines a ϖ -polygon without poles on its

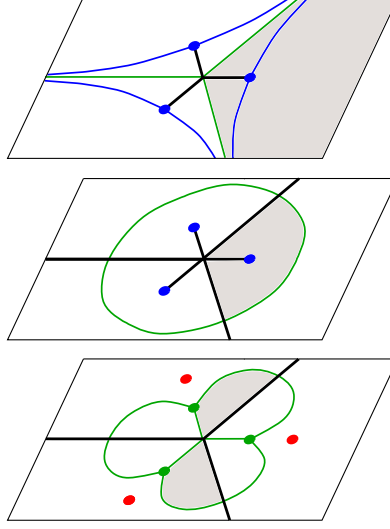


FIGURE 19. Figure for the hypothetical situation considered in the proof of Lemma 5.9. The shaded region is the ϖ -polygon contradicting Teichmüller's formula (5.32).

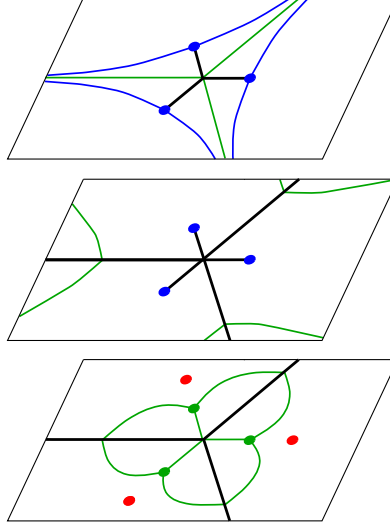


FIGURE 20. Trajectories of ϖ in the large after Lemma 5.9. Compare with the previous stage in Figure 18

closure, contradicting **P.3**. The only possibility left is the description claimed by the Lemma. \square

Again using **P.2** and **P.7**, we translate the previous Lemma to the trajectories emanating from $z_1^{(2)}, z_2^{(2)}$. The outcome is displayed in Figure 21.

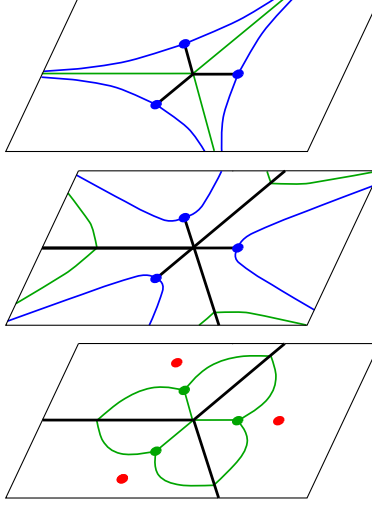


FIGURE 21. Trajectories of ϖ in the large after Lemma 5.10. Compare with the previous stage in Figure 20.

Lemma 5.11. *The trajectory $\gamma_0(\hat{z}_0^{(3)})$ never leaves $\tilde{\mathcal{R}}_3$ and extends to $\infty^{(3)}$ with critical angle $\theta_0^{(3)}$. The trajectory $\gamma_1(\hat{z}_0^{(3)})$ intersects the cut L_0 on $\tilde{\mathcal{R}}_3$ exactly once, moves to the sheet $\tilde{\mathcal{R}}_2$ and extends to $\infty^{(2)}$ along the critical direction $\theta_1^{(2)}$.*

Proof. An integral deformation argument similar to the one presented in the proof of Lemma 5.9 shows that any contour of the form $\gamma_k(\hat{z}_0^{(3)}) \cup \gamma_j(\hat{z}_0^{(3)})$, $j, k \in \{1, 2, 3, 4\}$, $j \neq k$, intersects each of the cuts L_0 and L_2 at most once. Moreover, these contours cannot be bounded closed loops in $\tilde{\mathcal{R}}_3$, otherwise we would get a contradiction to **P.3**.

There are two critical directions in the sector $-\frac{\pi}{3} < \arg z < \frac{\pi}{3}$ in $\tilde{\mathcal{R}}_3$, namely $\theta_0^{(3)}$ and $\theta_5^{(3)}$, so from the local behavior of trajectories near the pole $\infty^{(3)}$ we know that at most two trajectories from $\hat{z}_0^{(3)}$ can extend to $\infty^{(3)}$.

Combining the last two paragraphs, the only possibility left is that $\gamma_0(\hat{z}_0^{(3)})$ and $\gamma_3(\hat{z}_0^{(3)})$ stay in $\tilde{\mathcal{R}}_3$ and go to $\infty^{(3)}$ along the critical directions $\theta_0^{(3)}$ and $\theta_5^{(3)}$, respectively, and the trajectories $\gamma_1(\hat{z}_2^{(3)})$ and $\gamma_2(\hat{z}_2^{(3)})$ intersect the cuts L_0 and L_2 , respectively, and move to $\tilde{\mathcal{R}}_2$.

Consequently, we use **P.2** and **P.7** to get that $\gamma_1(\hat{z}_1^{(3)})$ has to intersect the branch cut L_0 on $\tilde{\mathcal{R}}_3$ and move to the sheet $\tilde{\mathcal{R}}_3$. Similarly as before, we also get that $\gamma_1(\hat{z}_1^{(3)})$ intersects L_0 at exactly one point. Indeed, due to the constrained geometry we have, this trajectory has to end up at a critical point on $\tilde{\mathcal{R}}_1 \cup \tilde{\mathcal{R}}_2$. Hence it has to cross L_0 an odd number of times. If $x_1 < y_1$ are any two points of intersection of $\gamma_1(\hat{z}_1^{(3)})$, we get $h(x_1, y_1) = 0$, as it follows from deformation of integrals as we did above. From Lemma 5.1 (ii) we then conclude that there can be at most two of such points x_1, y_1 . Since the number of intersections is odd, we conclude that actually there is exactly one intersection point.

Using again **P.2** and **P.7**, we translate the outcome of the previous paragraph to the trajectory $\gamma_0(\hat{z}_0^{(3)})$, concluding that it intersects L_2 exactly once, and thus

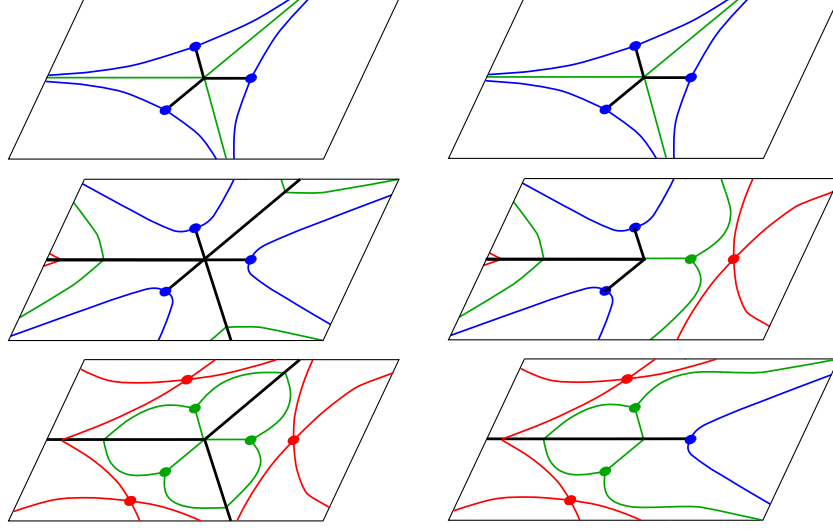


FIGURE 22. Critical graph of ϖ for $t_1 = 0$ before (left) and after (right) the regluing $\tilde{\mathcal{R}} \mapsto \mathcal{R}$.

it has to stay in $\tilde{\mathcal{R}}_2$. Consequently, the only possibility left for its behavior in the large is that it has to extend to $\infty^{(2)}$ along the critical direction $\theta_1^{(2)}$, concluding the proof. \square

Using the principles **P.2** and **P.7**, it is straightforward to get from Lemma 5.11 the behavior of the trajectories emanating from the double zeros $\hat{z}_j^{(3)}$, $j = 0, 1, 2$, hence concluding the description of the critical graph of ϖ for $t_1 = 0$, as can be seen in Figure 22. For later convenience, we also reverse the regluing $\tilde{\mathcal{R}}_j \mapsto \mathcal{R}_j$, and the result is also displayed in Figure 22.

5.4.2. Planar realization of the critical graph for $t_1 = 0$. A planar realization of \mathcal{G} for $t_1 = 0$ can be seen in Figure 23. It consists of a rectangle whose top and bottom are identified, and whose left and right rims correspond, respectively, to the poles $\infty^{(2)} = \infty^{(3)}$ and $\infty^{(1)}$. On each of these rims, there are a number of marked points, corresponding to the critical directions at the respective poles.

From its planar realization, it is easy to identify the strip and end domains of \mathcal{G} . We denote the strip domains by \mathcal{S}_j , $j = 1, \dots, 9$, labeling them according to Figure 23.

5.4.3. Deformation of the critical graph in the three-cut case. We now prove that the critical graph depicted in Figure 23 is always valid in the three-cut case, that is, for $(t_0, t_1) \in \mathcal{F}_1$. According to the principle **P.4**, this is the case as long as

- (i) Existing zeros of ϖ do not coalesce and there are no new zeros appearing. This is the case as the discussion at the beginning of Section 5.3 assures us.
- (ii) No new domains appear. Taking into account (i) above, this can only happen if a short trajectory changes its behavior. Since we do not have short trajectories for $t_1 = 0$, we are safe.

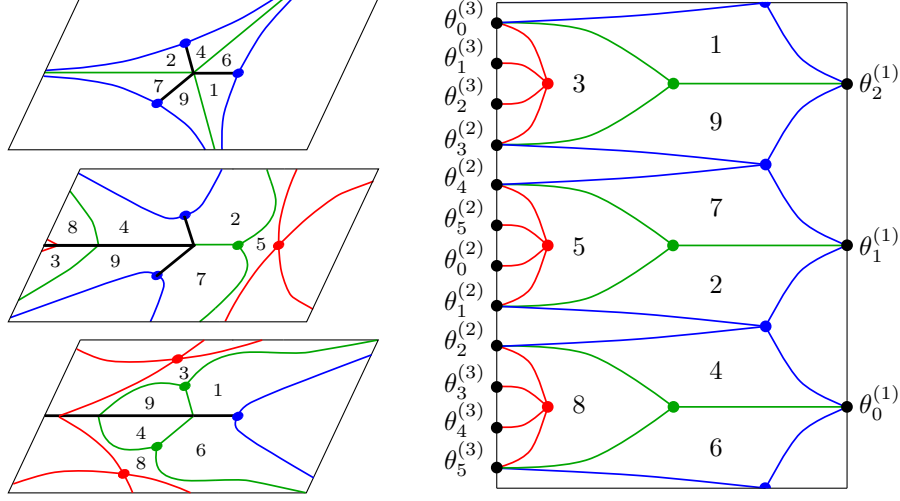


FIGURE 23. On the left panel the critical graph of ϖ in the three-cut case is displayed, and on the right panel its planar realization. The marked black dots on the rims of the rectangle correspond to the critical directions at the poles $\infty^{(1)}$ (right rim) and $\infty^{(2)} = \infty^{(3)}$ (left rim). In both pictures, the number j indicates the strip domain \mathcal{S}_j .

- (iii) The existing strip domains do not shrink. This amounts to showing that their widths do not vanish. For $j = 1, \dots, 5$, the identity $\sigma(\mathcal{S}_j) = |\tau_j|$ follows directly from (5.35) and the definition of τ_j given in (5.13)–(5.17). Consequently, $\sigma(\mathcal{S}_j) \neq 0$ for $j = 1, \dots, 5$ and $(t_0, t_1) \in \mathcal{F}_1$. Moreover, the symmetry under conjugation shows that $\sigma(\mathcal{S}_j) = \sigma(\mathcal{S}_{j-5})$ for $j = 6, \dots, 9$, thus $\sigma(\mathcal{S}_j) \neq 0$ for $j = 6, \dots, 9$ as well.

The considerations (i)–(iii) above hence show that the critical graph displayed in Figure 23 is valid for every choice $(t_0, t_1) \in \mathcal{F}_1$.

5.5. Critical graph in the one-cut case. We now describe the critical graph in the one-cut case $(t_0, t_1) \in \mathcal{F}_2$. We first describe the critical graph of ϖ for values of the parameter $(t_0, t_1) \in \mathcal{F}_2$ that are close to the critical curve γ_c and then prove that the topology of the critical graph remains unchanged when we deform the parameters (t_0, t_1) within \mathcal{F}_2 .

5.5.1. Critical graph in the one-cut case - short range. When (t_0, t_1) approaches the critical curve $\in \gamma_c$ from \mathcal{F}_1 , the critical points $z_1^{(j)}$ and $z_2^{(j)}$, $j = 1, 2$, of ϖ coalesce, thus the behavior of the critical trajectories emanating from these points can possibly (in fact, will) change. Choosing (t_0, t_1) sufficiently close to γ_c , the remaining trajectories emanating from the critical points $z_0^{(1)}$, $z_0^{(2)}$, $\hat{z}_0^{(2)}$, $\hat{z}_1^{(3)}$, $\hat{z}_2^{(3)}$ inherit their behavior already described for parameters on \mathcal{F}_1 . This is true because when we approach γ_c from \mathcal{F}_1 , each of such trajectories do not coalesce with other zeros of ϖ , and from principle **P.4** they have to preserve their behavior.

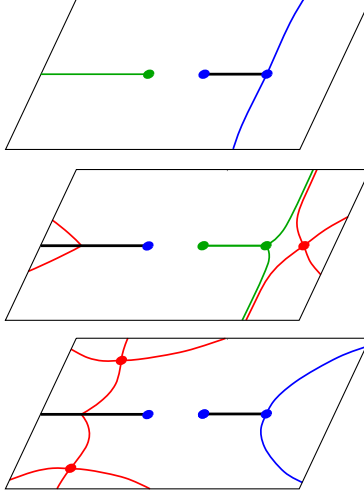


FIGURE 24. Trajectories that are preserved in the one-cut case when (t_0, t_1) is close to γ_c .

Taking into account the relations in the last two equations in (4.34), we get

$$\gamma_1(z_2^{(1)}) = \pi_1^{-1}((-\infty, z_2]), \quad \gamma_1(z_0^{(2)}) = \pi_2^{-1}([z_1, z_0]) = \gamma_0(z_1^{(2)}),$$

so the starting configuration is the one displayed on Figure 24, which at this moment we know it is valid whenever $(t_0, t_1) \in \mathcal{F}_2$ is chosen sufficiently close to γ_c .

Lemma 5.12. *The trajectories $\gamma_0(z_1^{(1)})$, $\gamma_1(z_1^{(1)})$, $\gamma_0(z_1^{(3)})$ and $\gamma_1(z_1^{(3)})$ do not cross the branch cut $[z_1, z_0]$ connecting \mathcal{R}_1 and \mathcal{R}_3 .*

The trajectories $\gamma_0(z_2^{(2)})$, $\gamma_1(z_2^{(2)})$, $\gamma_0(z_2^{(3)})$ and $\gamma_1(z_2^{(3)})$ do not cross the branch cut $(-\infty, z_2]$ connecting \mathcal{R}_2 and \mathcal{R}_3 .

Proof. We deal with $\gamma_0(z_1^{(1)})$. The result for the remaining trajectories follow analogously.

Suppose $\gamma_0(z_1^{(1)})$ crosses the branch cut $[z_1, z_0]$ at a point projecting to x_0 . Deforming the integral over $\gamma_0(z_1^{(1)})$ to the real line, we conclude

$$h_2(z_1, x_0) = \int_{z_1}^{x_0} \operatorname{Re}(\xi_2(x) - \xi_{3+}(x))dx = 0,$$

but this cannot occur, as it follows from Lemma 5.7 (ii) and our assumption that (t_0, t_1) is sufficiently close to γ_c . \square

Lemma 5.13. *The trajectories $\gamma_0(z_1^{(1)})$ and $\gamma_0(z_2^{(1)})$ extend to $\infty^{(1)}$ along the critical angle $\theta_0^{(1)}$.*

The trajectories $\gamma_1(z_1^{(1)})$ and $\gamma_2(z_2^{(1)})$ extend to $\infty^{(1)}$ along the critical angle $\theta_2^{(1)}$.

Proof. From Lemma 5.12, we know that $\gamma_0(z_1^{(1)})$ must stay on the sheet \mathcal{R}_1 , so either $\gamma_0(z_1^{(1)})$ intersects $\pi_1^{-1}([z_2, z_1])$ or it goes to $\infty^{(1)}$. If the former occurs, then we use **P.2** to get that $\gamma_0(z_1^{(1)}) = \gamma_3(z_1^{(1)})$, and consequently it determines a bounded ϖ polygon without poles on its closure, contradicting **P.3**. Hence we conclude that $\gamma_0(z_1^{(1)})$ extends to $\infty^{(1)}$, either along $\theta_0^{(1)}$ or $\theta_1^{(1)}$.

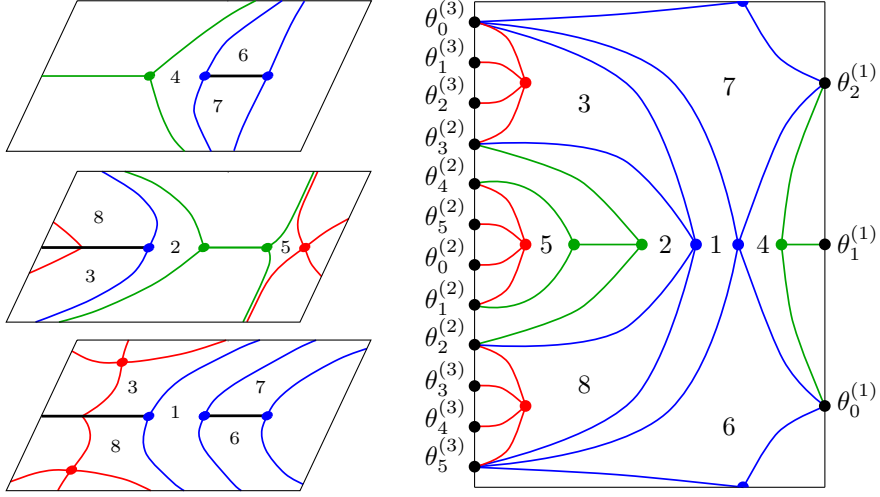


FIGURE 25. On the left the critical graph of ϖ for $(t_0, t_1) \in \mathcal{F}_2$, and on the right its planar realization. The marked black dots on the rims of the rectangle correspond to the critical directions at the poles $\infty^{(1)}$ (right rim) and $\infty^{(2)} = \infty^{(3)}$ (left rim). In both pictures, the number j indicates the strip domain \mathcal{S}_j .

Consequently, the conclusion above forces $\gamma_0(z_2^{(1)})$ to stay in \mathcal{R}_1 , so it also has to go to $\infty^{(1)}$ either along $\theta_0^{(1)}$ or $\theta_1^{(1)}$. We then apply (5.32) to the ϖ -polygon $D \subset \mathcal{R}_1$ determined by the trajectories $\gamma_0(z_2^{(1)})$ and $\gamma_1(z_2^{(1)})$. There are no critical points on D , so the right-hand side of (5.32) is equal to 2. Moreover, a simple computation shows that $\beta(z_2^{(1)}) = 0$, so

$$\beta(\infty^{(1)}) = 2 - \beta(z_2^{(1)}) = 2,$$

and then $\theta(\infty^{(1)}, D) = \frac{\pi}{3}$. Consequently, $\gamma_0(z_2^{(1)})$ extends to $\infty^{(1)}$ along $\theta^{(1)}$, and the same has to hold for $\gamma_0(z_1^{(1)})$.

Finally, we get the behavior of the trajectories $\gamma_1(z_1^{(1)})$ and $\gamma_2(z_2^{(1)})$ by simply applying the principle **P.2**. \square

Very similar arguments as for the previous proof also work to describe the behavior of the trajectories emanating from $z_1^{(j)}, z_2^{(j)}, j = 2, 3$. We skip the details.

The final outcome is the critical graph displayed in Figure 25, where we remind the reader that we are assuming $(t_0, t_1) \in \mathcal{F}_2$ is sufficiently close to the critical curve γ_c . In this figure, the planar version of the critical graph (as explained in Section 5.4.2) is also displayed. We denote the strip domains by $\mathcal{S}_j, j = 1, \dots, 8$, labeled as displayed in Figure 25.

5.5.2. Deformation of the critical graph in the one-cut case. We now prove that the critical displayed in Figure 25 is always valid in the one-cut case, that is, for the whole range $(t_0, t_1) \in \mathcal{R}_2$. Similarly as in Section 5.4.3, we use the principle **P.4** to conclude that this is the case as long as

- (i) The order of every critical point of ϖ is preserved and no new critical points appear. This is indeed the case, as discussed at the beginning of Section 5.3.
- (ii) No new domains appear. Taking into account (i) above, this can only occur if a short trajectory changes its behavior. In the present situation, the only critical trajectory is $\gamma_0(z_1^{(2)}) = \gamma_2(z_0^{(2)})$, which lives on the real line, so from principle **P.2** it is clear that this trajectory does not change its behavior.
- (iii) The strip domains do not shrink. As before, it is enough to verify that the widths $\sigma(\mathcal{S}_j)$, $j = 1, \dots, 8$, do not vanish for $(t_0, t_1) \in \mathcal{F}_2$. For $j = 1, \dots, 6$, these are given by $\sigma(\mathcal{S}_j) = |\tau_j|$, where τ_j is as in (5.26)–(5.31), so they do not vanish. Due to the symmetry under conjugation, the remaining widths satisfy $\sigma(\mathcal{S}_j) = \sigma(\mathcal{S}_{j-6})$, $j = 7, 8$, so these do not vanish as well.

From (i)–(iii) above, we finally conclude that the critical graph depicted in Figure 25 is valid for $(t_0, t_1) \in \mathcal{R}_2$.

6. PROOFS OF THEOREMS 2.3, 2.4, 2.9 AND 2.10

In Section 4.3 the Riemann surface \mathcal{R} was constructed as a three-sheeted cover of $\overline{\mathbb{C}}$ with sheets $\mathcal{R}_1, \mathcal{R}_2, \mathcal{R}_3$. Up to this moment, the cut γ_0 used in the construction of \mathcal{R}_1 and \mathcal{R}_2 in the three-cut case (carried out in Section 4.3.1) was quite arbitrary, but in what follows it is important to choose it in an optimal way.

From the analysis of the quadratic differential carried over in Section 5.4 (see in particular Figure 23), we know that the arc of trajectory $\gamma_0(z_1^{(3)}) \cap \mathcal{R}_3$ connects $z_1^{(3)}$ to a point z_* , where $z_* \in (-\infty, z_0)$. We then define $\Sigma_{*,1}$ to be the contour on the complex plane obtained by the projection of this arc of trajectory, that is,

$$\Sigma_{*,1} = \pi \left(\gamma_0(z_1^{(3)}) \cap \mathcal{R}_3 \right). \quad (6.1)$$

In this way $\Sigma_{*,1}$ is an arc with endpoints z_1 and z_* , and it is contained on the lower half plane. We additionally set

$$\Sigma_{*,2} = (\Sigma_{*,1})^* = \pi \left(\gamma_2(z_2^{(3)}) \cap \mathcal{R}_3 \right), \quad (6.2)$$

so that $\Sigma_{*,2}$ is an arc with endpoints z_2 and z_* that is contained on the upper half plane. Furthermore, denote

$$\Sigma_{*,0} = [z_*, z_0], \quad (6.3)$$

where z_* is the point of intersection of $\Sigma_{*,1}$ with the real axis as above.

Following the construction carried out in Section 4.3.1, we then set

$$\gamma_0 = \Sigma_{*,1} \cup \Sigma_{*,2}$$

and

$$\Sigma_* = \Sigma_{*,0} \cup \Sigma_{*,1} \cup \Sigma_{*,2} \quad (6.4)$$

so that the cut for the sheet \mathcal{R}_1 is simply given by

$$\gamma_0 \cup [z_*, z_0] = \Sigma_*.$$

Note also that with this sheet structure, we can further characterize the interval $\Sigma_{*,0}$ by

$$\Sigma_{*,0} = \pi \left(\gamma_1(z_0^{(2)}) \cap \mathcal{R}_2 \right).$$

For the rest of this paper, whenever we refer to the sheet structure $\mathcal{R}_1 \cup \mathcal{R}_2 \cup \mathcal{R}_3$ for \mathcal{R} in the three-cut case, we always assume the cut used in the sheet \mathcal{R}_1 to be

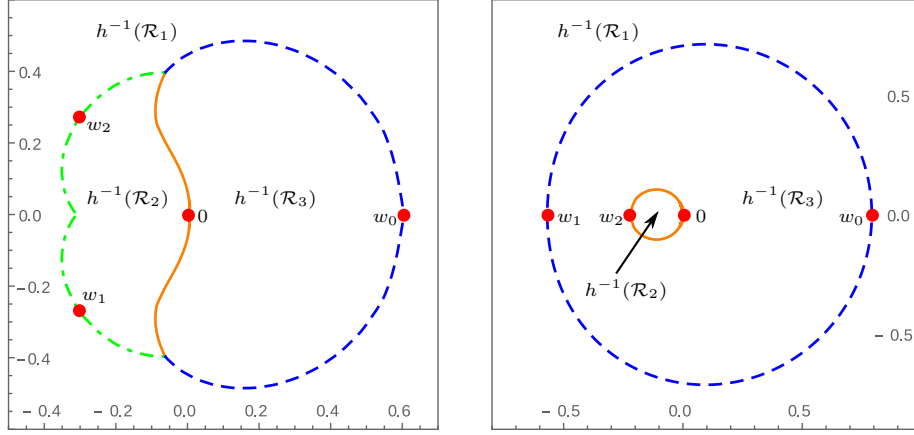


FIGURE 26. The partition of the w -plane into the inverse images of the sheets \mathcal{R}_1 , \mathcal{R}_2 and \mathcal{R}_3 under the conformal map h . The dots are the points w_0, w_1, w_2 and 0 , which are the inverse images of the branch points z_0, z_1, z_2 and $\infty^{(2)}$, respectively. In the left panel the three-cut case \mathcal{F}_1 is considered: the dashed line is the inverse image of the cut $\Sigma_{*,0}$ connecting \mathcal{R}_1 and \mathcal{R}_3 , the dot-dashed line is the inverse image of the cut $\Sigma_{*,1} \cup \Sigma_{*,2}$ connecting \mathcal{R}_1 and \mathcal{R}_2 and the solid line is the inverse image of the cut $(-\infty, z_*)$ connecting \mathcal{R}_2 and \mathcal{R}_3 . In the right panel the one-cut case \mathcal{F}_2 is considered: the dashed line is the inverse image of the cut (z_1, z_0) connecting \mathcal{R}_1 and \mathcal{R}_3 and the solid line is the inverse image of the cut $(-\infty, z_2)$ connecting \mathcal{R}_2 and \mathcal{R}_3 . Numerical output for the choices $r = 1/20$ and $a_0 = 1/10$ (three-cut) and $a_0 = 1/4$ (one-cut).

given by Σ_* as in (6.4). Furthermore, we orient the arcs of Σ_* outwards, that is, $\Sigma_{*,j}$ is oriented from z_* to z_j , $j = 0, 1, 2$.

In the one-cut case, we keep denoting

$$\Sigma_* = [z_1, z_0].$$

In this case it follows from the analysis in Section 5.5 that Σ_* can be alternatively expressed through the identity

$$\Sigma_* = \pi \left(\gamma_0(z_1^{(2)}) \right) = \pi \left(\gamma_1(z_0^{(2)}) \right), \quad (6.5)$$

see in particular Figure 25.

Theorem 2.5 assures us that the function $w \mapsto h(w)$ is a conformal map from $\overline{\mathbb{C}}$ to \mathcal{R} . Standard arguments on conformal mappings allow us to recover the inverse image of each of the sheets \mathcal{R}_1 , \mathcal{R}_2 and \mathcal{R}_3 under h . The outcome can be seen in Figure 26.

With these definitions, the set Σ_* satisfies all the geometric properties claimed by Theorem 2.9, except that we still have to prove the inclusion (2.24). Furthermore, the function ξ_1 in (2.15) admits a meromorphic continuation (that we keep denoting by ξ_1) to the whole sheet $\mathcal{R}_1 = \overline{\mathbb{C}} \setminus \Sigma_*$.

Recalling (3.25) *et seq.*, we also know that the function germ ξ_1 in (2.15) admits another meromorphic continuation S to a neighborhood G of $\mathbb{C} \setminus \Omega$, which is also the

Schwarz function of Ω . However, we emphasize that we do not know yet whether (2.24) is valid, and consequently we cannot be sure if $\xi_1 \equiv S$ in a full neighborhood of $\overline{\mathbb{C}} \setminus \Omega$.

Hence, for a moment we reserve the notation S for the meromorphic continuation of ξ_1 as the Schwarz function as above, and we use ξ_1 to denote the solution to (2.12) that is meromorphic in $\overline{\mathbb{C}} \setminus \Sigma_*$. Once we obtain (2.24), we can then conclude that these two meromorphic continuations coincide in a full neighborhood of $\overline{\mathbb{C}} \setminus \Omega$.

Proof of Theorem 2.9. We now prove all the conclusions of Theorem 2.9, except for the inclusion (2.24).

From the construction of the set Σ_* as above, it follows that ξ_1 is meromorphic on $\overline{\mathbb{C}} \setminus \Sigma_*$, with pole only at ∞ . Hence ξ_1 is analytic in $\mathbb{C} \setminus \Sigma_*$.

Suppose first that $(t_0, t_1) \in \mathcal{F}$. From the sheet structure constructed in Section 4.3.1 (and the cut Σ_* as in (6.4)), it holds true

$$\begin{aligned}\xi_{1-}(s) &= \xi_{3+}(s), \quad s \in \Sigma_{*,0}, \\ \xi_{1-}(s) &= \xi_{2+}(s), \quad s \in \Sigma_{*,1} \cup \Sigma_{*,2}.\end{aligned}$$

Since $\Sigma_{*,0}$, $\Sigma_{*,1}$ and $\Sigma_{*,2}$ are obtained as projections of arcs of the trajectories $\gamma_1(z_0^{(2)})$, $\gamma_0(z_1^{(3)})$ and $\gamma_2(z_2^{(3)})$, respectively (see (6.1)–(6.3)), we get

$$\begin{aligned}(\xi_{1+}(s) - \xi_{1-}(s))ds &= (\xi_{1+}(s) - \xi_{3+}(s))ds \in i\mathbb{R}, \quad s \in \Sigma_{0,*}, \\ (\xi_{1+}(s) - \xi_{1-}(s))ds &= (\xi_{1+}(s) - \xi_{2+}(s))ds \in i\mathbb{R}, \quad s \in \Sigma_{1,*} \cup \Sigma_{2,*}.\end{aligned}$$

This proves (2.25) in the three-cut case. Similarly, we use (6.5) to conclude that (2.25) is satisfied in the one-cut case as well. Furthermore, from its construction it immediately follows that Σ_* satisfies the properties claimed in (i) (in the three-cut case) and (ii) (in the one-cut case).

To prove that μ_* defined in (2.26) is a probability measure, first note that (2.25) automatically implies that it is a real measure. In the three-cut case, its density does not vanish on the arcs $\Sigma_{*,0}$, $\Sigma_{*,1}$ and $\Sigma_{*,2}$ of its support, so this measure has constant sign on each of these arcs. For $t_1 = 0$, we know that this density is positive in each of these arcs [15], so by continuity we conclude that this measure is positive for any pair $(t_0, t_1) \in \mathcal{F}_1$ as well. The total mass of μ_* is given by

$$\frac{1}{2\pi it_0} \int_{\Sigma_*} (\xi_{1-}(z) - \xi_{1+}(z))dz = \frac{1}{2\pi it_0} \oint_{\gamma} \xi_1(s)ds,$$

where γ is a contour positively oriented and encircling Σ_* . We deform γ to infinity and use the expansion (2.15) to get

$$\frac{1}{2\pi it_0} \int_{\Sigma_*} (\xi_{1-}(z) - \xi_{1+}(z))dz = -\frac{1}{t_0} \text{Res}(\xi_1, \infty) = 1,$$

so we conclude that in the three-cut case μ_* is indeed a probability measure.

To conclude that μ_* is positive in the one-cut case as well, note that the density of μ_* is continuous and does not vanish in the interval Σ_* , hence μ_* has constant sign along this interval. Calculations very similar as above show that the total mass of μ_* is 1, in particular μ_* has to be positive, and we then conclude that μ_* is a probability measure, as we want. \square

We remind that to conclude the proof of Theorem 2.9 we still have to verify the inclusion (2.24). To do so, we first have to prove some auxiliary results, which are

inspired from a similar analysis carried out by Balogh, Bertola, Lee and McLaughlin [6].

Recall that the principal value of the Cauchy transform C^λ of a finite and compactly supported measure λ is defined by

$$C^\lambda(z) = \lim_{\varepsilon \rightarrow 0} \int_{|s-z| \geq \varepsilon} \frac{d\lambda(s)}{s-z}, \quad z \in \mathbb{C}.$$

C^λ is analytic on the open sets of $\mathbb{C} \setminus \text{supp } \lambda$ and satisfies the identity

$$2 \frac{\partial U^\lambda}{\partial z}(z) = C^\lambda(z), \quad z \in \mathbb{C} \setminus \text{supp } \lambda, \quad (6.6)$$

where U^λ is the potential of λ as in (2.8).

Lemma 6.1. *For $(t_0, t_1) \in \mathcal{F}$ and V the cubic polynomial (1.12), the Cauchy transform of the measure μ_0 in (2.9) satisfies*

$$C^{\mu_0}(z) = \begin{cases} -\frac{1}{t_0}(\bar{z} - V'(z)), & z \in \bar{\Omega}, \\ -\frac{1}{t_0}(S(z) - V'(z)), & z \in \mathbb{C} \setminus \Omega. \end{cases} \quad (6.7)$$

whereas the Cauchy transform of μ_* in (2.26) satisfies

$$C^{\mu_*}(z) = -\frac{1}{t_0}(\xi_1(z) - V'(z)), \quad z \in \mathbb{C} \setminus \Sigma_*. \quad (6.8)$$

Proof. Suppose $z \in \mathbb{C} \setminus \bar{\Omega}$. Using Green's Theorem and the definition of the Schwarz function S , we can write

$$\begin{aligned} C^{\mu_0}(z) &= \frac{1}{\pi t_0} \iint_{\Omega} \frac{dA(s)}{s-z} \\ &= \frac{1}{2\pi i t_0} \int_{\partial\Omega} \frac{S(s)}{s-z} ds, \end{aligned}$$

where $\partial\Omega$ is oriented counterclockwise. The Schwarz function S is analytic on $\mathbb{C} \setminus \Omega$, so we can deform $\partial\Omega$ to ∞ in order to conclude

$$\begin{aligned} C^{\mu_0}(z) &= -\frac{1}{t_0} \text{Res} \left(\frac{S(s)}{s-z}, s=z \right) - \frac{1}{t_0} \text{Res} \left(\frac{S(s)}{s-z}, s=\infty \right) \\ &= -\frac{1}{t_0} (S(z) - V'(z)), \end{aligned}$$

where we computed the residue at ∞ using the fact that S is an analytic continuation of the function germ ξ_1 in (2.15). This is enough to prove the second equality in (6.7) for $z \in \mathbb{C} \setminus \bar{\Omega}$. Using continuity, this extends to $\partial\Omega$ as well.

Suppose now that $z \in \Omega$. Using the Cauchy-Green formula,

$$\begin{aligned} \bar{z} &= \frac{1}{2\pi i} \int_{\partial\Omega} \frac{\bar{s}}{s-z} ds - \frac{1}{\pi} \iint_{\Omega} \frac{dA(s)}{s-z} \\ &= \frac{1}{2\pi i} \int_{\partial\Omega} \frac{S(s)}{s-z} ds - t_0 C^{\mu_0}(s). \end{aligned}$$

Proceeding as before, we can compute the contour integral on the right-hand side above, concluding that

$$\bar{z} = V'(z) - t_0 C^{\mu_0}(s),$$

which is equivalent to the first equation in (6.7).

Finally, (6.8) follows again by a residue calculation, having in mind the identity

$$C^{\mu_*}(z) = \frac{1}{2\pi i t_0} \int_{\Sigma_*} \frac{\xi_{1-}(s) - \xi_{1+}(s)}{s - z} ds = \frac{1}{2\pi i t_0} \int_{\gamma} \frac{\xi_1(s)}{s - z} ds,$$

where we recall that Σ_* is oriented outwards, and γ is any positively oriented contour encircling Σ_* and for which z is on the exterior region of γ . \square

Recalling (1.12), denote by

$$\mathcal{U}_0(z) = 2U^{\mu_0}(z) + \mathcal{V}(z), \quad z \in \mathbb{C},$$

the total potential of μ_0 , and by

$$\mathcal{U}_*(z) = 2U^{\mu_*}(z) + \mathcal{V}(z), \quad z \in \mathbb{C}, \quad (6.9)$$

the total potential of μ_* .

Proof of Theorem 2.3. Since the partial derivatives of U^{μ_0} are continuous and C^{μ_0} is absolutely convergent in \mathbb{C} , the identity (6.6) for μ_0 is actually valid on Ω as well, and the first equation in (6.7) then says

$$\frac{\partial \mathcal{U}_0}{\partial z}(z) = 0, \quad z \in \Omega.$$

This identity suffices to conclude that \mathcal{U}_0 is constant, say l , on $\overline{\Omega}$, which is the same as (2.10).

The second equality in (6.7) provides an harmonic extension $\tilde{\mathcal{U}}_0$ of \mathcal{U}_0 to a neighborhood of $\partial\Omega$. More concretely, there is a neighborhood G of $\mathbb{C} \setminus \Omega$ and a constant c such that the harmonic function

$$\tilde{\mathcal{U}}_0(z) = -\frac{1}{t_0} \operatorname{Re} \int^z S(s) ds + \frac{|z|^2}{t_0} + c, \quad z \in G,$$

coincides with \mathcal{U}_0 in $\mathbb{C} \setminus \Omega$. Note also that the primitive above does not depend on the path of integration chosen within G , because the residue of S at ∞ is real.

We will prove that

$$\tilde{\mathcal{U}}_0(z_0 + \varepsilon\eta) = l + \frac{2\varepsilon^2}{t_0^2} + \mathcal{O}(\varepsilon^3), \quad \text{as } \varepsilon \rightarrow 0, \quad (6.10)$$

which is enough to conclude (2.11).

On $\partial\Omega$, we know that

$$\frac{\partial \tilde{\mathcal{U}}_0}{\partial z}(z) = -\frac{1}{t_0} (S(z) - \bar{z}) = 0,$$

so the (real) gradient of $\tilde{\mathcal{U}}_0$ vanishes on $\partial\Omega$. Furthermore, the Laplacian of $\tilde{\mathcal{U}}_0$ is

$$\Delta \tilde{\mathcal{U}}_0(z) = 4 \frac{\partial^2 \tilde{\mathcal{U}}_0}{\partial z \partial \bar{z}}(z) = \frac{4}{t_0}, \quad z \in \partial\Omega,$$

and the determinant of the Hessian $H(\tilde{\mathcal{U}}_0)$ of $\tilde{\mathcal{U}}_0$ is

$$\det H(\tilde{\mathcal{U}}_0) = 4 \left(\left(\frac{\partial^2 \tilde{\mathcal{U}}_0}{\partial z \partial \bar{z}} \right)^2 - \frac{\partial^2 \tilde{\mathcal{U}}_0}{\partial z^2} \frac{\partial^2 \tilde{\mathcal{U}}_0}{\partial \bar{z}^2} \right) = \frac{4}{t_0} (1 - |S'(z)|^2),$$

and the latter vanishes on $\partial\Omega$ because $|S'(z)| = 1$ there.

Hence we conclude that the eigenvalues of $H(\tilde{\mathcal{U}}_0)$ are $4/t_0$ and 0. Taking into account that $\tilde{\mathcal{U}}_0$ is constant along $\partial\Omega$, we see that the tangent vector to $\partial\Omega$ is an eigenvector for the eigenvalue 0, and consequently η is an eigenvector associated to $4/t_0$. This is enough to get (6.10). \square

Proof of Theorem 2.4. The conditions (2.10)–(2.11) are enough to conclude that μ_0 is the equilibrium measure of D in the external field \mathcal{V} [50, Theorem I.3.3]. The result is then an immediate consequence of [22, Theorem 4.1]. \square

To prove the inclusion (2.24), we need two more lemmas.

Lemma 6.2. *Suppose $(t_0, t_1) \in \mathcal{F}$. The total potential \mathcal{U}_* does not have a local minimum on Σ_* .*

Proof. Suppose first $z \notin \{z_*, z_0, z_1, z_2\}$. With respect to the outward orientation of Σ_* , denote by n_+ and n_- the normal vectors of Σ_* at z pointing to the positive and negative sides of Σ_* , respectively. Combining (6.6) and (6.8), it follows that

$$\begin{aligned} \frac{\partial \mathcal{U}_*}{\partial n_{\pm}}(z) &= 2 \operatorname{Re} \left(n_{\pm} \frac{\partial \mathcal{U}_{*\pm}}{\partial z}(z) \right) \\ &= \pm 2 \operatorname{Re} \left(n_{\pm} \left(C_{\pm}^{\mu_*}(z) + \frac{1}{t_0}(\bar{z} - V'(z)) \right) \right) \\ &= \pm \frac{2}{t_0} \operatorname{Re} \left(n_{\pm} (\bar{z} - \xi_{1\pm}(z)) \right). \end{aligned}$$

The vector tangent to Σ_* along its positive direction is $\tau_+ = -in_+$, and the equalities above then imply

$$\begin{aligned} \frac{\partial \mathcal{U}_*}{\partial n_+}(z) + \frac{\partial \mathcal{U}_*}{\partial n_-}(z) &= \frac{2}{t_0} \operatorname{Re} \left(n_+ (\xi_{1-}(z) - \xi_{1+}(z)) \right) \\ &= -\frac{2}{t_0} \operatorname{Im} \left(\tau_+ (\xi_{1-}(z) - \xi_{1+}(z)) \right). \end{aligned} \quad (6.11)$$

Since the measure μ_* is positive, we learn from (2.26) and the last equality that

$$\frac{\partial \mathcal{U}_*}{\partial n_+}(z) + \frac{\partial \mathcal{U}_*}{\partial n_-}(z) < 0,$$

so at least one of these directional derivatives is negative, thus z cannot be a local minimum.

Suppose now $z \in \{z_0, z_1, z_2\}$, say $z = z_j$. Using (6.8) and the relation (6.6),

$$U^{\mu_*}(u) = -\frac{1}{t_0} \operatorname{Re} \int_{z_j}^u \xi_1(s) ds + \frac{1}{t_0} \operatorname{Re}(V(u) - V(z_j)), \quad u \in G \setminus \Sigma_*, \quad (6.12)$$

where G is a sufficiently small neighborhood of z and the path of integration lies in $G \setminus \Sigma_*$. On G the function ξ_1 admits an expansion of the form

$$\xi_1(u) = \xi_1(z_j) + \mathcal{O}((u - z_j)^{1/2}), \quad u \in G \setminus \Sigma_*.$$

Using this expansion in (6.12), we then get

$$\begin{aligned}\mathcal{U}_*(u) &= -\frac{2}{t_0} \operatorname{Re}(\xi_1(z_j)u) + \frac{|u|^2}{t_0} + c + \mathcal{O}((u - z_j)^{3/2}), \\ &= -\frac{2}{t_0} \operatorname{Re} u \operatorname{Re} \xi_1(z_j) + \frac{2}{t_0} \operatorname{Im} u \operatorname{Im} \xi_1(z_j) \\ &\quad + \frac{(\operatorname{Re} u)^2 + (\operatorname{Im} u)^2}{t_0} + c + \mathcal{O}((u - z_j)^{3/2}), \quad u \in G \setminus \Sigma_*\end{aligned}$$

for some constant c . From (3.27) we know that $\xi_1(z_j) = h(w_j^{-1}) \neq 0$, so the leading contribution in the formula above is linear in $\operatorname{Re} u$ and $\operatorname{Im} u$, and consequently \mathcal{U}_* cannot have a local minimum at z_j .

It remains to verify that $z = z_*$ cannot be a local minimum in the three-cut case $(t_0, t_1) \in \mathcal{F}_1$. Consider the angle θ between $\Sigma_{*,2}$ and $\Sigma_{*,0}$ on the upper half plane, so that $\theta \leq \pi$. Assume for the moment that $\theta > \pi/2$. In this case, for $\epsilon > 0$ sufficiently small, the point $z_* + \epsilon i$ is in between $\Sigma_{*,0}$ and $\Sigma_{*,2}$, and using continuity we can conclude

$$\mathcal{U}_*(z_* + \epsilon i) = \lim_{\delta \rightarrow 0^+} \mathcal{U}_*(z_* + \epsilon i + \delta) = \mathcal{U}_*(z_*) + \epsilon \lim_{\delta \rightarrow 0^+} \frac{\partial \mathcal{U}_*}{\partial n_+}(z_* + \delta) + \mathcal{O}(\epsilon^2), \quad (6.13)$$

where $n_+ = i$ is the normal to $\Sigma_{*,0}$, and the error term is uniform in δ . Similarly,

$$\mathcal{U}_*(z_* - \epsilon i) = \lim_{\delta \rightarrow 0^+} \mathcal{U}_*(z_* - \epsilon i + \delta) = \mathcal{U}_*(z_*) + \epsilon \lim_{\delta \rightarrow 0^+} \frac{\partial \mathcal{U}_*}{\partial n_-}(z_* + \delta) + \mathcal{O}(\epsilon^2), \quad (6.14)$$

Proceeding as in (6.11) (and having in mind that in the present case $\tau_+ = 1$),

$$\lim_{\delta \rightarrow 0^+} \left(\frac{\partial \mathcal{U}_*}{\partial n_+}(z_* + \delta) + \frac{\partial \mathcal{U}_*}{\partial n_-}(z_* + \delta) \right) = -\frac{2}{t_0} \lim_{\delta \rightarrow 0^+} \operatorname{Im}(\xi_{1-}(z_* + \delta) - \xi_{1+}(z_* + \delta)).$$

As before, we use that the density of μ_* is positive on $\Sigma_{*,0}$ and does not vanish on z_* to conclude that the limit above is strictly negative. Taking into account (6.13)–(6.14), this is enough to conclude that z_* is not a point of minimum.

It only remains to prove the inequality $\theta > \pi/2$. When $t_1 = 0$, then $\theta = 3\pi/2$ and we are done. Since θ varies continuously with t_1 , it is enough to prove that $\theta \neq \pi/2$.

To the contrary, suppose $\theta = \pi/2$. In this case, the vector tangent to $\Sigma_{*,2}$ converges to i as $z \rightarrow z_*$ along $\Sigma_{*,2}$, so that from (2.25) we learn

$$(\xi_{1+}(z_*) - \xi_{1-}(z_*)) \in \mathbb{R},$$

where the \pm boundary values are with respect to $\Sigma_{*,2}$. But in this case $\xi_{1+}(z_*) \in \mathbb{R}$ as well, so we conclude that $\xi_{1-}(z_*) \in \mathbb{R}$, and consequently all the solutions to (2.12) are real for $z = z_*$. But this cannot occur, because $z_* < z_0$ and we know from Theorem 4.1 that the discriminant of (2.12) is negative on the interval $(-\infty, z_0)$. \square

Lemma 6.3. *The total potential \mathcal{U}_* does not have a local minimum on Ω .*

Proof. From Lemma 6.2, we know that \mathcal{U}_* does not attain a minimum on Σ_* , so if $p \in \Omega$ is a point of minimum of \mathcal{U}_* , then the gradient of \mathcal{U}_* should vanish at p . This means that

$$0 = \frac{\partial \mathcal{U}_*}{\partial z}(p) = C^{\mu_*}(p) + \frac{1}{t_0}(\bar{p} - V'(p)) = \frac{1}{t_0}(\bar{p} - \xi_1(p)), \quad (6.15)$$

where for the first equality we used the definition of \mathcal{U}_* given in (6.9) together with the identity (6.6), and for the last equality we used (6.8). That is, we conclude that

the point p where \mathcal{U}_* attains its minimum should satisfy $\xi_1(p) = \bar{p}$. Let w be such that

$$h(w) = p, \quad h\left(\frac{1}{w}\right) = \xi_1(p) = \bar{p}. \quad (6.16)$$

We know from Theorem 2.2 that h maps $\partial\mathbb{D}$ to $\partial\Omega$. Since $p \in \Omega$, we learn from this that $|w| \neq 1$, so the point $\tilde{w} := 1/\bar{w}$ is different from w . Furthermore, because the rational function h has real coefficients,

$$h(\tilde{w}) = \overline{h(w^{-1})} = \overline{\xi_1(p)} = p = h(w), \quad (6.17)$$

and also

$$h\left(\frac{1}{\tilde{w}}\right) = \overline{h(w)} = \bar{p} = \xi_1(p) = h\left(\frac{1}{w}\right). \quad (6.18)$$

Since $\tilde{w} \neq w$, the pairs $(h(w^{-1}), h(w))$ and $(h(\tilde{w}^{-1}), h(\tilde{w}))$ represent distinct points on \mathcal{R} . In virtue of the equalities (6.16)–(6.18), we conclude that p is a zero of the discriminant of (2.12). But $p \notin \Sigma_*$, so in particular it cannot be a branch point. Thus $p = \hat{z}_j$ for some j , and from Theorem 2.6 we learn that p cannot be on Ω . Hence (6.15) cannot hold on $\Omega \setminus \Sigma_*$, and the proof is complete. \square

Proof of (2.24). Fix t_0 . When $t_1 = 0$, the set Σ_* is explicitly given by (4.8), and (2.24) is valid in this case. Suppose now that (2.24) is not valid for some value of t_1 . Continuity arguments show that for the smallest of such value, say \tilde{t}_1 , it holds true

$$\Sigma_* \subset \bar{\Omega} \quad \text{and} \quad \partial\Omega \cap \Sigma_* \neq \emptyset. \quad (6.19)$$

Recalling that ξ_1 and S coincide in a neighborhood of ∞ , the inclusion in (6.19) implies $\xi_1 \equiv S$ on the whole set $\mathbb{C} \setminus \Omega$. Thus, still for the given pair (t_0, \tilde{t}_1) , the second identity in (6.7) combined with (6.8) then says that

$$C^{\mu_0}(z) = C^{\mu_*}(z), \quad z \in \mathbb{C} \setminus \Omega. \quad (6.20)$$

Taking into account (6.6), we further get

$$\mathcal{U}_*(z) - \mathcal{U}_0(z) = c, \quad z \in \mathbb{C} \setminus \Omega,$$

for some constant c . This constant is equal to

$$\begin{aligned} c &= \lim_{z \rightarrow \infty} (U^{\mu_*}(z) - U^{\mu_0}(z)) \\ &= \lim_{z \rightarrow \infty} \left(\iint \log \left| 1 - \frac{s}{z} \right| d\mu_0(s) - \int \log \left| 1 - \frac{s}{z} \right| d\mu_*(s) \right) = 0. \end{aligned}$$

In particular, it follows from Theorem 2.3 that

$$\mathcal{U}_*(z) > l, \quad \text{for } z \in \mathbb{C} \setminus \bar{\Omega} \text{ sufficiently close to } \partial\Omega, \quad (6.21)$$

and

$$\mathcal{U}_*(z) = l, \quad z \in \partial\Omega. \quad (6.22)$$

The function \mathcal{U}_* is continuous on $\bar{\Omega}$, so it has a minimum in this set. Using Lemma 6.3 and (6.22), we thus conclude

$$\mathcal{U}_*(z) > l, \quad z \in \Omega. \quad (6.23)$$

From (6.19), we know that there exists $p \in \partial\Omega \cap \Sigma_*$. From (6.21)–(6.23) we learn that p is a local minimum of \mathcal{U}_* , but this is in contradiction with Lemma 6.2.

Hence (2.24) always holds true, and the proof of Theorem 2.9 is complete. \square

Proof of Theorem 2.10. Having in mind (2.24), we now know that $\xi_1 \equiv S$ on $\mathbb{C} \setminus \Omega$. Proceeding as in (6.20)–(6.23), we conclude

$$\mathcal{U}_*(z) = \mathcal{U}_0(z), \quad z \in \mathbb{C} \setminus \Omega, \quad (6.24)$$

$$\mathcal{U}_*(z) > l, \quad z \in \Omega, \quad (6.25)$$

where l is the constant from Theorem 2.3. From the definition of \mathcal{U}_0 and \mathcal{U}_* it follows that (6.24) is equivalent to (2.27). Furthermore, by Theorem 2.3 we know that $\mathcal{U}_0 \equiv l$ on Ω , and (6.25) then becomes (2.28). \square

7. RIEMANN-HILBERT ANALYSIS IN THE THREE-CUT CASE

In this section we perform the Riemann-Hilbert/Steepest Descent analysis for the multiple orthogonal polynomial $P_{n,n}$ (given in Definition 2.12) in the three-cut case $(t_0, t_1) \in \mathcal{F}_1$.

The analysis is similar to the one presented by Bleher and Kuijlaars in [15] for $t_1 = 0$. The main difference here is that we construct the g -functions only with the help of the ξ -functions, without relying on any vector equilibrium problem. Although our g -functions could also be given in terms of the solution to a vector equilibrium problem, we do not elaborate in this direction.

For $j = 0, 1, 2$, we extend $\Sigma_{*,j}$ given in Section 6 to a contour Σ_j in the following way. For $j = 0$, simply set $\Sigma_j = [z_*, \hat{z}_0]$. For $j = 2$, we take $\Sigma_2 \setminus \Sigma_{*,2}$ to be an arc from z_2 to \hat{z}_2 contained in the projection of the strip domain \mathcal{S}_3 of the quadratic differential ϖ , that is,

$$\Sigma_2 \setminus (\Sigma_{*,2} \cup \{\hat{z}_2\}) \subset \pi(\mathcal{S}_3), \quad (7.1)$$

where we recall that the strip domain \mathcal{S}_3 is labeled as in Figure 23. Lastly we extend $\Sigma_{*,1}$ imposing the conjugation property

$$\Sigma_1 \setminus \Sigma_{*,1} = (\Sigma_2 \setminus \Sigma_{*,2})^*. \quad (7.2)$$

In this way,

$$\Sigma_1 \setminus (\Sigma_{*,1} \cup \{\hat{z}_1\}) \subset \pi(\mathcal{S}_8), \quad (7.3)$$

where the strip domain \mathcal{S}_8 is given as in Figure 23. We refer the reader to Figure 27.

The arc Σ_j is oriented from z_* to \hat{z} . We then set

$$\Sigma = \Sigma_0 \cup \Sigma_1 \cup \Sigma_2,$$

and consider the multiple orthogonal polynomial $P_{n,n}$ in Definition 2.12 with this choice of Σ .

7.1. Multiple orthogonality in terms of Airy functions. The multiple orthogonality conditions (2.42) can be stated in terms of solutions to the Airy equation $y'' = zy$. The Airy function Ai is the special solution to the Airy equation determined by the asymptotic behavior

$$\begin{aligned} \text{Ai}(z) &= \frac{z^{-1/4}}{2\sqrt{\pi}} e^{-\frac{2}{3}z^{3/2}} (1 + \mathcal{O}(z^{-3/2})), \\ \text{Ai}'(z) &= -\frac{z^{1/4}}{2\sqrt{\pi}} e^{-\frac{2}{3}z^{3/2}} (1 + \mathcal{O}(z^{-3/2})), \end{aligned}$$

valid when $z \rightarrow \infty$, $-\pi < \arg z < \pi$. It admits the integral representation

$$\text{Ai}(z) = \frac{1}{2\pi i} \int_{\Gamma_0} e^{\frac{1}{3}s^3 - zs} ds, \quad z \in \mathbb{C},$$

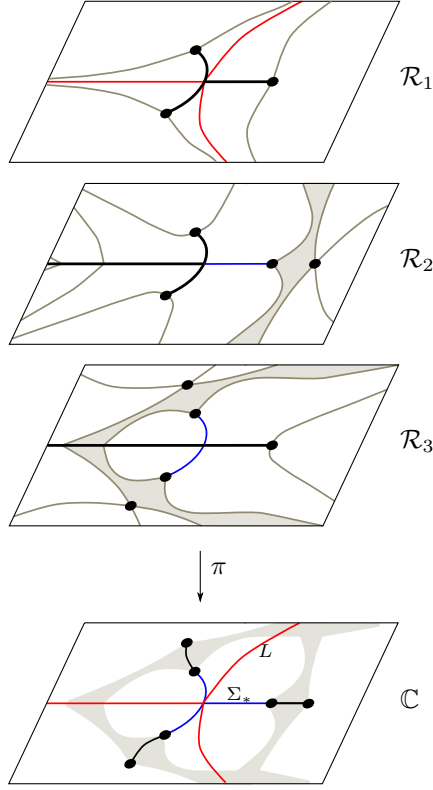


FIGURE 27. Illustration of properties (7.1) and (7.9). The trajectories highlighted on \mathcal{R} in blue and red are projected onto \mathbb{C} to the contours Σ_* , L , also respectively represented in blue and red. Σ_* consists of the union of the three trajectories projected from \mathcal{R}_2 , \mathcal{R}_3 , whereas L consists of the pieces projected from \mathcal{R}_1 . In addition, we extend Σ_* to Σ by constraining $\Sigma \setminus \Sigma_*$ to lie within the shaded region on \mathbb{C} , which consists of the projections of the gray strip domains on \mathcal{R} . The arcs of $\Sigma \setminus \Sigma_*$ are depicted in black.

where Γ_0 is a contour as in Section 2.7, see (2.31) *et seq.* For Γ_1, Γ_2 , ω also given as in Section 2.7, set

$$y_j(z) = \omega^j \text{Ai}(\omega^j z) = \frac{1}{2\pi i} \int_{\Gamma_j} e^{\frac{1}{3}s^3 - zs} ds, \quad z \in \mathbb{C}, \quad j = 0, 1, 2, \quad (7.4)$$

where we recall that $\omega = e^{2\pi i/3}$. Note that the integral representations above, in combination with contour deformation, immediately imply that

$$y_0(z) + y_1(z) + y_2(z) = \text{Ai}(z) + \omega \text{Ai}(\omega z) + \omega^2 \text{Ai}(\omega^2 z) = 0. \quad (7.5)$$

Using the functions y_0, y_1 and y_2 in (7.4) and setting $c_n = (n/t_0)^{2/3}$, the conditions (2.42) can be rewritten as

$$\begin{aligned} \sum_{l=0}^2 \int_{\Sigma_l} P_{n,n}(z) z^k e^{\frac{n}{t_0} V(z)} y_l(c_n(z-t_1)) dz &= 0, \quad k = 0, \dots, \left\lfloor \frac{n}{2} \right\rfloor - 1, \\ \sum_{l=0}^2 \int_{\Sigma_l} P_{n,n}(z) z^k e^{\frac{n}{t_0} V(z)} y'_l(c_n(z-t_1)) dz &= 0, \quad k = 0, \dots, \left\lfloor \frac{n}{2} \right\rfloor - 1. \end{aligned} \quad (7.6)$$

7.2. The Riemann-Hilbert problem Y . For simplicity of presentation, we assume for now on n even. The case n odd can be treated similarly, after appropriate (and non essential) modifications.

Consider the following Riemann-Hilbert problem for Y .

- $Y : \mathbb{C} \setminus \Sigma \rightarrow \mathbb{C}^{3 \times 3}$ is analytic;
- $Y_+(z) = Y_-(z) J_Y(z)$, $z \in \Sigma$, where

$$J_Y(z) = \begin{pmatrix} 1 & e^{\frac{n}{t_0} V(z)} y_j(c_n(z-t_1)) & e^{\frac{n}{t_1} V(z)} y'_j(c_n(z-t_1)) \\ 0 & 1 & 0 \\ 0 & 0 & 1 \end{pmatrix}, \quad z \in \Sigma_j;$$

- $Y(z) = (I + \mathcal{O}(z^{-1})) \begin{pmatrix} z^n & 0 & 0 \\ 0 & z^{-\frac{n}{2}} & 0 \\ 0 & 0 & z^{-\frac{n}{2}} \end{pmatrix}, \quad z \rightarrow \infty;$
- $Y(z) = \begin{pmatrix} \mathcal{O}(1) & \mathcal{O}(\log(z - \hat{z}_j)) & \mathcal{O}(\log(z - \hat{z}_j)) \\ \mathcal{O}(1) & \mathcal{O}(\log(z - \hat{z}_j)) & \mathcal{O}(\log(z - \hat{z}_j)) \\ \mathcal{O}(1) & \mathcal{O}(\log(z - \hat{z}_j)) & \mathcal{O}(\log(z - \hat{z}_j)) \end{pmatrix}, \quad z \rightarrow \hat{z}_j, \quad j = 0, 1, 2.$
- $Y(z)$ is remains bounded when $z \rightarrow z_*$.

Here and in what follows, Σ is oriented outwards, that is, towards ∞ , see Figure 28.

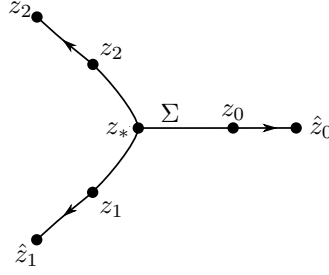
It turns out that the polynomial $P_{n,n}$ uniquely exists if, and only if, the Riemann Hilbert problem above has a solution. In such a case, the polynomial $P_{n,n}$ is recovered through

$$P_{n,n} = Y_{1,1}. \quad (7.7)$$

As one of the consequences of our analysis, we get that for sufficiently large n , the Riemann-Hilbert problem above has a solution, and thus the polynomial $P_{n,n}$ exists for n sufficiently large.

7.3. First transformation: $Y \mapsto X$. The first transformation, essentially the same as in [15], has the goal of reducing the jump matrix of Y to nontrivial 2×2 blocks. Define

$$\begin{aligned} y_3(z) &= 2\pi i (\omega^2 \text{Ai}(\omega z) - \omega \text{Ai}(\omega^2 z)), \\ y_4(z) &= \omega y_3(\omega z), \\ y_5(z) &= \omega^2 y_3(\omega^2 z). \end{aligned}$$

FIGURE 28. Contour Σ for the RHP for Y .

Using the identities $1 - \omega = i\sqrt{3}\omega^2$ and $1 - \omega^2 = -i\sqrt{3}\omega$, in combination with (7.5), we also get

$$\begin{aligned}
 y_3(z) &= \frac{2\pi}{\sqrt{3}}((1 - \omega) \operatorname{Ai}(\omega z) + (1 - \omega^2)\omega^2 \operatorname{Ai}(\omega^2 z)) \\
 &= \frac{2\pi}{\sqrt{3}}(-\omega \operatorname{Ai}(\omega z) - \omega^2 \operatorname{Ai}(\omega^2 z) + \operatorname{Ai}(\omega z) + \operatorname{Ai}(\omega^2 z)) \\
 &= \frac{2\pi}{\sqrt{3}}(\operatorname{Ai}(z) + \operatorname{Ai}(\omega z) + \operatorname{Ai}(\omega^2 z))
 \end{aligned}$$

This last identity immediately implies that $y_3(\omega z) = y_3(z)$, and consequently $y_4(z) = \omega y_3(z)$ and $y_5(z) = \omega^2 y_3(z)$.

Additionally, set

$$L_0 = (-\infty, z_*] = \pi(\mathcal{R}_1 \cap \gamma_1(z_0^{(2)})) \quad (7.8)$$

and

$$L_2 = \pi(\mathcal{R}_1 \cap \gamma_0(z_1^{(3)})), \quad L_1 = L_2^* = \pi(\mathcal{R}_1 \cap \gamma_2(z_2^{(3)})), \quad (7.9)$$

where $\pi : \mathcal{R} \rightarrow \overline{\mathbb{C}}$ is the canonical projection as before, see Figure 27. L_1 and L_2 are unbounded analytic arcs with a common finite endpoint $z_* \in \mathbb{R}$, and they extend to ∞ along the angles $\frac{\pi}{3}$ and $-\frac{\pi}{3}$, respectively. We set the orientation on L_j to be outwards, that is, from z_* to ∞ .

Remark 7.1. For ease of presentation, in what follows we assume that $L_j \cap \Sigma_* = \{z_*\}$. If L_j intersects Σ_* in more points, it is still possible to carry out the Riemann-Hilbert analysis along the same lines as we present here, with appropriate and non essential modifications. Numerical experiments indicate that the condition $L_j \cap \Sigma_* = \{z_*\}$ always holds true anyway.

The union $L = L_0 \cup L_1 \cup L_2$ divides the plane into three domains, henceforth denoted G_0, G_1, G_2 , where G_j is uniquely defined through the condition that \hat{z}_j is contained in G_j , see Figure 29.

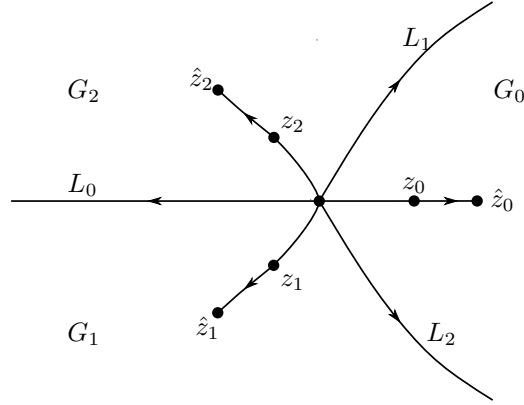


FIGURE 29. Contour $\Sigma \cup L$, $L = L_0 \cup L_1 \cup L_2$, for the RHP's for X and T , and the sectors G_0 , G_1 , G_2 .

We make the transformation

$$X(z) = \begin{pmatrix} 1 & 0 & 0 \\ 0 & \frac{c_n^{-1/4}}{\sqrt{2\pi}} & 0 \\ 0 & 0 & i\frac{c_n^{1/4}}{\sqrt{2\pi}} \end{pmatrix} Y(z) \begin{pmatrix} 1 & 0 & 0 \\ 0 & y'_{j+3}(c_n(z-t_1)) & -y'_j(c_n(z-t_1)) \\ 0 & -y_{j+3}(c_n(z-t_1)) & y_j(c_n(z-t_1)) \end{pmatrix} \\ \times \begin{pmatrix} 1 & 0 & 0 \\ 0 & 1 & 0 \\ 0 & 0 & -2\pi i \end{pmatrix}, \quad z \in G_j, \quad j = 0, 1, 2. \quad (7.10)$$

It follows as in [15, pp. 1297–1301] that X satisfies the following RHP

- $X : \mathbb{C} \setminus (\Sigma \cup L) \rightarrow \mathbb{C}^{3 \times 3}$ is analytic;
- $X_+(z) = X_-(z)J_X(z)$, $z \in \Sigma \cup L$, where J_X is given by

$$J_X(z) = \begin{pmatrix} 1 & 0 & 0 \\ 0 & \omega^2 & 1 \\ 0 & 0 & \omega \end{pmatrix}, \quad z \in L; \quad J_X(z) = \begin{pmatrix} 1 & e^{\frac{n}{t_0}V(z)} & 0 \\ 0 & 1 & 0 \\ 0 & 0 & 1 \end{pmatrix}, \quad z \in \Sigma.$$

- X has the same endpoint conditions as Y at z_* , \hat{z}_j , $j = 0, 1, 2$.
- $X(z) = (I + \mathcal{O}(z^{-1}))A(z)Q(z)$, $z \rightarrow \infty$,
where

$$A(z) = \begin{pmatrix} 1 & 0 & 0 \\ 0 & z^{1/4} & 0 \\ 0 & 0 & z^{-1/4} \end{pmatrix} \times \begin{cases} \begin{pmatrix} 1 & 0 & 0 \\ 0 & \frac{1}{\sqrt{2}} & -\frac{i}{\sqrt{2}} \\ 0 & -\frac{i}{\sqrt{2}} & \frac{1}{\sqrt{2}} \end{pmatrix}, & z \in G_0, \\ \begin{pmatrix} 1 & 0 & 0 \\ 0 & -\frac{i}{\sqrt{2}} & -\frac{1}{\sqrt{2}} \\ 0 & \frac{1}{\sqrt{2}} & \frac{i}{\sqrt{2}} \end{pmatrix}, & z \in G_1, \\ \begin{pmatrix} 1 & 0 & 0 \\ 0 & \frac{i}{\sqrt{2}} & \frac{1}{\sqrt{2}} \\ 0 & -\frac{1}{\sqrt{2}} & -\frac{i}{\sqrt{2}} \end{pmatrix}, & z \in G_2. \end{cases} \quad (7.11)$$

and

$$Q(z) = \begin{cases} \begin{pmatrix} z^n & 0 & 0 \\ 0 & z^{-\frac{n}{2}} e^{\frac{2n}{3t_0}(z-t_1)^{3/2}} & 0 \\ 0 & 0 & z^{-\frac{n}{2}} e^{-\frac{2n}{3t_0}(z-t_1)^{3/2}} \end{pmatrix} & z \in G_0, \\ \begin{pmatrix} z^n & 0 & 0 \\ 0 & z^{-\frac{n}{2}} e^{-\frac{2n}{3t_0}(z-t_1)^{3/2}} & 0 \\ 0 & 0 & z^{-\frac{n}{2}} e^{\frac{2n}{3t_0}(z-t_1)^{3/2}} \end{pmatrix} & z \in G_1 \cup G_2, \end{cases}$$

7.4. Second transformation: $X \mapsto T$. The second transformation has the goal of removing the n -dependence from the asymptotics of X .

Introduce the g -functions

$$\begin{aligned} g_1(z) &= \int_{z_0}^z \xi_1(s) ds + c_1, & z \in \mathbb{C} \setminus (\Sigma_* \cup L_0), \\ g_2(z) &= \int_{z_*}^z \xi_2(s) ds + c_2, & z \in \mathbb{C} \setminus (\Sigma_{*,1} \cup \Sigma_{*,2} \cup L_0), \\ g_3(z) &= \int_{z_0}^z \xi_3(s) ds + c_3, & z \in \mathbb{C} \setminus (\Sigma_{*,0} \cup L_0), \end{aligned} \quad (7.12)$$

where for g_2 the path of integration starts along $(z_*, +\infty)$ and

$$c_2 = -\pi i t_0 - \int_{\Sigma_{*,2}} (\xi_{1+}(s) - \xi_{2+}(s)) ds, \quad c_1 = c_3 = \int_{z_*}^{z_0} \xi_{3-}(s) ds. \quad (7.13)$$

The constant c_2 can be alternatively expressed as

$$c_2 = -\pi i t_0 + 2\pi i t_0 \mu_*(\Sigma_{*,2}) = -\pi i t_0 + 2\pi i t_0 \mu_*(\Sigma_{*,1}) = -\pi i t_0 \mu_*(\Sigma_{*,0}), \quad (7.14)$$

where μ_* is given by Theorem 2.9. In particular, c_2 is purely imaginary.

We could as well express one of the g -functions in terms of the other two through $\sum \xi_j = V'$, but we found more convenient to work with three g -functions instead.

The asymptotics (2.15) can be rewritten as

$$\begin{aligned} \xi_1(z) &= V'(z) + \frac{t_0}{z} + \mathcal{O}(z^{-2}), \\ \xi_2(z) &= -(z - t_1)^{1/2} - \frac{t_0}{2z} + \mathcal{O}(z^{-3/2}), & z \rightarrow \infty \\ \xi_3(z) &= (z - t_1)^{1/2} - \frac{t_0}{2z} + \mathcal{O}(z^{-3/2}), \end{aligned}$$

which in turn give

$$\begin{aligned} g_1(z) &= V(z) + l_1 + t_0 \log z + \mathcal{O}(z^{-1}), \\ g_2(z) &= -\frac{2}{3}(z - t_1)^{3/2} + l_2 - \frac{t_0}{2} \log z + \mathcal{O}(z^{-1/2}), & z \rightarrow \infty \\ g_3(z) &= \frac{2}{3}(z - t_1)^{3/2} + l_3 - \frac{t_0}{2} \log z + \mathcal{O}(z^{-1/2}), \end{aligned} \quad (7.15)$$

for some constants l_1, l_2, l_3 .

Lemma 7.1. *For the constants l_2, l_3, c_2 and c_3 as in (7.12)–(7.15), it is valid*

$$l_3 = l_2, \quad c_2 = i \operatorname{Im} c_3. \quad (7.16)$$

Proof. From the asymptotics (7.15),

$$\begin{aligned} g_{3+}(z) - g_{2-}(z) &= \frac{2}{3}((z - t_1)_+^{3/2} + (z - t_1)_-^{3/2}) + l_3 - l_2 \\ &\quad - \frac{t_0}{2}(\log z)_+ + \frac{t_0}{2}(\log z)_- + \mathcal{O}(z^{-1/2}) \\ &= l_3 - l_2 + \pi i t_0 + \mathcal{O}(z^{-1/2}), \quad z \in L_0 \end{aligned}$$

On another hand, from the definition of g_2 and g_3 ,

$$\begin{aligned} g_{3+}(z) - g_{2-}(z) &= c_3 - c_2 + \int_{z_0}^{z_*} \xi_{3-}(s) ds - \int_{z_*}^{z_2} (\xi_{1+}(s) - \xi_{2+}(s)) ds, \\ &= -c_2 + \int_{z_*}^{z_2} (\xi_{1-}(s) - \xi_{1+}(s)) ds = \pi i t_0, \quad z \in L_0, \end{aligned}$$

where for the second equality we used the jump condition $\xi_{1\pm} = \xi_{2\mp}$ in $\Sigma_{*,2}$, which follows from the sheet structure constructed in Section 4.3.1.

To get the second equality in (7.16), just note that

$$\begin{aligned} 2i \operatorname{Im} c_3 &= c_3 + \overline{c_3} = \int_{z_*}^{z_0} (\xi_{3-}(s) - \overline{\xi_{3-}(s)}) ds \\ &= \int_{z_*}^{z_0} (\xi_{1+}(s) - \xi_{1-}(s)) ds \\ &= -2\pi i t_0 \mu_*(\Sigma_{*,0}) = 2c_2, \end{aligned}$$

where for the second equality we used the jump equalities in (4.31) and for the last equality we used (7.14). □

The second transformation is given by

$$\begin{aligned} T(z) &= \begin{pmatrix} e^{\frac{n}{t_0} l_1} & 0 & 0 \\ 0 & e^{\frac{n}{t_0} l_2} & 0 \\ 0 & 0 & e^{\frac{n}{t_0} l_2} \end{pmatrix} X(z) \\ &\quad \times \begin{cases} \begin{pmatrix} e^{\frac{n}{t_0}(V(z)-g_1(z))} & 0 & 0 \\ 0 & e^{-\frac{n}{t_0} g_3(z)} & 0 \\ 0 & 0 & e^{-\frac{n}{t_0} g_2(z)} \end{pmatrix}, & z \in G_0 \\ \begin{pmatrix} e^{\frac{n}{t_0}(V(z)-g_1(z))} & 0 & 0 \\ 0 & e^{-\frac{n}{t_0} g_2(z)} & 0 \\ 0 & 0 & e^{-\frac{n}{t_0} g_3(z)} \end{pmatrix}, & z \in G_1 \cup G_2 \end{cases} \end{aligned} \quad (7.17)$$

It follows that T is the solution to the following RHP,

- $T : \mathbb{C} \setminus (\Sigma \cup L) \rightarrow \mathbb{C}^{3 \times 3}$ is analytic;

- $T_+(z) = T_-(z)J_T(z)$, $z \in \Sigma \cup L$, where J_T is given by

$$J_T(z) = \begin{cases} \begin{pmatrix} e^{\frac{n}{t_0}(g_1-(z)-g_{1+}(z))} & e^{\frac{n}{t_0}(g_1-(z)-g_{3+}(z))} & 0 \\ 0 & e^{\frac{n}{t_0}(g_3-(z)-g_{3+}(z))} & 0 \\ 0 & 0 & e^{\frac{n}{t_0}(g_2-(z)-g_{2+}(z))} \end{pmatrix}, & z \in \Sigma_0, \\ \begin{pmatrix} e^{\frac{n}{t_0}(g_1-(z)-g_{1+}(z))} & e^{\frac{n}{t_0}(g_1-(z)-g_{2+}(z))} & 0 \\ 0 & e^{\frac{n}{t_0}(g_2-(z)-g_{2+}(z))} & 0 \\ 0 & 0 & e^{\frac{n}{t_0}(g_3-(z)-g_{3+}(z))} \end{pmatrix}, & z \in \Sigma_1 \cup \Sigma_2, \\ \begin{pmatrix} e^{\frac{n}{t_0}(g_1-(z)-g_{1+}(z))} & 0 & 0 \\ 0 & \omega^2 e^{\frac{n}{t_0}(g_2-(z)-g_{2+}(z))} & e^{\frac{n}{t_0}(g_2-(z)-g_{3+}(z))} \\ 0 & 0 & \omega e^{\frac{n}{t_0}(g_3-(z)-g_{3+}(z))} \end{pmatrix}, & z \in L_0, \\ \begin{pmatrix} 1 & 0 & 0 \\ 0 & \omega^2 e^{-\frac{n}{t_0}(g_2(z)-g_3(z))} & 1 \\ 0 & 0 & \omega e^{-\frac{n}{t_0}(g_3(z)-g_2(z))} \end{pmatrix}, & z \in L_1, \\ \begin{pmatrix} 1 & 0 & 0 \\ 0 & \omega^2 e^{-\frac{n}{t_0}(g_3(z)-g_2(z))} & 1 \\ 0 & 0 & \omega e^{-\frac{n}{t_0}(g_2(z)-g_3(z))} \end{pmatrix}, & z \in L_2; \end{cases}$$

- T satisfies the same endpoint conditions as X when $z \rightarrow z_*, \hat{z}_j$, $j = 0, 1, 2$.
- $T(z) = (I + \mathcal{O}(z^{-1}))A(z)$, as $z \rightarrow \infty$.

Our next goal is to simplify the jump matrix J_T further. For this purpose it is convenient to introduce the functions

$$\begin{aligned} \Phi_0(z) &= \frac{1}{t_0} \int_{z_0}^z (\xi_1(s) - \xi_3(s)) ds, \\ \Phi_1(z) &= \frac{1}{t_0} \int_{z_1}^z (\xi_1(s) - \xi_2(s)) ds, \quad z \in \mathbb{C} \setminus (\Sigma_* \cup L_0), \\ \Phi_2(z) &= \frac{1}{t_0} \int_{z_2}^z (\xi_1(s) - \xi_2(s)) ds. \end{aligned} \quad (7.18)$$

and also

$$\begin{aligned} \Psi_j(z) &= \frac{1}{t_0} \int_{z_*}^z (\xi_2(s) - \xi_3(s)) ds, \quad z \in \mathbb{C} \setminus (\Sigma_* \cup L_0), \quad j = 0, 1, \\ \Psi_2(z) &= \frac{1}{t_0} \int_{z_*}^z (\xi_3(s) - \xi_2(s)) ds, \quad z \in \mathbb{C} \setminus (\Sigma_* \cup L_0). \end{aligned} \quad (7.19)$$

where the paths of integration for Ψ_0 , Ψ_1 and Ψ_2 are as follows.

- If $\text{Im } z \geq 0$, then the path of integration for Φ_0 emanates from z_* in the sector between L_0 and Σ_2 on the upper half plane. If $\text{Im } z < 0$, then the path of integration for Φ_0 emanates from z_* in the sector between L_0 and Σ_1 on the lower half plane.
- For $j = 1, 2$, the path of integration for Ψ_j emanates from z_* in the sector between L_j and Σ_{j+1} on G_{j+1} .

The main properties of the functions Φ_j and Ψ_j are collected in the next proposition.

Proposition 7.2. *The functions g_j, Φ_j, Ψ_j , $j = 0, 1, 2$, satisfy*

(A) *For $z \in \Sigma_{*,0}$,*

- (i) $g_{1+}(z) - g_{1-}(z) = t_0 \Phi_{0+}(z)$,
- (ii) $g_{2+}(z) - g_{2-}(z) = 0$,
- (iii) $g_{3+}(z) - g_{3-}(z) = t_0 \Phi_{0-}(z)$,
- (iv) $g_{3+}(z) - g_{1-}(z) = 0$,
- (v) $\operatorname{Re} \Phi_{0\pm}(z) = 0$,
- (vi) $\Phi_{0+}(z) + \Phi_{0-}(z) = 0$,
- (vii) $\Psi_{1+}(z) + \Psi_{2-}(z) = \Phi_{0+}(z) + \frac{2c_2}{t_0}$.

(B) *For $j = 1, 2$ and $z \in \Sigma_{*,j}$,*

- (i) $g_{1+}(z) - g_{1-}(z) = t_0 \Phi_{j+}(z)$,
- (ii) $g_{2+}(z) - g_{2-}(z) = t_0 \Phi_{j-}(z)$,
- (iii) $g_{3+}(z) - g_{3-}(z) = 0$,
- (iv) $g_{2+}(z) - g_{1-}(z) = (-1)^{j+1} \pi i t_0$,
- (v) $\operatorname{Re} \Phi_{j\pm} = 0$,
- (vi) $\Phi_{j+}(z) + \Phi_{j-}(z) = 0$,
- (vii) $\Phi_{j-1,-}(z) + (-1)^{j+1} \Psi_{j+1,+}(z) = \Phi_{j+}(z) - \frac{c_2}{t_0} - \pi i$.

(C) *For $z \in \Sigma_0 \setminus \Sigma_{j,0}$,*

$$g_3(z) - g_1(z) = -t_0 \Phi_0(z).$$

(D) *For $j = 1, 2$, and $z \in \Sigma_j \setminus \Sigma_{*,j}$,*

$$g_2(z) - g_1(z) = -t_0 \Phi_j(z) + (-1)^{j+1} \pi i t_0.$$

(E) *$\operatorname{Re} \Phi_j$ is negative on $\Sigma_j \setminus \Sigma_{*,j}$, $j = 0, 1, 2$.*

(F) *For $j = 0, 1, 2$, the functions $\operatorname{Im} \Phi_{j+}$ and $\operatorname{Im} \Phi_{j-}$ are decreasing and increasing, respectively, along the orientation of $\Sigma_{*,j}$.*

(G) *For $z \in L_0$,*

- (i) $\Psi_{0+}(z) + \Psi_{0-}(z) = 0$,
- (ii) $\operatorname{Re} \Psi_{0\pm}(z) = 0$,
- (iii) $g_{1+}(z) - g_{1-}(z) = -2\pi i t_0$,
- (iv) $g_{2+}(z) - g_{2-}(z) = t_0 \Psi_{0+}(z) + 2c_2 + 2\pi i t_0$,
- (v) $g_{3+}(z) - g_{3-}(z) = t_0 \Psi_{0-}(z) - 2c_2$,
- (vi) $g_{3+}(z) - g_{2-}(z) = \pi i t_0$.
- (vii) $\Phi_{2-}(z) - \Phi_{1+}(z) = \Psi_{0+}(z) + \frac{2c_2}{t_0} + 2\pi i$.

(H) *For $j = 1, 2$, and $z \in L_j$,*

- (i) $\Psi_{j+}(z) = \Psi_{j-}(z)$,
- (ii) $\operatorname{Re} \Psi_j(z) = 0$,
- (iii) $g_3(z) - g_2(z) = (-1)^j t_0 \Psi_j(z) + (-1)^{j+1} c_2$
- (iv) $\Phi_{j-1}(z) - \Phi_{j+1}(z) = \Psi_j(z) - \frac{c_2}{t_0} + \pi i$.

(I) *For $j = 0, 1, 2$, the function $\operatorname{Im} \Psi_{j+}$ is decreasing along the orientation of L_j .*

Proof. To see that the conditions (A)–(v) and (B)–(v) are true, note that from the sheet structure constructed in Section 4.3.1, it follows that

$$\Phi_{j\pm}(z) = \int_{z_j}^z (\xi_{1\pm}(s) - \xi_{1\mp}(s))ds, \quad z \in \Sigma_*.$$

Since Σ_* satisfies (2.25), the right-hand side above has to be purely imaginary, leading to (A)–(v) and (B)–(v).

Similarly, to get (G)–(ii) and (H)–(ii) we note that (7.8)–(7.9) say that L_j coincides with the projection of a trajectory on the first sheet of the quadratic differential (5.2). From the definition of ϖ in (5.1)–(5.2) and of its trajectories (5.3), and taking also into account that $z_* \in L$, we thus get

$$\operatorname{Re} \int_{z_*}^z (\xi_{2+}(s) - \xi_{3+}(s))ds = 0, \quad z \in L,$$

which is enough to conclude (G)–(ii) and (H)–(ii).

The remaining conditions claimed in (A)–(D) and (G)–(H) follow in a straightforward manner, once one has in mind the sheet structure for the spectral curve \mathcal{R} (see Sections 4.3.1 and the beginning of Section 6), and also equations (7.13)–(7.14) and (7.16). We skip the details for these computations.

Recalling that $\xi_1 < \xi_3$ on (z_0, \hat{z}_0) , see (4.30), we get (E) for $j = 0$.

Note that the analytic continuation of the function Φ_2 (that we keep denoting by Φ_2) coincides (up to a multiplicative real factor) with the primitive Υ in (5.34) on the strip domain $\mathcal{U} = \mathcal{S}_3$. In particular, Φ_2 maps \mathcal{S}_3 to a vertical strip on \mathbb{C} whose one of the boundary components is the imaginary axis, and consequently the sign of $\operatorname{Re} \Phi_2$ is constant on \mathcal{S}_3 . The trajectory $\gamma_0(z_2^{(3)})$ is contained in one of the components of $\partial\mathcal{S}_3$, is mapped by Φ_2 to the imaginary axis and extends to ∞ along the angle $\theta_0^{(3)} = \pi/6$. Using the expansion (2.15) it follows that

$$\Phi_2(z) = \frac{z^3}{3t_0} + \mathcal{O}(z) = i \frac{|z|^3}{3t_0} + \mathcal{O}(z), \quad \text{as } z \rightarrow \infty \text{ along } \gamma_0(z_2^{(3)}),$$

thus $\gamma_0(z_2^{(3)})$ is mapped by Φ_2 to $i\mathbb{R}_+$. Hence, because Φ_2 is conformal, we conclude that the left-hand side of $\gamma_0(z_2^{(3)})$ in the orientation from $z_2^{(3)}$ to ∞ (that is, \mathcal{S}_3) is mapped by Φ_2 to the left-hand side of $i\mathbb{R}_+$ in the natural orientation. Since the sign of $\operatorname{Re} \Phi_2$ is constant on \mathcal{S}_3 , this is enough to conclude that $\operatorname{Re} \Phi_2(z) < 0$ on \mathcal{S}_3 . In virtue of (7.3), we conclude (E) for $j = 2$. Finally, (E) for $j = 1$ follows in a similar fashion, or also noticing the symmetry relations $\Phi_2(\bar{z}) = \Phi_1(\bar{z})$ and (7.2).

For (F), denote by γ_z the sub arc of $\Sigma_{*,j}$ from z to z_j . It follows from (7.18) that we can write

$$\Phi_{j\pm}(z) = \frac{1}{t_0} \int_{z_j}^z (\xi_{1\pm}(s) - \xi_{1\mp}(s))ds = \pm 2\pi i \mu_*(\gamma_z).$$

The measure μ_* is positive, so $\mu_*(\gamma_z)$ is decreasing along $\Sigma_{*,j}$, and (F) follows from the equation above.

We now proceed to prove (I). We already know that

$$\operatorname{Im} \Psi_{j+}(z) = \Psi_{j+}(z), \quad z \in L_j, \quad (7.20)$$

as it follows from (G)–(ii) and (H)–(ii). The derivative of Ψ_{j+} is, up to a sign, equal to $\xi_{2+} - \xi_{3+}$, which does not vanish along L_j . Combining with (7.20) we

learn that $\text{Im } \Psi_{j+}$ is monotone along L_j . Taking into account that L_j extends to ∞ with angle $\pi - 2j\pi/3$ and using the asymptotics (2.15), we learn

$$\begin{aligned}\Psi_{j+}(z) &= \epsilon \frac{4}{3} z^{3/2} + \mathcal{O}(z^{1/2}) \\ &= -\frac{4i}{3} |z|^{3/2} + \mathcal{O}(z^{1/2}), \quad \text{as } z \rightarrow \infty \text{ along } L_j,\end{aligned}$$

where $\epsilon = -1$ for $j = 0, 1$ and $\epsilon = 1$ for $j = 2$. In virtue of the previous comments, this is enough to conclude (G)–(ii) and (H)–(ii). \square

The jump matrix J_T can then be rewritten as

$$J_T(z) = \begin{cases} \begin{pmatrix} e^{-n\Phi_{j+}(z)} & 1 & 0 \\ 0 & e^{-n\Phi_{j-}(z)} & 0 \\ 0 & 0 & 1 \end{pmatrix}, & z \in \Sigma_{*,j}, \quad j = 0, 1, 2, \\ \begin{pmatrix} 1 & e^{n\Phi_j(z)} & 0 \\ 0 & 1 & 0 \\ 0 & 0 & 1 \end{pmatrix}, & z \in \Sigma_j \setminus \Sigma_{*,j}, \quad j = 0, 1, 2, \\ \begin{pmatrix} 1 & 0 & 0 \\ 0 & \omega^2 e^{-n(\Psi_{0+}(z) + \alpha_0)} & 1 \\ 0 & 0 & \omega e^{-n(\Psi_{0-}(z) - \alpha_0)} \end{pmatrix}, & z \in L_0, \\ \begin{pmatrix} 1 & 0 & 0 \\ 0 & \omega^2 e^{-n(\Psi_j(z) - \alpha_j)} & 1 \\ 0 & 0 & \omega e^{n(\Psi_j(z) - \alpha_j)} \end{pmatrix}, & z \in L_j, \quad j = 1, 2. \end{cases}$$

where we set

$$\alpha_0 = \frac{2c_2}{t_0}, \quad \alpha_1 = \alpha_2 = \frac{c_2}{t_0}.$$

Remark 7.2. Our second transformation $X \mapsto T$ should be compared with the sequence of transformations $X \mapsto V \mapsto U \mapsto T$ in [15].

7.5. Opening of lenses: $T \mapsto S$. Based on the properties of the functions Φ_j , Ψ_j , we now open lenses around the contours Σ_* , L . We denote by

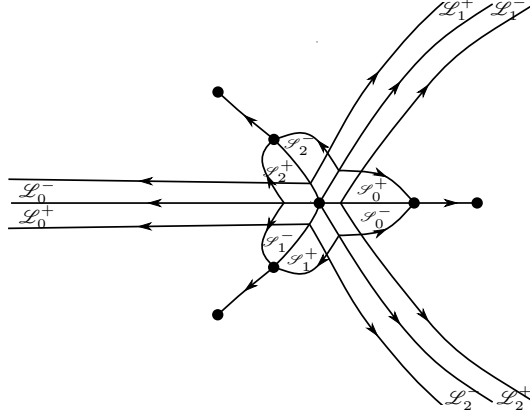
$$\mathcal{S} = \mathcal{S}^+ \cup \mathcal{S}^-$$

the (open) lens around the contour Σ_* , with the convention that \mathcal{S}^+ and \mathcal{S}^- are the parts of \mathcal{S} lying on the upper and lower sides of Σ_* , respectively. Furthermore, $\partial\mathcal{S}^+$ and $\partial\mathcal{S}^-$ denote the parts of the boundary of \mathcal{S} lying on the upper and lower sides of Σ_* , respectively. In addition, we assume that $\partial\mathcal{S}$ intersects $\Sigma_{*,j}$ only at the endpoint z_j and, moreover, $\partial\mathcal{S}^\pm$ is chosen so that it intersects the contour L_j , $j = 0, 1, 2$, at a point other than z_* . We also set \mathcal{S}_j^\pm and $\partial\mathcal{S}_j^\pm$ to be the parts of \mathcal{S}^\pm and $\partial\mathcal{S}^\pm$ on the \pm -sides of $\Sigma_{*,j}$, $j = 0, 1, 2$, respectively. We refer the reader to Figure 30 for a depiction of this lens.

We claim that the lens \mathcal{S} can be chosen so that

$$\text{Re } \Phi_j(z) > 0, \quad z \in \partial\mathcal{S}_j^\pm \setminus \{z_j\}, \quad j = 0, 1, 2. \quad (7.21)$$

To see this, we use Proposition 7.2 (F) and the Cauchy-Riemann equations to get that $\text{Re } \Phi_j$ is increasing in both normal directions to $\Sigma_{*,j}$. Taking into account that $\text{Re } \Phi_{j\pm} = 0$ along $\Sigma_{*,j}$ (see Proposition 7.2 (A)–(v) and (B)–(v)) and reducing \mathcal{S} if necessary, (7.21) follows.

FIGURE 30. Lenses \mathcal{S} , \mathcal{L} determining the contour Σ_S .

In the very same spirit, we construct the lens

$$\mathcal{L} = \mathcal{L}^+ \cup \mathcal{L}^-$$

around L , where \mathcal{L}^\pm denotes the part of \mathcal{L} on the \pm -side of L , and as before we use $\partial\mathcal{L}^\pm$ to denote the part of the boundary of \mathcal{L} that is on the \pm -side of L , and \mathcal{L}_j^\pm , $\partial\mathcal{L}_j^\pm$ to denote the respective parts of \mathcal{L}^\pm , $\partial\mathcal{L}^\pm$ on the \pm -sides of L_j , $j = 0, 1, 2$. We additionally assume that $\partial\mathcal{L}_j^\pm$ does not intersect L_j and for some $\varepsilon > 0$ small,

$$\arg z \rightarrow \pi - \frac{2\pi i}{3}j \pm \varepsilon, \quad \text{as } z \rightarrow \infty \text{ along } \partial\mathcal{L}_j^\pm.$$

In an analogous manner as in (7.21), we claim that \mathcal{L} can be chosen so that

$$\begin{aligned} \operatorname{Re} \Psi_0(z) &> 0, \quad z \in \partial\mathcal{L}_0^\pm, \\ \pm \operatorname{Re} \Psi_j(z) &> 0, \quad z \in \partial\mathcal{L}_j^\pm, \quad j = 1, 2. \end{aligned} \tag{7.22}$$

Indeed, similarly as before we combine Cauchy-Riemann equations and Proposition 7.2 (I) to conclude that $\operatorname{Re} \Psi_j$ is increasing in the direction normal to L_j (pointing towards the positive side of L_j). Taking into account that $\operatorname{Re} \Psi_{j+} = 0$ along L_j (see (G)–(ii) and (H)–(ii)), Ψ_j is continuous along L_j for $j = 1, 2$ (see (H)–(i)) and reducing \mathcal{L} if necessary, this leads to the inequalities in (7.22) on $\partial\mathcal{L}_j^\pm$, $j = 1, 2$, and also on $\partial\mathcal{L}_0^+$. Finally, the inequality for $\partial\mathcal{L}_0^-$ then follows from the inequality on $\partial\mathcal{L}_0^+$ and the jump condition (G)–(i).

The lips $\partial\mathcal{L}_j^\pm$, $\partial\mathcal{L}_j^\pm$ of the lenses are oriented outwards, that is, towards ∞ , see Figure 30.

We are finally ready to open lenses. Set

$$S(z) = T(z), \quad z \in \mathbb{C} \setminus (\mathcal{S} \cup \mathcal{L}), \tag{7.23}$$

and

$$S(z) = T(z) \times \begin{cases} \begin{pmatrix} 1 & 0 & 0 \\ \mp e^{-n\Phi_j(z)} & 1 & 0 \\ 0 & 0 & 1 \end{pmatrix}, & z \in \mathcal{S}_j^\pm \setminus \mathcal{L}, \\ \begin{pmatrix} 1 & 0 & 0 \\ 0 & 1 & 0 \\ 0 & \mp \omega^\mp e^{-n(\Psi_0(z) \pm \alpha_0)} & 1 \end{pmatrix}, & z \in \mathcal{L}_0^\pm \setminus \mathcal{S}, \\ \begin{pmatrix} 1 & 0 & 0 \\ 0 & 1 & 0 \\ 0 & \mp \omega^\mp e^{\mp n(\Psi_j(z) - \alpha_j)} & 1 \end{pmatrix}, & z \in \mathcal{L}_j^\pm \setminus \mathcal{S}, j \neq 0. \\ \begin{pmatrix} 1 & 0 & 0 \\ \pm e^{-n\Phi_{\pm 1}(z)} & 1 & 0 \\ \omega^\pm e^{-n(\Psi_0(z) + \Phi_{\pm 1}(z) \pm \alpha_0)} & \mp \omega^\mp e^{-n(\Psi_0(z) \pm \alpha_0)} & 1 \end{pmatrix}, & z \in \mathcal{L}_0^\pm \cap \mathcal{S}_{\pm 1}^\mp \\ \begin{pmatrix} 1 & 0 & 0 \\ \pm e^{-n\Phi_{j\pm 1}(z)} & 1 & 0 \\ \omega^\pm e^{\mp n(\Psi_j(z) \pm \Phi_{j\pm 1}(z) - \alpha_j)} & \mp \omega^\mp e^{\mp n(\Psi_j(z) - \alpha_j)} & 1 \end{pmatrix}, & z \in \mathcal{L}_j^\pm \cap \mathcal{S}_{j\pm 1}^\mp, j \neq 0 \end{cases} \quad (7.24)$$

where $\omega^+ = \omega$, $\omega^- = \omega^{-1} = \omega^2$ and all indices are understood modulo 3.

Denote

$$\Gamma_S = \Sigma \cup L \cup \partial \mathcal{S} \cup \partial \mathcal{L}.$$

The matrix S satisfies the following RHP.

- $S : \mathbb{C} \setminus \Gamma_S \rightarrow \mathbb{C}^{3 \times 3}$ is analytic;
- $S_+(z) = S_-(z)J_S(z)$, $z \in \Gamma_S$, where the jump matrix J_S is given by

$$J_S(z) = \begin{cases} \begin{pmatrix} 0 & 1 & 0 \\ -1 & 0 & 0 \\ 0 & 0 & 1 \end{pmatrix}, & z \in \Sigma_* \\ \begin{pmatrix} 1 & 0 & 0 \\ 0 & 0 & 1 \\ 0 & -1 & 0 \end{pmatrix}, & z \in L \\ \begin{pmatrix} 1 & e^{n\Phi_j(z)} & 0 \\ 0 & 1 & 0 \\ 0 & 0 & 1 \end{pmatrix}, & z \in \Sigma_j \setminus \Sigma_{*,j}, \\ \begin{pmatrix} 1 & 0 & 0 \\ e^{-n\Phi_j(z)} & 1 & 0 \\ 0 & 0 & 1 \end{pmatrix}, & z \in \partial\mathcal{S}_j \setminus \mathcal{L}, \\ \begin{pmatrix} 1 & 0 & 0 \\ 0 & 1 & 0 \\ 0 & \omega^\mp e^{-n(\Psi_0(z) \pm \alpha_0)} & 1 \end{pmatrix}, & z \in \partial\mathcal{L}_0^\pm \setminus \mathcal{S}, \\ \begin{pmatrix} 1 & 0 & 0 \\ 0 & 1 & 0 \\ 0 & \omega^\mp e^{\mp n(\Psi_j(z) + \alpha_j)} & 1 \end{pmatrix}, & z \in \partial\mathcal{L}_j^\pm \setminus \mathcal{S}, j \neq 0, \\ \begin{pmatrix} 1 & 0 & 0 \\ e^{-n\Phi_{\pm 1}(z)} & 1 & 0 \\ \mp e^{-n(\Psi_0(z) + \Phi_{\pm 1} \pm \alpha_0)} & 0 & 1 \end{pmatrix}, & z \in \partial\mathcal{S}_{\pm 1}^\mp \cap \mathcal{L} \\ \begin{pmatrix} 1 & 0 & 0 \\ e^{-n\Phi_{j\pm 1}(z)} & 1 & 0 \\ \mp e^{\mp n(\Psi_j(z) \pm \Phi_{j\pm 1}(z) - \alpha_j)} & 0 & 1 \end{pmatrix}, & z \in \partial\mathcal{S}_{j\pm 1}^\mp \cap \mathcal{L}, j \neq 0, \end{cases}$$

and

$$J_S(z) = \begin{cases} \begin{pmatrix} 1 & 0 & 0 \\ 0 & 1 & 0 \\ \mp \omega^\pm e^{-n(\Psi_0(z) + \Phi_{\pm 1}(z) \pm \alpha_j)} & \omega^\mp e^{-n(\Psi_0(z) \pm \alpha_0)} & 1 \end{pmatrix}, & z \in \partial\mathcal{L}_0^\pm \cap \mathcal{S} \\ \begin{pmatrix} 1 & 0 & 0 \\ 0 & 1 & 0 \\ \mp \omega^\pm e^{\mp n(\Psi_j(z) \pm \Phi_{j\pm 1}(z) - \alpha_j)} & \omega^\mp e^{\mp n(\Psi_j(z) - \alpha_j)} & 1 \end{pmatrix}, & z \in \partial\mathcal{L}_j^\pm \cap \mathcal{S}, j \neq 0, \end{cases}$$

- S has the same endpoint behavior as X when $z \rightarrow z_*, \hat{z}_j, j = 0, 1, 2$,
- $S(z) = (I + \mathcal{O}(z^{-1}))A(z)$, as $z \rightarrow \infty$.

The jump conditions above can be verified directly from the definition of S , once one has in hands Lemma 7.1 and Proposition 7.2. The remaining conditions on the RHP above follow directly from the RHP for T . We skip the details.

7.6. The global parametrix. As we will see in a moment, the jump matrix J_S converges to the identity matrix on $\Gamma_S \setminus (\Sigma_* \cup L)$. Hence, neglecting the jumps on

$\Gamma_S \setminus (\Sigma_* \cup L)$, we are led to the Riemann-Hilbert problem for M , commonly called the *global parametrix*.

- $M : \mathbb{C} \setminus (\Sigma_* \cup L) \rightarrow \mathbb{C}^{3 \times 3}$ is analytic;
- $M_+(z) = M_-(z)J_M(z)$, $z \in \Sigma_* \cup L$, where

$$J_M(z) = \begin{cases} \begin{pmatrix} 0 & 1 & 0 \\ -1 & 0 & 0 \\ 0 & 0 & 1 \end{pmatrix}, & z \in \Sigma_*, \\ \begin{pmatrix} 1 & 0 & 0 \\ 0 & 0 & 1 \\ 0 & -1 & 0 \end{pmatrix}, & z \in L; \end{cases} \quad (7.25)$$

- $M(z) = \mathcal{O}((z - z_j)^{-1/4})$ as $z \rightarrow z_j$, $j = 0, 1, 2$;
- M remains bounded as $z \rightarrow z_*$.
- $M(z) = (I + \mathcal{O}(z^{-1}))A(z)$ as $z \rightarrow \infty$;

We postpone the construction of the parametrix to Section 9.

7.7. The local parametrices. Denote by

$$D_\delta(z_j) = \{z \in \mathbb{C} \mid |z - z_j| < \delta\}, \quad j = 0, 1, 2,$$

the disk of radius $\delta > 0$ around z_j and set

$$D_\delta = \bigcup_{j=0}^2 D_\delta(z_j). \quad (7.26)$$

For $\delta > 0$ sufficiently small, we search for a matrix P , called the *local parametrix*, solution to the following RHP.

- $P : D_\delta \setminus \Gamma_S \rightarrow \mathbb{C}^{3 \times 3}$ is analytic;
- $P_+(z) = P_-(z)J_S(z)$, $z \in \Gamma_S \cap D_\delta$;
- $P(z) = (I + \mathcal{O}(n^{-1}))M(z)$, as $n \rightarrow \infty$ uniformly for $z \in \partial D_\delta$, where M is the global parametrix constructed in Section 7.6;

Note that the non trivial jumps for P only come on the upper left 2×2 corner of J_S , so this is essentially a 2×2 RHP.

As we are in the three-cut case $(t_0, t_1) \in \mathcal{F}_1$, the function Φ_j has order of vanishing $3/2$ at z_j , that is,

$$\Phi_j(z) = \text{const} \times (z - z_j)^{\frac{3}{2}}(1 + \mathcal{O}(z - z_j)^{1/2}), \quad \text{as } z \rightarrow z_j, \quad j = 0, 1, 2,$$

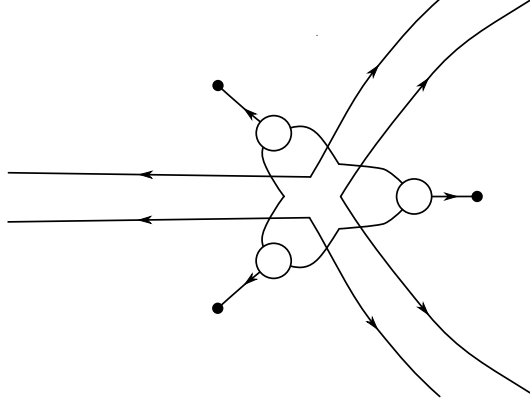
and the local parametrix can be constructed out of Airy functions, see for instance [18]. We skip this construction here.

7.8. Final transformation: $S \mapsto R$. We arrived at the final step of our analysis. For D_δ as in (7.26) and M and P the global and local parametrices considered in Sections 7.6 and 7.7, respectively, we make the final transformation

$$R(z) = \begin{cases} S(z)M(z)^{-1}, & z \in \mathbb{C} \setminus (\Gamma_S \cup D_\delta), \\ S(z)P(z)^{-1}, & z \in D_\delta \setminus \Gamma_S. \end{cases} \quad (7.27)$$

Since the jumps of M and P coincide with the jumps of S on $\Sigma_* \cup L$ and $\Gamma_S \cap D_\delta$, respectively, it follows that R satisfies a RHP on the contour

$$\Gamma_R = \partial D_\delta \cup (\Gamma_S \setminus (D_\delta \cup L \cup \Sigma_*)),$$

FIGURE 31. Contour Σ_R for the jump of the RHP for R .

where each piece of ∂D_δ is oriented in the clockwise direction, see Figure 31. More precisely,

- $R : \mathbb{C} \setminus \Gamma_R \rightarrow \mathbb{C}^{3 \times 3}$ is analytic;
- $R_+(z) = R_-(z)J_R(z)$, $z \in \Gamma_R$, where

$$J_R(z) = \begin{cases} M(z)J_S(z)M(z)^{-1}, & z \in \Gamma_R \setminus \partial D_\delta, \\ P(z)M(z)^{-1}, & z \in \partial D_\delta. \end{cases}$$

- $R(z) = I + \mathcal{O}(z^{-1})$, $z \rightarrow \infty$.

It follows from (7.21), (7.22) and the definition of the jump J_S that for some positive constant c ,

$$J_R(z) = I + \mathcal{O}(e^{-nc}), \quad z \in \Gamma_R \setminus \partial D_\delta,$$

whereas from the RHP for P it follows that

$$J_R(z) = I + \mathcal{O}(n^{-1}), \quad z \in \partial D_\delta,$$

where the implicit terms in the last two formulas above are uniform in z . As a consequence [18], we conclude that for n large enough the RHP for R is uniquely solvable and

$$R(z) = I + \mathcal{O}\left(\frac{1}{n(1+|z|)}\right), \quad n \rightarrow \infty, \quad (7.28)$$

uniformly on $\mathbb{C} \setminus \Gamma_R$.

Thus we can invert the series of transformations performed

$$Y \mapsto X \mapsto T \mapsto S \mapsto R$$

to conclude that the RHP for Y is uniquely solvable and, moreover, translate (7.28) into asymptotic information about Y (see Section 10 below for an example) concluding the steepest descent analysis.

8. RIEMANN-HILBERT ANALYSIS IN THE ONE-CUT CASE

We proceed to the Riemann-Hilbert/Steepest Descent analysis in the one-cut case $(t_0, t_1) \in \mathcal{F}_2$. We do not give much details, and mostly highlight the main differences comparing to the three-cut case carried out in Section 7. The focus

is on the jumps and parametrices, the remaining aspects of the steepest descent analysis are the same as in the three-cut case.

Following Theorem 2.9, for $(t_0, t_1) \in \mathcal{F}_2$ we denote $\Sigma_* = [z_1, z_0]$. The first step is to define the contours Σ and L in the same spirit as (7.1) and (7.9). As before, these are defined taking into account the critical graph of the quadratic differential ϖ . The parts of Σ and L lying on the real line are defined by

$$\Sigma_0 = [z_2, \hat{z}_0], \quad L_0 = (-\infty, z_2] = \pi \left(\gamma_1(z_2^{(1)}) \right).$$

To construct Σ_1, Σ_2, L_1 and L_2 , we rely on the critical graph of ϖ . For $\pi : \mathcal{R} \rightarrow \overline{\mathbb{C}}$ the canonical projection and \mathcal{S}_3 the strip domain determined by the condition that $\hat{z}_2^{(3)}$ and $z_2^{(3)}$ are the critical points on its boundary (see Figure 25), we consider an oriented contour Σ_2 from z_2 to \hat{z}_2 , contained in the upper half plane, and satisfying

$$\Sigma_2 \setminus \{z_2, \hat{z}_2\} \subset \pi(\mathcal{S}_3 \cap \mathcal{R}_3), \quad (8.1)$$

and set $\Sigma_1 = (\Sigma_2)^*$, $\Sigma = \Sigma_0 \cup \Sigma_1 \cup \Sigma_2$. Furthermore, define

$$L_1 = \pi \left(\gamma_0(z_2^{(1)}) \right), \quad L_2 = (L_1)^* = \pi \left(\gamma_2(z_2^{(1)}) \right), \quad (8.2)$$

and then set $L = L_0 \cup L_1 \cup L_2$, see Figure 32. Choosing Σ_1 and Σ_2 appropriately, we can also be sure that $L \cap \Sigma = \{z_2\}$.

For this choice of Σ , we consider the diagonal sequence of multiple orthogonal polynomials $(P_{n,n})$ in Definition 2.12. As before, such polynomials can be alternatively characterized by (7.6). Furthermore, assuming n even as before, $P_{n,n}$ is alternatively described by the Riemann-Hilbert problem Y given in Section 7.2.

As in the three-cut situation, the contour L defined above splits the complex plane into three regions G_0, G_1, G_2 , where G_j contains the point \hat{z}_j , $j = 0, 1, 2$. The first transformation $Y \mapsto X$ is exactly the same as in Section 7.3, see Figure 33 for a display of the jump contours.

The second transformation $X \mapsto T$ is also similar as for the three-cut case. The only difference is concerned the starting points of integration in the definition of the g -functions.

More precisely, we define

$$\begin{aligned} g_1(z) &= \int_{z_0}^z \xi_1(s) ds + c_1, & z \in \mathbb{C} \setminus (-\infty, z_0), \\ g_2(z) &= \int_{z_2}^z \xi_2(s) ds + c_2, & z \in \mathbb{C} \setminus (-\infty, z_2), \\ g_3(z) &= \int_{z_0}^z \xi_3(s) ds + c_3, & z \in \mathbb{C} \setminus (-\infty, z_0), \end{aligned} \quad (8.3)$$

where

$$c_1 = c_3 = \int_{z_2}^{z_0} \xi_{3-}(s) ds, \quad c_2 = -\pi i t_0.$$

As in (7.15), g_1, g_2 and g_3 admit the asymptotic expansion

$$\begin{aligned} g_1(z) &= V(z) + l_1 + t_0 \log z + \mathcal{O}(z^{-1}), \\ g_2(z) &= -\frac{2}{3}(z - t_1)^{3/2} + l_2 - \frac{t_0}{2} \log z + \mathcal{O}(z^{-1/2}), \\ g_3(z) &= \frac{2}{3}(z - t_1)^{3/2} + l_3 - \frac{t_0}{2} \log z + \mathcal{O}(z^{-1/2}), \end{aligned} \quad z \rightarrow \infty$$

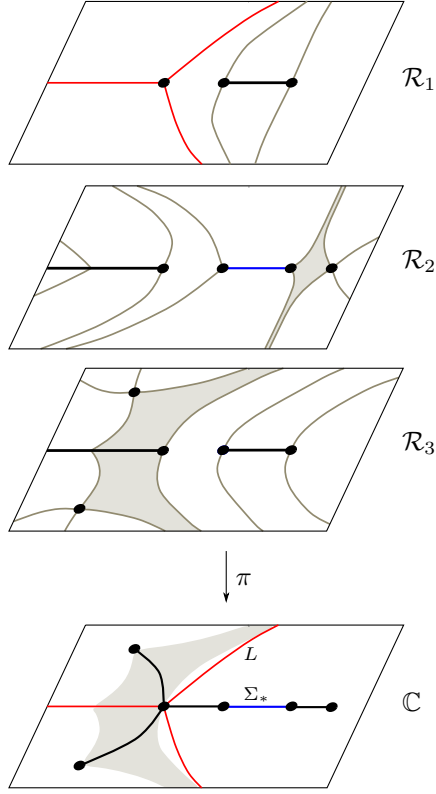


FIGURE 32. Illustration of properties (8.1) and (8.2). The trajectories highlighted on \mathcal{R} in blue and red are projected onto \mathbb{C} to the contours Σ_* , L , also respectively represented in blue and red. Σ_* is the interval in blue color, whereas L consists of the pieces projected from \mathcal{R}_1 . In addition to the pieces on the real line, we extend Σ_* to Σ by constraining $\Sigma \setminus (\Sigma_* \cup \mathbb{R})$ to lie within the shaded region on \mathbb{C} , which consists of the projections of the gray strip domains on \mathcal{R} . The arcs of $\Sigma \setminus \Sigma_*$ on the complex plane are depicted in black.

and the proof of Lemma 7.1 carries over without any essential modification, leading to $l_2 = l_3$ and $c_2 = i \operatorname{Im} c_3$.

For the g -functions as in (8.3), we make the transformation $X \mapsto T$ as in (7.17). The resulting RH-problem characterizing T is similar to the one presented in Section 7.4. The jump contour is given by $\Sigma \cup L$, see Figure 33 and, after simplifications,

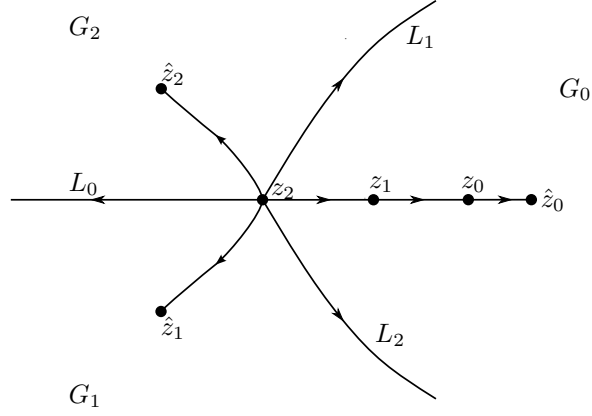


FIGURE 33. Contour $\Sigma \cup L$ for the RHP's for X and T , and the sectors G_0, G_1, G_2 .

its jump matrix J_T reduces to

$$J_T(z) = \left\{ \begin{array}{ll} \begin{pmatrix} e^{\frac{n}{t_0}(g_1-(z)-g_{1+}(z))} & 1 & 0 \\ 0 & e^{\frac{n}{t_0}(g_3-(z)-g_{3+}(z))} & 0 \\ 0 & 0 & 1 \end{pmatrix}, & z \in (z_1, z_0), \\ \begin{pmatrix} 1 & e^{\frac{n}{t_0}(g_1-(z)-g_{3+}(z))} & 0 \\ 0 & 1 & 0 \\ 0 & 0 & 1 \end{pmatrix}, & z \in (z_2, z_1) \cup (z_0, \hat{z}_0), \\ \begin{pmatrix} 1 & e^{\frac{n}{t_0}(g_1(z)-g_2(z))} & 0 \\ 0 & 1 & 0 \\ 0 & 0 & 1 \end{pmatrix}, & z \in \Sigma_1 \cup \Sigma_2, \\ \begin{pmatrix} 1 & 0 & 0 \\ 0 & \omega^2 e^{\frac{n}{t_0}(g_2-(z)-g_{2+}(z))} & 1 \\ 0 & 0 & \omega e^{\frac{n}{t_0}(g_3-(z)-g_{3+}(z))} \end{pmatrix}, & z \in L_0, \\ \begin{pmatrix} 1 & 0 & 0 \\ 0 & \omega^2 e^{\frac{n}{t_0}(g_3(z)-g_2(z))} & 1 \\ 0 & 0 & \omega e^{\frac{n}{t_0}(g_2(z)-g_3(z))} \end{pmatrix}, & z \in L_1, \\ \begin{pmatrix} 1 & 0 & 0 \\ 0 & \omega^2 e^{\frac{n}{t_0}(g_2(z)-g_3(z))} & 1 \\ 0 & 0 & \omega e^{\frac{n}{t_0}(g_3(z)-g_2(z))} \end{pmatrix}, & z \in L_2. \end{array} \right.$$

Analogously to (7.18), (7.19), we now consider

$$\begin{aligned}
\Phi_0(z) &= \frac{1}{t_0} \int_{z_0}^z (\xi_1(s) - \xi_3(s)) ds, & z \in \mathbb{C} \setminus (-\infty, z_0), \\
\Phi_1(z) &= \frac{1}{t_0} \int_{z_1}^z (\xi_1(s) - \xi_3(s)) ds, & z \in \mathbb{C} \setminus ((-\infty, z_2) \cup (z_1, +\infty)), \\
\Phi_2(z) &= \frac{1}{t_0} \int_{z_2}^z (\xi_1(s) - \xi_2(s)) ds + \Phi_1(z_2), & z \in \mathbb{C} \setminus ((-\infty, z_2) \cup (z_1, +\infty)),
\end{aligned} \tag{8.4}$$

and also

$$\Psi(z) = \frac{1}{t_0} \int_{z_2}^z (\xi_2(s) - \xi_3(s)) ds, \quad z \in \mathbb{C} \setminus ((-\infty, z_2) \cup (z_1, +\infty)).$$

The jump matrix J_T is then expressed in terms of these functions as

$$J_T(z) = \begin{cases} \begin{pmatrix} e^{-n\Phi_{0+}(z)} & 1 & 0 \\ 0 & e^{-n\Phi_{0-}(z)} & 0 \\ 0 & 0 & 1 \end{pmatrix}, & z \in (z_1, z_0), \\ \begin{pmatrix} 1 & e^{n\Phi_0(z)} & 0 \\ 0 & 1 & 0 \\ 0 & 0 & 1 \end{pmatrix}, & z \in (z_0, \hat{z}_0), \\ \begin{pmatrix} 1 & e^{n\Phi_1(z)} & 0 \\ 0 & 1 & 0 \\ 0 & 0 & 1 \end{pmatrix}, & z \in (z_2, z_1), \\ \begin{pmatrix} 1 & e^{n\Phi_2(z)} & 0 \\ 0 & 1 & 0 \\ 0 & 0 & 1 \end{pmatrix}, & z \in \Sigma_1 \cup \Sigma_2, \\ \begin{pmatrix} 1 & 0 & 0 \\ 0 & \omega^2 e^{-n\Psi_+(z)} & 1 \\ 0 & 0 & \omega e^{-\Psi_-(z)} \end{pmatrix}, & z \in L_0, \\ \begin{pmatrix} 1 & 0 & 0 \\ 0 & \omega^2 e^{-n\Psi(z)} & 1 \\ 0 & 0 & \omega e^{n\Psi(z)} \end{pmatrix}, & z \in L_1, \\ \begin{pmatrix} 1 & 0 & 0 \\ 0 & \omega^2 e^{n\Psi(z)} & 1 \\ 0 & 0 & \omega e^{-n\Psi(z)} \end{pmatrix}, & z \in L_2. \end{cases}$$

The jump matrices above are in a suitable form for the opening of lenses. We open the lens \mathcal{S} around (z_1, z_0) and denote by \mathcal{S}^\pm the part of \mathcal{S} on the \pm -side of (z_1, z_0) , and by $\partial\mathcal{S}^\pm$ the component of the boundary of $\partial\mathcal{S}$ on the \pm -side of (z_1, z_0) . Similarly, \mathcal{L}_j^\pm denotes the part of \mathcal{L} on the \pm -side of L_j , and ∂L_j^\pm denotes the component of the boundary of \mathcal{L} on the \pm -side of L_j . Additionally, we open the lens \mathcal{L} in such a way that it does not intersect Σ , see Figure 34.

The functions Φ_0 and Φ_1 satisfy

$$\Phi_0(z) < 0, \quad z \in (z_0, \hat{z}_0], \quad \Phi_1(z) < 0, \quad z \in [z_2, z_1). \tag{8.5}$$

Moreover, due to the construction of Σ_1, Σ_2 and L as in equations (8.1)–(8.2), we can be sure that (after reducing the lenses if necessary)

$$\begin{aligned}
\operatorname{Re} \Phi_0(z) &> 0, & z \in \partial \mathcal{S}^\pm \setminus \{z_0, z_1\}, \\
\operatorname{Re} \Phi_2(z) &< 0, & z \in \Sigma_1 \cup \Sigma_2, \\
\operatorname{Re} \Psi(z) &> 0, & z \in \partial \mathcal{L}_0^\pm \setminus \{z_2\}, \\
\pm \operatorname{Re} \Psi(z) &> 0, & z \in \partial \mathcal{L}_1^\pm \setminus \{z_2\}, \\
\mp \operatorname{Re} \Psi(z) &> 0, & z \in \partial \mathcal{L}_2^\pm \setminus \{z_2\}.
\end{aligned} \tag{8.6}$$

These conditions will assure the jumps for the next transformation have the right decaying properties. We stress that due to the constant $\Phi_1(z_2)$ in the definition of Φ_2 in (8.4), the strict inequality $\operatorname{Re} \Phi_2 < 0$ also holds true at the endpoint z_2 of Σ_1 and Σ_2 .

We then set

$$S(z) = T(z), \quad z \text{ outside the lenses } \mathcal{S} \cup \mathcal{L},$$

and on the lenses

$$S(z) = T(z) \times \begin{cases} \begin{pmatrix} 1 & 0 & 0 \\ \mp e^{-n\Phi_0(z)} & 1 & 0 \\ 0 & 0 & 1 \end{pmatrix}, & z \in \mathcal{S}^\pm, \\ \begin{pmatrix} 1 & 0 & 0 \\ 0 & 1 & 0 \\ 0 & \mp \omega^\mp e^{-n\Psi(z)} & 1 \end{pmatrix}, & z \in \mathcal{L}_0^\pm \\ \begin{pmatrix} 1 & 0 & 0 \\ 0 & 1 & 0 \\ 0 & \mp \omega^\mp e^{\mp n\Psi(z)} & 1 \end{pmatrix}, & z \in \mathcal{L}_1^\pm, \\ \begin{pmatrix} 1 & 0 & 0 \\ 0 & 1 & 0 \\ 0 & \mp \omega^\mp e^{\pm n\Psi(z)} & 1 \end{pmatrix}, & z \in \mathcal{L}_2^\pm. \end{cases}$$

Then S satisfies a Riemann-Hilbert problem on the contour Γ_S shown in Figure 34. The jump matrix J_S coincides with J_T outside the lenses, and on the

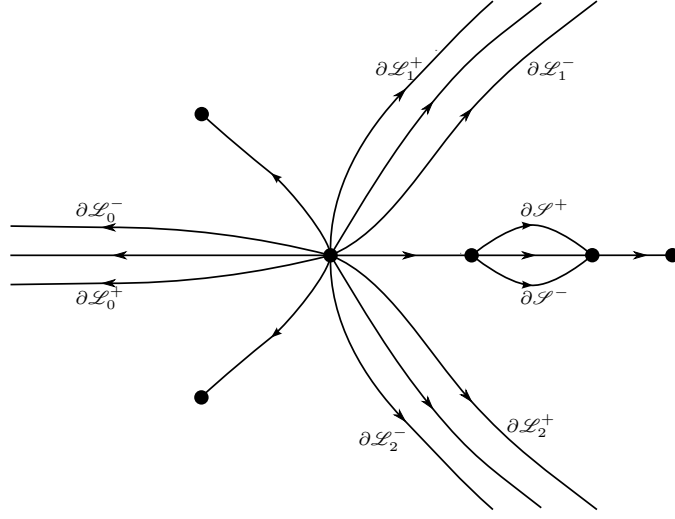


FIGURE 34. The boundary components of the lenses \mathcal{S} , \mathcal{L} determining the contour Γ_S for S .

remaining parts of Γ_S it is given by

$$J_S(z) = \begin{cases} \begin{pmatrix} 0 & 1 & 0 \\ -1 & 0 & 0 \\ 0 & 0 & 1 \end{pmatrix}, & z \in (z_1, z_0) \\ \begin{pmatrix} 1 & 0 & 0 \\ 0 & 0 & 1 \\ 0 & -1 & 0 \end{pmatrix}, & z \in L \\ \begin{pmatrix} 1 & 0 & 0 \\ e^{-n\Phi_0(z)} & 1 & 0 \\ 0 & 0 & 1 \end{pmatrix}, & z \in \partial\mathcal{S}^\pm, \\ \begin{pmatrix} 1 & 0 & 0 \\ 0 & 1 & 0 \\ 0 & \omega^\mp e^{-n\Psi(z)} & 1 \end{pmatrix}, & z \in \partial\mathcal{L}_0^\pm \\ \begin{pmatrix} 1 & 0 & 0 \\ 0 & 1 & 0 \\ 0 & \omega^\mp e^{\mp n\Psi(z)} & 1 \end{pmatrix}, & z \in \partial\mathcal{L}_1^\pm \\ \begin{pmatrix} 1 & 0 & 0 \\ 0 & 1 & 0 \\ 0 & \omega^\mp e^{\pm n\Psi(z)} & 1 \end{pmatrix}, & z \in \partial\mathcal{L}_2^\pm \end{cases}$$

The next step is the construction of the parametrices. In virtue of (8.5)–(8.6), the jump matrix J_S is exponentially small on the lipses of the lenses as well as in $\Sigma \setminus [z_1, z_0]$, as long as we stay away from the endpoints z_0, z_1, z_2 . Near z_2 , the jumps for S on Σ are still exponentially small, so for the local parametrix near z_2 we only have to take into account the jumps coming from L and $\partial\mathcal{L}$.

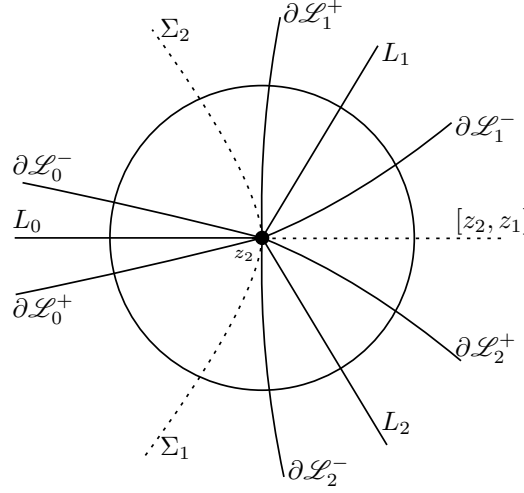


FIGURE 35. Blow up of the jump contours for S near z_2 . The solid lines represent L and $\partial\mathcal{L}$, so these are contours for the jumps of the local parametrix P . The dashed lines represent Σ , and since J_S is exponentially small in these contours, they are not taken into account for the construction of P near z_2 , so P is analytic across these contours.

More concretely,

- The RHP for the global parametrix M is essentially the same as in Section 7.6, having in mind that $\Sigma_* = (z_1, z_0)$. We refer to Section 9.3 for details.
- The local parametrices near z_0, z_1 are constructed out of Airy functions in exactly the same way as in Section 7.7. A little more care should be taken for the parametrix near z_2 . As we already observed, the jumps for S on Σ near z_2 are exponentially small, so we neglect them for the construction of the local parametrix near z_2 . Hence the jump condition on $D_\delta(z_2)$ becomes

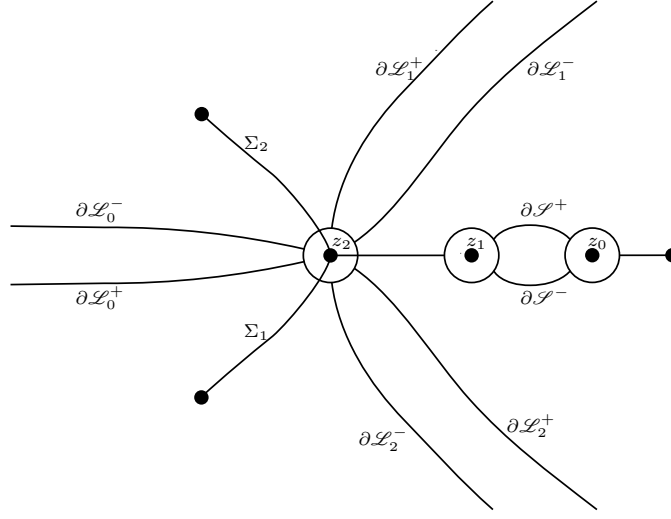
$$P_+(z) = P_-(z)J_S(z), \quad z \in D_\delta(z_2) \cap (L \cup \partial\mathcal{L}),$$

see Figure 35 for the jump contours of P near z_2 . The remaining RHP is essentially 2×2 . Although there are nine rays emanating from z_2 instead of the usual four rays, this parametrix is still constructed out of Airy functions, see for instance [39].

The final transformation $S \mapsto R$ is similar as in Section 7.8, equation (7.27). The contour Σ_R for R is displayed in Figure 36.

As in the three-cut case, it turns out that the jump matrix J_R is close to the identity as $n \rightarrow \infty$: on the lipses of the lenses \mathcal{S} and \mathcal{L} , this is true because of (8.5)–(8.6), whereas on the boundary of D_δ , this is true from the construction of the local parametrix. We only have to be careful about the jumps inside $D_\delta(z_2)$ that are not canceled by the local parametrix, which are given by

$$J_R(z) = P(z)J_S(z)P(z)^{-1} = P(z)J_T(z)P(z)^{-1}, \quad z \in \Sigma \cap D_\delta(z_2).$$

FIGURE 36. Contours for the jumps of R .

Since P is bounded near z_2 , the second inequality in (8.6) together with the identity above assure us that J_R is exponentially small for $z \in \Sigma \cap D_\delta(z_2)$.

As the final outcome, we get that the jump matrix J_R satisfies

$$J_R(z) = I + \mathcal{O}(n^{-1}), \quad n \rightarrow \infty,$$

uniformly in J_R , and the analysis is concluded in a similar fashion as in Section 7.8.

9. CONSTRUCTION OF THE GLOBAL PARAMETRIX

In this section we prove the existence of the global parametrix in the three-cut and one-cut cases. We also construct its first row explicitly.

It is convenient to perform a regluing of the sheets forming the Riemann surface \mathcal{R} , in much the same spirit as used for $t_1 = 0$ in Section 5.1.

To do so, recall the definition of the contours L_1 and L_2 given in (7.9) and (8.2) in the three-cut and one-cut cases, respectively, which defined the sector G_0 containing the point z_0 , as shown in Figures 29 and 33.

We construct a new Riemann surface

$$\tilde{\mathcal{R}} = \tilde{\mathcal{R}}_1 \cup \tilde{\mathcal{R}}_2 \cup \tilde{\mathcal{R}}_3,$$

obtained from the original surface \mathcal{R} after interchanging the sectors $\pi^{-1}(G_0) \cap \mathcal{R}_2$ and $\pi^{-1}(G_0) \cap \mathcal{R}_3$. Thus the sheets $\tilde{\mathcal{R}}_1$ and $\tilde{\mathcal{R}}_2$ are connected crosswise along Σ_* and the sheets $\tilde{\mathcal{R}}_2$ and $\tilde{\mathcal{R}}_3$ are connected crosswise along L . In the three-cut case, the branch points of $\tilde{\mathcal{R}}$ are

$$z_j^{(1)} = z_j^{(2)}, \quad j = 0, 1, 2, \quad \infty^{(2)} = \infty^{(3)},$$

whereas in the one-cut case the branch points are

$$z_j^{(1)} = z_j^{(2)}, \quad j = 0, 1, \quad z_2^{(2)} = z_2^{(3)}, \quad \infty^{(2)} = \infty^{(3)}.$$

We also denote

$$\tilde{\mathcal{R}}_{j,k} = \pi^{-1}(G_k) \cap \mathcal{R}_j, \quad j = 1, 2, \quad k = 0, 1, 2, \quad (9.1)$$

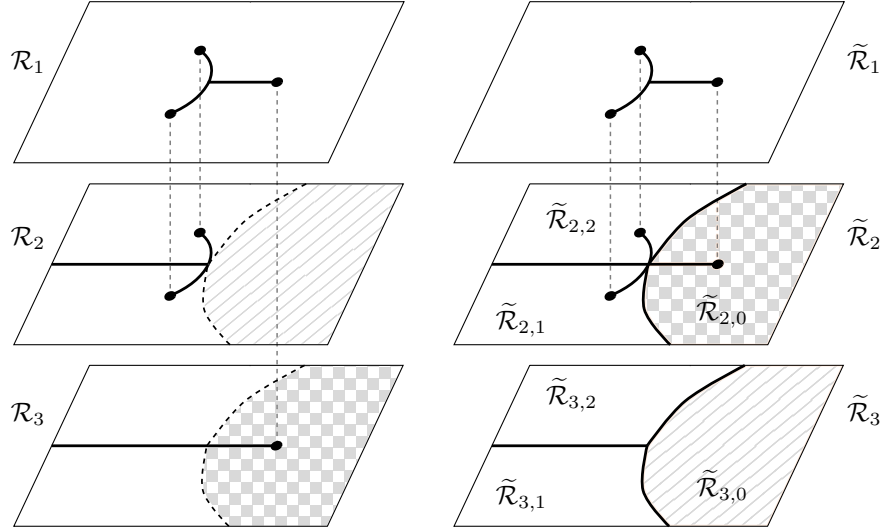


FIGURE 37. The sheet structure for \mathcal{R} (left panel) and $\tilde{\mathcal{R}}$ (right panel) in the three-cut case. The dashed lines on \mathcal{R}_2 and \mathcal{R}_3 are the (preimages through π of) the curves L_1 and L_2 . They bound the shaded areas, which are interchanged between the sheets to create the new sheets $\tilde{\mathcal{R}}_2$ and $\tilde{\mathcal{R}}_3$. On the right panel we also distinguish the set $\tilde{\mathcal{R}}_{j,k}$'s defined in (9.1).

and refer to Figures 37 and 38 for a depiction of the regluing and the sets (9.1) in the three-cut and one-cut cases, respectively.

It is also convenient to denote by $\Sigma_{*,+}^{(k)}$ and $\Sigma_{*,-}^{(k)}$ the positive and negative sides of the cut Σ_* on the sheet $\tilde{\mathcal{R}}_k$. Ditto for the other quantities $\Sigma_{*,j,\pm}^{(k)}$, $L_{\pm}^{(k)}$ and $L_{j,\pm}^{(k)}$. In particular, note that

$$\Sigma_{*,\pm}^{(1)} = \Sigma_{*,\mp}^{(2)}, \quad L_{\pm}^{(2)} = L_{\mp}^{(3)}.$$

We orient each arc of $\Sigma_*^{(k)}$ and $L^{(k)}$ according to the orientation induced from their projection Σ_* and L . Thus, for instance, the positive side of $\Sigma_{*,+}^{(1)}$ lies on the sheet $\tilde{\mathcal{R}}_1$, whereas the negative side of $\Sigma_{*,+}^{(1)}$ lies on the sheet $\tilde{\mathcal{R}}_2$.

9.1. The inverse of the rational parametrization. According to Theorem 2.5, the rational function h induces the bijection (2.16) between $\overline{\mathbb{C}}$ and \mathcal{R} , and consequently between $\overline{\mathbb{C}}$ and $\tilde{\mathcal{R}}$. This means that there exist three meromorphic functions

$$\psi_j : \tilde{\mathcal{R}}_j \rightarrow \overline{\mathbb{C}}, \quad j = 1, 2, 3, \quad (9.2)$$

for which

$$\psi : \tilde{\mathcal{R}} \rightarrow \overline{\mathbb{C}}, \quad \psi|_{\tilde{\mathcal{R}}_j} = \psi_j, \quad j = 1, 2, 3, \quad (9.3)$$

is the inverse of h .

Set

$$\begin{aligned} \mathcal{W}_j &= \psi(\tilde{\mathcal{R}}_j), \quad j = 1, 2, 3, \\ \mathcal{W}_{j,k} &= \psi(\tilde{\mathcal{R}}_{j,k}), \quad j = 2, 3, \quad k = 0, 1, 2, \end{aligned} \quad (9.4)$$

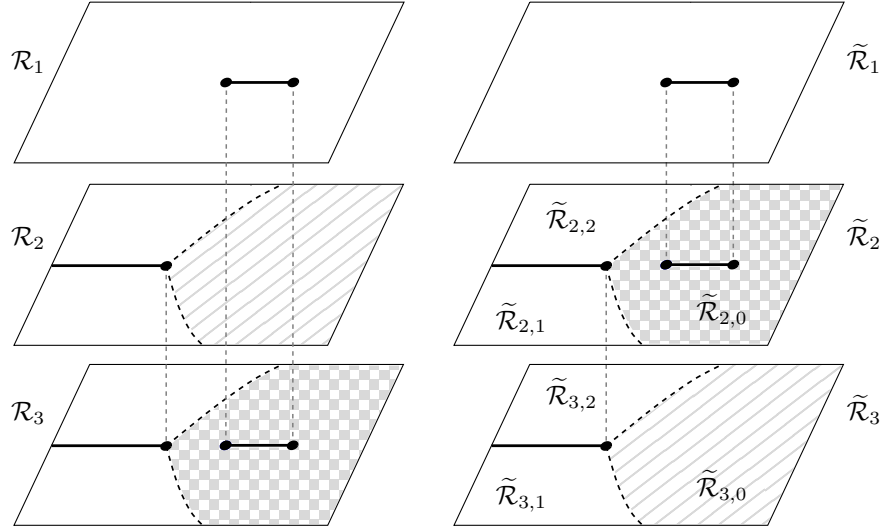


FIGURE 38. The sheet structure for \mathcal{R} (left panel) and $\tilde{\mathcal{R}}$ (right panel) in the one-cut case. The dashed lines on \mathcal{R}_2 and \mathcal{R}_3 are the (preimages through π of) the curves L_1 and L_2 . They bound the shaded areas, which are interchanged between the sheets to create the new sheets $\tilde{\mathcal{R}}_2$ and $\tilde{\mathcal{R}}_3$. On the right panel we also distinguish the set $\tilde{\mathcal{R}}_{j,k}$'s defined in (9.1).

and also

$$\begin{aligned}\Xi &= \psi(\Sigma_{*,+}^{(1)}), \\ \Lambda_j &= \psi(L_{j,+}^{(2)}), \quad j = 0, 1, 2, \\ \Lambda &= \psi(L_+^{(2)}) = \Lambda_0 \cup \Lambda_1 \cup \Lambda_2.\end{aligned}\tag{9.5}$$

In the three-cut case, we also define

$$\Xi_j = \psi(\Sigma_{*,j,+}^{(1)}), \quad j = 0, 1, 2,\tag{9.6}$$

so that $\Xi = \Xi_1 \cup \Xi_2 \cup \Xi_3$.

Using basic properties of conformal maps, the sets (9.4)–(9.6) can be described in the w -plane. The outcome for (9.4) can be seen in Figure 39. The sets (9.5)–(9.6) are displayed in Figures 40 and 41 in the three-cut and one cut-cases, respectively.

Remark 9.1. The function ψ_1 in (9.2) is analytic in $\mathbb{C} \setminus \Sigma_*$ and maps $\mathbb{C} \setminus \Omega$ conformally to $\mathbb{C} \setminus \mathbb{D}$. Since the point $\infty^{(1)}$ on \mathcal{R}_1 corresponds to the point ∞ on the w -plane through ψ , we automatically get that

$$\lim_{z \rightarrow \infty} \psi_1(z) = \infty.$$

Furthermore, using the Implicit Function Theorem,

$$\lim_{z \rightarrow \infty} \psi_1'(z) = \lim_{w \rightarrow \infty} \frac{1}{h'(w)} = \frac{1}{r}.$$

This shows that ψ_1 in (9.2) coincides with the function ψ_1 appearing in Theorem 2.15.

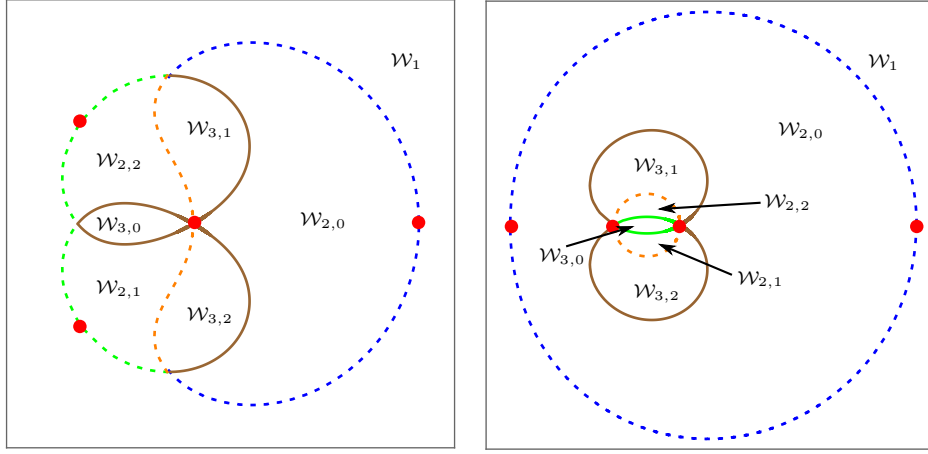


FIGURE 39. The partition of the w -plane into the sets $\mathcal{W}_{j,k}$'s in the three-cut (left panel) and one-cut (right panel) cases. The dashed lines display the inverse images of the cuts for the original Riemann surface \mathcal{R} (compare with Figure 26), and the solid lines display the new cuts arising after the regluing that defines $\tilde{\mathcal{R}}$. Numerical output for the choices $r = 1/20$ and $a_0 = 1/10$ (three-cut) and $a_0 = 1/4$ (one-cut).

9.2. Construction of the global parametrix in the three-cut case. In [15], the global parametrix is constructed for $t_1 = 0$ using meromorphic differentials. In this section we reproduce their arguments to construct the parametrix in the general three-cut case.

On the Riemann surface $\tilde{\mathcal{R}}$, consider the meromorphic differential η , defined by the condition that it has simple poles at each of the branch points $z_0^{(1)}, z_1^{(1)}, z_2^{(1)}$ and $\infty^{(2)}$, with residues

$$\text{Res}(\eta, z_j^{(1)}) = -\frac{1}{2}, \quad \text{Re}(\eta, \infty^{(2)}) = \frac{3}{2}, \quad (9.7)$$

and no other poles. Since the sum of residues is zero, such an η exists. It is also unique, because the genus of $\tilde{\mathcal{R}}$ is zero.

The set $\Sigma_{*,+}^{(1)} \cup L_+^{(2)}$ is connected and consists of a finite union of analytic arcs. Its image through the inverse ψ in (9.3) is the set $\Xi \cup \Lambda$, which can be geometrically described with standard arguments in conformal mapping, and is displayed in Figure 40. Since $\mathbb{C} \setminus (\Xi \cup \Lambda)$ and $\tilde{\mathcal{R}} \setminus (\Sigma_{*,+}^{(1)} \cup L_+^{(2)})$ are conformally equivalent, it readily follows from Figure 40 that the domain $\tilde{\mathcal{R}} \setminus (\Sigma_{*,+}^{(1)} \cup L_+^{(2)}) \subset \tilde{\mathcal{R}}$ is simply connected and does not contain poles of η . In particular, this implies that the function

$$u(p) = \int_{\infty^{(1)}}^p \eta, \quad p \in \tilde{\mathcal{R}} \setminus (\Sigma_{*,+}^{(1)} \cup L_+^{(2)}),$$

where the integration goes along any path that does not cross $\Sigma_{*,+}^{(1)} \cup L_+^{(2)}$, is well defined and analytic.

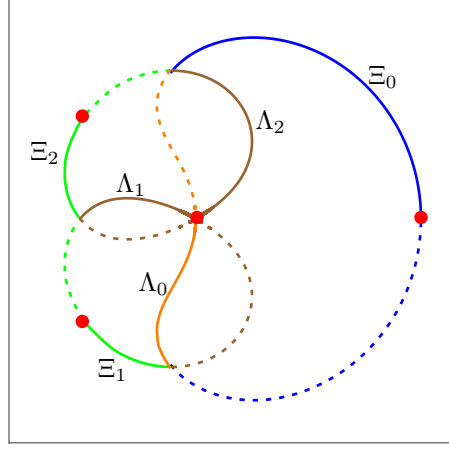


FIGURE 40. In solid lines the sets Λ_j and Ξ_j , $j = 0, 1, 2$, are displayed; these are the image through ψ of the jumps for m . In dashed lines, the remaining images through ψ of the cuts of $\tilde{\mathcal{R}}$ are shown. The solid lines also correspond to the jump contours for f in the three-cut case. Numerical output for $r = 1/20$ and $a_0 = 1/10$.

From Figure 40 and conformal equivalence, it follows that for a given $p \in \Sigma_{*,+}^{(1)} \cup L_+^{(2)}$, we can write the difference $u_+(p) - u_-(p)$ as an integral over a closed contour going around exactly one of the branch points $z_j^{(1)}$. Consequently we learn from (9.7) and the Residues Theorem that

$$u_+(p) - u_-(p) = \pm \pi i, \quad p \in \Sigma_{*,+}^{(1)} \cup L_+^{(2)}. \quad (9.8)$$

We thus define

$$m(p) = e^{u(p)}, \quad p \in \tilde{\mathcal{R}} \setminus \Sigma_{*,+}^{(1)} \cup L_+^{(2)}.$$

Note that (9.8) implies that

$$m_+(p) = -m_-(p), \quad p \in \Sigma_{*,+}^{(1)} \cup L_+^{(2)}. \quad (9.9)$$

Set

$$m_k = m|_{\tilde{\mathcal{R}}_k}, \quad k = 1, 2, 3.$$

The functions m_1 , m_2 and m_3 are analytic in $\mathbb{C} \setminus \Sigma_*$, $\mathbb{C} \setminus (\Sigma_* \cup L)$ and $\mathbb{C} \setminus L$, respectively. Combining with the condition (9.9) we immediately get that

$$(m_{1+}(z), m_{2+}(z), m_{3+}(z)) = (m_{1-}(z), m_{2-}(z), m_{3-}(z)) J_M(z), \quad z \in \Sigma_* \cup L. \quad (9.10)$$

In addition, (9.7) gives

$$m_k(z) = \mathcal{O}\left((z - z_j)^{-1/4}\right), \quad z \rightarrow z_j, \quad k = 1, 2, \quad (9.11)$$

and also

$$m_k(z) = \mathcal{O}(z^{-3/4}), \quad z \in \infty, \quad k = 2, 3. \quad (9.12)$$

Furthermore, since $u(\infty^{(1)}) = 0$, we also have

$$m_1(z) = 1 + \mathcal{O}(z^{-1}), \quad z \rightarrow \infty. \quad (9.13)$$

In summary, (9.10)–(9.13) tell us that the row vector (m_1, m_2, m_3) satisfies the conditions for the first row of M .

To construct the remaining rows of M , consider a basis $f_1 \equiv 1, f_2, f_3$ of the vector space of functions analytic on $\tilde{\mathcal{R}} \setminus \{\infty^{(2)}\}$, with at most a double pole at $\infty^{(2)}$. Denote $f_{j,k} = f_j|_{\tilde{\mathcal{R}}_k}$ and consider the auxiliary matrix

$$B = \begin{pmatrix} m_1 & m_2 & m_3 \\ m_1 f_{2,1} & m_2 f_{2,2} & m_3 f_{2,3} \\ m_1 f_{3,1} & m_2 f_{3,2} & m_3 f_{3,3} \end{pmatrix}. \quad (9.14)$$

Using (9.10), we learn

$$B_+(z) = B_-(z)J_M(z), \quad z \in \Sigma_* \cup L. \quad (9.15)$$

Furthermore, it follows from the analyticity of the $f_{j,k}$'s near finite points, and also the local behavior (9.11)–(9.13), that B satisfies the endpoint conditions for M .

Because $\det J_M = 1$, we also learn from (9.15) that $\det B$ is entire. Furthermore, a simple analysis of its entries shows that $B(z) = \mathcal{O}(z^{1/4})$ as $z \rightarrow \infty$. Since the functions f_1, f_2 and f_3 are linearly independent, this is enough to show that $\det B$ is equal to a non-zero constant. In particular, B is always invertible.

By inspection one can see that the function A in (7.11) satisfies $A_+ = A_- J_M$ on L , and using (9.15) we thus conclude that BA^{-1} is analytic on $\mathbb{C} \setminus \Sigma_*$. As $A(z) = \mathcal{O}(z^{1/4})$ and $B(z) = \mathcal{O}(z^{1/4})$, we see that BA^{-1} is bounded near ∞ , and thus admits a series expansion of the form

$$(BA^{-1})(z) = C + \mathcal{O}(z^{-1}), \quad z \rightarrow \infty,$$

for some constant matrix C , which is non-singular because $\det A, \det B \neq 0$. We already observed that B satisfies (9.15) and also the endpoint conditions for M . It thus finally follows that

$$M(z) = C^{-1}B(z), \quad z \in \mathbb{C} \setminus (\Sigma_* \cup L)$$

is the desired global parametrix.

9.3. Construction of the global parametrix in the one-cut case. The Riemann-Hilbert problem for the global parametrix in the one-cut case assumes the following form.

- $M : \mathbb{C} \setminus (\Sigma_* \cup L) \rightarrow \mathbb{C}^{3 \times 3}$ is analytic;
- $M_+(z) = M_-(z)J_M(z)$, $z \in \Sigma_* \cup L$, where J_M is defined as in (7.25).
- $M(z) = \mathcal{O}((z - z_j)^{-1/4})$ as $z \rightarrow z_j$, $j = 0, 1, 2$.
- $M(z) = (I + \mathcal{O}(z^{-1}))A(z)$, as $z \rightarrow \infty$.

Following the ideas carried out in Section 9.2, we start the construction of M from its first row.

As in Section 9.2, there exists a meromorphic differential η on $\tilde{\mathcal{R}}$ uniquely defined through the conditions that it has simple poles at the branch points $z_0^{(1)}, z_1^{(1)}, z_2^{(2)}$ and $\infty^{(2)}$, with residues

$$\text{Res}(\eta, z_0^{(1)}) = \text{Res}(\eta, z_1^{(1)}) = \text{Res}(\eta, z_2^{(2)}) = -\frac{1}{2}, \quad \text{Res}(\eta, \infty^{(2)}) = \frac{3}{2}, \quad (9.16)$$

and no other poles.

We then consider the function

$$u(p) = \int_{\infty^{(1)}}^p \eta, \quad p \in \tilde{\mathcal{R}} \setminus (\Sigma_{*,+}^{(1)} \cup L_{0,+}^{(2)}).$$

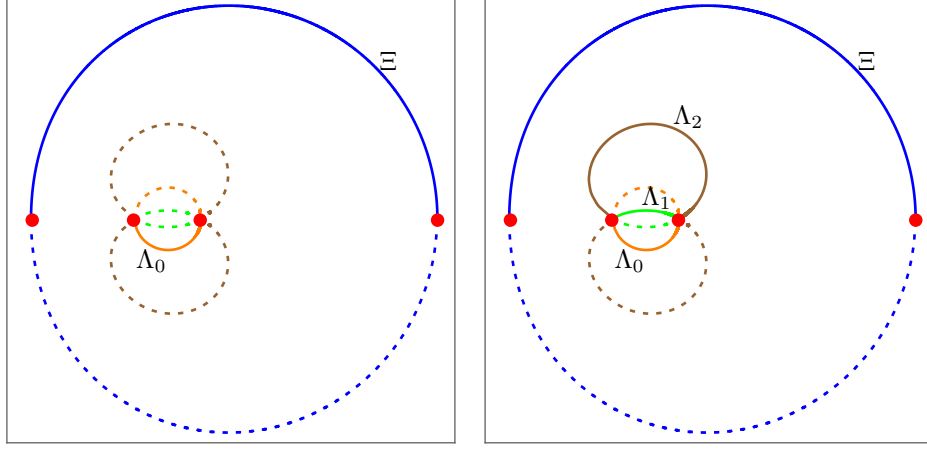


FIGURE 41. The solid lines are the images through ψ of the jumps for \tilde{m} and m in the left and right panels, respectively. The dashed lines are the images of the remaining cuts. The solid lines in the right panel also correspond to the jump contours for f in the one-cut case. Numerical output for $r = 1/20$ and $a_0 = 1/4$.

The image of $\Sigma_{*,+}^{(1)} \cup L_{0,+}^{(2)}$ through ψ is the set $\Xi \cup \Lambda_0$, which is shown in the left panel of Figure 41. From this figure and conformal equivalence, it easily follows that the set $\tilde{\mathcal{R}} \setminus (\Sigma_{*,+}^{(1)} \cup L_{0,+}^{(2)})$ is not simply connected, and thus $u(p)$ depends on the path of integration chosen. However, in virtue of (9.16), it follows after a residue calculation that the value $u(p)$ is well defined modulo $2\pi i$. Having this in mind, it also holds true

$$u_+(p) - u_-(p) = \pi i \pmod{2\pi i}, \quad p \in \Sigma_{*,+}^{(1)} \cup L_{0,+}^{(2)}. \quad (9.17)$$

We then define

$$\tilde{m}(p) = e^{u(p)}, \quad p \in \tilde{\mathcal{R}} \setminus (\Sigma_{*,+}^{(1)} \cup L_{0,+}^{(2)}),$$

and also

$$m(p) = \begin{cases} -\tilde{m}(p), & p \in \mathcal{W}_{2,2} \cup \mathcal{W}_{3,1} \\ \tilde{m}(p), & \text{elsewhere.} \end{cases}$$

The functions \tilde{m} and m are analytic on $\tilde{\mathcal{R}} \setminus (\Sigma_{*,+}^{(1)} \cup L_{0,+}^{(2)})$ and $\tilde{\mathcal{R}} \setminus (\Sigma_{*,+}^{(1)} \cup L_+^{(2)})$, respectively. Furthermore, from (9.17)

$$\tilde{m}_+(p) = -\tilde{m}_-(p), \quad p \in \Sigma_{*,+}^{(1)} \cup L_{0,+}^{(2)},$$

and consequently, from the definition of m we get

$$m_+(p) = -m_-(p), \quad p \in \Sigma_{*,+}^{(1)} \cup L_+^{(2)}. \quad (9.18)$$

We refer the reader to Figure 41 for a display of the jump contours for \tilde{m} and m in the w -plane.

Further setting

$$m_j = m|_{\tilde{\mathcal{R}}_j}, \quad j = 1, 2, 3,$$

it follows in the same way as we did in Section 9.2, equations (9.7)–(9.13), that the first row of the global parametrix M is (m_1, m_2, m_3) . The remaining rows of M

can be obtained in exactly the same way as we did in Section 7.6, equation (9.14) *et seq.* We skip the details.

9.4. Explicit construction of the first row. In Sections 9.2 and 9.3, we constructed the first row of the global parametrix in terms of the function m , which, in virtue of (9.9)–(9.13) (see also (9.18)) is unique solution to the following Riemann-Hilbert problem.

- $m : \tilde{\mathcal{R}} \setminus (\Sigma_{*,+}^{(1)} \cup L_+^{(2)}) \rightarrow \mathbb{C}$ is analytic;
- $m_+(z) = -m_-(z)$, $z \in \Sigma_{*,+}^{(1)} \cup L_+^{(2)}$;
- If z_j is a branch point for the sheet $\tilde{\mathcal{R}}_k$, then

$$m_k(z) = \mathcal{O}((z - z_k)^{-1/4}), \quad z \rightarrow z_j, \quad (9.19)$$

and as $z \rightarrow \infty$,

$$m_1(z) = 1 + \mathcal{O}(z^{-1}), \quad m_k(z) = \mathcal{O}(z^{-3/4}), \quad k = 2, 3. \quad (9.20)$$

- In the three-cut case, $m_k(z)$ remains bounded as $z \rightarrow z_*$.

It turns out that the Riemann-Hilbert problem above can be solved explicitly with the help of the rational parametrization h and its inverse ψ in (9.3). If we seek for m of the form

$$f(w) = m(h(w)), \quad (9.21)$$

then it follows that f should satisfy the following scalar Riemann-Hilbert problem.

- $f : \mathbb{C} \setminus (\Xi \cup \Lambda) \rightarrow \mathbb{C}$ is analytic;
- $f_+(w) = -f_-(w)$, $w \in \Xi \cup \Lambda$;
- $f(w) \rightarrow 1$ as $w \rightarrow \infty$ and $f(w) \rightarrow 0$ as $w \rightarrow 0$.
- $f(w) = \mathcal{O}((w - w_j)^{-1/2})$ as $w \rightarrow w_j$, $j = 0, 1, 2$.

We remark that the 1/4-blow-ups for m become 1/2-blow-ups because the points z_0, z_1 and z_2 are branch points.

The jumps for f are shown in Figure 40 and in the right panel of Figure 41 for the three-cut and one-cut cases, respectively.

Thus the natural choice for f is

$$f(w) = \left(\frac{w^3}{(w - w_0)(w - w_1)(w - w_2)} \right)^{1/2}, \quad w \in \mathbb{C} \setminus (\Xi \cup \Lambda),$$

where the branch of the square root is uniquely determined by the condition that $f(w) \rightarrow 1$ as $w \rightarrow \infty$ and with branch cuts on $\Xi \cup \Lambda$.

We know that w_0, w_1 and w_2 are the zeros of h' (see Lemma 3.10), and consequently of the monic polynomial $\tilde{h}(w) = w^3 r^{-1} h'(w)$ as in (3.28). This means that

$$\frac{w^3}{r} h'(w) = (w - w_0)(w - w_1)(w - w_2),$$

which expresses that

$$f(w) = \left(\frac{r}{h'(w)} \right)^{1/2}. \quad (9.22)$$

From the Inverse Function Theorem, we know that $h'(w) = 1/\psi'(z)$, where ψ is given in (9.3) and $w = \psi(z)$. Returning back to (9.22) and using (9.21), we thus get that m is given by

$$m(z) = \sqrt{r\psi'(z)}, \quad z \in \tilde{\mathcal{R}} \setminus (\Sigma_{*,+}^{(1)} \cup L_+^{(2)}).$$

Recalling (9.3), we finally arrive at the expressions for the first line (m_1, m_2, m_3) of M , namely

$$m_j(z) = \sqrt{r\psi'_j(z)}, \quad j = 1, 2, 3, \quad (9.23)$$

where the branch cuts for the square root of ψ_1 , ψ_2 and ψ_3 are determined from the ones in (9.22). In particular, the branch cut for m_1 is taken on Σ_* .

10. PROOFS OF THEOREMS 2.14 AND 2.15

We now prove Theorems 2.14 and 2.15. The arguments are valid both in the three-cut and one-cut cases.

Proof of Theorem 2.15. Unfolding the transformations in the Riemann-Hilbert analysis, we get in particular

$$\begin{aligned} P_{n,n}(z) &= Y_{1,1}(z) \\ &= X_{1,1}(z) \\ &= T_{1,1}(z)e^{\frac{n}{t_0}(g_1(z)-V(z)-l_1)}, \quad z \in \mathbb{C} \setminus \Sigma, \end{aligned}$$

we refer to (7.7), (7.10) and (7.17) for the three-cut case, and remind that these transformations are the same in the one-cut case (with the appropriate definition of the function g_1). For any fixed compact $K \subset \mathbb{C} \setminus \Sigma_*$, we can reduce the lens \mathcal{S} and the set D_δ in such a way that

$$K \cap (\overline{\mathcal{S}} \cup \overline{D_\delta}) = \emptyset,$$

and in this case it follows further that $T_{1,1} = S_{1,1}$ on K (see for instance (7.23) and (7.24)), so

$$P_{n,n}(z) = S_{1,1}(z)e^{-\frac{n}{t_0}(g_1(z)-V(z)-l_1)}, \quad z \in K. \quad (10.1)$$

From (7.27) and the estimate (7.28), we know that as $n \rightarrow \infty$

$$\begin{aligned} S_{1,1}(z) &= R_{1,1}(z)M_{1,1}(z) + R_{1,2}(z)M_{2,1}(z) + R_{1,3}(z)M_{3,1}(z) \\ &= (1 + \mathcal{O}(n^{-1}))M_{1,1}(z), \quad z \in K. \end{aligned}$$

where for the last equality we also used that the first column of M remains bounded away from Σ_* , which is a direct consequence of the RHP satisfied by M . Also note that the implicit term above is uniform on K . Returning this last equation into (10.1), we conclude

$$P_{n,n}(z) = (1 + \mathcal{O}(n^{-1}))M_{1,1}(z)e^{\frac{n}{t_0}(g_1(z)-V(z)-l_1)} \quad (10.2)$$

uniformly on the compact $K \subset \mathbb{C} \setminus \Sigma_*$.

From (9.23) and from the definition of g_1 in (7.12) and (8.3), it immediately follows that

$$M_{1,1}(z) = \sqrt{r\psi'_1(z)}, \quad g_1(z) = G(z) + c_1,$$

where G is as in (2.44). Returning this information back to (10.2), we get (2.45) for the constant $c = c_1 - l_1$. \square

Proof of Theorem 2.14. Since ψ_1 is the inverse of h on $\tilde{\mathcal{R}}_1$, the derivative ψ'_1 does not vanish on $\mathbb{C} \setminus \Sigma_*$, so from (2.45) we conclude that the zeros of $P_{n,n}$ accumulate on the star Σ_* in the large n limit.

Suppose now that $\mu_{n_k} \xrightarrow{*} \nu$, where (μ_{n_k}) is a subsequence of the sequence of zero counting measures (μ_n) defined in (2.43). The zeros of $P_{n,n}$ accumulate on Σ_* , so we must have

$$\text{supp } \nu \subset \Sigma_*.$$

For any $z \in \mathbb{C} \setminus \Sigma_*$, it follows from (10.2) that

$$\begin{aligned} U^\nu(z) &= - \int \log |s - z| d\nu(s) \\ &= - \lim_{k \rightarrow \infty} \frac{1}{n_k} \log |P_{n_k, n_k}(z)| = - \frac{1}{t_0} \text{Re}(g_1(z) - V(z) - l_1). \end{aligned}$$

Having in mind (6.6) and (6.8), this last identity implies that

$$C^\nu(z) = - \frac{1}{t_0} (g'_1(z) - V'(z)) = - \frac{1}{t_0} (\xi_1(z) - V'(z)) = C^{\mu_*}(z), \quad z \in \mathbb{C} \setminus \Sigma_*.$$

Using the same arguments as in (6.20) *et seq.*, we thus conclude

$$U^\nu(z) = U^{\mu_*}(z), \quad z \in \mathbb{C} \setminus \Sigma_*.$$

Since Σ_* has planar Lebesgue measure zero, the above equation says that the potential of the measures ν and μ_* coincide a.e. in \mathbb{C} . From the Unicity Theorem [50, Theorem II.2.1] we get $\nu = \mu_*$, concluding the proof. \square

APPENDIX A. ANALYSIS OF THE WIDTH PARAMETERS

In the appendix, we analyze the parameters τ_j 's that were used in Section 5. To do so, we need some preliminary lemmas. For the next results, we recall that w_0 and w_1 are given by Lemma 3.10.

Lemma A.1. *For $(t_0, t_1) \in \mathcal{F}$, it is valid*

$$w_0 > r^{1/3}. \tag{A.1}$$

Additionally, for $(t_0, t_1) \in \mathcal{F}_2$,

$$|w_1| < r^{1/3}, \tag{A.2}$$

and

$$w_1 > -\frac{2a_0}{3r}, \tag{A.3}$$

and consequently,

$$|w_1| < w_0. \tag{A.4}$$

Proof. Recall that w_0 is the unique positive solution to

$$h'(w) = 0,$$

so $h'(w) < 0$ for positive w only if $w < w_0$. Simple calculations then show

$$h'(r^{1/3}) = -r - 2a_0 r^{1/3} < 0, \quad 0 < r < \frac{1}{2}.$$

giving us (A.1).

For the second inequality, we recall that w_1 is the smallest (negative) root of h' and, furthermore, $h'(w) \rightarrow r > 0$ as $w \rightarrow -\infty$, so that $h(w) > 0$ on the interval $(-\infty, w_1)$. Simple computations show that

$$h'(-r^{1/3}) = r \left(3 - \frac{2a_0}{r^{2/3}} \right).$$

For fixed a_0 , the function $r \mapsto 3 - 2a_0/r^{2/3}$ is increasing, so it attains its maximum when r is chosen so that the corresponding pair (t_0, t_1) belongs to the critical curve γ_c . Using (2.22), we see that this maximum is

$$3 - \frac{3s^2}{s^2} = 0,$$

thus we get that $h'(-r^{1/3}) < 0$. Since we already observed that h' is positive on $(-\infty, w)$, this is enough to conclude that $w_1 < -r^{1/3} < 0$, which is equivalent to (A.2).

To get (A.3), we note that the function

$$a_0 \mapsto -\frac{2a_0}{3r}$$

is decreasing, so it attains its maximum value along γ_c . Recalling that $w_1 > -1$ (see Lemma 3.10) and using (2.48), we get

$$-\frac{2a_0}{3r} < -\frac{2(3s^2/2)}{s^3} = -\frac{1}{s} < -1 < w_1.$$

Finally, the inequality (A.4) trivially follows from (A.1)–(A.2). \square

Lemma A.2. *Suppose $(t_0, t_1) \in \mathcal{F}_2$. Then*

$$\frac{1}{w_0} + \frac{1}{w_1} > -1 \tag{A.5}$$

where w_0 and w_1 are the zeros of h' as in Lemma 3.10.

Proof. From the explicit expression of h in (2.3), we trivially have

$$h''(w) = \frac{4a_0r}{w^3} + \frac{6r^2}{w^4} = \frac{2r}{w^4}(3rw + 2a_0) \tag{A.6}$$

Since $h'(w_j) = 0$, the chain rule gives us

$$\frac{\partial w_j}{\partial a_0} = -\frac{\frac{\partial h'}{\partial a_0}(w_j)}{h''(w_j)} = \frac{2r}{w_j^2 h''(w_j)}.$$

Using (A.6), we thus get

$$\begin{aligned} \frac{\partial}{\partial a_0} \left(\frac{1}{w_0} + \frac{1}{w_1} \right) &= - \left(\frac{1}{w_0^2} \frac{\partial w_0}{\partial a_0} + \frac{1}{w_1^2} \frac{\partial w_1}{\partial a_0} \right) \\ &= - \left(\frac{1}{3rw_0 + 2a_0} + \frac{1}{3rw_1 + 2a_0} \right). \end{aligned} \tag{A.7}$$

We know that $w_0 > 0$ and also $3rw_1 + 2a_0 > 0$, as it follows from Lemma 3.10 and (A.3), respectively. From (A.7) we thus conclude that the function

$$a_0 \mapsto \frac{1}{w_0} + \frac{1}{w_1}$$

is decreasing, so it attains its minimum along the critical curve Γ_c . On Γ_c , it follows from (2.21) that

$$h'(w) = \frac{s(w-1)(2s+w^2+w)}{w^3},$$

where $s \in (0, 1/8)$, so that in this case

$$w_0 = 1, \quad w_1 = \frac{1}{2}(-1 - \sqrt{1-8s}),$$

and consequently for every choice of parameters in \mathcal{F}_2 , it holds true

$$\frac{1}{w_0} + \frac{1}{w_1} > 1 - \frac{2}{1 + \sqrt{1 - 8s}} > -1,$$

as we want. \square

A.1. Width parameters in the three-cut case. Recall that the non vanishing of the parameters τ_j , $j = 1, 2, 3, 4, 5$, introduced in (5.13)–(5.17), were used in Section 5.4.3 to prove that the critical graph of the quadratic differential ϖ remains unchanged in \mathcal{F}_1 . We now verify that these quantities do not vanish.

Proposition A.3. *For $(t_0, t_1) \in \mathcal{F}_1$, we have $\tau_5 < 0$.*

Proof. Follows directly from (4.30) and (5.17). \square

Proposition A.4. *For $(t_0, t_1) \in \mathcal{F}_1$, we have $\tau_1 > 0$.*

Proof. The rational parametrization $(\xi, z) = (h(w^{-1}), h(w))$ given by Theorem 2.2 induces the change of variables $s = h(w)$, $\xi_j = h(w^{-1})$, from which it follows that

$$\int_{z_2}^{z_0} \xi_1 ds = \int_{w_2}^{w_0} h\left(\frac{1}{w}\right) h'(w) dw, \quad \int_{z_2}^{z_0} \xi_2 ds = \int_{w_2}^{\tilde{w}_0} h\left(\frac{1}{w}\right) h'(w) dw,$$

where w_2, w_0, \tilde{w}_0 satisfy

$$z_2 = h(w_2), \quad \xi_1(z_2) = h(w_2^{-1}) = \xi_2(z_2), \quad (\text{A.8})$$

$$z_0 = h(w_0) = h(\tilde{w}_0), \quad \xi_1(z_0) = h(w_0^{-1}), \quad \xi_2(z_0) = h(\tilde{w}_0^{-1}). \quad (\text{A.9})$$

We should remark that w_0 and w_2 are the same points given by Lemma 3.10.

Hence,

$$\tau_1 = \operatorname{Re} \int_{z_2}^{z_0} (\xi_1(s) - \xi_2(s)) ds = \operatorname{Re} \int_{\tilde{w}_0}^{w_0} h\left(\frac{1}{w}\right) h'(w) dw. \quad (\text{A.10})$$

We can further simplify the integral above in the following way,

$$\begin{aligned} \int_{\tilde{w}_0}^{w_0} h\left(\frac{1}{w}\right) h'(w) dw &= \int_{\tilde{w}_0}^{w_0} \left(h\left(\frac{1}{w}\right) - a_0 \right) h'(w) dw + a_0 \int_{\tilde{w}_0}^{w_0} h'(w) dw \\ &= \int_{\tilde{w}_0}^{w_0} \left(h\left(\frac{1}{w}\right) - a_0 \right) h'(w) dw, \end{aligned}$$

where in the last step we used the first equation in (A.9).

We use the definition of h in (2.3) to compute explicitly the last integral above, arriving at

$$\int_{\tilde{w}_0}^{w_0} h\left(\frac{1}{w}\right) h'(w) dw = F(w_0) - F(\tilde{w}_0) + r^2(1 - 4a_0^2 - 2r^2)(\log w_0 - \log \tilde{w}_0), \quad (\text{A.11})$$

where

$$F(w) = \frac{r^3}{3} w^3 + r^2 a_0 w^2 - 2r^3 a_0 w + \frac{4r^3 a_0}{w} + \frac{r^2 a_0}{w^2} + \frac{2r^3}{3w^3}$$

is determined by the condition that $F(w) + r^2(1 - 4a_0^2 - 2r^2) \log w$ is the primitive of $h(w^{-1})(h(w) - a_0)$.

The next step is to express \tilde{w}_0 in terms of w_0 . The equation

$$h(w) - z_0 = \frac{r}{w^2} \left(w^3 + \frac{a_0 - z_0}{r} w^2 + 2a_0 w + r \right) = 0$$

has w_0 as a solution with double multiplicity and \tilde{w}_0 as a simple solution, that is

$$w^3 + \frac{a_0 - z_0}{r}w^2 + 2a_0w + r = (w - w_0)^2(w - \tilde{w}_0).$$

This gives us the relation

$$\tilde{w}_0 = -\frac{r}{w_0^2}. \quad (\text{A.12})$$

After some calculations, we are thus reduced to

$$\begin{aligned} F(w_0) - F(\tilde{w}_0) = \frac{r + w_0^3}{3w_0^6} & (2w_0^9 - 3a_0w_0^7 + r(r^2 - 2)w_0^6 + 15a_0r^2w_0^5 \\ & + 3a_0r(1 - 2r^2)w_0^4 + r^2(2 - r^2)w_0^3 - 3a_0r^3w_0^2 + r^5) \end{aligned}$$

The expression $h'(w_0) = 0$ gives us additionally $w_0^3 = 2a_0w_0 + 2r$. Replacing every multiple power of 3 in the expression under brackets above, we get

$$\begin{aligned} F(w_0) - F(\tilde{w}_0) = \frac{r + w_0^3}{3w_0^6} & ((30a_0^2r^2 + 4a_0^3)w_0^3 + ra_0(r^2(12 - 8a_0) + 10a_0)w_0^2 \\ & + 6a_0r^2(5 - r^2)w_0 + 12r^3 + 3r^5). \quad (\text{A.13}) \end{aligned}$$

Recalling Theorem 3.6, we know that $0 < a_0, r < 1$, so the expression between parentheses above is a polynomial in w_0 with positive coefficients. Because $w_0 > 0$ (Lemma 3.10), we finally conclude

$$F(w_0) - F(\tilde{w}_0) > 0. \quad (\text{A.14})$$

We now take care of the log terms in (A.11). From the definition of a_0 in (2.4),

$$0 \leq a_0 \leq \frac{1 - 4r^2}{2} < \frac{1}{2},$$

and this gives us $4a_0^2 \leq 2a_0$. Having also in mind $r < 1$,

$$1 - 4a_0^2 - 2r^2 > 1 - 2r - 2a_0 > 0, \quad (\text{A.15})$$

where in the last step we used (3.21). Using also (A.12), we get

$$\text{Re}((1 - 4a_0^2 - 2r^2)(\log w_0 - \log \tilde{w}_0)) = (1 - 4a_0^2 - 2r^2) \log \frac{w_0^3}{r} > 0,$$

because $w_0^3 > r$, see (A.1). Plugging this last equation and (A.14) into (A.11), and having in mind (A.10), we arrive at the desired result. \square

Remark A.1. Note that (A.12) and (A.13) also hold if we replace w_0 and \tilde{w}_0 by w_j and \tilde{w}_j , respectively, where w_j is a zero of $h'(w) = 0$ and \tilde{w}_j is the simple zero of $h(w) - h(w_j) = 0$.

Remark A.2. The keen reader might notice that a combination of (A.11)–(A.13) establishes the equivalence between (2.47) and (2.48). In fact, the mother body phase transition determined by γ_c^- corresponds to the vanishing of τ_1 . Unlike for $t_1 > 0$, the transition across γ_c^- does not correspond to the coalescence of critical points of the quadratic differential ϖ (or, equivalently, of the points z_j and \hat{z}_j given by Theorem 2.6). Instead, it corresponds to the shrinking of the domains \mathcal{S}_1 and \mathcal{S}_6 in Figure 23.

Proposition A.5. *For $(t_0, t_1) \in \mathcal{F}_1$, we have*

$$\tau_2 > 0, \quad (\text{A.16})$$

$$\tau_3 < 0. \quad (\text{A.17})$$

We have not been able to verify Proposition A.5 analytically, so we verified it numerically as explained next.

We start with (A.16). As in the proof of Proposition A.4, we perform the change of variables $z = h(w)$, $\xi_j = h(w^{-1})$, and arrive at

$$\int_{z_0}^{z_2} \xi_1(s) ds = H(w_2) - H(w_0), \quad \int_{z_0}^{z_2} \xi_3(s) ds = H(\tilde{w}_2) - H(w_0), \quad (\text{A.18})$$

where w_0, w_2 are as in Lemma 3.10, \tilde{w}_2 is the simple zero of $h(w) - z_2$, so alternatively given by

$$\tilde{w}_2 = -\frac{r}{w_2^2}, \quad (\text{A.19})$$

see Remark A.1, and $H(w)$ is the primitive of $h'(w)h(w^{-1})$, explicitly given by

$$\begin{aligned} H(w) = & \frac{r^3}{3} w^3 + a_0 r^2 w^2 + a_0 r (1 - 2r^2) w \\ & + \frac{2a_0^2 r + 4a_0 r^3}{w} + \frac{2a_0 r^2}{w^2} + \frac{2r^3}{3w^3} - r^2 (4a_0^2 + 2r^2 - 1) \log w \end{aligned} \quad (\text{A.20})$$

In the expression above, we choose the main branch of the logarithm - actually the branch chosen is not important, because at the end we will be only interest in the real part of H . Taking the difference between the two expressions in (A.18), the integral in Equation (5.14) gets the form

$$\begin{aligned} \tau_2 = \operatorname{Re} \int_{z_0}^{z_2} (\xi_1(s) - \xi_3(s)) ds &= \operatorname{Re} H(w_2) - \operatorname{Re} H(\tilde{w}_2) \\ &= \operatorname{Re} H(w_2) - \operatorname{Re} H\left(-\frac{r}{w_2^2}\right). \end{aligned} \quad (\text{A.21})$$

Note that the right hand side of (A.21) is given only in terms of a_0, r . We then use (A.21) for numerical computation of the integral as follows.

For given r, a_0 , we first solve

$$h'(w) = 0,$$

pick w_2 as the only solution with positive imaginary part (see Lemma 3.10), compute \tilde{w}_2 through (A.19) and finally get the difference $\operatorname{Re} H(w_2) - \operatorname{Re} H(\tilde{w}_2)$. By varying $r \in (0, 1/2)$ and $a_0 \in (0, \alpha)$, where

$$\alpha = \alpha(r) = \min\{3/2r^{2/3}, (1 - 2r)/2\} = \begin{cases} \frac{3}{2}r^{2/3}, & r \leq \frac{1}{8}, \\ \frac{1-2r}{2}, & \frac{1}{8} < r < \frac{1}{2}, \end{cases}$$

we are sure to be covering every possible choice $(t_0, t_1) \in \mathcal{F}_1$ (see Proposition 2.7).

With this idea in mind, we evaluated τ_2 numerically with Mathematica in 300-digit precision for the range

$$r = \frac{1}{2} \frac{j}{5000}, \quad a_0 = \frac{\alpha(r)}{5000} k, \quad j, k = 1, \dots, 5000, \quad (\text{A.22})$$

verifying that in this case $\tau_2 > 0$.

For (A.17) we proceed similarly as before to get

$$\tau_3 = \operatorname{Re} \int_{z_2}^{\hat{z}_2} (\xi_1(s) - \xi_2(s)) ds = \operatorname{Re} H(\hat{w}_2) - \operatorname{Re} H(\hat{w}_2^{-1})$$

where \hat{w}_2 is the parameter on the w -plane for which $\xi_1(\hat{z}_2) = h(\hat{w}_2^{-1})$, $\xi_2(\hat{z}_2) = h(\hat{w}_2)$. Recalling Corollary 4.6, \hat{w}_2 is alternatively characterized as the only zero of the function f appearing in (4.20)–(4.21) that belongs to $\{w \in \mathbb{C} \mid \operatorname{Im} w > 0, |w| > 1\}$. Note that the coefficient $t_0 - 2t_1$ of f in (4.20)–(4.21) can be written only in terms of r, a_0 with the help of the system (2.19)–(2.20).

So the numerical procedure here is to find all the zeros of f , select \hat{w}_2 and then compute the left hand side of (A.17) through (A.12). (A.17) was again evaluated in the range (A.22) and 300-digit precision, and we verified that in this case $\tau_3 < 0$.

The outcome of the numerical evaluation of τ_2 and τ_3 for several choices of r can be seen in Figures 42–44 and Figures 45–47, respectively.

Proposition A.6. *For $(t_0, t_1) \in \mathcal{F}_1$ it is valid*

$$\tau_4 > 0.$$

Proof. From (2.15) we see that the residue at infinity of ξ_1 is purely imaginary, thus

$$\operatorname{Re} \int_{z_2}^{z_*} \xi_1(s) ds + \operatorname{Re} \int_{z_*}^{z_1} \xi_1(s) ds = \operatorname{Re} \int_{z_2}^{z_1} \xi_1(s) ds, \quad (\text{A.23})$$

where, as in (5.16), $x_* < z_*$ and on both sides of (A.23) the paths of integration are taken in $\mathbb{C} \setminus ((-\infty, z_*] \cup \Sigma_*)$.

For the remaining integral in (5.16), we deform the path of integration across Σ_* to get

$$\int_{z_2}^{z_*} \xi_2(s) ds + \int_{z_*}^{z_1} \xi_3(s) ds = \int_{z_2}^{z_0} \xi_1(s) ds + \int_{z_0}^{z_1} \xi_3(s) ds. \quad (\text{A.24})$$

Combining (A.23) and (A.24), we obtain

$$\begin{aligned} \tau_4 &= \operatorname{Re} \int_{z_2}^{z_*} (\xi_1(s) - \xi_2(s)) ds + \operatorname{Re} \int_{z_*}^{z_1} (\xi_1(s) - \xi_3(s)) ds = \operatorname{Re} \int_{z_0}^{z_1} (\xi_1(s) - \xi_3(s)) ds \\ &= \operatorname{Re} \int_{z_0}^{z_2} (\xi_1(s) - \xi_3(s)) ds \\ &= \tau_2 \end{aligned}$$

where for the third equality we used the symmetry under conjugation. From (A.16) we get the desired result. \square

A.2. Width parameters in the one-cut case. We now proceed to the analysis of the τ_j 's in (5.26)–(5.31).

Proposition A.7. *For $(t_0, t_1) \in \mathcal{F}_2$, the quantities τ_1 , τ_2 , τ_4 and τ_5 , given respectively by (5.26), (5.27), (5.29) and (5.30), are never zero.*

Proof. Each of the integrals can be deformed to either one of the intervals $[z_2, z_1]$ or $[z_0, \hat{z}_0]$, where the respective integrand $\xi_j - \xi_k$ is real, continuous and never zero (see (4.34)), and hence does not change sign. \square

Proposition A.8. *For $(t_0, t_1) \in \mathcal{F}_2$, the quantity τ_6 given in (5.31) is strictly negative.*

Proof. Recall that w_0, w_1 and w_2 are the zeros of h' (see Lemma 3.10) and \tilde{w}_j is the simple solution to $h(w) - h(w_j) = 0$ (see Remark A.1). Proceeding in a similar manner as for Proposition A.4 (see in particular (A.10)–(A.13)), we get

$$\begin{aligned}\tau_6 &= \operatorname{Re} \int_{w_0}^{w_1} h\left(\frac{1}{w}\right) h'(w) dw - \operatorname{Re} \int_{\tilde{w}_0}^{\tilde{w}_1} h\left(\frac{1}{w}\right) h'(w) dw \\ &= \frac{r + w_1^3}{3w_1^3} q(w_1) - \frac{r + w_0^3}{3w_0^3} q(w_0) + 3r^2(1 - 4a_0r^2 - 2r^2) \log \left| \frac{w_1}{w_0} \right|,\end{aligned}\quad (\text{A.25})$$

where here q is given by

$$q(w) = \frac{12r^3 + 3r^5}{w^3} + \frac{6a_0r^2(5 - r^2)}{w^2} + \frac{a_0r((12 - 8a_0)r^2 + 10a_0)}{w} + 30a_0^2r^2 + 4a_0^3.$$

From (A.4) and (A.15),

$$3r^2(1 - 4a_0r^2 - 2r^2) \log \left| \frac{w_1}{w_0} \right| < 0. \quad (\text{A.26})$$

To deal with the first two terms on the right hand side of (A.25), rewrite

$$\begin{aligned}\frac{r + w_0^3}{3w_0^3} q(w_0) - \frac{r + w_1^3}{3w_1^3} q(w_1) &= \\ &= \left(\frac{r + w_0^3}{3w_0^3} - \frac{r + w_1^3}{3w_1^3} \right) q(w_0) + \frac{r + w_1^3}{3w_1^3} (q(w_0) - q(w_1))\end{aligned}\quad (\text{A.27})$$

From the rough estimate $0 < a_0, r < 1$ (see Theorem 3.6) it follows that the coefficients of q are positive, thus

$$q(w_0) > 0, \quad (\text{A.28})$$

because $w_0 > 0$, see Lemma 3.10. Furthermore, from (A.2),

$$\frac{r + w_1^3}{3w_1^3} > 0. \quad (\text{A.29})$$

Clearly,

$$\frac{r + w_0^3}{3w_0^3} - \frac{r + w_1^3}{3w_1^3} = \frac{r(w_0^3 - w_1^3)}{w_0^3(-w_1)^3} > 0, \quad (\text{A.30})$$

where for the last conclusion we used $w_1 < 0 < w_0$, see Lemma 3.10. Summarizing, a combination of (A.26)–(A.30) shows that the right-hand side of (A.25) is negative if we can prove that

$$q(w_0) - q(w_1) > 0. \quad (\text{A.31})$$

To see that (A.31) holds true, write

$$\begin{aligned}q(w_0) - q(w_1) &= (12r^3 + 3r^5) \left(\frac{1}{w_0^3} - \frac{1}{w_1^3} \right) + \left(\frac{1}{w_0} - \frac{1}{w_1} \right) \\ &\quad \times \left(6a_0r^2(5 - r^2) \left(\frac{1}{w_0} + \frac{1}{w_1} \right) + a_0r((12 - 8a_0)r^2 + 10a_0) \right)\end{aligned}\quad (\text{A.32})$$

Using again $w_1 < 0 < w_0$,

$$\frac{1}{w_0^3} - \frac{1}{w_1^3}, \frac{1}{w_0} - \frac{1}{w_1} > 0. \quad (\text{A.33})$$

In addition, using (A.5)

$$\begin{aligned}
6a_0r^2(5-r^2)\left(\frac{1}{w_0} + \frac{1}{w_1}\right) + a_0r((12-8a_0)r^2 + 10a_0) \\
\geq -6a_0r^2(5-r^2) + a_0r((12-8a_0)r^2 + 10a_0) \\
= a_0r[a_0(10-8r^2) + 6r(r^2 + 2r - 5)]
\end{aligned} \tag{A.34}$$

The term between brackets on the right-hand side above is increasing with a_0 , so it attains its minimum along the critical curve γ_c . Using (2.22), we get

$$a_0(10-8r^2) + 6r(r^2 + 2r - 5) = 3s^2(2s^7 - 4s^6 + 4s^4 - 10s + 5) > 0,$$

thus the left-hand side of (A.34) is positive as well. Combining this with (A.32)–(A.33), we conclude (A.31), and the proof is complete. \square

Proposition A.9. *The width τ_3 in (5.28) is strictly negative.*

As for the Proposition A.9, we verified that $\tau_3 < 0$ numerically as explained next.

Proceeding as in (A.18)–(A.21) we get

$$\int_{z_2}^{\hat{z}_2} (\xi_1(s) - \xi_2(s)) ds = H(\hat{w}_2) - H\left(\frac{1}{\hat{w}_2}\right) + H(w_2) - H\left(-\frac{r}{w_2}\right),$$

where w_2 and \hat{w}_2 are given by Lemma 3.10 and Corollary 4.6, respectively (see also Remark A.1), and the function H is given in (A.20). Thus

$$\tau_3 = \operatorname{Re} H(\hat{w}_2) - \operatorname{Re} H\left(\frac{1}{\hat{w}_2}\right) + H(w_2) - H\left(-\frac{r}{w_2}\right). \tag{A.35}$$

We use this last expression to verify that $\tau_3 < 0$ for

$$0 < r < \frac{1}{8}, \quad \frac{3}{2}r^{2/3} < a_0 < \frac{1-2r}{2},$$

which corresponds to $(t_0, t_1) \in \mathcal{F}_2$ (see Proposition 2.7). We evaluated (A.35) for

$$r = \frac{1}{8} \frac{j}{5000}, \quad a_0 = \frac{3r^{2/3}}{2} \frac{5000-k}{5000} + \frac{1-2r}{2} \frac{k}{5000}, \quad j, k = 1, \dots, 5000,$$

using Mathematica with 300-digit precision and verified that $\tau_3 < 0$. The outcome for several values of r and the whole corresponding range of a_0 can be seen in Figures 48–49.

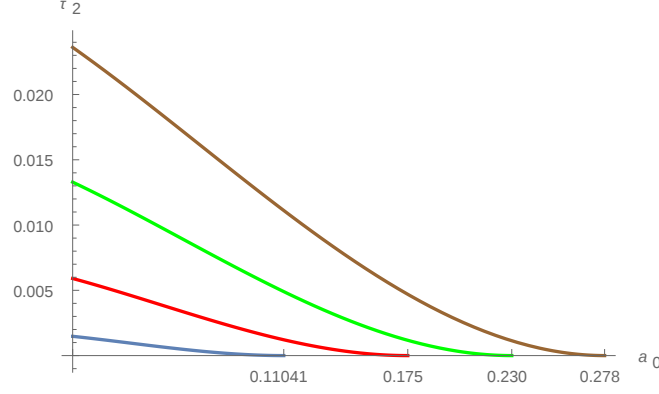


FIGURE 42. Plot of τ_2 as a function of a_0 in the three-cut case for $r = 1/50, 2/50, 3/50, 4/50$ (from bottom to top). For these choices of r , the extremal values of a_0 are attained in the critical line γ_c , so that a_0 ranges from 0 to the correspond critical value $3r^{2/3}/2$, in the present case given by 0.1105..., 0.1754..., 0.2298... and 0.2784..., respectively.

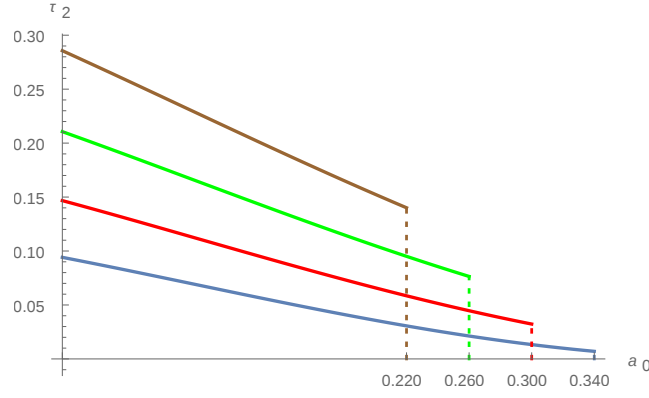


FIGURE 43. Plot of τ_2 as a function of a_0 in the three-cut case for $r = 8/50, 10/50, 12/50, 14/50$ (from bottom to top). For these choices of r , the extremal values of a_0 are attained in the critical line Γ_c , so that a_0 ranges from 0 to the correspond critical value $(1 - 2r)/2$, in the present case given by 0.34, 0.3, 0.26 and 0.22, respectively.

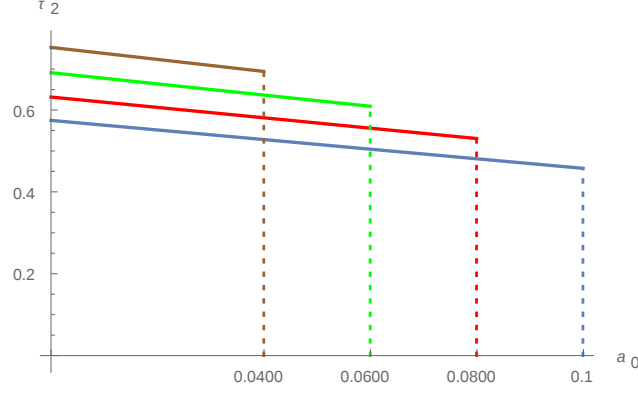


FIGURE 44. Plot of τ_2 as a function of a_0 in the three-cut case for $r = 20/50, 21/50, 22/50, 23/50$ (from bottom to top). For these choices of r , the extremal values of a_0 are attained in the critical line Γ_c , so that a_0 ranges from 0 to the correspond critical value $(1 - 2r)/2$, in the present case given by 0.1, 0.08, 0.06 and 0.04, respectively.

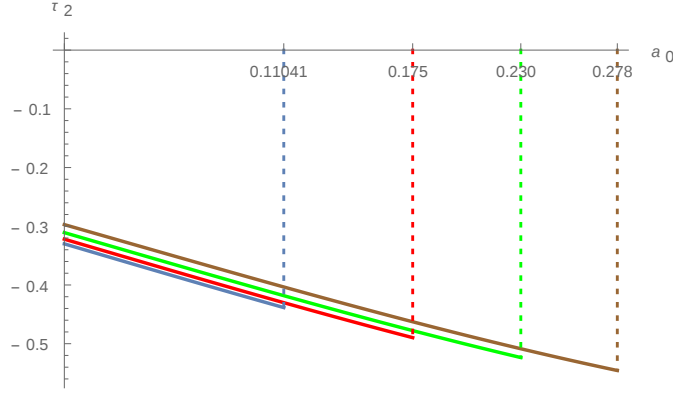


FIGURE 45. Plot of τ_3 as a function of a_0 in the three-cut case for $r = 1/50, 2/50, 3/50, 4/50$ (from bottom to top). For these choices of r , the extremal values of a_0 are attained in the critical line γ_c , so that a_0 ranges from 0 to the correspond critical value $3r^{2/3}/2$, in the present case given by 0.1105..., 0.1754..., 0.2298... and 0.2784..., respectively.

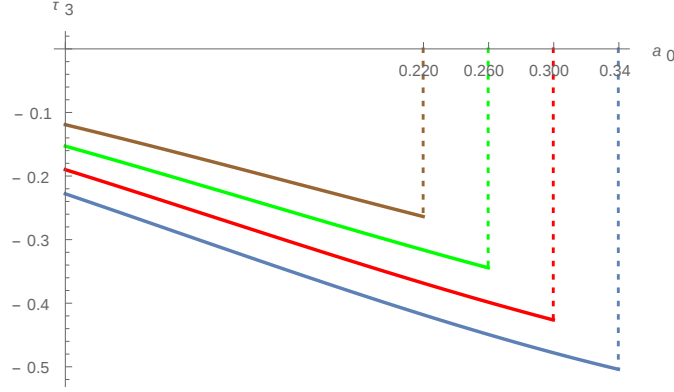


FIGURE 46. Plot of τ_3 as a function of a_0 in the three-cut case for $r = 8/50, 10/50, 12/50, 14/50$ (from bottom to top). For these choices of r , the extremal values of a_0 are attained in the critical line Γ_c , so that a_0 ranges from 0 to the correspond critical value $(1 - 2r)/2$, in the present case given by 0.34, 0.3, 0.26 and 0.22, respectively.

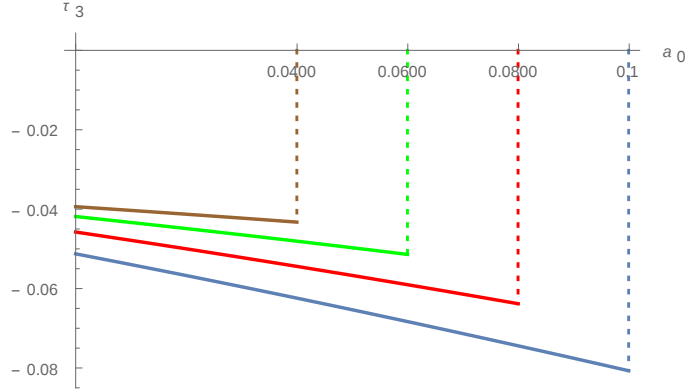


FIGURE 47. Plot of τ_3 as a function of a_0 in the three-cut case for $r = 20/50, 21/50, 22/50, 23/50$ (from bottom to top). For these choices of r , the extremal values of a_0 are attained in the critical line Γ_c , so that a_0 ranges from 0 to the correspond critical value $(1 - 2r)/2$, in the present case given by 0.1, 0.08, 0.06 and 0.04, respectively.

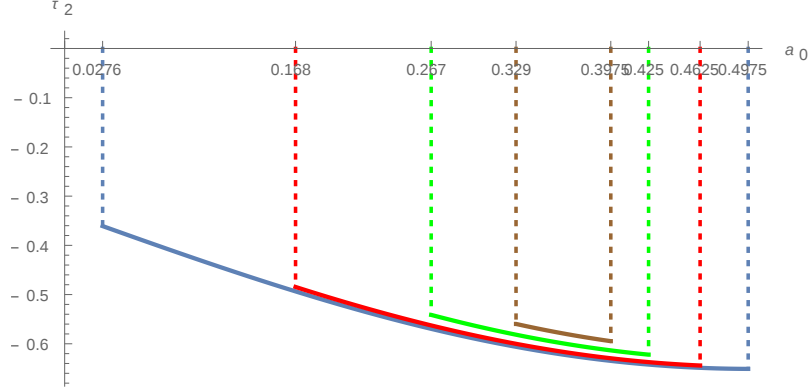


FIGURE 48. Plot of τ_3 as a function of a_0 in the one-cut case for $r = 1/400, 15/400, 30/400, 41/400$ (from bottom to top). For these choices of r , the minimal value for a_0 is along γ_c , thus given by $3r^{2/3}/3$, whereas the maximal value for a_0 is along Γ_c , hence corresponding to $(1 - 2r)/2$. In the present case, the minimal values are 0.0276..., 0.1680..., 0.2667... and 0.32852..., respectively, whereas the maximal values are 0.4975, 0.4625, 0.425 and 0.3975, respectively.

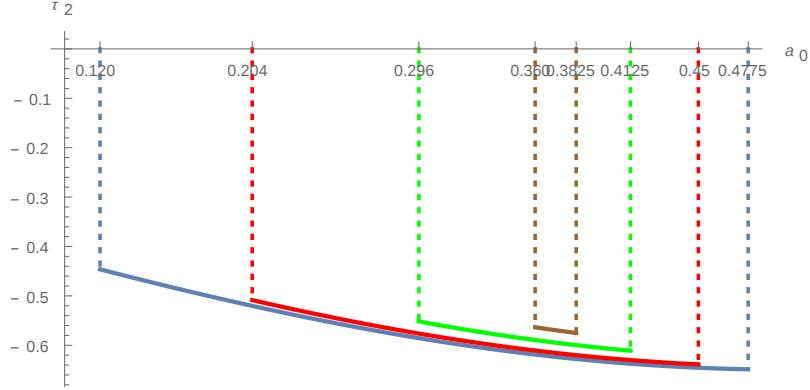


FIGURE 49. Plot of τ_3 as a function of a_0 in the one-cut case for $r = 9/400, 20/400, 35/400, 47/400$ (from bottom to top). For these choices of r , the minimal value for a_0 is along γ_c , thus given by $3r^{2/3}/3$, whereas the maximal value for a_0 is along Γ_c , hence corresponding to $(1 - 2r)/2$. In the present case, the minimal values are 0.1195..., 0.2035..., 0.2956... and 0.3598..., respectively, whereas the maximal values are 0.4775, 0.45, 0.4125 and 0.3825, respectively.

ACKNOWLEDGEMENTS

We thank F. Balogh, B. Gustafsson, A. Kuijlaars, S.-Y. Lee, R. Riser and E. Saff for useful discussions.

The first author was partially supported by the National Science Foundation project DMS-1265172.

The second author was supported by FWO Flanders project G.0934.13 and the FP7 IRSES grant RIMMP Random and Integrable Models in Mathematical Physics. He gratefully acknowledges the hospitality of the Department of Mathematical Sciences, Indiana University Purdue University Indianapolis, where a substantial part of this work was carried out during his visits in April-2014 and October-2014.

REFERENCES

- [1] D. Aharonov and H. S. Shapiro, *Domains on which analytic functions satisfy quadrature identities*, J. Anal. Math. **30** (1976), 39–73.
- [2] Y. Ameur, H. Hedenmalm and N. G. Makarov, *Random normal matrices and Ward identities*, Ann. Probab. **43** (2015), no. 3, 1157–1201.
- [3] Y. Ameur, H. Hedenmalm and N. G. Makarov, *Fluctuations of eigenvalues of random normal matrices*, Duke Math. J. **159** (2011), no. 1, 31–81.
- [4] A. I. Aptekarev, P. M. Bleher and A. B. J. Kuijlaars, *Large n limit of Gaussian random matrices with external source. II*, Comm. Math. Phys. **259** (2005), no. 2, 367–389.
- [5] A. I. Aptekarev, A. B. J. Kuijlaars and W. Van Assche, *Asymptotics of Hermite-Pade rational approximants for two analytic functions with separated pairs of branch points (case of genus 0)*, Int. Math. Res. Pap. **2008** (2008).
- [6] F. Balogh, M. Bertola, S.-Y. Lee and K. D. T-R McLaughlin, *Strong asymptotics of the orthogonal polynomials with respect to a measure supported on the plane*, Comm. Pure Appl. Math. **68** (2015), no. 1, 112–172.
- [7] F. Balogh, T. Grava and D. Merzi, *Orthogonal polynomials for a class of measures with discrete rotational symmetries in the complex plane*, ArXiv:1509.05331
- [8] L. Baratchart, H. Stahl and M. Yattselev, *Weighted extremal domains and best rational approximation*, Adv. Math. **229** (2012), no. 1, 357–407.
- [9] B. Beckermann, V. Kalyagin, A. C. Matos and F. Wielonsky, *Equilibrium problems for vector potentials with semidefinite interaction matrices and constrained masses*, Constr. Approx. **37** (2013), no. 1, 101–134.
- [10] M. Bertola, *Boutroux curves with external field: equilibrium measures without a variational problem*, Anal. Math. Phys. **1** (2011), no. 2-3, 167–211.
- [11] P. M. Bleher and A. Deaño, *Painlevé I double scaling limit in the cubic matrix model*, ArXiv:1310.3768.
- [12] P. M. Bleher, S. Delvaux and A. B. J. Kuijlaars, *Random matrix model with external source and a constrained vector equilibrium problem*, Comm. Pure Appl. Math. **64** (2011), no. 1, 116–160.
- [13] P. M. Bleher and A. B. J. Kuijlaars, *Large n limit of Gaussian random matrices with external source. I*, Comm. Math. Phys. **252** (2004), no. 1-3, 43–76.
- [14] P. M. Bleher and A. B. J. Kuijlaars, *Large n limit of Gaussian random matrices with external source. III*, Comm. Math. Phys. **270** (2007), no. 2, 481–517.
- [15] P. M. Bleher and A. B. J. Kuijlaars, *Orthogonal polynomials in the normal matrix model with a cubic potential*, Adv. Math. **230** (2012), no. 3, 1272–1321.
- [16] P. M. Bleher and K. Liechty, *Six-vertex model with partial domain wall boundary conditions: ferroelectric phase*, J. Math. Phys. **56** (2015), no. 2, 023302, 28.
- [17] L.-L. Chau and O. Zaboronsky, *On the structure of correlation functions in the normal matrix model*, Comm. Math. Phys. **196** (1998), no. 1, 203–247.
- [18] P. Deift, *Orthogonal polynomials and random matrices: A Riemann-Hilbert approach*, Courant Lecture Notes, no. 3, American Mathematical Society, 2000.

- [19] P. Deift, A. R. Its and X. Zhou, *A Riemann-Hilbert approach to asymptotic problems arising in the theory of random matrix models and also in the theory of integrable statistical mechanics*, Ann. of Math. **146** (1997), 149–235.
- [20] M. Duits and A.B.J. Kuijlaars, *Painlevé I asymptotics for orthogonal polynomials with respect to a varying quartic weight*, Nonlinearity **19** (2006), no. 10, 2211–2245.
- [21] P. Elbau, *Random normal matrices and polynomial curves*, Ph.D. thesis, ETH Zurich, 2006, arXiv:0707.0425.
- [22] P. Elbau and G. Felder, *Density of eigenvalues of random normal matrices*, Comm. Math. Phys. **259** (2005), no. 2, 433–450.
- [23] A. A. Gonchar and E. A. Rakhmanov, *Equilibrium distributions and the rate of rational approximation of analytic functions*, Mat. Sb. (N.S.) **134(176)** (1987), no. 3, 306–352, 447.
- [24] B. Gustafsson, *Lectures on balayage*, Clifford Algebras and Potential Theory, University of Joensuu Department of Mathematics, Sirkka-Liisa Eriksson, 2002, Proceedings of the summer school held in Mekrijärvi, June 24–28, 2002, pp. 17–63.
- [25] B. Gustafsson, *On mother bodies of convex polyhedra*, SIAM J. Math. Anal. **29** (1998), no. 5, 1106–1117.
- [26] B. Gustafsson, *On quadrature domains and an inverse problem in potential theory* J. Anal. Math. **55** (1990), 172–216.
- [27] B. Gustafsson and Y.-L. Lin, *On the dynamics of roots and poles for solutions of the Polubarinova-Galin equation*, Ann. Acad. Sci. Fenn. Math. **38** (2013), no. 1, 259–286.
- [28] B. Gustafsson, M. Putinar, E. B. Saff and N. Stylianopoulos, *Bergman polynomials on an archipelago: estimates, zeros and shape reconstruction*, Adv. Math. **222** (2009), no. 4, 1405–1460.
- [29] A. Hardy and A. B. J. Kuijlaars, *Weakly admissible vector equilibrium problems*, J. Approx. Theory **164** (2012), no. 6, 854–868.
- [30] H. Hedenmalm and N. G. Makarov, *Coulomb gas ensembles and Laplacian growth*, Proc. Lond. Math. Soc. (3) **106** (2013), no. 4, 859–907.
- [31] D. Huybrechts, A. B. J. Kuijlaars and N. Lejon, *Zero distribution of complex orthogonal polynomials with respect to exponential weights*, J. Approx. Theory **184** (2014), 28–54.
- [32] J. A. Jenkins, *Univalent functions and conformal mapping*, Ergebnisse der Mathematik und ihrer Grenzgebiete. Neue Folge, Heft 18. Reihe: Moderne Funktionentheorie, Springer-Verlag, Berlin-Göttingen-Heidelberg, 1958.
- [33] S. Kamvissis, *Comment on “Existence and regularity for an energy maximization problem in two dimensions”* [S. Kamvissis and E. A. Rakhmanov, J. Math. Phys. **46**, 083505 (2005)], J. Math. Phys. **50** (2009), 104101, 3.
- [34] S. Kamvissis, K. D. T.-R. McLaughlin and P. D. Miller, *Semiclassical soliton ensembles for the focusing nonlinear Schrödinger equation*, Ann. of Math. Stud., vol. 154, Princeton Univ. Press, Princeton, NJ, 2003, xii+265.
- [35] S. Kamvissis and E. A. Rakhmanov, *Existence and regularity for an energy maximization problem in two dimensions*, J. Math. Phys. **46** (2005), no. 8, 083505, 24.
- [36] I. K. Kostov, I. Krichever, M. Mineev-Weinstein, P. B. Wiegmann and A. Zabrodin, *The τ -function for analytic curves*, Random matrix models and their applications, Math. Sci. Res. Inst. Publ., vol. 40, Cambridge Univ. Press, Cambridge, 2001, pp. 285–299.
- [37] A. B. J. Kuijlaars and A. López, *A vector equilibrium problem for the normal matrix model and multiple orthogonal polynomials on a star*, arXiv: 1401.2419.
- [38] A. B. J. Kuijlaars and G. L. F. Silva, *S-curves in polynomial external fields*, J. Approx. Theory **191** (2015), 1–37.
- [39] A. B. J. Kuijlaars and A. Tovbis, *The supercritical regime in the normal matrix model with cubic potential*, Adv. Math. **283** (2015), 530–587.
- [40] S.-Y. Lee and N. G. Makarov *Topology of quadrature domains*, J. Amer. Math. Soc., to appear.
- [41] S.-Y. Lee, R. Teodorescu and P. Wiegmann *Viscous shocks in Hele-Shaw flow and Stokes phenomena of the Painlevé I transcendent*, Phys. D **240** (2011), no. 13, 1080–1091.
- [42] D. H. U. Marchetti, T. Pereira and A. M. Veneziani *Asymptotic integral kernel for ensembles of random normal matrices with radial potentials*, J. Math. Phys. **53** (2012), no. 2, 023303, 21.
- [43] D. H. U. Marchetti, T. Pereira and A. M. Veneziani *Conformal deformation of equilibrium measures in normal random ensembles*, J. Phys. A **44** (2011), no. 7, 075202, 21.

- [44] A. Martínez-Finkelshtein and E. A. Rakhmanov, *Critical measures, quadratic differentials, and weak limits of zeros of Stieltjes polynomials*, Comm. Math. Phys. **302** (2011), no. 1, 53–111.
- [45] A. Martínez-Finkelshtein and G. L. F. Silva, *Critical measures for vector energy: global structure of trajectories of quadratic differentials*, ArXiv:1509.06704.
- [46] H. N. Mhaskar and E. B. Saff, *The distribution of zeros of asymptotically extremal polynomials*, J. Approx. Theory **65** (1991), no. 3, 279–300.
- [47] C. Pommerenke, *Univalent functions - With a chapter on quadratic differentials by G. Jensen*, Vandenhoeck & Ruprecht, Gottingen, 1975.
- [48] E. A. Rakhmanov, *Orthogonal polynomials and S-curves*, Contemp. Math., vol. 578, Amer. Math. Soc., Providence, RI, 2012. MR 2964146
- [49] R. Riser, *Universality in Gaussian Normal Matrices*, Ph.D. thesis, ETH Zurich, 2012, arXiv:1312.0068.
- [50] E. B. Saff and V. Totik, *Logarithmic potentials with external fields*, Grundlehren der Mathematischen Wissenschaften [Fundamental Principles of Mathematical Sciences], vol. 316, Springer-Verlag, Berlin, 1997, Appendix B by T. Bloom.
- [51] T. V. Savina, V. E. Shatalov and B. Yu. Sternin, *On a minimal element for a family of bodies producing the same external gravitational field*, Appl. Anal. **84** (2005), no. 7, 649–668.
- [52] J. R. Sendra, F. Winkler and S. Pérez-Díaz, *Rational algebraic curves: a computer algebra approach*, Algorithms and Computation in Mathematics, vol. 22, Springer, Berlin, 2008.
- [53] T. Sjödin, *Mother bodies of algebraic domains in the complex plane*, Complex Var. Elliptic Equ. **51** (2006), no. 4, 357–369.
- [54] H. Stahl, *Extremal domains associated with an analytic function. I, II*, Complex Variables Theory Appl. **4** (1985), no. 4, 311–324, 325–338.
- [55] ———, *The structure of extremal domains associated with an analytic function*, Complex Variables Theory Appl. **4** (1985), no. 4, 339–354.
- [56] ———, *Orthogonal polynomials with complex-valued weight function. I, II*, Constr. Approx. **2** (1986), no. 3, 225–240, 241–251.
- [57] K. Strebel, *Quadratic differentials*, Ergebnisse der Mathematik und ihrer Grenzgebiete (3) [Results in Mathematics and Related Areas (3)], vol. 5, Springer-Verlag, Berlin, 1984.
- [58] D. Zidarov, *Inverse Gravimetric Problem in Geoprospecting and Geodesy* Developments in Solid Earth Geophysics, Elsevier, 1990. 284 pages.

(PB) DEPARTMENT OF MATHEMATICAL SCIENCES, INDIANA UNIVERSITY-PURDUE UNIVERSITY
INDIANAPOLIS, 402 N. BLACKFORD ST., INDIANAPOLIS, IN 46202, USA.

E-mail address: pbleher@iupui.edu

(GS) KU LEUVEN, DEPARTMENT OF MATHEMATICS, CELESTIJNENLAAN 200B BUS 2400, B-3001
LEUVEN, BELGIUM

E-mail address: guilherme.silva@wis.kuleuven.be